Biomimetic polymer vesicles : towards structural and functional cell biomimicry

Ariane Peyret

Thèse présentée

pour obtenir le grade de

DOCTEUR DE L'UNIVERSITÉ DE BORDEAUX

Ecole Doctorale des Sciences Chimiques

Spécialité : Polymères

par **Ariane PEYRET**

Vésicules Polymères Biomimétiques : vers un biomimétisme cellulaire structurel et fonctionnel

Biomimetic Polymer Vesicles: towards structural and functional cell biomimicry

Directeur de Thèse: Sébastien Lecommandoux

Soutenue le 24/10/2017

Devant la commission d'examen formée de :

Mme LI Min Hui	Directrice de recherche, CNRS, Chimie Paris Tech	Rapporteur
M. TRIBET Christophe	Directeur de recherche, CNRS, ENS Paris	Rapporteur
M. HADZIIOANNOU Georges	Professeur, Université de Bordeaux	Président
M. HUCK Wilhelm	Professeur, Radboud University, Nijmegen	Examinateur
Mme FARCET Céline	Ingénieur de recherche, L'Oréal Paris	Examinateur
M. LECOMMANDOUX Sébastien	Professeur, Bordeaux INP	Examinateur
M. McCLENAGHAN Nathan	Directeur de recherche, CNRS, Bordeaux	Examinateur
M. NASSOY Pierre	Directeur de recherche, CNRS, Bordeaux	Examinateur

J'écris ces quelques lignes qui ne seront jamais assez suffisantes pour témoigner de la profonde gratitude que je ressens envers tous ceux qui m'ont aidée d'une manière ou d'une autre dans le cadre de cette thèse. J'ai passé des années exceptionnelles au sein du LCPO, et ce grâce à toutes les personnes mentionnées ci-dessous. Ce fut une aventure humaine et scientifique, riche en émotions et découvertes, ces quelques années resteront toujours gravées dans ma mémoire.

I first of all would like to thank my jury, for agreeing to evaluate my work. Thank you to my referees Dr. Min-Hui Li and Dr. Christophe Tribet and of course to Pr. Wilhelm Huck, Dr. Céline Farcet, Dr. Nathan McClenaghan, Dr. Pierre Nassoy and the jury president, Pr. Georges Hadziioannou.

Un grand merci au Pr. Henri Cramail, directeur du labo au début de ma thèse, pour m'avoir accueillie au sein du LCPO.

Je souhaite remercier tout particulièrement mon directeur de thèse et actuel directeur du LCPO, le professeur Sébastien Lecommandoux pour m'avoir fait confiance toutes ces années, d'abord en stage puis pour ce projet de thèse ambitieux. Merci infiniment pour toute la liberté que tu m'as laissée. J'ai eu la chance de pouvoir évoluer et diriger mes recherches dans la direction que je souhaitais, tout en recevant tes conseils avisés au long du chemin. Tu t'es toujours rendu disponible, que ce soit le temps de 2 minutes en passant devant le bureau, par e-mails au milieu de la nuit ou au téléphone depuis d'autres continents ! Merci de m'avoir permis de partir présenter mes travaux à l'étranger et d'assister à des conférences d'un haut niveau scientifique qui m'ont inspirée et motivée. Je réalise que c'était une grande chance et de belles opportunités pour moi. Merci également de m'avoir si souvent rassurée, re-motivée et ré-orientée lorsque j'étais perdue devant les (nombreux !) obstacles auxquels nous avons été confrontés durant cette thèse. Je suis extrêmement fière des travaux qu'on a faits et du bout de chemin parcouru ensemble. Je pense avoir énormément appris en travaillant à tes côtés, tu avoueras notamment que mes schémas sont un peu moins moches qu'avant… C'était vraiment un honneur de pouvoir travailler avec toi, au sein de l'équipe. Je ressors grandie de cette expérience et j'espère que nous aurons l'occasion de collaborer dans le futur, qui sait... !!

Merci au Ministère de l'Enseignement Supérieur et de la Recherche pour avoir financé cette thèse.

Une pensée particulière et un grand merci à Jun Mougnier, ami de longue date, qui m'a orientée vers le LCPO il y a plusieurs années de ça.

Un merci à Romain Jagu, mon stagiaire de Master pour tout le travail qu'il a fait sans se décourager ! J'en profite pour remercier aussi tous les stagiaires du « loft » à cette période-là, particulièrement Manue, Justine et Mathieu pour leur bonne humeur et tous les excellents moments passés ensemble !

Je souhaiterai remercier Elizabeth Gillies, pour sa gentillesse, son encadrement, sa disponibilité et ses conseils lors du stage qui a précédé ma thèse, durant lequel nous avons collaboré sur un beau projet.

Un grand merci à Arnaud Tron et Nathan McClenaghan pour leur aide précieuse lors de notre collaboration au début de ma thèse. Merci pour votre accueil au sein de votre labo et merci de m'avoir initiée à de nouvelles techniques expérimentales avec patience ! Votre aide a été indispensable.

Un énorme merci à toute l'équipe de Pierre Nassoy et particulièrement Kevin, Maxime, Amaël et Nestor/Nelson/Norbert pour leur accueil chaleureux et cette belle nouvelle collaboration sur un projet ambitieux ! C'était un honneur de pouvoir faire partie de votre équipe l'espace de quelques mois. J'ai extrêmement apprécié tous nos échanges et chacune de mes visites était instructive.

Je souhaite également remercier chaleureusement toutes les personnes qui ont participé de près ou de loin à l'aventure de « Ma thèse en 180 secondes » et particulièrement Delphine et Marie. C'était un projet qui me tenait à cœur, je n'y serai jamais arrivée sans toute l'aide que j'ai reçue. Merci à Seb de m'avoir permis de participer et tous mes collègues et partenaires pour leur aide et leur soutien.

En ce qui concerne le LCPO, merci à toutes les personnes qui nous facilitent la vie au quotidien au sein du laboratoire : Nicole, Corine, Bernadette, Claude, Loïc, Catherine et Dominique (qui j'espère se souviendra de nos conversations à propos de Georges). Votre aide nous est précieuse ! Des remerciements également à tous les experts techniques, non seulement pour votre aide sur le fonctionnement des machines, mais également pour tout le temps passé à réfléchir à nos côtés et à analyser, décortiquer les résultats. Merci donc à Cédric, Anne-Laure, Gégé, Eric, Nico et Amélie.

Manu…tu mérites bien un paragraphe! On peut dire que tu as adoré me faire la vie dure pendant trois ans ! Tu m'as fait du chantage au chocolat lorsque je te demandais de l'aide, tu as adoré te moquer de moi, tu m'as grondée quand la salle du confocal était en désordre, tu t'es attribué tout le mérite de nos travaux, tu as fait de moi un poisson bleu idiot, et j'en passe… Pourtant, malgré le cactus piquant que tu es en surface, tu as un cœur en chocolat tout mou. Tu as été mon papa du confocal pendant cette thèse, tu as su me faire rire pour me déstresser et surtout garder ton sérieux quand il le fallait. Merci pour ton aide précieuse, ton envie de bien faire et ton perfectionnisme qui ont si souvent réussi à me re-motiver. Merci pour tous ces excellents moments, toutes ces heures passées devant l'écran du confocal à attendre des explosions qui n'arrivaient jamais au bon moment. Tu es une personne unique, cette thèse n'aurait pas été la même sans toi, ton énergie et ton humour !

Je souhaite remercier particulièrement Jeff, Christophe, Bertrand, Olivier et Babeth, non seulement pour votre aide au quotidien mais également et surtout pour votre bonne humeur qui ont contribué à l'excellente ambiance du N2 ! Vous m'avez tous aidée à un moment ou un autre et vos conseils m'ont été précieux. Sur un plan humain, merci pour tous les bons moments passés ensemble, les discussions et les verres à la parcelle ! C'était un plaisir et un honneur de travailler dans votre équipe. J'en profite pour remercier quelques anciens membres de la Team 3 : Julie et Colin qui m'ont encadrée en stage avant ma thèse, je garde un excellent souvenir du bout de chemin parcouru à vos côtés ; mais aussi Silvia, Camille, Marie, Lucas, Romain, Annie, Ann, Shusheng, Cony, Rosine et Tuyen. Un merci chaleureux à tous les doctorants et post-docs de l'équipe. Votre présence au quotidien fait du N2 et de nos laboratoires un environnement de travail extrêmement agréable où règnent sympathie et bonne humeur ! Merci particulier à Marie, Ye, Michèle, Julien, Vangelis, Gaugau et Loulou : quel bonheur de travailler dans ce bureau !

J'ai eu la chance de rencontrer des personnes formidables et de partager bien plus qu'un quotidien en laboratoire. Merci pour ces nouvelles amitiés, merci pour tous ces bons moments, les pauses cafés, les repas Caes, toutes ces soirées (beaucoup de soirées !), les weekends et vacances passés ensemble ! Sans vous, rien n'aurait été pareil. Merci donc premièrement à Lélé : tu es une personne formidable avec un cœur énorme. Tu as toujours été là pour m'écouter, faire semblant de rire à mes blagues et partager les bons moments comme les mauvais. Tu as été une épaule et un soutien essentiel. Merci à P-L la police, Ursule Mais Heu, Mr Berto, Bakka, Kentain, Tutur, Sav', QP, Lulu (2), Sofiem, Julien, Cédric, Martin C., Martin F., Guillaume Go., Gaelle, Coralie, Esra, Monica, Boris, Dounia, Michou, Guillaume Ga., Jérémie, Laura,

Margot, Romain, Océane, Geoffrey, Alex, Benji, Mehdi, Fiona, la team B8 : Cindy, Ségo & Camille, le bureau N2, et particulièrement la team bling-bling. Gaugau, tu es une belle personne, tu m'as énormément inspirée pendant cette thèse et bien souvent remotivée. Merci pour ton soutien, ta patience, tes cours de golf et tes bons mojitos! Loulou, que dire ? Je ne sais pas ce que j'aurai fait sans toi. Merci d'avoir supporté mes humeurs (et mes Pious), merci de m'avoir écoutée, épaulée, conseillée au quotidien. Merci pour tous ces moments, toutes ces pauses café, balades digestives, batailles d'eau ou de nunchaku, dé-réglages de chaises, fous-rires, et j'en passe. Merci d'avoir été mon meilleur ami pendant ces trois années !

Une pensée pour tous les amis qui ont suivi cette thèse de près ou de loin : Laura, Amélie, Agathe, Franck, Jean, Mel, Gwen, Audrey, Aurore, Thibaut, Stef, Lisa, Anaïs, Arthur, Flo, etc…

Enfin, un énorme merci à ma famille grecque et française, ainsi qu'à ma belle-famille. A mes parents et mon frère particulièrement pour leurs conseils et soutien sans faille au quotidien. Je n'y serai jamais arrivée sans vous. Lulu, merci non pas pour les trois années passées, mais pour les sept dernières et toutes celles qui suivront. Cette thèse tu l'as vécue avec moi. Ton soutien et ta patience m'ont été indispensables et je t'en serai pour toujours reconnaissante. Tu as été à mes côtés pour vivre réussites et échecs pendant lesquels j'ai constamment pu compter sur tes encouragements et ton soutien. Merci pour tout ce que tu m'as apporté, cette thèse, je n'y serai jamais arrivée sans toi.

A ma famille

A Lulu

General table of contents

Résumé

Ce projet de thèse s'inscrit dans le contexte de travaux de recherche sur le biomimétisme cellulaire. La volonté de recréer artificiellement des mimes de cellules biologiques à base de matériaux synthétiques a fait l'objet de nombreuses études depuis déjà plusieurs dizaines d'années. Les premières vésicules synthétiques ayant été formées en laboratoire sont les liposomes, formés par l'assemblage de lipides dont les avantages en termes de biocompatibilité, d'encapsulation et délivrance d'actifs thérapeutiques, ou encore d'utilisation comme bioréacteurs ne sont plus à démontrer. Des systèmes plus complexes ont été développés avec le temps en s'inspirant de ces modèles et notamment des structures compartimentées permettant l'encapsulation de plusieurs molécules et la possibilité de réaliser des réactions chimiques ou enzymatiques en cascade, en milieu confiné. Ces systèmes innovants ont été inspirés par la structure compartimentée de la cellule biologique eucaryote dont les compartiments internes permettent de séparer, de protéger et de fournir des environnements différents aux espèces encapsulées, tout en les gardant proches au sein du cytoplasme. L'expansion de ces structures biomimétiques synthétiques a permis de voir naître des systèmes extrêmement complexes mimant non seulement la compartimentalisation mais également une partie de la fonction cellulaire, à savoir certaines réactions métaboliques sous forme de réactions confinées en cascade dans des bioréacteurs artificiels à base principalement de lipides ou de polymères.

Les travaux de cette thèse s'inscrivent dans ce contexte de biomimétisme cellulaire, à l'interface de la science des polymères et des biomatériaux. Sans ce contexte, nous avons utilisé les concepts les plus avancés dans les domaines de l'auto-assemblage des copolymères à blocs, des procédés de formulation, de la photochimie ou de la biophysique des membranes et des interfaces afin d'élaborer des systèmes innovants. L'objectif principal qui a fait l'objet de trois ans de recherche était de repousser les limites du mimétisme en développant des systèmes compartimentés dont les sous-compartiments répondraient à des stimuli externes pour libérer indépendamment des espèces encapsulées. Il s'agissait donc de proposer une structure compartimentée innovante et « intelligente » et de démontrer la libération contrôlée d'espèces *via* différents « *triggers* » externes (chapitres 3 et 4). De plus, des travaux ont été effectués sur le développement et l'étude d'une membrane asymétrique polymère-lipide mimant de manière plus proche en terme de propriétés de perméabilité et de mobilité la membrane cellulaire (chapitre 2). Enfin, les derniers mois ont été consacrés à la mise en place d'un nouveau projet en collaboration portant sur l'étude de l'interaction entre des mimes synthétiques de cellules (polymersomes) et des cellules biologiques (chapitre 5). Après une présentation du contexte

bibliographique permettant de positionner mon étude (Chapitre 1), les principales recherches et découvertes réalisées sont résumées ci-dessous pour chaque chapitre.

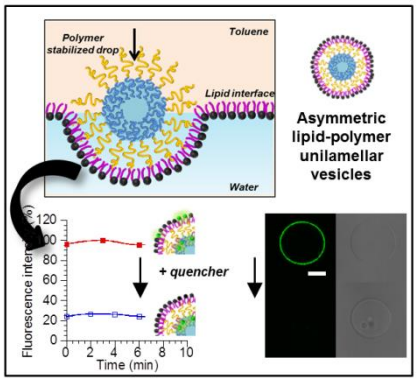

Chapitre 2 : *Développement d'une membrane synthétique asymétrique lipide/polymère mimant les caractéristiques structurelles et physiques principales d'une membrane cellulaire biologique*

Les membranes cellulaires biologiques sont caractérisées par une répartition asymétrique des lipides qui la composent. De nombreux travaux de recherche sont axés sur le développement de membranes asymétriques synthétiques mimant les membranes naturelles dans le but de faciliter la compréhension de phénomènes biophysiques fondamentaux étroitement liés à cette structuration particulière. La technique d'émulsion-centrifugation a été utilisée pour préparer des vésicules biomimétiques géantes dont la membrane interne est formée d'une monocouche de poly(oxyde d'éthylène)-*b*-poly(butadiène) (PBut-*b*-PEO, copolymère amphiphile) et dont la membrane externe est formée d'une monocouche de 1-palmito-2-oleyl-sn-glycero-3-phosphocholine (POPC, lipide). L'asymétrie totale de la membrane a été prouvée grâce à des tests d'extinction de fluorescence, avec l'insertion d'un lipide « tagué » au sein de la couche lipidique. De plus, la stabilité de l'asymétrie dans le temps a été mesurée expérimentalement par des mesures de diffusion transverse des lipides de la couche externe vers la couche interne. Le temps auquel la moitié des lipides a diffusé vers la couche interne, ou temps de demi-vie, a été estimé à 7,5 heures. Ce temps est en accord avec le temps de diffusion de lipides dans certaines membranes (peut varier entre quelques heures et plusieurs jours en fonction du lipide et du type de membrane) et confirme la ressemblance des membranes synthétiques obtenues au regard des propriétés physiques visées. Des mesures de recouvrement de fluorescence après photoblanchiment ont permis de déterminer le coefficient de diffusion d'un lipide « tagué » avec de la rhodamine inséré dans la couche lipidique POPC externe. Ce coefficient de diffusion a été estimé à 1,8±0.50 $\mu m^2/s$ à 25 °C and 2.3±0.7 $\mu m^2/s$ à 37 °C, des valeurs comprises entre les coefficients de diffusion de membranes purement lipidiques ou purement polymères et proches des valeurs de diffusion des lipides dans les membranes biologiques. Ces données ont permis de confirmer la fiabilité des vésicules à membrane asymétrique développées grâce à la technique d'émulsion-centrifugation, qui constitue un moyen précis et efficace pour préparer ces systèmes. Il a de plus été démontré que différents lipides peuvent être utilisés par ce même protocole permettant ainsi de moduler les propriétés de membrane.

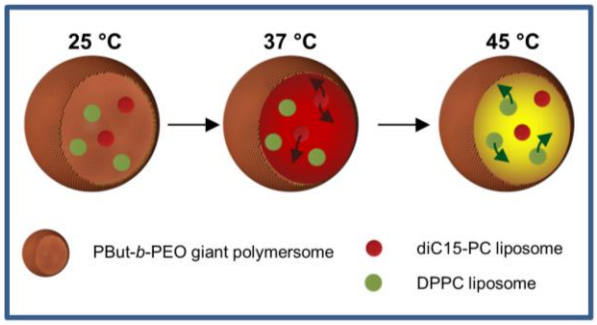

Chapitre 3 : *Des nano-liposomes encapsulés dans des polymersomes géants comme systèmes multi-compartimentés avec libération contrôlée par la température*

Les résultats obtenus sur les travaux concernant la multi-compartimentalisation et la libération contrôlée au sein de systèmes biomimétiques synthétiques sont présentés dans ce chapitre. Différents nano-liposomes à base de POPC, DMPC (1,2-dimyristoyl-sn-glycero-3-phosphocholine), diC15-PC (1,2-dipentadecanoyl-sn-glycero-3-phosphocholine) et DPPC (1,2-dipalmitoyl-sn-glycero-3-phosphocholine) ont été formés par la méthode de réhydratation d'un film de lipide suivie d'une extrusion. Des analyses DLS ont permis de confirmer un diamètre d'environ 100 nm pour les différentes vésicules. Ces liposomes ont ensuite été encapsulés séparément puis co-encapsulés dans des polymersomes PBut-*b*-PEO géants par la méthode d'émulsion-centrifugation. Les systèmes multi-compartimentés ainsi obtenus ont été caractérisés par microscopie confocale et spectroscopie UV-visible. Aucune fusion entre les liposomes ou avec la membrane PBut-*b*-PEO n'a été observée quel que soit le type de lipide confirmant la versatilité de la méthode. Dans un second temps, la libération contrôlée d'espèces a été démontrée. Des liposomes diC15-PC et DPPC ont été co-encapsulés dans des vésicules PBut-*b*-PEO. Les lipides ont été choisis en fonction de leur température de transition (Tt) de phase au-delà de laquelle la membrane devient perméable, permettant ainsi la diffusion des espèces encapsulées. Les liposomes diC15-PC et DPPC ont une Tt respective de 35 et 41 °C. Ainsi, il a été montré par spectroscopie de fluorescence et microscopie confocale qu'à température contrôlée (37 et 45 °C), il est possible de libérer *in vitro* dans les polymersomes géants de manière successive deux fluorophores, le bleu de méthylène et la fluorescéine, respectivement encapsulés dans chacun des deux types de liposomes. Le système développé possède la structuration multi-compartimentée d'une cellule biologique eucaryote et permet des libérations contrôlées de manière indépendante par la température. Ces systèmes pourraient être utilisés comme micro-réacteurs avec la possibilité d'initier des réactions chimiques ou enzymatiques en cascade de manière contrôlée grâce à la température.

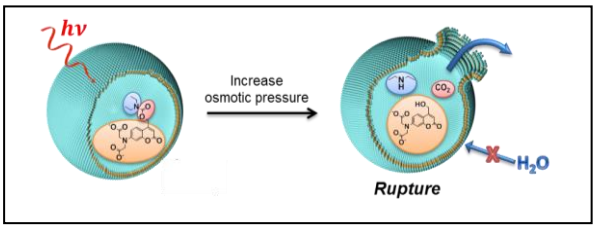

Chapitre 4 : *Ruptures contrôlées de polymersomes grâce à la pression osmotique*

Les travaux présentés dans ce chapitre concernent le développement d'une méthode de haute précision permettant une rupture contrôlée de polymersomes suite à un déséquilibre osmotique. Des molécules fluorescentes ont été encapsulées dans des vésicules PBut-*b*-PEO préparées par la méthode d'émulsion-centrifugation. La première, un dérivé photo-clivable du coumarin (N-diethyl, O-({7-[bis(carboxymethyl)-amino]coumarin-4-yl}methyl carbamate, λ_{exc}=405 nm), a été synthétisée en collaboration avec l'Institut des Sciences Moléculaires (ISM, équipe du Dr. N. McClenaghan). Les deux autres, la calcéine (λ_{exc}=488 nm) et le bleu de méthylène (λ_{exc}=633 nm) produisent des espèces oxygénées réactives. Il a été démontré qu'à forte concentration et sous irradiation, ces molécules se clivent et génèrent ainsi une augmentation de pression osmotique. Lorsque ces molécules sont irradiées à l'intérieur de polymersomes PBut-*b*-PEO sous microscope confocal, la différence de pression osmotique générée couplée à la très faible perméabilité de la membrane ($\approx P \sim 3.1 \pm 1.6$ µm·s^{-1}) entraîne la formation rapide (quelques secondes) d'un pore qui provoque une une ouverture irréversible de la vésicule conduisant à sa rupture. La formation de ce pore est liée au choc hypotonique qui génère des pressions importantes de l'eau sur la membrane. Des mesures de pression osmotique, de RMN et d'absorbance en particulier ont permis de confirmer que l'augmentation de pression osmotique générée par le clivage des molécules irradiées est bien responsable de l' « explosion » des polymersomes.

Il a ensuite été montré que ce phénomène de rupture peut être parfaitement contrôlé dans le temps et l'espace. Comme preuve de concept, deux lots de polymersomes PBut-*b*-PEO ont été préparés, l'un encapsulant des nano-polymersomes et de la calcéine et l'autre des nano-liposomes et du bleu de méthylène. Ces nano-vésicules ont été libérées séparément par rupture successives des lots de polymersomes PBut-*b*-PEO après irradiations respectives à 488 puis 633 nm, correspondant respectivement aux longueurs d'onde d'absorption maximales de la calcéine et du bleu de méthylène.

Enfin, pour confirmer ces résultats, une seconde étude de choc osmotique sur des vésicules PBut-*b*-PEO a été conduite. Celle-ci implique un choc hypertonique lié à la photo-polymérisation UV d'acrylamide *in situ.* Des premiers tests ont été réalisés pour établir les paramètres de polymérisation induisant une rapide (inférieure à 5 min) et importante diminution de pression osmotique. Ainsi, il a été trouvé que des concentrations en monomère de 10, 20 et

40 g/L pouvaient générer des différences de pression osmotique entre 100 et 150 mOsm associées à une augmentation notable de viscosité après 5 min d'irradiation UV (lampe mercure-xenon, 200 W). Ces différents paramètres de photo-polymérisation ont ensuite été testés *in situ* au sein de polymersomes géants PBut-*b*-PEO en observation directe sous microscope confocal. Il a été observé que les polymersomes subissent une rupture rapide pour 20 et 40 g/L en monomère acrylamide en présence de 0,25 et 0,50 % (masse volumique) respectifs de photo-amorceur (Irgacure 2959). A contrario, même à forte concentration en monomère et sous irradiation prolongée, les vésicules restent stables pour 0,10 % d'amorceur, indiquant que l'augmentation de viscosité (faible pour ces conditions) intervient probablement dans le processus de rupture. Des contrôles sans amorceur ont été effectués dans les mêmes conditions pour confirmer que la rupture des vésicules est uniquement une conséquence de la diminution de pression osmotique générée par la production de poly(acrylamide). Ces travaux confirment les résultats précédents et constituent une approche solide, originale et généralisable pour des problématiques de libération contrôlée.

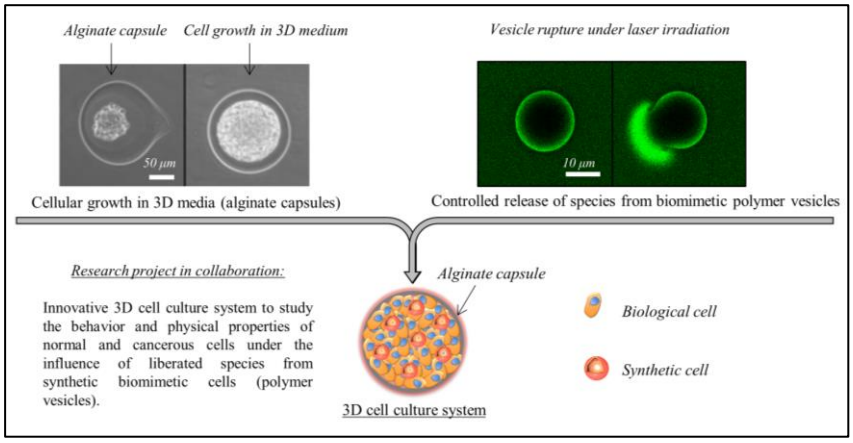

Chapitre 5 : *Co-culture de cellules synthétiques polymères et de cellules biologiques dans des capsules d'alginate 3D*

Ces derniers travaux de recherches constituent la base d'un nouveau projet en collaboration avec l'équipe du Dr. P. Nassoy (Laboratoire Photonique Numérique et Nanosciences, LP2N UMR 5298) et notre laboratoire. L'équipe du Dr. Nassoy a récemment développé un système qui s'appuie sur une technique de micro-fluidique pour former de manière fiable et reproductible des capsules d'alginate biocompatibles dans lesquelles il est possible d'encapsuler et de faire croître différents types cellulaires de manière tridimensionnelle (3D). L'objectif du projet est de cultiver des cellules biologiques en milieu 3D en présence de polymersomes (cellules artificielles) et d'étudier le comportement de cellules saines ou tumorales sous l'action de molécules environnantes nocives ou thérapeutiques libérées de manière contrôlée par les polymersomes.

Les premiers travaux de recherche du projet ont été axés sur l'optimisation du protocole d'encapsulation des cellules dans les capsules alginate pour permettre la co-encapsulation avec les polymersomes et leur co-culture. Les paramètres du système de micro-fluidique ont été conservés et les principales modifications ont concerné la préparation des vésicules par la technique d'émulsion-centrifugation. En particulier, le glucose a été remplacé par du sorbitol dont la concentration a été ajustée pour ne pas générer de choc osmotique lors de la mise en contact avec les cellules. De plus, il a été déterminé que différents lots de polymersomes devaient être combinés lors de l'encapsulation pour augmenter le rendement d'encapsulation. L'optimisation du protocole a été suivie par microscopies optiques et confocales. Des premiers tests de co-encapsulation ont été effectués avec des cellules souches humaines. Malgré un bon rendement, les cellules n'ont survécu que quelques heures après encapsulation. En effet, les cellules souches sont connues pour être extrêmement sensibles et ont probablement pu être déstabilisées par des traces de toluène résiduel. Il a donc été décidé de poursuivre les tests avec des lignées d'adipocytes de souris, connues pour être extrêmement résistantes. Les premiers tests effectués ont démontré une survie jusqu'à 4 jours après co-encapsulation avec les polymersomes dans les capsules alginate 3D.

Ces premiers résultats constituent de solides bases et une suite optimiste à ce nouveau projet de recherche en collaboration entre le LP2N et le LCPO. Par la suite, les résultats des travaux de cette thèse sur la libération contrôlée d'espèces à partir de vésicules synthétiques compartimentées seront utilisés pour étudier le comportement de cellules biologiques en réponse à une libération environnante d'espèces nocives ou thérapeutiques.

Pour résumer, les travaux de cette thèse ont apporté différentes avancées significatives dans le domaine du biomimétisme cellulaire *via* l'auto-assemblage contrôlé de systèmes copolymères. Une structure compartimentée innovante à base de polymères et de lipides a été développée pour permettre des co-encapsulations d'espèces au sein d'un même système, ainsi que leur libération successive contrôlée par des variations de température ou de pression osmotique. Un nouveau modèle de membrane biomimétique asymétrique a aussi été élaboré et des tests sont en cours pour observer le comportement de cellules biologiques co-cultivées avec des cellules synthétiques en milieu 3D.

Ces travaux forment le fondement pour de nouvelles perspectives à l'interface des domaines de la thérapie cellulaire et de la biologie synthétique. Les systèmes développés représentent tout d'abord des modèles de compréhension fondamentale de systèmes biologiques complexes. En prolongement de ces travaux, il serait intéressant d'étudier, au sein de milieux 3D, la libération contrôlée d'actifs thérapeutiques à partir de systèmes compartimentés à proximité de cellules biologiques et d'étudier leur impact notamment sur l'évolution de tumeurs dans le but d'envisager de nouvelles stratégies thérapeutiques. De plus, les systèmes compartimentés à libération contrôlée développés pourraient servir de bioréacteurs pour des réactions confinées contrôlées en cascade avec des applications en biocatalyse. Enfin, les membranes synthétiques asymétriques présentées permettent d'envisager la préparation de nouvelles cellules synthétiques avec des propriétés de membrane mieux contrôlées et mieux adaptées à la réalité.

List of abbreviations

ABTS	2,2'-azinobis(3-ethylbenzothiazoline-6-sulfonic acid
ADH	alcohol dehydrogenase
aGHUV	asymmetric giant hybrid unilamellar vesicles
AP	alkaline phosphatase
AL	alginate solution
CalB	*candida antartica* lipase B
cDICE	continuous droplet interface crossing encapsulation
CD	cyclodextrin
CS	cell suspension
DDAO	dichlorodimethylacridinone
DEX-*b*-PCL	dextran-*b*-poly(ε-caprolactone)
diC15-PC	1,2-dipentadecanoyl-sn-glycero-3-phosphocholine
DLS	dynamic light scattering
DMPC	1,2-dimyristoyl-sn-glycero-3-phosphocholine
DOPC	1,2-dioleoyl-s*n*-glycero-3-phosphocholine
DOPE-rhod	1,2-dioleoyl-sn-glycero-3-phosphoethanolamine-N-(lissamine rhodamine B sulfonyl)
DOPS	1,2-dioleoyl-s*n*-glycero-3-phospho-L-serine
DOX	doxorubicin
DPBF	1,3-diphenylisobenzofuran
DPPC	1,2-dipalmitoyl-sn-glycero-3-phosphocholine
ECM	extracellular matrix
EGFP	enhanced green fluorescent protein
FRAP	fluorescence recovery after photobleaching
GHUV	giant hybrid polymer-lipid unilamellar vesicles
GOx	glucose oxidase
GR	glutathione reductase
GSH	glutathione sulfhydryl
GSSG	poly(N-vinylpyrrolidone)-*b*-cholesterol acrylate)
GUVs	giant unilamellar vesicles
HRP	horseradish peroxidase
IS	intermediate solution
LbL	layer-by-layer
LHUV	large hybrid unilamellar vesicles
LiPs	liposomes in polyersomes
LRB	1,2-dioleoyl-sn-glycero-3-phosphoethanolamine-N-(lissamine rhodamine B sulfonyl)
LUVs	large unilamellar vesicles
MβCD	methyl-β-cyclodextrin
MB	methylene blue
MLVs	multi-lamellar vesicles
NaN_3	sodium azide
PA	phosphatidic acid
PAH	polyallylamine hydrochloride
PBut-*b*-PEO	poly(butadiene)-*b*-poly(ethylene oxide)

PDMS	poly(dimethylsiloxane)
PE-NBD	1,2-diphytanoyl-sn-glycero-3-phosphoethanolamine-N-(7-nitro-2-1,3-benzoxadiazol-4-yl)
PEG-*b*-PLA	poly(ethylene glycol)-*b*-poly(lactic acid)
PEG-*b*-PSBA	poly(ethylene glycol)-*b*-poly(styrene boronic acid)
PEO-*b*-PCL	poly(ethylene oxide)-*b*-poly(ε-caprolactone)
PEO-*b*-PCL-*b*-PDEA	poly(ethylene oxide)-*b*-poly(caprolactone)-*b*-poly(2-(diethylamino) ethyl metacrylate)
PG	phosphatidylglycerol
PMA	poly(methacrylic acid)
PMOXA-*b*-PDMS-*b*-PMOXA	poly[-(2-methyloxazoline)-*b*-poly-(dimethylsiloxane)-*b*-poly-(2-methyloxazoline)]
PMT	photomultiplier
POPC	phosphatidylcholine
POPS or PS	phosphatidylserine
PS-*b*-PIAT	poly(styrene)-*b*-poly(L-isocyanoalanine(2-tiophen-3-yl-ethyl) amide)
PSS	polystyrene sulfonate
PTMC-*b*-PGA	poly(trimethylene carbonate)-*b*-poly(L-glutamic acid)
PVA	polyvinyl alcohol
PVPc	poly(N-vinylpyrrolidone)-*b*-cholesterol acrylate)
ROI	region of interest
ROS	reactive oxygen species
SM	sphingomyelin
SUVs	small unilamellar vesicles
TEM	transmission electron microscopy
Tt	transition temperature
w-o-w	water-in-oil-in-water

General Introduction

Nature has inspired all scientists from different research areas, ranging from molecular biology to materials science, over the world for decades. How life was maintained and has evolved over millions of years has led researchers to investigate Nature's most complex designs and use them as a source of inspiration to constantly improve our world. Re-creating bio-inspired processes, a strategy most commonly termed *biomimicry*, constitutes a step towards understanding them. As J. Benyus wrote : « Biomimicry is the process of looking at a leaf and trying to figure out how to make a better solar cell » or in other terms, biomimicry is « innovation inspired by Nature ».[1]

More than a scientific strategy to engineer new systems inspired by Nature, biomimicry has in fact become a common way of thinking. As an example, when imagining a new drug formulation, we first ask how Nature would do it? How systems in nature contain both hydrophilic and hydrophobic molecules? How does nature protect certain molecules from others in the same system? How does nature activate enzymes only when needed? *Etc.*… Understanding how nature does it so well – as R. Feynman said "She's always got better imagination than we have" – and the answers to these questions often constitute a starting point in elaborating innovative strategies, and new materials or products.[2]

In the domain of nanomedicine, one example of how Nature has inspired technology concerns how to invade and treat cancer cells. In this context, researchers are studying and trying to mimic the structure and function of viruses, which have the ability to penetrate certain kinds of cells before replicating, and use these mimics as cancer-treating drug delivery vehicles.[3,4]

In the context of this PhD project, some of the major questions and challenges that we decided to tackle were:

- How can we improve the current artificial cell models and make them more realistic in terms of structural and functional resemblance?
- How can we encapsulate many distinct species within a same system while keeping them separated and protected from the others?
- How can we control the *in vitro* independent release of these species?

We especially asked ourselves how nature solves this last particular issue, and more specifically, how eukaryotic cells manage to segregate different species (enzymes, proteins, glycoproteins,…) within their lumen while perfectly controlling their independent activity. The first chapter details our findings on the answers to these questions and how researchers have

used them in creating smart bio-inspired systems. With the help of these previous findings, we thus focused on cell membrane asymmetry and compartmentalization to develop tunable biomimetic structures that could then be used as scaffolds for independent release of species *via* different triggers. Hence, the following chapters sum up how nature inspired us to innovate in the field of cellular biomimetics on cell structure and function mimicry, keeping in mind, as T. Edison said, that "Genius is one per cent inspiration, ninety-nine per cent perspiration".

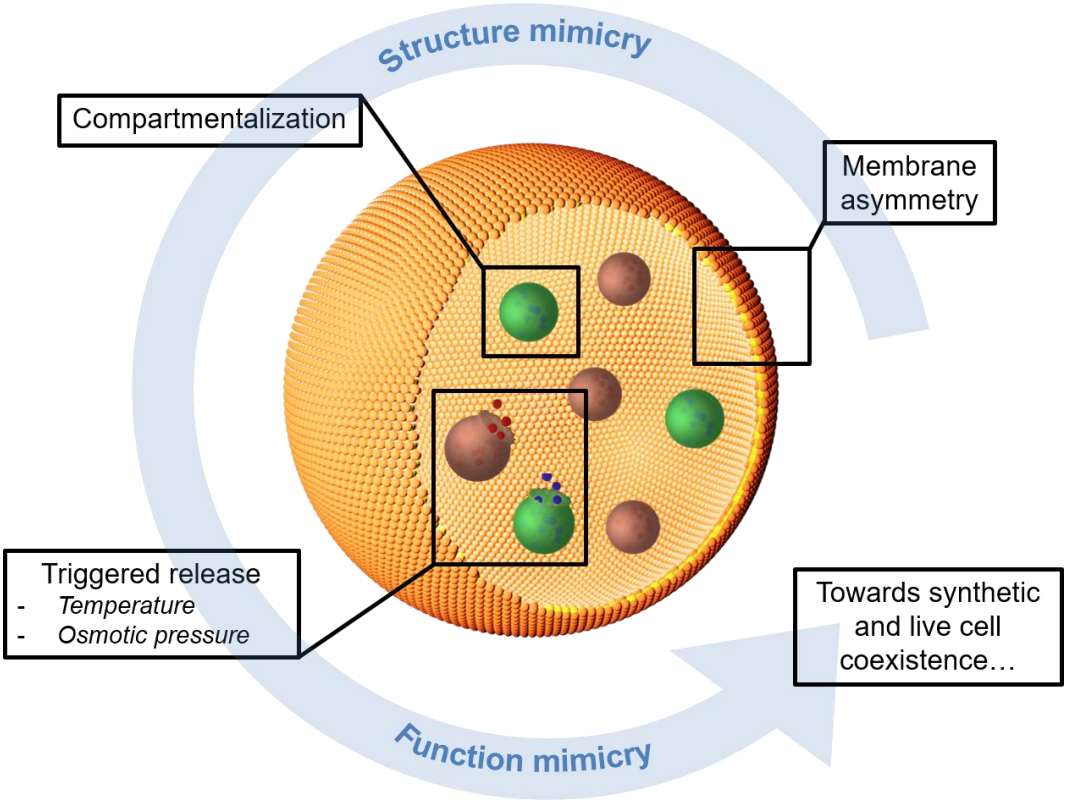

Figure 1. Thesis general outline

References

[1] J. M. Benyus, *Biomimicry: Innovation Inspired by Nature*, Harper Collins, **2009**.
[2] R. Feynman, **1979**.
[3] J.-W. Yoo, D. J. Irvine, D. E. Discher, S. Mitragotri, *Nat. Rev. Drug Discov.* **2011**, *10*, 521–535.
[4] C. Schatz, S. Louguet, J.-F. Le Meins, S. Lecommandoux, *Angew. Chem. Int. Ed.* **2009**, *48*, 2572–2575.

Chapter 1: State of the art

1. Introduction

Prokaryotes, which include bacteria and archea, were the only form of life for millions of years on earth before the emergence of the more complex eukaryotes. The first description of the cell was attributed to R. Hooke in the 1660s in his book *Micrographia,* one of the earliest works on microscopy. He observed a slice of cork at the microscopic level and termed the constituting units "cells" or "pores". Since then, the origins of the emergence of cells still remain a mystery but the "cell theory" or the idea that the cell is the basic component of living organisms, gave rise to a common definition for the cell as *the basic structural, functional and biological common unit of every living organism*.[1,2] More precisely, the eukaryotic cells are "soft wet machines" that are compartmentalized, able to replicate and evolve, need energy and host metabolic reactions for self-replication and maintenance.[2]

One of the main structural features of natural eukaryotic cells is their asymmetric membrane, in terms of bilayer lipid and protein composition, which induces very specific physical properties affecting fluidity, permeability, mechanical strength or curvature.[3–5] However, the most important structural characteristics are their inner compartments, termed organelles, which allow isolation and protection of different species inside the cytoplasm.[6] This compartmentalized structure is crucial for cellular function since it allows the cell to host multiple simultaneous metabolic reactions with high accuracy and specificity and is what makes eukaryotic cells highly complex systems sometimes referred to as "micro-factories".[7–9]

Their complex architecture, which distinguishes them from simpler non-compartmentalized prokaryotic cells, has challenged researchers from all over the world to develop synthetic cellular mimics and use them as models to further understand the origins of cellular evolution, to provide solid bases for the analysis of the diverse biophysical processes occurring at cell membranes and lastly, to develop vesicle-based platforms for biomedical applications.[10–18] For a long time, the lipid composition of cellular membranes made lipid vesicles, or "liposomes", the most strategic choice in the designing of cell-like systems. However, the recent development of polymer-based vesicles, termed "polymersomes", allowed new insight into the fields of biomimicry and nanomedicine.[19] Indeed, the higher molar masses conferred by polymers and their chemical tunability make polymer vesicles more robust, stable and less permeable than their lipid analogues, and have proven to be essential features in developing drug carriers with targeting capabilities and controlled release.[20–25]

Combining cell structure mimicry, mainly membrane composition and compartmentalization, with cell function mimicry or the ability of the cells to carry out confined complex chemical or enzymatic transformations in artificial minimal cells constitutes the ultimate challenge and has been a common dream for researchers for decades now.[8,26–31]

The present chapter focuses on cell structural and functional biomimicry and the recent advances in the field of synthetic biology to further push the boundaries of designing artificial cell-like systems. Even if very interesting contributions concern the elaboration of cell-like machinery in droplets, mainly using microfluidic approaches, we will focus on systems based on self-assembled membranes. In the first part, we discuss the latest advances in the development of structural mimics to achieve artificial compartmentalized systems and asymmetric membranes. In the second part, we present confined enzymatic reactions in synthetic nano or micro-reactors that mimic functional minimal cells or organelles and lastly, the most advanced synthetic cell-like systems that exhibit chemical or enzymatic compartmentalized reactions.

2. Eukaryotic cell structure mimicry

2.1. Compartmentalization in synthetic cells: mimicking structural organelles

Eukaryotes developed compartmentalized structures as a way to optimize the chemistry and physics conferred by a single bilayer. The use of multiple inner compartments (*e.g*. the nucleus) has been a successful improvement to allow the occurrence of different simultaneous metabolic reactions in close proximity while keeping the enzymes and substrates protected. Chemists, physico-chemists and biologists have tried to synthetically reproduce and take advantage of this compartmentalized structure to develop smart nano- or micro-reactors, artificial minimal cells as well as new drug carrier platforms.[32] These systems could benefit from the bilayer within-a-bilayer structure where the inner compartments are protected from the outer environment by a double barrier physical effect, to permit better protection and optimized release of encapsulated species. In this part, we discuss the main different strategies that have been developed to afford multicompartment bioinspired particulate systems based on liposomes and polymersomes, self-assembled from amphiphilic lipids and block copolymers respectively.

Zasadzinski and co-workers where among the first to introduce compartmentalized lipidic architectures termed “vesosomes” with the idea of providing multifunctional drug delivery

systems.[33] These vesosomes consist of small unilamellar liposomes entrapped within a larger liposome. Briefly, negatively charged phosphatidylserine lipid bilayers were folded into cochleate cylinders upon complexation with calcium. Vesosomes were formed by unrolling the cylinders onto preformed liposomes *via* biotin-streptavidin interactions and modulation of calcium concentration with a chelating agent (Figure 1).

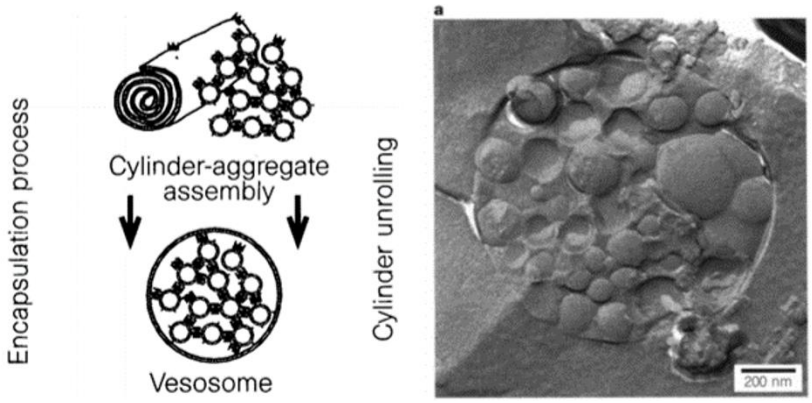

Figure 1. Vesosome encapsulation process and freeze-fracture transmission electron micrograph of the resulting liposomes-in-liposome.[33]

This approach was a first major step on the road to synthetic compartmentalized architectures but suffered from poor encapsulation efficiency (5-15 %) and purity with no real control on the formed objects (mixture of vesosomes and free liposomes). Since then, new encapsulation and purification strategies that preserve the integrity of the encapsulated vesicles and avoid their fusion have been elaborated to address these issues. Especially, Huck and co-workers recently presented the formation of uniform multi-compartment liposomes using microfluidics.[34] Their method (based on surfactant-assisted microfluidics and controlled dewetting of water-in-oil-in-water double emulsions) allows a fine control over the size and number of compartments of the resulting vesosomes which have been shown to serve as scaffolds for cell-free gene expression. In a recent work, these multi-compartment liposomes were presented as artificial minimal cell models demonstrating their great potential for such applications.[35,36]

Polymers also constitute promising materials for the development of compartmentalized systems. Their higher molecular weight is responsible for a thicker membrane that brings more stability and mechanical strength to the polymersomes. In addition, their synthetic nature

enables their chemical modification to allow polymer vesicles to respond to external stimuli such as pH or temperature.

The first polymersome-in-polymersome system was described by Chern and co-workers in 2008.[37] They prepared polymer vesicles by a water-in-oil-in-water (w1-o-w2) double emulsion technique and showed that they could tune vesicle size by adjusting the ratio of solvents used for the oil phase. Thus, they used a first set of vesicles as the w1 phase of a second w1-o-w2 double emulsion to encapsulate them in larger vesicles made from the same poly(acrylic acid)-*b*-poly(distearin acrylate) copolymer. Interestingly, the insertion of pH responsive acrylic acid units in the membrane allowed to reversibly tune membrane permeability by adjusting the pH and to control the encapsulation of small molecules through the transmembrane channels resulting from the pH modifications. Since then, other elaborate systems have been introduced and especially, Weitz and coworkers were pioneers in this field by coupling microfluidics to the double emulsion technique to improve size control and reproducibility.[38,39]

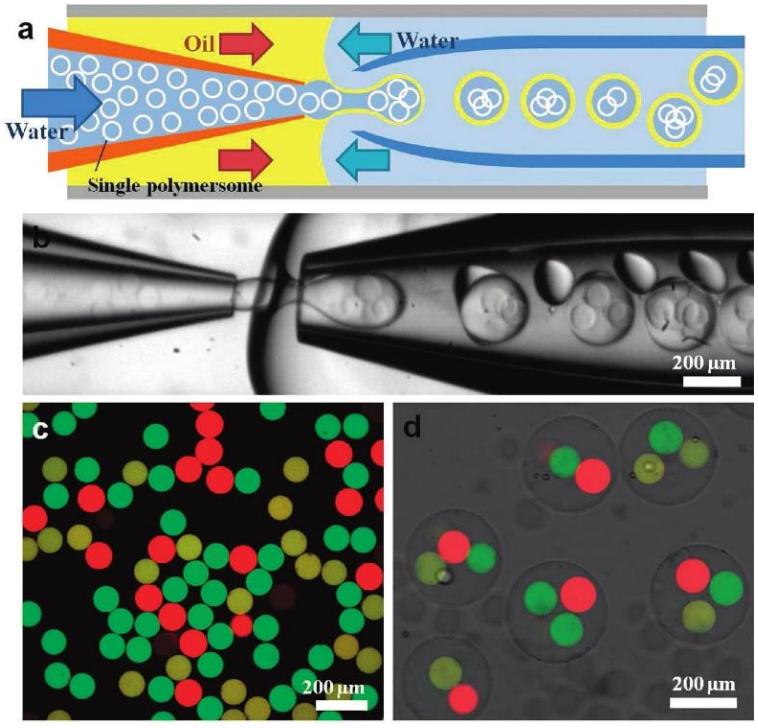

Figure 2. Polymersome-in-polymersome formation by microfluidics coupled to double emulsion.[38] a) Schematic illustration of the device. b) Optical microscopy image showing injection of polymersomes from the microfluidic capillary into the double emulsion drops, c) and d) optical and confocal microscope images of the resulting single and multiple inner polymersomes.

They formed poly(ethylene glycol)-*b*-poly(lactic acid) (PEG-*b*-PLA) polymersomes from w-o-w double emulsion drops using a microcapillary microfluidic device that allowed fine tuning of the vesicle size (Figure 2. a), b)). In a similar manner to the previously discussed double emulsion approach by Chern and coworkers, the resultant monodisperse polymersomes (Figure 2. c)) were re-injected in another microcapillary device as the water phase of the double emulsion to afford multicompartment polymersomes (Figure 2. d)). The main advantage of this technique is the ability to control the number of inner compartments by tuning the flow rate of the different phases and the diameter of the microcapillary. To go a bit further, the authors showed that they could achieve programmed release of encapsulated components from the degradation of the inner polymersomes by tuning the permeability of the PEG-*b*-PLA membrane. They observed that adding a fraction of PLA homopolymer in the hydrophobic region of the bilayer increased vesicle stability for up to two months whereas free-PLA homopolymer membrane underwent hydrolysis upon a few days. Therefore, membrane degradation and subsequent release of loaded components can be sequentially controlled by tuning the composition of the bilayer membrane. Similarly, Colin and coworkers developed a simple glue-free microfluidic device made of fused silica capillaries and T-junctions to overcome the incompatibility issues often encountered between solvents and the poly(dimethylsiloxane) (PDMS) devices or glues.[40] They showed that these simple devices allowed formation of multicompartment polymersomes made of poly(butadiene)-*b*-poly(ethylene oxide) (PBut-*b*-PEO). However, while double emulsion techniques allow precise control on vesicle size and number, the drying process needed for solvent evaporation can lead to vesicle destabilization and involves traces of solvent left in the bilayer of the vesicles which is a major drawback for biomedical applications.

Several approaches for constructing multicompartmentalized systems involving little or no traces of solvent were also reported. Among them, film rehydration followed by direct dissolution to afford polymersomes-in-polymersomes of at least two compartments was developed by Nallani and coworkers.[41]

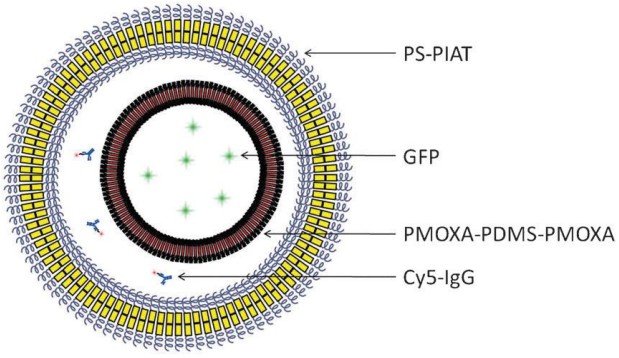

Figure 3. Schematic representation of a multicompartmentalized polymersome.[41]

The process is based on a sequential self-assembly of two different block copolymers: poly[-(2-methyloxazoline)-*b*-poly-(dimethylsiloxane)-*b*-poly-(2-methyloxazoline)] (PMOXA-*b*-PDMS-*b*-PMOXA) and poly(styrene)-*b*-poly(L-isocyanoalanine(2-tiophen-3-yl-ethyl) amide) (PS-*b*-PIAT). PMOXA-*b*-PDMS-*b*-PMOXA polymersomes were first formed through film rehydration. Then, the solution of polymersomes was used as the aqueous phase for the direct dissolution of PS-*b*-PIAT (dissolved in THF) yielding larger vesicles encapsulating the PMOXA-*b*-PDMS-*b*-PMOXA smaller polymersomes (Figure 3). A green fluorescent GFP dye was loaded into the lumen of the inner vesicles and a red fluorescent Cy5-IgG dye inside the outer ones. The resulting yellow fluorescence observed under confocal microscopy observation confirmed the compartmentalized structure. However, the presence of numerous individual red and green spots indicated the presence of single inner or outer polymersomes along with the desired multicompartment structure. Thus, a significant drawback of this approach is the low encapsulation efficiency.

Lecommandoux *et al.* presented at the same period a different protocol to form cellular structural mimics with their polymersomes-in-gelly polymersomes system by taking into account the molecular crowding of the cytoplasm of biological cells.[42] They formed nanosize polymersomes of poly(trimethylene carbonate)-*b*-poly(L-glutamic acid) (PTMC-*b*-PGA) by solvent displacement (also coined nanoprecipitation) and loaded them into the lumen of giant poly(butadiene)-*b*-poly(ethylene oxide) (PBut-*b*-PEO) polymersomes *via* an emulsion-centrifugation protocol inspired from literature.[43]

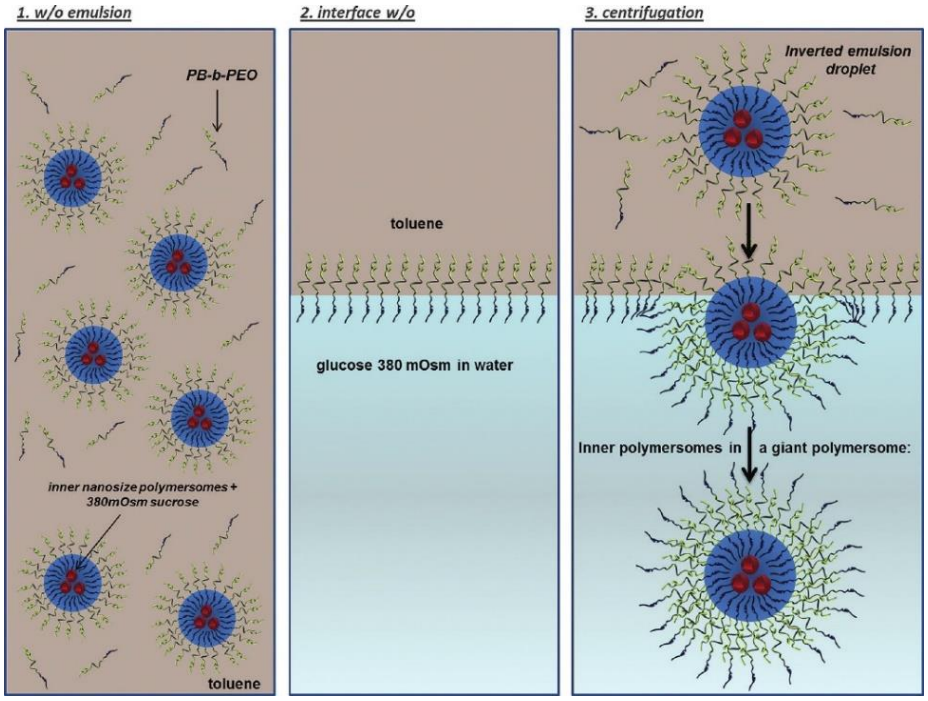

Figure 4. Schematic representation of the emulsion-centrifugation protocol to form giant unilamellar vesicles.[42]

An emulsion of PBut-*b*-PEO stabilized sucrose droplets in toluene is formed by vigorous hand shaking and then poured over a glucose-toluene interface stabilized by the same copolymer. The difference of density between glucose and sucrose allows the droplets to cross the interface with the help of centrifugation (Figure 4). The resulting giant unilamellar vesicles (GUVs) are recovered in the lower glucose phase. The main advantage of this process is its tunability as almost any objects can be quantitatively loaded into the giant polymersomes *via* solubilization in the initial sucrose phase (as shown for the small inner red vesicles (nanosize PTMC-*b*-PGA polymersomes in the study) in Figure 4). To go a bit further, the authors "gellified" the lumen of the GUVs by encapsulating, together with the nanosize polymersomes, highly viscous alginate or dextran solutions and studied the subsequent 2D motion of the inner vesicles (artificial organelles) which were shown to have a 6.6 times smaller diffusion coefficient as compared with the uncrowded lumen. This study constitutes a step further in the field of cellular structural mimics as the system both mimics organelles and the cytoplasm of biological cells in a simplified way. In addition, the authors studied the double barrier effect of the inner and outer vesicle membranes by encapsulating an anti-cancer drug named doxorubicin (DOX), a well-known anticancer drug, in the inner polymersomes.[44] They demonstrated a decreased release rate of DOX from the inner polymersomes of the multi-compartment system, as compared with the release rate of DOX from just the nano-vesicles (about twice faster), proving the utility of

such a system as a drug-carrier platform to allow better protection and controlled release of loaded drugs.

Since both lipids and polymers possess interesting properties for constructing cellular mimics a last strategy for designing biomimetic compartmentalized structures resides in combining the two. Following this idea, Caruso and coworkers developed "capsosomes" defined as liposomes incorporated into a polymer carrier capsule.[14,45,46]

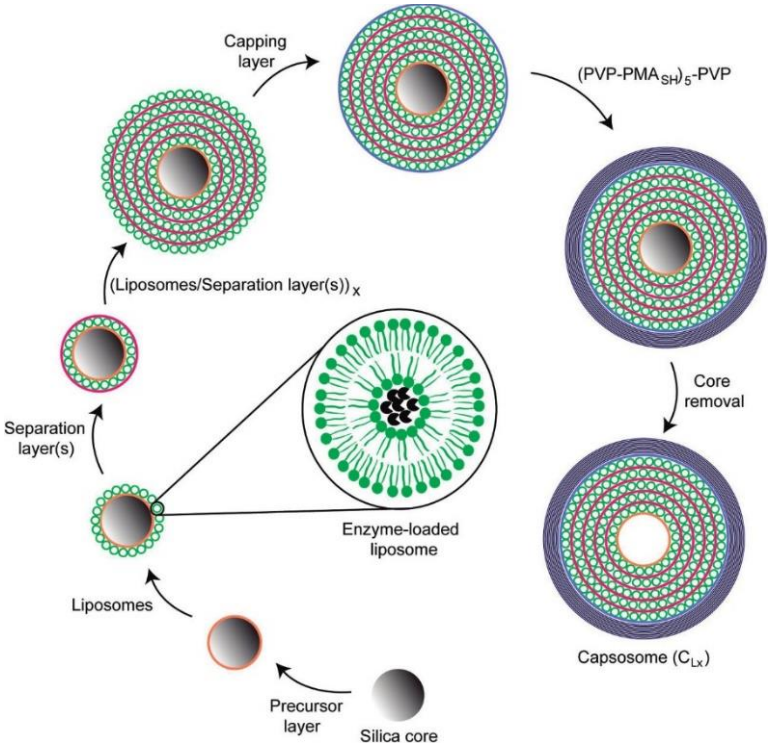

Figure 5. Schematic illustration of capsosome assembly. A silica core is coated with a polymer layer and liposomes alternatively. Dissolution of the core results in a capsosome with multiple layers and intact (loaded) liposomes.[45]

Polymer capsules are assembled following a layer-by-layer (LbL) assembly technique where alternating polymer layers are deposited on a sacrificial template core.[47–49] Liposomes are coated between each layer of polymer as shown in Figure 5. After the sequential deposition of all layers, the core is dissolved and stable capsosomes are obtained. The authors show that they can control the number of sub-compartments (maximizing it up to 160 000 liposomes assembled onto a 3 µm silica core particle) as well as their spatial position (free floating or attached to the polymeric capsule wall).[45,46] These systems could be promising as therapeutic carriers as the LbL technique allows a high degree of tunability (number of layers, shape, permeability of the polymer capsule through the choice of polymer) and the liposomes permit

encapsulation of both hydrophobic and hydrophilic drugs with potential triggered release through temperature variations.[45]

These compartmentalized vesicular systems and their synthesis all represent innovative advances in the field of cellular structure mimics and a major milestone in the development of new drug delivery systems. As discussed later in this manuscript, another key objective is to use these structures as compartmentalized nano- or micro-reactors for cascade chemical or enzymatic reactions.

2.2. Membrane properties: mimicking the membrane asymmetry of eukaryotic cells

2.2.1. Cell membrane asymmetry

1972 was a milestone in research biology when the famous fluid mosaic model was proposed as an interpretation of biological membrane structure by Singer and Nicolson (Figure 6).[50] Biological membranes were defined as "[…] analogous to a two-dimensional oriented solution of integral proteins (or lipoproteins) in the viscous phospholipid bilayer solvent." This model provided a solid base to start explaining membrane organization ("mosaic") and predicted many membrane phenomena regulated by lipid and protein dynamic rearrangement ("fluid").

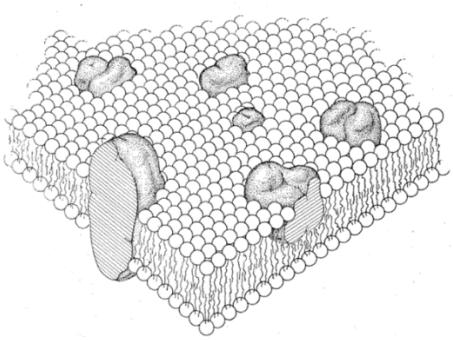

Figure 6. Schematic three-dimensional representation of the fluid mosaic structure of the membrane, reproduced with permission from [50]. Globular proteins inserted into a lipid matrix.

Around that same period of time, Bretscher introduced the concept of "asymmetry" to characterize membrane structure through the different repartition of lipids and proteins across the two leaflets of the bilayer.[4,51] One of his five guidelines for membrane structure was that the basis of a biological membrane is a bilayer enriched with choline lipid derivatives and

glycolipids in the exoplasmic side and amino-phospholipids in the cytoplasmic side.[4] Evidence of asymmetry was already supported with several examples involving selective binding of substrates to one side or the other or phospholipase digestion.[52–54] For example, ferritin was shown to specifically bind to oligosaccharides with *d*-mannose or *d*-glucose residues on the outer surface of erythrocyte membranes and not on the inner cytoplasmic surface.[55]

While proteins were also shown to be unevenly organized between both leaflets, asymmetry in biological membranes mostly comes from the distribution of lipids, which play a major structural and functional role. Indeed, their amphiphilicity allows them to spontaneously form membranes in the form of small compartments to segregate internal constituents from the external medium. They also act as messengers in signal transduction and molecular recognition processes and they are used for energy storage.[56] It is now well-established that the differences in constituents between both sides of the bilayer have a strong impact on membrane physical properties such as permeability, membrane curvature (linked to the intrinsic asymmetric nature of lipids), shape or surface charge (negatively-charged phospholipids on the cytoplasmic side).[3,5,57,58] Consequently, disruption of the normal membrane asymmetry often has significant physiological consequences such as blood coagulation or recognition and removal of apoptotic cells by macrophages.[59–61] For example, phosphatidylserine exposure on the outer leaflet is a sign for cell death.[62–65] These processes are essential for cell development but if unregulated, they could be the source of pathologic conditions.[66] Thus, maintaining the repartition of constituents and mainly lipids between the two leaflets and hence maintaining asymmetry, is crucial for the proper functioning of membrane regulated cellular phenomena.[56,59,67] As such, a lot of energy is invested by the cell to maintain the non-random distribution of species across the bilayer with the help of transporter enzymes such as flippases (ATP-dependent) or floppases (ATP independent) which are in charge of controlling the transmembrane distribution of lipids [66,68–73].

The study of biological membranes has been facilitated by the preparation of synthetic symmetric lipid membranes either supported or in the form of vesicular systems.[74] Models with asymmetric membranes would however be more realistic in cell structural biomimicry studies but they have been difficult to establish experimentally mostly because of a lack of reliable methods to precisely control and quantify the asymmetry. Still, over the last few years, significant progress has been made on the preparation of such model systems using mostly lipid-only membranes.[75] There are however many other possibilities to form asymmetric membranes with cell mimicking properties by using alternative synthetic pathways or

constituents such as polymers or peptides. The goal of this review is to gather and summarize the main cell mimicking asymmetric membrane models that have been proposed and studied over the last years. We aim at providing a non-exhaustive review of the different systems with respect to geometry and composition, focusing on the most relevant synthetic routes.

We firstly describe the main different methodologies to prepare asymmetric membranes made exclusively from lipids. We then outline innovative approaches that have been presented with polymers and finally give an overview of a few systems that combine both lipids and polymers. These systems are schematically illustrated in Figure 7, which presents the main preparation routes, compositions and morphologies that have been reported for asymmetric lipid and polymer membrane.

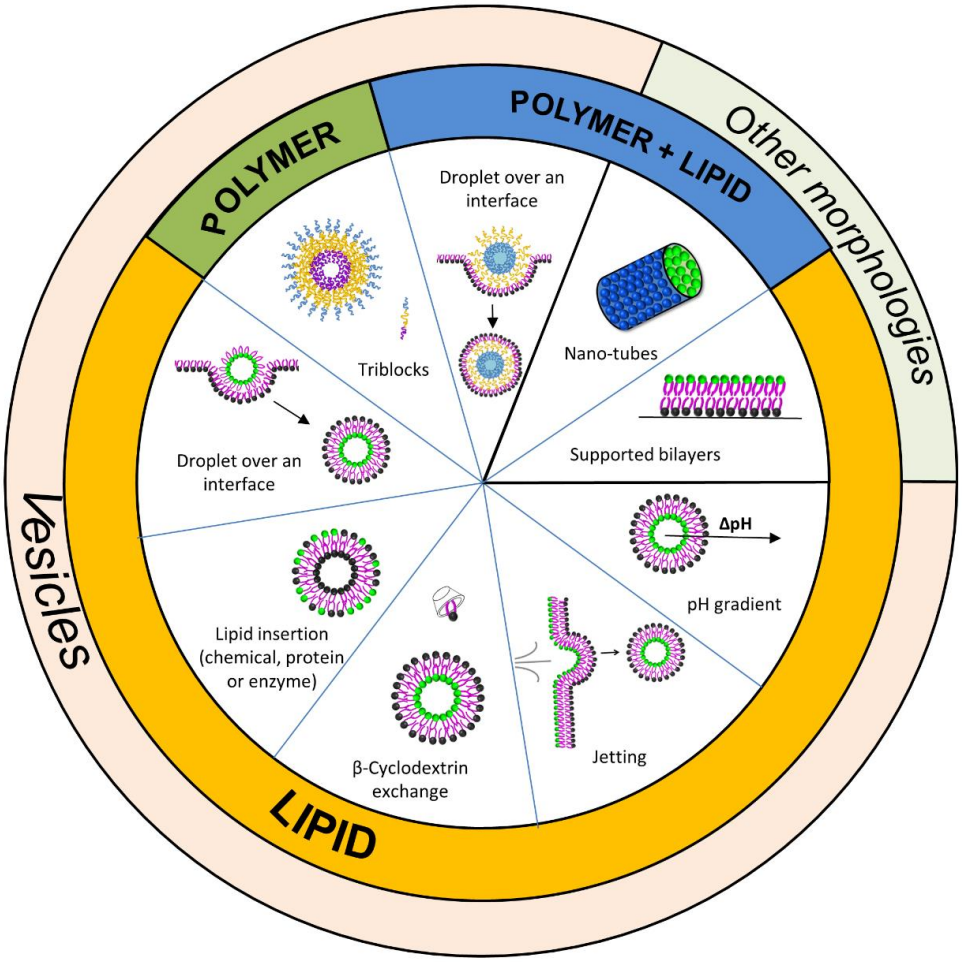

Figure 7. Schematic representation of some of the reported strategies to afford synthetic asymmetric membranes with respect to composition and morphology. pH gradient,[76] lipid insertion by proteins / enzymes or chemicals,[77–79] β-cyclodextrin,[80–82] droplet over an interface,[83–86] jetting,[87], supported bilayers,[88] nano-tubes,[89,90] triblock polymers.[91–93]

2.2.2. Design of asymmetric membranes based on lipids

Lipids are the main constituent of all biological membranes.[56,69] Their amphiphilic character is responsible for their spontaneous organization in two leaflets that together form a bilayer. Their polar headgroup is oriented towards the external aqueous environment while their hydrophobic tail (hydrocarbon chains) form the core of the membrane. Lipid-only asymmetric synthetic bilayer systems have been widely used and have proven to be highly successful models to study membrane properties.[75,94] The wide available pool of lipids makes them suitable candidates to form different geometries through various processes detailed below.

Early examples of synthesized asymmetry in small and large vesicles relied on lipid transfer techniques involving lipid exchange proteins or enzymes.[77–79] Lipid transfer proteins were discovered in the 1980s in the group of Zilversmit after investigating how lipid components from plasma lipoproteins were taken up by liver cells.[78] Several groups studied the translocation rate of lipids from one monolayer to the other using the lipid exchange or conversion technique essentially by means of NMR after exposing small lipid vesicles to an exchange protein or often to a phospholipase enzyme that converts phosphatidylcholine (POPC) to phosphatidic acid (PA).[79,95,96] The lipid translocation (or flip-flop) rates varied from minutes to a few days depending on the system.[79,95] Other examples of generating transmembrane bilayer asymmetry involve spontaneous transfer of a lipid from a donor to an acceptor lipid vesicle when the two populations are in close contact or a chemical control with a sodium ascorbate induced extinction of paramagnetism of spin-labelled lipids in the outer monolayer of lipid vesicles.[96,97]

Later on, the pH gradient technique was proposed by Cullis and coworkers to induce transverse asymmetry in lipid bilayers.[76] They showed that they could influence the positioning of weak acid lipids such as phosphatidylglycerol (PG) by applying a transmembrane pH gradient in lipid vesicles (inside basic and outside acidic or the reverse). Charged lipids are known to move very slowly from one monolayer to the other but it was expected that using protonated (uncharged) PG lipids would facilitate the movement. It was found that when POPC vesicles with a fraction of PG were prepared with a transmembrane pH gradient (inside basic), almost 90 % of PG located in the inner monolayer. Interestingly, the reverse pH gradient led to the opposite asymmetry and the same vesicles formed with zwitterionic lipids only retained a symmetric distribution of lipids thus confirming the influence of pH on the movement of weak acid lipids.[76]

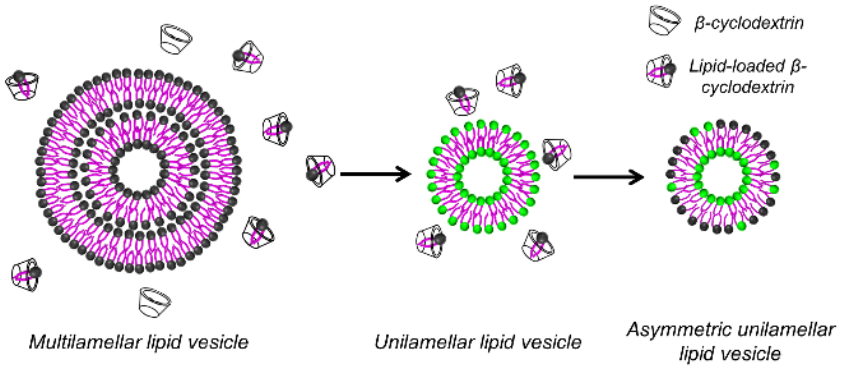

Figure 8. Schematic representation of methyl-β-cyclodextrin (MβCD) mediated lipid exchange to form asymmetric unilamellar lipid vesicles. Multilamellar lipid vesicles are incubated with β-cyclodextrin to form lipid- MβCD complexes. Unilamellar lipid vesicles are then incubated with an excess of the complexes to generate the asymmetric vesicles.

Strategies based on the ability of cyclodextrin (CD) derivatives to bind and exchange phospholipids have been developed in the laboratory of E. London in the last decade to afford vesicles comprising an asymmetrical distribution of lipids between the bilayers.[98,99] Methyl-β-cyclodextrin (MβCD) molecules have the ability to bind hydrophobic species within their cavity and thus have attracted much attention as potential carriers for cholesterol, lipophilic drugs or other molecules with low solubility.[100] In one of their initial study, sphingomyelin (SM) multi-lamellar vesicles (MLVs) were obtained by rehydration of a dried lipid film. The assemblies were then incubated with highly concentrated MβCD to form SM-MβCD complexes which were purified and incubated with pre-formed small unilamellar lipid vesicles (SUVs) to allow insertion of SM in the outer lipid monolayer (Figure 8).[98] High performance thin layer chromatography confirmed a rapid (within minutes) exchange of about 80 % lipid with the outer monolayer of the SUVs whereas control samples with SUVs incubated with SM in the absence of MβCD only showed traces of exchanged SM. Fluorescence anisotropy measurements of fluorescent probes added to the vesicles were used to confirm asymmetry which was stable over a few days. The authors also showed that cholesterol could be inserted into these asymmetric SUVs by performing a second successive MβCD exchange step, confirming the versatility of the process. Following studies by the same group introduced the production of asymmetric large and giant unilamellar vesicles (respectively LUVs and GUVs) through the same MβCD-mediated lipid exchange with the aim of studying how asymmetry impacts ordered domain formation and inter-leaflet coupling in cell bilayer membranes.[80–82,99] The advantages of this method are essentially that it requires minimum equipment and that

different molecules can be exchanged by this process, proving the flexibility of the method. The versatility in terms of vesicle size (SUVs, LUVs and GUVs) that can be used is also an important aspect as sometimes, methods to yield asymmetric vesicles are restricted/more efficient with a certain vesicle size (either giant or small/large). However, multiple steps (incubation, centrifugation, purification, …) are needed to yield the asymmetric vesicles making this method quite tedious.

Over the last decade, there has been a growing interest in the development of new synthetic routes with higher control and precision to afford synthetic asymmetric lipid vesicles. Several groups reported on innovative protocols to generate membrane asymmetry with a special focus on giant vesicles (GUVs) that are thought to constitute more adequate cell mimics in terms of membrane physical properties but, also, they have as a main strength facile manipulation and observation, as compared with small vesicles, which allows researchers to dig deeper into membrane properties.[83–85,101–103]

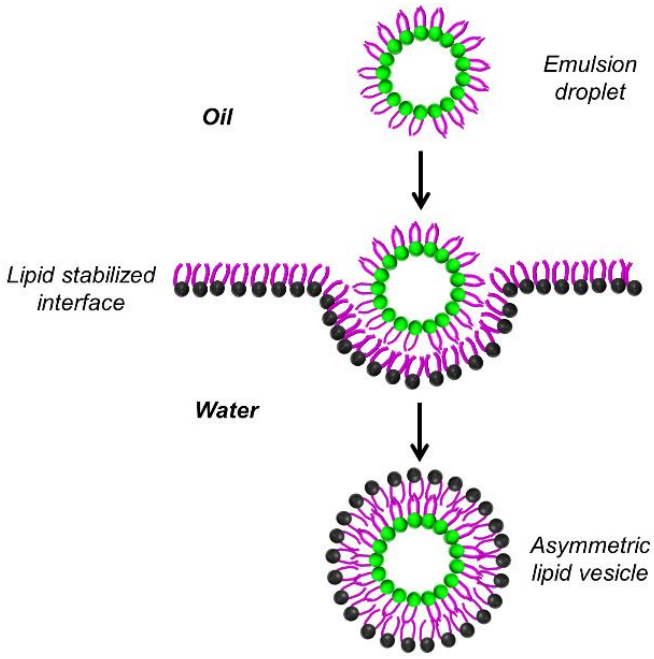

Figure 9. Schematic representation of the "droplet over an interface" method to generate asymmetric lipid vesicles. An aqueous droplet stabilized by a lipid is poured over a different lipid-stabilized oil-water interface.

Rather than through membrane exchange, giant asymmetric lipid vesicles can be assembled by emulsion methods where lipid-stabilized aqueous droplets are forced through a lipid-stabilized oil-water interface to generate the bilayer membrane. This process is referred as "droplet over

an interface" method (Figure 9).[103,104] Weitz and coworkers presented this method to prepare LUVs (about 500 nm) with an inner leaflet of POPC and outer leaflet of phosphatidylserine (POPS), or the reverse. Centrifugation was used to help the lipid-stabilized aqueous droplets to cross the lipid-stabilized oil/water interface. One should note that the preparation of asymmetric SUVs was also previously demonstrated by a similar protocol.[105] The membrane asymmetry of the vesicles and its stability overtime were demonstrated with a fluorescence-quenching assay. The layer-by-layer assembly allowed insertion of a fluorescently tagged lipid in one of the bilayer leaflets (POPC monolayer or POPS monolayer) and the fluorescence was measured before and after addition of a fluorescence quencher on the outer medium. For example, when the dye was inserted in the lipid-stabilized interface (outer leaflet of the vesicle membrane), about 95 % fluorescence was lost upon addition of the quencher to the vesicle solution, indicating an almost total asymmetry (no flip from the outer to the inner monolayer). Overall, authors demonstrated that highly asymmetric structures could be obtained using this technique, with varying amphiphile molecules (they also performed a test with a lipid-polymer asymmetric membrane). A few years later, the group of Takagi followed a similar procedure to prepare cell-sized (GUVs) asymmetric vesicles with the aim of facilitating manipulation of "biological" vesicles under a controlled environment.[83] Rather than through centrifugation, the authors used a sugar weight gradient to induce spontaneous transfer of the denser lipid-stabilized sucrose droplets through an oil-glucose interface, a strategy that significantly increased vesicle yield.[83] Other improvements of the "droplet over an interface", also referred to as "emulsion-centrifugation" method involved microfluidics as an efficient way to produce size-controlled monodisperse emulsion droplets.[85] In addition, the continuous droplet interface crossing encapsulation (cDICE) method has been described as an efficient way to produce giant vesicles with high throughput production of size-tunable monodisperse vesicles.[106,107] Vesicles are formed through continuous dripping of droplets off a capillary while forcing their passage through an interface using a centrifugal force. The authors presented the use of the cDICE method to form giant asymmetric vesicles.[108]

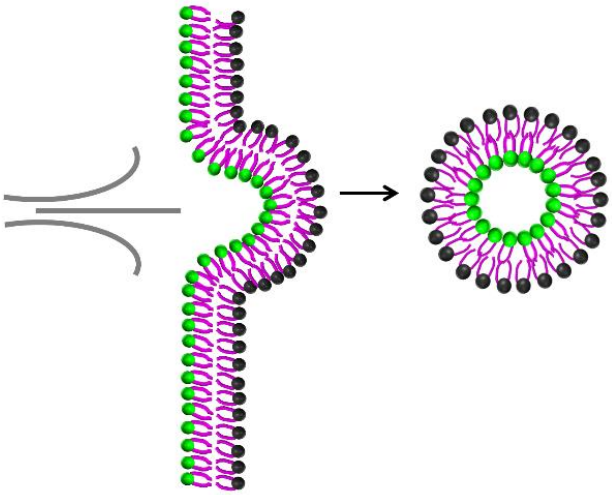

Figure 10. Schematic representation of « jetting ». A jet flow is applied on a lipid asymmetric bilayer. Its deformation leads to the formation of asymmetric lipid vesicles.

Finally, uncommon original techniques have been presented to construct lipid vesicles comprising an asymmetric membrane. Especially, microfluidic jetting has been introduced.[84,87,109,110] The main concept is that a jet flow is used to deform a lipid bilayer and induce formation of vesicles (Figure 10). Kamiya and coworkers formed cell-sized asymmetric 1,2-dioleoyl-*sn*-glycero-3-phosphocholine (DOPC) / 1,2-dioleoyl-*sn*-glycero-3-phospho-L-serine (DOPS) vesicles using this technique by induced break up of a phospholipid microtube formed by applying a jet flow on a lipid planar bilayer.[87] They demonstrated that upon deformation of the lipid bilayer with an applied jet flow, the microtube breakdowns in two distinct vesicle populations of respectively 100-200 µm and 3-20 µm in diameter. With this method, authors were able to produce monodisperse asymmetric vesicles with little residual solvent in the membrane to investigate lipid flip-flop. In addition, *in vitro* membrane protein synthesis was demonstrated, proving the biological relevance of the system.

Another approach resides in focusing on the membrane alone in the form of a supported lipid bilayer, instead of designing objects which require a precise control over the final shape and which might complicate membrane study. In particular, supported lipid bilayers have been broadly studied and used as membrane models.[111] They consist of a lipid bilayer either fixed or freely deposited on a solid surface (*e.g.* gold or mica) and are classically formed by the Langmuir-Blodgett technique (transfer of successive lipid monolayers) or by vesicle fusion (liposomes deposited and allowed to fuse on the surface).[112] In a recent study, dioleoylphosphatidylcholine (DOPC) supported bilayers were formed by vesicle fusion and

MβCD was used to enrich the upper DOPC leaflet with sphingomyelin (SM) thus generating an asymmetric bilayer which stayed stable for up to a few hours, before SM started flipping to the lower leaflet.[88] While this approach does not allow a precise control over the degree of asymmetry it is however tunable, easy to handle and free of solvent, making it suitable to reconstruct synthetic asymmetric membranes. Similar studies showed the formation of asymmetric domains in supported bilayers.[113,114]

Overall, important advances have been made in the field of asymmetric membrane models, especially in the last decade, using lipidic systems. The different proposed technologies to construct lipid-based membrane asymmetry allowed gaining more control into the design of synthetic membranes. In addition, these approaches have considerably helped the investigation and understanding of lipid dynamics in biological membranes.

2.2.3. Design of asymmetric membranes based on block copolymers

When thinking of designing biological membrane mimics, lipids come as an obvious choice as a starting material. However, cellular membranes are much more complex than pure lipid bilayers.[115] Proteins, glycoproteins, glycolipids, glycans or cholesterol that are incorporated in cell membranes convey precise mechanical properties that cannot be adequately represented by lipid-only membrane models.[75] More recently, new synthetic asymmetric membranes have been proposed, with other constituting materials and morphologies, with the shared goal of determining to which extent asymmetry influences membrane properties.

A promising approach in the field of cellular membrane mimics resides in the use of polymers. Because of their synthetic nature which makes them chemically stable and tunable, polymers have attracted a lot of attention for the bottom-up assembly of cell mimics, especially in the form of polymer vesicles, or polymersomes, which possess tougher and thicker membranes than their lipid analogues.[11,14,19,29,116,117] Zhang and coworkers presented a phase-guided assembly technique to form giant polymersomes from two amphiphilic diblock copolymers: poly(ethylene oxide)-*b*-poly(ε-caprolactone) (PEO-*b*-PCL) and dextran-*b*-poly(ε-caprolactone) (DEX-*b*-PCL).[118] The vesicles self-assembled from an aqueous two-phase system, where PEO formed the continuous phase and dextran the dispersed phase. Phase separation led DEX-*b*-PCL to align at the surface of the dextran droplets (with dextran facing the interior) and PEG-*b*-PCL to form the outer leaflet of the bilayer, with PEG facing the continuous phase. The asymmetry of the GUVs was confirmed by means of NMR and fluorescence experiments. To

go a bit further, the authors showed that they could encapsulate erythropoietin with high encapsulation efficiency (ascribed to the thermodynamically favored partition) and a well-preserved bioactivity thus proving the biological relevance of their system.

A majority of investigated copolymers have an AB structure, where A is hydrophilic and B is hydrophobic, which self-assemble into symmetric membranes. However, ABC triblock copolymers (A and C water soluble blocks and B hydrophobic middle block) were recently introduced to form polymersomes bearing an asymmetric membrane upon film rehydration.[91–93,119,120] When using such polymers, there are three different conformations that can be obtained following vesicle formation: A block on the inside and C on the outside, the reverse, or a mixture of A and C on either side (symmetric). Due to their intrinsic asymmetric nature, if the orientation of the triblocks can be controlled or influenced inside the membrane, it is thus possible to afford total asymmetry. For example, designing triblocks with different molecular weights for the A and C blocks should result in the longer one segregating on the outside of the vesicle due to a larger radius of curvature (differing volume fraction) and the smaller one segregating on the inside.[93,121] Using charged blocks is another technique to help block segregation on either side of the membrane as has been shown by Zhong and coworkers who formed biodegradable chimaeric polymersomes from poly(ethylene oxide)-*b*-poly(caprolactone)-*b*-poly(2-(diethylamino) ethyl metacrylate) (PEO-*b*-PCL-*b*-PDEA) triblock copolymers with an outer PEO block and inner PDEA charged block assumed to facilitate efficient protein encapsulation and stabilization.[120] Others have used cleavable peptide-linked triblock copolymers to form vesicles with asymmetric membranes that can undergo shape transformation into multicavity vesicles upon cleavage.[122]

While vesicles with asymmetric membranes formed from polymers are still in an early research stage, they hold promise in the design of new synthetic cellular analogues and have great potential for biomedical applications.

2.2.4. Membrane asymmetry in hybrid lipid-polymer systems

Mixing lipids and polymers to form synthetic asymmetric membranes has not been much exploited so far, but presents a lot of potential in the field of cell membrane biomimicry. Indeed, combining the advantages of lipid biocompatibility and polymer chemical versatility provides a powerful way to prepare membranes with cell mimicking physical properties.

Although vesicles appear as an optimal choice in the field of cell biomimicry, alternative morphologies comprising asymmetric membranes have been investigated. In particular, tubular structures have been presented.[89,90,123] As illustrated by Liedberg and co-authors, an equimolar proportion of poly(butadiene)-*b*-poly(ethylene oxide) and POPC led to the formation of nano-tubular vesicles. They also demonstrated that asymmetry generates a net spontaneous curvature, with the lipid segregating into the inner compressed leaflet, that is required for the stabilization of the tubular morphology.[90] Interestingly, amphiphilic peptides were also considered in generating spontaneous membrane asymmetry in nanotubes or nanoribbons.[89,123]

Over the last years, reconstitution of model membrane systems have helped researchers gain more insight into the complex machinery of cellular processes, and particularly into the dynamics of lipids. Especially, the construction of asymmetric synthetic membranes through a variety of different methods and components open new opportunities to dig deeper into our understanding of the cell machinery and could lead to the development of new therapeutic approaches where lipids should play a major role. However new strategies are desirable to reach stable artificial asymmetric membranes with high control and precision. These systems would help our understanding of the importance of lipid asymmetric distribution in cell membranes and uncover how asymmetry is initially formed and maintained.

3. Combining eukaryotic cell structure and function mimicry in synthetic micro-reactors

As previously discussed, eukaryotic cells differ from prokaryotic cells by their compartmentalized structure. Indeed, inner compartments, termed organelles, serve as separated reactors for different metabolic reactions to take place simultaneously and independently inside the cell. Such compartmentalized reactions are not found in prokaryotic cells, which consist of a single cellular wall comprising all the metabolic materials. Chemical or enzymatic reactions confined in reconstituted biomimetic nano- or micro-compartments could be used to study and improve catalytic processes.[13] In this part, we describe some of the main reported *in vitro* single and multi-compartment systems that confine chemical or enzymatic reactions, as mimics of cells or artificial organelles.[18,29,124]

3.1. Single compartment

Vesicle nanoreactors have attracted much attention over the last years.[12,94,125,126] As exploited by cellular systems, performing a reaction in the confined lumen of a vesicle has several advantages such as enhanced reactivity due to concentration effects. In addition, a restricted location of catalysts, substrates and products allows for their protection and the closed system confines specific reacting conditions, as is for example the case for lysosomes, which exhibit a lower pH than the cytoplasm. Thus, researchers have designed single compartment vesicular systems that can be utilized to carry out simple or complex reactions. As will be further discussed, an important feature of these systems is the permeability of the membrane as either the catalyst and substrates are encapsulated together inside the lumen of the vesicle, or just one of them with a selectively permeable membrane that allows diffusion of species from the outer medium.

Some groups have focused on the elaboration of synthetic minimal cells which are characterized as structures containing the minimal and sufficient number of components to be defined as alive or at least capable of displaying some of the fundamental functions of a living cell.[127] Especially, *in vitro* protein reconstitution and self-replication have been studied.[26,128–131] Luisi and co-workers have presented the production of functional Enhanced Green Fluorescent Protein (EGFP) inside POPC liposomes.[128] A cell-free kit composed of a set of enzymes, ribosomes, tRNA, substrates and cofactors were encapsulated in POPC liposomes together with a plasmid encoding for EGFP. Fluorescence experiments demonstrated that about 10 % protein was synthesized inside the vesicles in the presence of RNase A in the outer medium (preventing protein synthesis). While similar previous work carried out protein synthesis using commercial extracts with little information on content concentration and composition, the authors claim that the novelty of the present study is the detailed knowledge of all components, which represents a step further in the construction of semi-synthetic minimal cells. However, the film rehydration followed by extrusion technique to afford liposomes generated vesicles with low control over the shape and encapsulation efficiency. To overcome these limitations, Weitz and co-authors developed a microfluidic technique to form well-defined polymersomes that can efficiently encapsulate bioactive materials.[129]

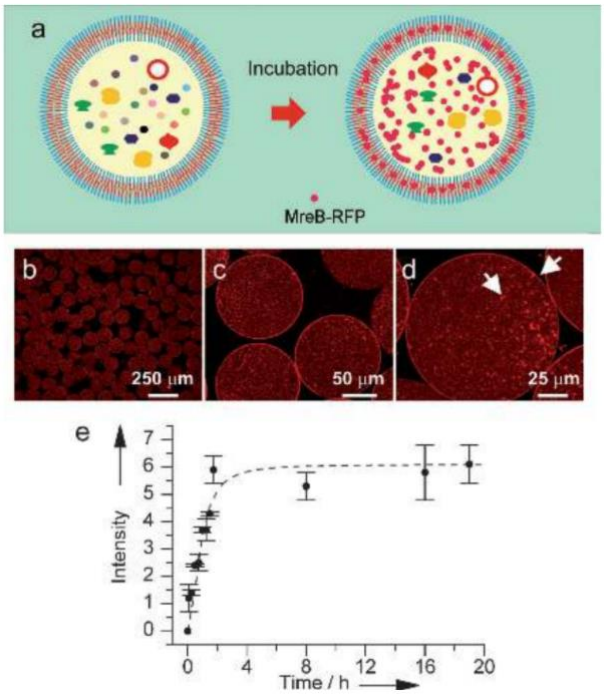

Figure 11. Protein expression in polymersomes formed by a microfluidic technique. a) schematic representation of a polymersome containing the protein expression solution before and after production of MreB-RFP protein. b-d) confocal images of PEG-b-PLA polymersomes after production of MreB-RFP, located in the membrane and inside the lumen. e) Protein expression overtime represented by an increase of fluorescence.[129]

A capillary microfluidic device was used to produce monodisperse W/O/W double emulsion drops for the production of poly(ethylene glycol)-*b*-poly(lactic acid) (PEG-*b*-PLA) polymersomes. E. Coli ribosomal extract (required for protein expression) and the DNA plasmid encoding for the MreB red fluorescent protein (MreB-RFP), responsible for maintaining bacteria's shape, formed the inner water phase (lumen of the vesicles) (Figure 11. a)). After evaporation of the residual solvent from the membranes, the polymersomes were incubated at 32 °C to allow protein production from mRNA translation. After two hours, fluorescence spectroscopy measurements showed a maximum of intensity indicating efficient protein synthesis (Figure 11. e)). In addition, confocal observations allowed to visualize protein positioning in the membrane and in suspension inside the lumen of the vesicles (Figure 11. b-d)). The authors further showed that an osmotic shock could trigger the release of the proteins through the semi-permeable PEG-*b*-PLA vesicle membrane.

In both previous examples, all the necessary biological materials participating in protein synthesis were encapsulated into the lumen of the vesicles. This approach prevents any control

on the beginning of the reaction which starts immediately after encapsulation. To circumvent this issue, cascade reactions have been presented where enzymes are caged inside vesicles with semi-permeable membranes that let small molecules diffuse. The reaction is triggered by adding the substrate in the outer medium which then diffuses inside the vesicle to react with the enzyme. Especially, the group of Van Hest presented polystyrene-*b*-poly(L-isocyanoalanine(2-thiophen-3-yl-ethyl)amide) (PS-*b*-PIAT) permeable polymersomes with positional assembly of enzymes in the lumen and in the membrane of the vesicle.[132,133]

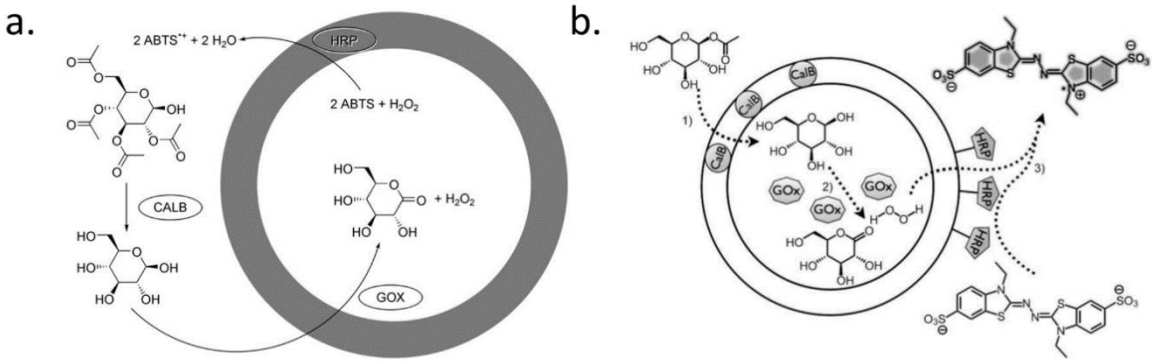

Figure 12. Schematic representations of two cascade reaction systems with PS-b-PIAT polymersomes involving three enzymes : GOx, CalB and HRP. The cascade reaction is initiated by the addition of glucose acetate in the outer medium[132,133] a) HRP is located inside the membrane, GOx in the lumen and CalB is free in the outer medium.[133] b) CalB is located inside the membrane, Gox in the lumen and HRP is attached on the outer leaflet of the membrane.[132]

PS-*b*-PIAT is a rod-coil type copolymer that self-assembles into water to form porous polymersomes that exhibit a high degree of diffusion.[134] These vesicles have been shown to allow small molecules to move across the membrane while large molecules such as proteins cannot.[135] The group showed that a cascade reaction involving three enzymes (*Candida Antarctica* lipase B (CalB), glucose oxidase (GOx), and horseradish peroxidase (HRP)) could be initiated by adding glucose acetate in the outer medium. In one of their studies (Figure 12. a)), glucose acetate is hydrolyzed by CalB in the outer medium to generate glucose which then enters the vesicle to be converted into its lactone form and hydrogen peroxide by GOx. In a last step hydrogen peroxide is used by HRP to oxidize 2,2'-azinobis(3-ethylbenzothiazoline-6-sulfonic acid) (ABTS) into its colored radical cation resulting in an increase of absorbance followed by spectroscopy to evaluate the progress of the reaction.[133] A similar study was

performed with the same system and cascade reaction but with positional assembly of the three enzymes: inside the lumen (GOx), into the membrane (CalB) and tethered to the membrane (HRP) (Figure 12. b)).[132] Utilizing a nanoreactor as a scaffold to perform a cascade reaction involving multiple substrates and enzymes is of great interest as all the reaction components are kept in close proximity. In addition, using a semi-permeable membrane is a first step towards controlling the initiation of the reaction. However the diffusion is not selective over the type of molecules and the majority of copolymers do not have a semi-permeable nature.

Other authors focused on improving the movement of molecules across the membrane.[117] Meier and co-workers were among the first to exploit natural membrane channels which can be reconstituted in synthetic vesicles to form pores with well-defined sizes.[136] The group reported on the assembly of PMOXA-*b*-PDMS-*b*-PMOXA triblock copolymers into vesicular stuctures in which they incorporated a transmembrane bacterial porin OmpF.[137] Porins are well-characterized nonspecific membrane channels which are located into the outer membrane of bacteria.[138] These channels allow passive diffusion of small solutes such as ions or nutrients across the membrane.

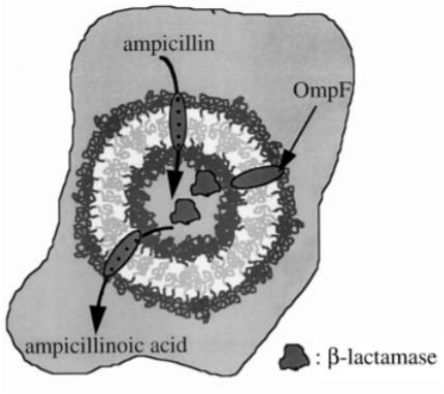

Figure 13. PMOXA-b-PDMS-b-PMOXA nanoreactor with transmembrane OmpF protein channel. Ampicillin from the outer medium diffuses into the vesicle to be converted into ampicillinoic acid by β-lactamase.[137]

The authors demonstrated that the presence of OmpF in the membrane was necessary to allow outer ampicillin to enter the nanoreactor and be converted into ampicillinoic acid by β-lactamase within the aqueous lumen as no reaction was observed in the absence of porin (Figure 13). Since then the use of porins and other transmembrane channels have been exploited as a means to permeabilize membranes.[37,139–142]

A last alternative in generating permeability, is by using stimuli-responsive polymers to induce pore formation in synthetic vesicle membranes. Several studies report on triggering permeability by partially turning a hydrophobic copolymer block into a hydrophilic block by applying an external stimulus. Especially, redox, pH or temperature sensitive polymers have been studied.[117,119,143–148]

Van Hest and co-authors designed polymersomes consisting of stimuli-responsive poly(ethylene glycol)-*b*-poly(styrene boronic acid) (PEG-*b*-PSBA) amphiphilic block copolymers (Figure 14. A).[148] Boronic acid derivatives have been studied and are known to strongly bind to sugar molecules.[149,150] The authors demonstrated that addition of sugar molecules into the polymersome solution at basic pH resulted in disassembly of the vesicles mediated by the strong binding of boronic acid moieties with the sugars and the subsequent increase of the PSBA block solubility in water. Polymersomes were thus constructed with a mixture of PEG-*b*-PS and PEG-*b*-PSBA (10 wt%). The addition of sugar molecules in the outer medium resulted in phase separation between the non-polar PS block and the polar PSBA block upon binding of sugars with boronic acid at high pH. Consequently, the PEG-*b*-PSBA copolymers dissolved in water leaving pores well dispersed throughout the bilayer membrane of the vesicles (Figure 14. B) as confirmed by DLS and TEM analyses.

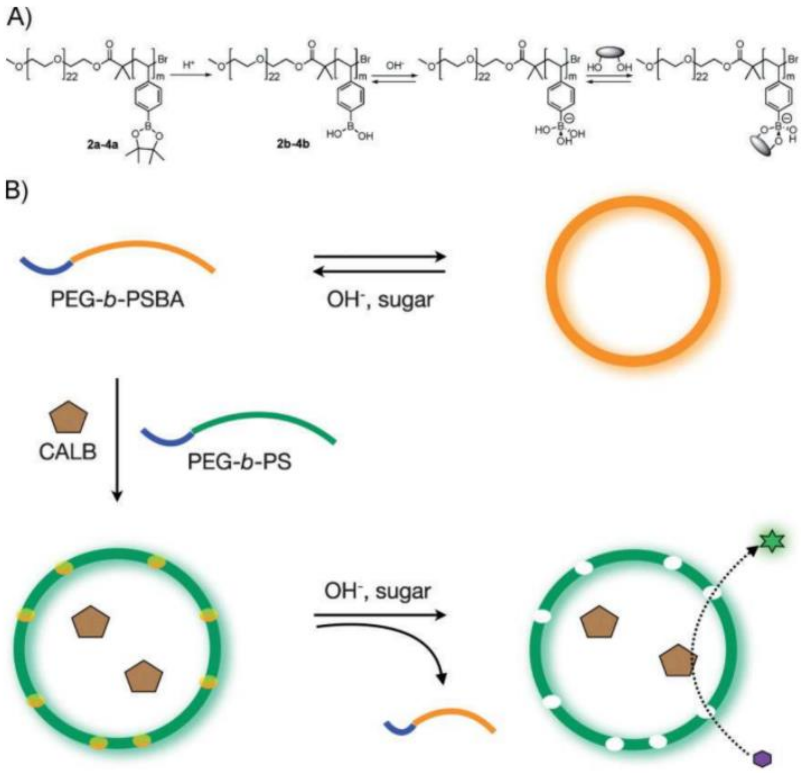

Figure 14. Mechanism of pore formation in PEG-b-PSBA polymersomes.[148] A) Molecular structure of poly(ethylene glycol)-b-poly(styrene boronic acid) (PEG-b-PSBA) amphiphilic block copolymers and their equilibrium with sugar molecules. B) Schematic representation of size-selective pore formation in PEG-b-PSBA polymersomes induced by the sugar-responsiveness of boronic acid.

To demonstrate the potential use of this system as a bioreactor, CalB enzyme was encapsulated into the lumen of the pore-containing polymersomes (Figure 14. B). Fluorescence intensity was monitored after the introduction of a pro-fluorescent substrate in the outer medium. When non-permeable polymersomes were used (before addition of sugar moieties) no increase of the fluorescence intensity was observed. However, the introduction of pores into the membrane allowed the substrate to enter the vesicle and by hydrolyzed into its fluorescent product by CalB. The authors also showed that the rate of the reaction could be tuned by varying the amount of PEG-*b*-PSBA inserted into the membrane of the vesicles.

In summary, functional cell biomimicry in the form of artificial organelles has been demonstrated with the use of single-compartment catalytic systems. It was shown that many strategies have been proposed to tune membrane permeability to allow better control and precision over reaction rates and initiation.

3.2.Multi-compartment

As previously discussed, nanoreactors in the form of single compartments hosting catalytic reactions constitute adequate organelle or prokaryotic cell mimics. However, mimicking the multi-compartmentalized structure of the eukaryotic cell would offer many more possibilities to develop systems that can host multiple chemical or enzymatic reactions, and especially cascade reactions. Compartmentalized catalytic systems have recently been developed and constitute an important advance in the field of cell biomimicry. The idea is to separate substrates and catalysts in individual compartments that are all kept in close proximity within a larger scaffold. Such a structure would for instance allow protecting species from each other in the case they were incompatible, or could offer different specific environments often necessary for enzyme activity.

One of the earliest reports on compartmentalized catalytic reactions was presented by Sukhorukov and co-workers.[151] They introduced shell-in-shell polyelectrolyte microcapsules formed by the LbL technique. Briefly, a six-step protocol was followed to afford ball-in-ball calcium carbonate inner and outer compartments coated with polyelectrolyte multilayers of polystyrene sulfonate (PSS) and polyallylamine hydrochloride (PAH). EDTA treatment was then performed to dissolve calcium carbonate. The authors further encapsulated glucose oxidase in the outer capsule and peroxidase in the inner capsule to demonstrate the use of their system as a compartmentalized catalytic scaffold (Figure 15. a), b)). When glucose was added in the outer medium, it diffused to the outer shell through the semi-permeable membrane and was subsequently converted by glucose oxidase into its lactone form with production of hydrogen peroxide. Hydrogen peroxide then diffused into the inner shell to allow conversion of amplex red to the highly fluorescent resorufin by peroxidase. Confocal images showed that resorufin formed quickly into the inner shell after addition of amplex red to the outer medium and then diffuses into the outer shell thus proving the effective separation of substrates and enzymes in the two-compartment system (Figure 15. c)).

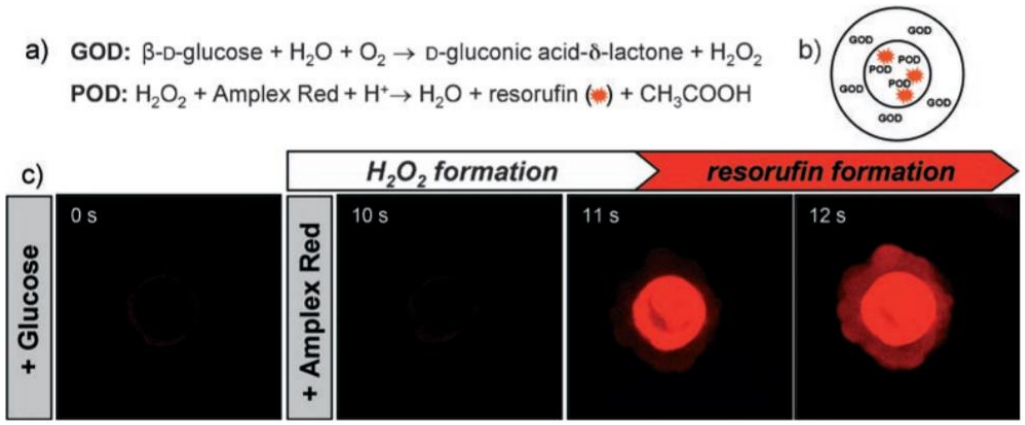

Figure 15. Compartmentalized enzymatic cascade reactions using glucose oxidase (GOD) and peroxidase (POD). a) Reaction schemes, b) localization of GOD and POD in the shell-in-shell microcapsules, c) confocal images taken after the addition of glucose and amplex red to the outer medium.[151]

A few years later, a more complex polymersomes-in-polymersome structure was presented by Lecommandoux and co-authors using an emulsion-centrifugation approach.[152] The authors showed the possibility to perform a three-enzyme catalyzed compartmentalized cascade reaction inside the lumen of giant PBut-*b*-PEO polymersomes. The cascade reaction involves a monooxygenase (PAMO), a lipase (CalB) and an alcohol dehydrogenase (ADH) that turn a pro-fluorescent substrate into a fluorescent product. Several initial tests were performed in bulk with all the enzymes free in solution, CalB in PS-*b*-PIAT nano-reactors, or CalB and ADH in nano-reactors to demonstrate that reaction intermediates could easily travel across the semi-permeable membrane of the different compartments as only a slight decrease of the reaction rate was observed. Next, the PS-*b*-PIAT loaded CalB and ADH were encapsulated together with free PAMO and other reagents inside the lumen of giant PBut-*b*-PEO polymersomes. An increase in fluorescence intensity monitored by confocal analysis proved the effective generation of the final fluorescent product and thus the success of the cascade reaction. Finally, the authors demonstrated the need to compartmentalize enzymes by replacing CalB with an alcalase by showing that alcalase severely decreases the reaction rate by degrading other enzymes if not protected from the others inside a nano-reactor.

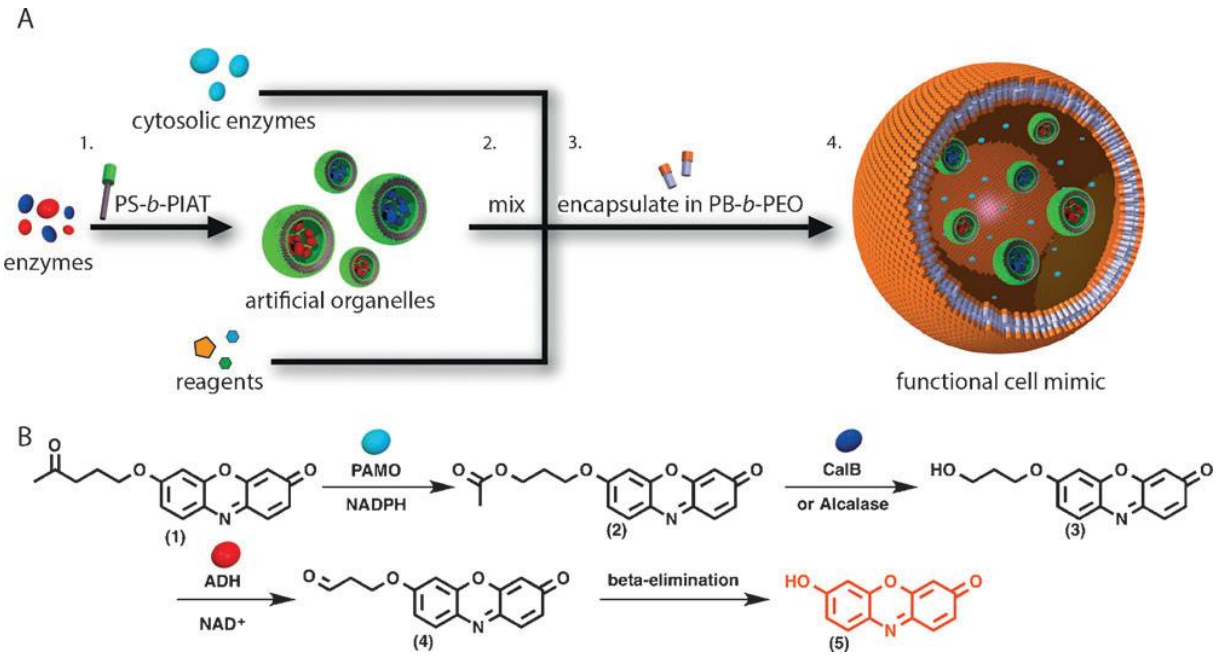

Figure 16. Compartmentalized three-enzyme catalytic system in PBut-b-PEO polymersomes.[152] A) scheme of the compartmentalized structure with initial encapsulation of enzymes in PS-b-PIAT nano-reactors and subsequent encapsulation into giant PBut-b-PEO polymersomes, B) general reaction scheme for the three-enzyme catalytic process.

This example presents one of the first multicompartmentalized synthetic systems that structurally and functionally mimics eukaryotic cells with the presence of functional organelle mimics encapsulated inside a larger vesicle. Such architecture provides an efficient way to study cellular processes and could easily be tuned with other multi-step reaction pathways. However, as in other compartmentalized catalytic structures, the reaction rate is defined by the rate at which substrates and products diffuse across the semi-permeable membrane of the inner nano-compartments.

As previously discussed, the choice of semi-permeable polymers is rather limited and other strategies have been introduced. Especially, the insertion of protein pores inside the membrane have been presented.[37,137,139–141] Ces *et al.* described a three-step cascade enzymatic reaction pathway in compartmentalized liposomes bearing transmembrane α-hemolysin protein pores.[153] Two- or three-compartment lipidic vesicles were formed by phase transfer of water-in-oil droplets to an aqueous solution. The number and content of compartments (two or three) could be tuned by the number of expelled droplets from a tubing. The reaction involved transformation of lactose into glucose by lactase, which was then oxidized by GOx yielding hydrogen peroxide. In a last step, amplex red was oxidized by hydrogen peroxide to fluorescent

resorufin in the presence of HRP (Figure 17. a)). Each enzyme was segregated in a different compartment and communication between compartments was facilitated by the diffusion of substrates and products through hemolysin transmembrane pores.[154] Confocal observations allowed to follow the reaction rate by monitoring the increase in fluorescence intensity inside the compartments (Figure 17. b), c), d)). Control experiments without transmembrane hemolysin confirmed that the pores were necessary for the substrates to diffuse through the compartments for efficient resorufin production.

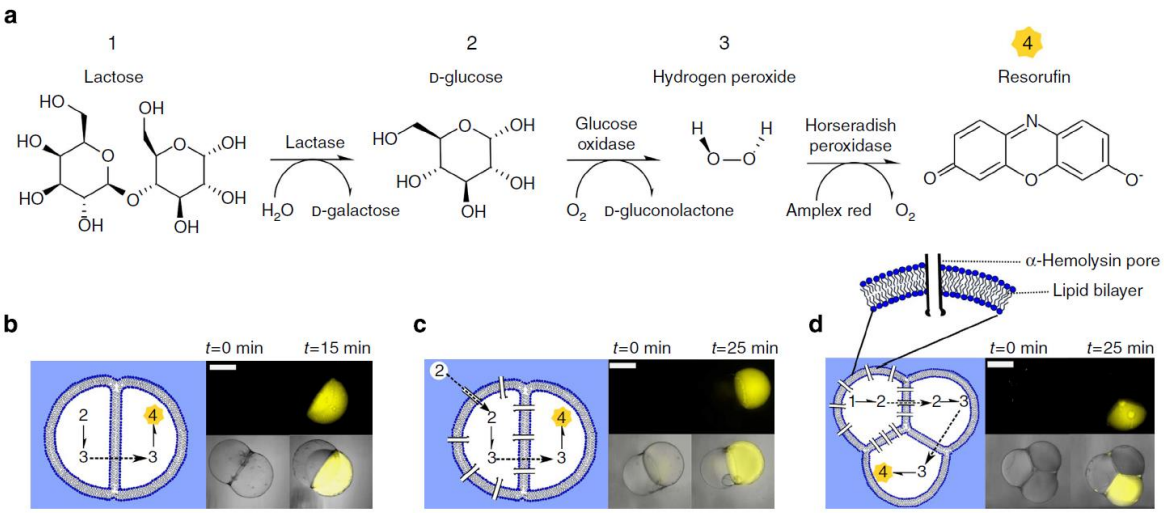

Figure 17. Spatially segregated reaction sequences in multi-compartment vesicles.[153] a) Three-enzyme catalytic reaction scheme involving lactase, GOx and HRP. Glucose is produced from lactose by lactase and is subsequently oxidized by GOx to gluconolactone with formation of hydrogen peroxide. Amplex red is then converted into fluorescent resorufin by hydrogen peroxide and HRP. b), c) and d) Confocal images of resorufin formation in the compartmentalized system and schematic representations of the multi-compartment systems bearing two (b), c)) or three (d)) compartments and α-hemolysin pores (c), d)).

Colloidosomes and capsosomes were also introduced as compartmentalized structures hosting enzymatic reactions.[155,156] The few examples presented here all constitute major advances in the field of cellular mimics. Indeed, compartmentalization have been synthetically engineered in vesicular structures, either in the form of small compartments entrapped in a larger compartment or in the form of adjacently joined compartments. These architectures have been used to mimic functional organelles and segregate multiple enzymes to carry out cascade reactions in a single system. These studies present highly elaborate and complex structures which constitute important advances towards a common goal: reaching eukaryotic cell mimics.

4. Towards smart biomimetic eukaryotic cell models: cascade reactions induced by external stimuli

For the cells to function properly, temporal and positional control of the biological processes are required. As previously discussed, positional control can be achieved with compartmentalized structures that allow precise localization of the different substrates and catalysts.[157] However, for most reported systems, a last major challenge that remains is the ability to initiate confined cascade reactions 'on demand' and especially, to find triggers to control the beginning of chemical or enzymatic reactions in compartmentalized systems which for now, are most often dictated by the slow diffusion of substrates through membranes.[151–153]

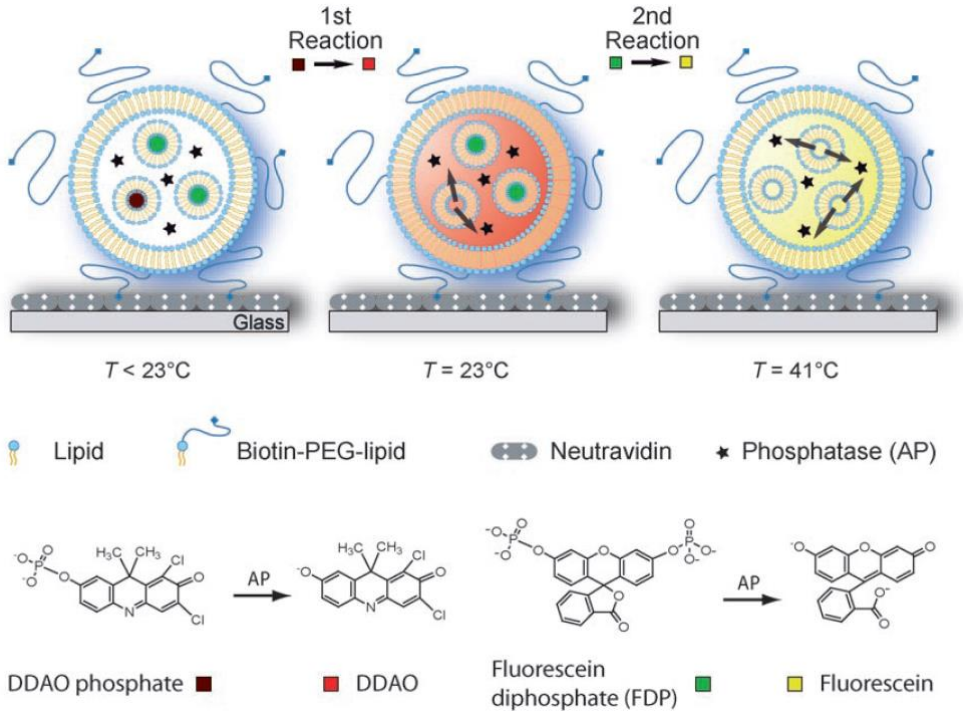

Figure 18. Schematic representation of two consecutive enzymatic reactions triggered by a release of cargo from SUVs inside a LUV reactor at defined transition temperatures (Tts).[158] LUVs comprise biotin on their surface for immobilization on neutravidin-coated glass slide. At 23°C dichlorodimethylacridinone (DDAO) phosphate is release from SUVs with Tt = 23 °C. DDAO is converted by alkaline phosphatase (AP, free in the lumen of LUVs) into is fluorescent product. At 41 °C, fluorescein diphosphate is released from SUVs with Tt = 41 °C to be converted into its fluorescent product by AP.

An elegant multi-compartment lipidic system (liposomes-in-liposome) was presented by Vogel and co-workers.[158] Small unilamellar lipid vesicles (SUVs) were entrapped into the lumen of large unilamellar lipid vesicles (LUVs) (Figure 18). Lipids were chosen carefully depending on their specific ordered-fluid phase transition temperature (Tt) to accurately define the

temperature at which the SUVs could release their cargo inside the LUVs. Two different SUV compositions were enclosed into the lumen of a LUV: DMPC/DMPG = 4:1 SUVs and DPPC/DPPG = 9:1 SUVs with respective Tts of approximately 23 °C and 41 °C. The successive increase of temperature above the different Tts induced controlled SUV membrane permeabilization and subsequent release of cargo inside LUVs. This architecture presents both the compartmentalized structure of biological cells and the controlled release of different reactants and constitutes a major improvement of existing biomimetic systems with the potential of controlling the initiation of compartmentalized reactions. As a proof of concept, the authors showed the temperature-controlled release of pro-fluorescent substrates from SUVs and subsequent mixing with a free alkaline phosphatase (AP) enzyme enclosed inside the lumen of the LUVs (Figure 18). Two different substrates could be release independently at the two defined Tts (23 and 41 °C) to be converted by AP into their fluorescent products. The increase of fluorescence intensity monitored by fluorescence correlation spectroscopy was a proof of the efficient release of substrates from the SUVs.

Temperature was also used as a trigger in other studies on biomimetic sub-compartmentalized assemblies, termed capsosomes, by Caruso and coworkers.[45,159] As previously described, capsosomes are formed from LbL assembly of polymers onto a sacrificial silica template. Here, glutathione reductase enzyme (GR) was encapsulated into cholesterol containing liposomes (DPPC:cholesterol = 4:1) which were deposited onto poly(N-vinylpyrrolidone)-*b*-cholesterol acrylate) (PVPc) layers adsorbed on the silica particles. GR is responsible for the reduction of glutathione disulfide (GSSG) into its sulfhydryl form (GSH). The liposomes were then capped with PVPc and poly(methacrylic acid) (PMA) polymer layers before dissolution of the silica sacrificial particles by treatment with acid to afford liposomes-loaded capsosomes. The incubation of GSSG with the capsosomes resulted in an increase of absorbance at 37 °C because of GSH production, but not at 24 °C thus proving that the reagents don't permeate inside the liposomes below the Tt of the lipids and confirming the temperature dependency of the capsosomes-confined reaction. In order to demonstrate that this system permits efficient triggered cascade catalytic reaction, the authors co-encapsulated a polymer-peptide conjugate together with the GR-loaded liposomes inside the lumen of the capsosomes (Figure 19). The peptide was fluorescently labelled and attached to the polymer by a disulfide linker.[160] Upon increase of temperature, GSSG is converted into GSH by GR. GSH then cleaves the disulfide linkage of the polymer-peptide conjugate enabling its release from the capsosomes, as verified by fluorescence microscopy and flow cytometry.

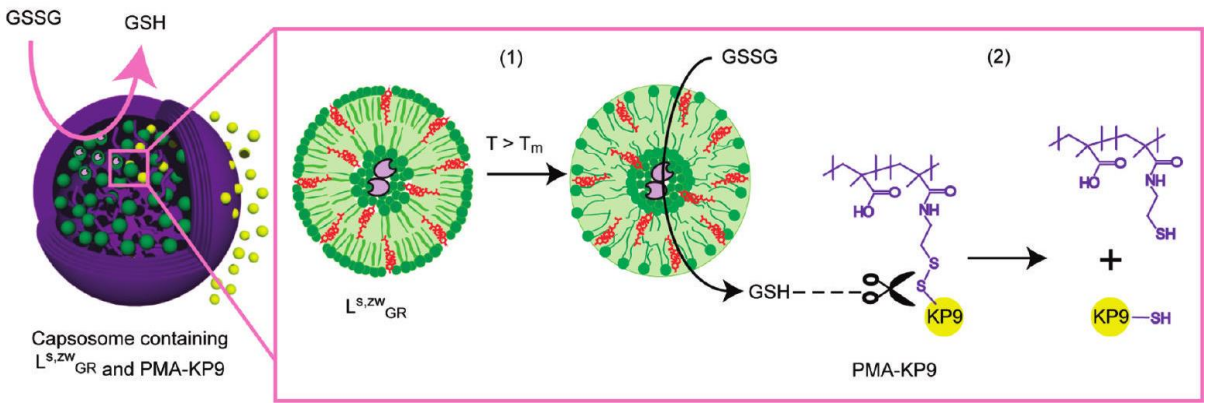

Figure 19. Schematic representation of the liposomes-loaded capsosomes and the temperature triggered reduction of glutathione disulfide (GSSG) into glutathione sulfhydryl (GSH) by glutathione reductase (GR) followed by the cleavage of the polymer-peptide conjugate (PMA-KP9) and liberation of the peptide.[159]

The fact that no reaction could be initiated below the Tt of the lipids indicates the efficiency of this system as a suitable design for performing multistep catalytic cascade reactions requiring rapid mixing within a confined environment.

The previously discussed examples constitute recent innovative compartmentalized systems that can host triggered cascade reactions and represent elegant combinations of structural and functional cell biomimicry. While some few other elaborate systems have been presented, triggering chemical or enzymatic cascade reactions in multi-compartmentalized structures is still in an early research stage and more progress has to be done to achieve better temporal control in the initiation of catalytic reactions.

5. Conclusions

Considerable progress has been made over the last decade in the design of new eukaryotic cellular mimics. Complex synthetic architectures that more and more resemble those of biological cells have been engineered and these studies have led researchers to gain more insight into the cell mechanical, chemical and physical properties. Especially, artificial compartmentalized structures and asymmetric membranes have been developed. In addition, functional mimicry has been reached with the construction and use of synthetic nano- and micro-reactors.

It is only recently that structural and functional cell mimicry have been combined to afford better cell mimics and mostly through structures hosting compartmentalized cascade reactions. However, a lot of progress still has to be made to reach models with a higher level of precision over the catalytic processes and the controlled segregation of species.

The work carried out during this PhD thesis aims at providing new tools to enrich the already existing toolbox for constructing biomimetic systems. A special focus has been made on innovative compartmentalized structures and asymmetric membranes. Additionally, a major part of the carried work was dedicated to finding new ways to trigger enzymatic or chemical reactions in compartmentalized systems as a way to improve the already existing synthetic catalytic structures.

The first part of the manuscript is focused on structural cell mimicry research findings and mostly, we present a novel type of synthetic compartmentalized architecture relying on polymers and lipids and the design of an asymmetric lipid-polymer synthetic membrane. The second part presents our research on triggers for reactions using osmotic pressure variations to induce controlled rupture of vesicles. Finally, the last part is dedicated to our recent findings on mixing synthetic polymeric vesicles (model cells) with biological cells and the study of their co-existence.

6. References

[1] P. Mazzarello, *Nat. Cell Biol.* **1999**, *1*, E13–E15.

[2] S. Mann, *Acc. Chem. Res.* **2012**, *45*, 2131–2141.

[3] J. E. Rothman, J. Lenard, *Science* **1977**, *195*, 743–753.

[4] M. S. Bretscher, *Nature* **1972**, *236*, 11–12.

[5] P. F. Devaux, *Biochemistry (Mosc.)* **1991**, *30*, 1163–1173.

[6] B. Alberts, A. Johnson, J. Lewis, M. Raff, K. Roberts, P. Walter, **2002**.

[7] K. Khoshmanesh, A. Z. Kouzani, S. Nahavandi, S. Baratchi, J. R. Kanwar, *Comput. Biol. Chem.* **2008**, *32*, 315–331.

[8] J. W. Szostak, D. P. Bartel, P. L. Luisi, *Nature* **2001**, *409*, 387–390.

[9] W. Martin, *Philos. Trans. R. Soc. Lond. B Biol. Sci.* **2010**, *365*, 847–855.

[10] B. C. Buddingh', J. C. M. van Hest, *Acc. Chem. Res.* **2017**, DOI 10.1021/acs.accounts.6b00512.

[11] M. Marguet, C. Bonduelle, S. Lecommandoux, *Chem. Soc. Rev.* **2012**, *42*, 512–529.

[12] L. Schoonen, J. C. M. van Hest, *Adv. Mater.* **2016**, *28*, 1109–1128.

[13] R. J. R. W. Peters, I. Louzao, J. C. M. van Hest, *Chem. Sci.* **2012**, *3*, 335–342.

[14] B. Städler, A. D. Price, R. Chandrawati, L. Hosta-Rigau, A. N. Zelikin, F. Caruso, *Nanoscale* **2009**, *1*, 68–73.

[15] R. Chandrawati, F. Caruso, *Langmuir* **2012**, *28*, 13798–13807.

[16] D. A. Hammer, N. P. Kamat, *FEBS Lett.* **2012**, *586*, 2882–2890.

[17] A. Pohorille, D. Deamer, *Trends Biotechnol.* **2002**, *20*, 123–128.

[18] Y. Zhang, W. C. Ruder, P. R. LeDuc, *Trends Biotechnol.* **2008**, *26*, 14–20.

[19] B. M. Discher, Y.-Y. Won, D. S. Ege, J. C.-M. Lee, F. S. Bates, D. E. Discher, D. A. Hammer, *Science* **1999**, *284*, 1143–1146.

[20] X. Hu, Y. Zhang, Z. Xie, X. Jing, A. Bellotti, Z. Gu, *Biomacromolecules* **2017**, DOI 10.1021/acs.biomac.6b01704.

[21] F. Ahmed, P. J. Photos, D. E. Discher, *Drug Dev. Res.* **2006**, *67*, 4–14.

[22] R. Rodríguez-García, M. Mell, I. López-Montero, J. Netzel, T. Hellweg, F. Monroy, *Soft Matter* **2011**, *7*, 1532–1542.

[23] L. Messager, J. Gaitzsch, L. Chierico, G. Battaglia, *Curr. Opin. Pharmacol.* **2014**, *18*, 104–111.

[24] F. Meng, Z. Zhong, J. Feijen, *Biomacromolecules* **2009**, *10*, 197–209.

[25] J. S. Lee, J. Feijen, *J. Controlled Release* **2012**, *161*, 473–483.

[26] P. Stano, P. L. Luisi, *Chem. Commun.* **2010**, *46*, 3639–3653.

[27] M. Forlin, R. Lentini, S. S. Mansy, *Curr. Opin. Chem. Biol.* **2012**, *16*, 586–592.

[28] J. C. Blain, J. W. Szostak, *Annu. Rev. Biochem.* **2014**, *83*, 615–640.

[29] N. P. Kamat, J. S. Katz, D. A. Hammer, *J. Phys. Chem. Lett.* **2011**, *2*, 1612–1623.

[30] P. Tanner, S. Egli, V. Balasubramanian, O. Onaca, C. G. Palivan, W. Meier, *FEBS Lett.* **2011**, *585*, 1699–1706.

[31] B. A. Grzybowski, W. T. S. Huck, *Nat. Nanotechnol.* **2016**, *11*, 585–592.

[32] T. Trantidou, M. Friddin, Y. Elani, N. J. Brooks, R. V. Law, J. M. Seddon, O. Ces, *ACS Nano* **2017**, DOI 10.1021/acsnano.7b03245.

[33] S. A. Walker, M. T. Kennedy, J. A. Zasadzinski, *Nature* **1997**, *387*, 61–64.

[34] N.-N. Deng, M. Yelleswarapu, W. T. S. Huck, *J. Am. Chem. Soc.* **2016**, *138*, 7584–7591.

[35] N.-N. Deng, M. Yelleswarapu, L. Zheng, W. T. S. Huck, *J. Am. Chem. Soc.* **2017**, *139*, 587–590.

[36] N.-N. Deng, W. T. S. Huck, *Angew. Chem. Int. Ed Engl.* **2017**, *56*, 9736–9740.

[37] H.-C. Chiu, Y.-W. Lin, Y.-F. Huang, C.-K. Chuang, C.-S. Chern, *Angew. Chem. Int. Ed.* **2008**, *47*, 1875–1878.
[38] S.-H. Kim, H. C. Shum, J. W. Kim, J.-C. Cho, D. A. Weitz, *J. Am. Chem. Soc.* **2011**, *133*, 15165–15171.
[39] H. C. Shum, Y. Zhao, S.-H. Kim, D. A. Weitz, *Angew. Chem. Int. Ed.* **2011**, *50*, 1648–1651.
[40] A. Perro, C. Nicolet, J. Angly, S. Lecommandoux, J.-F. Le Meins, A. Colin, *Langmuir* **2011**, *27*, 9034–9042.
[41] Z. Fu, M. A. Ochsner, H.-P. M. de Hoog, N. Tomczak, M. Nallani, *Chem. Commun.* **2011**, *47*, 2862–2864.
[42] M. Marguet, O. Sandre, S. Lecommandoux, *Langmuir* **2012**, *28*, 2035–2043.
[43] E. Mabrouk, D. Cuvelier, L.-L. Pontani, B. Xu, D. Lévy, P. Keller, F. Brochard-Wyart, P. Nassoy, M.-H. Li, *Soft Matter* **2009**, *5*, 1870–1878.
[44] M. Marguet, L. Edembe, S. Lecommandoux, *Angew. Chem. Int. Ed.* **2012**, *51*, 1173–1176.
[45] R. Chandrawati, L. Hosta-Rigau, D. Vanderstraaten, S. A. Lokuliyana, B. Städler, F. Albericio, F. Caruso, *ACS Nano* **2010**, *4*, 1351–1361.
[46] L. Hosta-Rigau, S. F. Chung, A. Postma, R. Chandrawati, B. Städler, F. Caruso, *Adv. Mater.* **2011**, *23*, 4082–4087.
[47] B. G. D. Geest, S. D. Koker, G. B. Sukhorukov, O. Kreft, W. J. Parak, A. G. Skirtach, J. Demeester, S. C. D. Smedt, W. E. Hennink, *Soft Matter* **2009**, *5*, 282–291.
[48] L. L. del Mercato, P. Rivera-Gil, A. Z. Abbasi, M. Ochs, C. Ganas, I. Zins, C. Sönnichsen, W. J. Parak, *Nanoscale* **2010**, *2*, 458–467.
[49] P. T. Hammond, *Mater. Today* **2012**, *15*, 196–206.
[50] S. J. Singer, G. L. Nicolson, *Science* **1972**, *175*, 720–731.
[51] M. S. Bretscher, *Science* **1973**, *181*, 622–629.
[52] A. J. Verkleij, R. F. A. Zwaal, B. Roelofsen, P. Comfurius, D. Kastelijn, L. L. M. van Deenen, *Biochim. Biophys. Acta BBA - Biomembr.* **1973**, *323*, 178–193.
[53] R. F. Zwaal, B. Roelofsen, C. M. Colley, *Biochim. Biophys. Acta* **1973**, *300*, 159–182.
[54] T. L. Steck, G. Dawson, *J. Biol. Chem.* **1974**, *249*, 2135–2142.
[55] G. L. Nicolson, S. J. Singer, *Proc. Natl. Acad. Sci.* **1971**, *68*, 942–945.
[56] G. van Meer, D. R. Voelker, G. W. Feigenson, *Nat. Rev. Mol. Cell Biol.* **2008**, *9*, 112–124.
[57] H. Lodish, A. Berk, S. L. Zipursky, P. Matsudaira, D. Baltimore, J. Darnell, **2000**.
[58] S. Manno, Y. Takakuwa, N. Mohandas, *Proc. Natl. Acad. Sci. U. S. A.* **2002**, *99*, 1943–1948.
[59] B. Fadeel, D. Xue, *Crit. Rev. Biochem. Mol. Biol.* **2009**, *44*, 264–277.
[60] B. R. Lentz, *Prog. Lipid Res.* **2003**, *42*, 423–438.
[61] R. F. A. Zwaal, A. J. Schroit, *Blood* **1997**, *89*, 1121–1132.
[62] V. A. Fadok, D. R. Voelker, P. A. Campbell, J. J. Cohen, D. L. Bratton, P. M. Henson, *J. Immunol. Baltim. Md 1950* **1992**, *148*, 2207–2216.
[63] V. A. Fadok, P. M. Henson, *Curr. Biol.* **1998**, *8*, R693–R695.
[64] B. Verhoven, R. A. Schlegel, P. Williamson, *J. Exp. Med.* **1995**, *182*, 1597–1601.
[65] R. A. Schlegel, P. Williamson, *Cell Death Differ.* **2001**, *8*, 551–563.
[66] D. L. Daleke, *J. Lipid Res.* **2003**, *44*, 233–242.
[67] J. M. Boon, B. D. Smith, *Med. Res. Rev.* **2002**, *22*, 251–281.
[68] F. J. Sharom, *IUBMB Life* **2011**, *63*, 736–746.
[69] T. Pomorski, S. Hrafnsdóttir, P. F. Devaux, G. van Meer, *Semin. Cell Dev. Biol.* **2001**, *12*, 139–148.
[70] P. F. Devaux, *FEBS Lett.* **1988**, *234*, 8–12.
[71] M. Seigneuret, P. F. Devaux, *Proc. Natl. Acad. Sci. U. S. A.* **1984**, *81*, 3751–3755.
[72] M. Bitbol, P. F. Devaux, *Proc. Natl. Acad. Sci. U. S. A.* **1988**, *85*, 6783–6787.

[73] G. van Meer, *Cold Spring Harb. Perspect. Biol.* **2011**, *3*, a004671.
[74] A. Iglic, *Advances in Planar Lipid Bilayers and Liposomes*, Academic Press, **2012**.
[75] D. Marquardt, B. Geier, G. Pabst, *Membranes* **2015**, *5*, 180–196.
[76] M. J. Hope, T. E. Redelmeier, K. F. Wong, W. Rodrigueza, P. R. Cullis, *Biochemistry (Mosc.)* **1989**, *28*, 4181–4187.
[77] L. W. Johnson, M. E. Hughes, D. B. Zilversmit, *Biochim. Biophys. Acta BBA - Biomembr.* **1975**, *375*, 176–185.
[78] D. B. Zilversmit, *J. Lipid Res.* **1984**, *25*, 1563–1569.
[79] M. G. Low, D. B. Zilversmit, *Biochim. Biophys. Acta BBA - Biomembr.* **1980**, *596*, 223–234.
[80] H.-T. Cheng, E. London, *Biophys. J.* **2011**, *100*, 2671–2678.
[81] Q. Lin, E. London, *PLOS ONE* **2014**, *9*, e87903.
[82] F. A. Heberle, D. Marquardt, M. Doktorova, B. Geier, R. F. Standaert, P. Heftberger, B. Kollmitzer, J. D. Nickels, R. A. Dick, G. W. Feigenson, et al., *Langmuir* **2016**, *32*, 5195–5200.
[83] T. Hamada, Y. Miura, Y. Komatsu, Y. Kishimoto, M. Vestergaard, M. Takagi, *J. Phys. Chem. B* **2008**, *112*, 14678–14681.
[84] D. L. Richmond, E. M. Schmid, S. Martens, J. C. Stachowiak, N. Liska, D. A. Fletcher, *Proc. Natl. Acad. Sci. U. S. A.* **2011**, *108*, 9431–9436.
[85] P. C. Hu, S. Li, N. Malmstadt, *ACS Appl. Mater. Interfaces* **2011**, *3*, 1434–1440.
[86] A. Peyret, E. Ibarboure, J.-F. Le Meins, S. Lecommandoux, *Submited* **n.d.**
[87] K. Kamiya, R. Kawano, T. Osaki, K. Akiyoshi, S. Takeuchi, *Nat. Chem.* **2016**, *8*, 881–889.
[88] I. Visco, S. Chiantia, P. Schwille, *Langmuir ACS J. Surf. Colloids* **2014**, *30*, 7475–7484.
[89] S. Li, A. K. Mehta, A. N. Sidorov, T. M. Orlando, Z. Jiang, N. R. Anthony, D. G. Lynn, *J. Am. Chem. Soc.* **2016**, *138*, 3579–3586.
[90] S. K. Lim, A. S. W. Wong, H.-P. M. de Hoog, P. Rangamani, A. N. Parikh, M. Nallani, S. Sandin, B. Liedberg, *Soft Matter* **2017**, *13*, 1107–1115.
[91] A. F. Mason, P. Thordarson, *ACS Macro Lett.* **2016**, 1172–1175.
[92] E. V. Konishcheva, U. E. Zhumaev, W. P. Meier, *Macromolecules* **2017**, *50*, 1512–1520.
[93] R. Stoenescu, W. Meier, *Chem. Commun.* **2002**, 3016–3017.
[94] F. Fernandez-Trillo, L. M. Grover, A. Stephenson-Brown, P. Harrison, P. M. Mendes, *Angew. Chem. Int. Ed.* **2017**, *56*, 3142–3160.
[95] B. de Kruijff, P. Baken, *Biochim. Biophys. Acta BBA - Biomembr.* **1978**, *507*, 38–47.
[96] R. E. Pagano, O. C. Martin, A. J. Schroit, D. K. Struck, *Biochemistry (Mosc.)* **1981**, *20*, 4920–4927.
[97] H. M. McConnell, R. D. Kornberg, *Biochemistry (Mosc.)* **1971**, *10*, 1111–1120.
[98] H.-T. Cheng, Megha, E. London, *J. Biol. Chem.* **2009**, *284*, 6079–6092.
[99] S. Chiantia, P. Schwille, A. S. Klymchenko, E. London, *Biophys. J.* **2011**, *100*, L1–L3.
[100] T. G. Anderson, A. Tan, P. Ganz, J. Seelig, *Biochemistry (Mosc.)* **2004**, *43*, 2251–2261.
[101] K. Kamiya, R. Kawano, T. Osaki, K. Akiyoshi, S. Takeuchi, *Nat. Chem.* **2016**, *advance online publication*, DOI 10.1038/nchem.2537.
[102] W. L. Hwang, M. Chen, B. Cronin, M. A. Holden, H. Bayley, *J. Am. Chem. Soc.* **2008**, *130*, 5878–5879.
[103] S. Pautot, B. J. Frisken, D. A. Weitz, *Proc. Natl. Acad. Sci.* **2003**, *100*, 10718–10721.
[104] S. Pautot, B. J. Frisken, D. A. Weitz, *Langmuir* **2003**, *19*, 2870–2879.
[105] Z. Xiao, M. Xu, M. Li, Z. Lu, Y. Wei, *Supramol. Sci.* **1998**, *5*, 619–622.
[106] M. Abkarian, E. Loiseau, G. Massiera, *Soft Matter* **2011**, *7*, 4610–4614.
[107] C. Claudet, M. In, G. Massiera, *Eur. Phys. J. E* **2016**, *39*, 9.
[108] M. C. Blosser, B. G. Horst, M. Abkarian, G. Massiera, S. L. Keller, *Biophys. J.* **2012**, *102*, 97a.

[109] J. C. Stachowiak, D. L. Richmond, T. H. Li, F. Brochard-Wyart, D. A. Fletcher, *Lab. Chip* **2009**, *9*, 2003–2009.
[110] J. C. Stachowiak, D. L. Richmond, T. H. Li, A. P. Liu, S. H. Parekh, D. A. Fletcher, *Proc. Natl. Acad. Sci.* **2008**, *105*, 4697–4702.
[111] E. Sackmann, *Science* **1996**, *271*, 43–48.
[112] J. M. Sanderson, *Mol. Membr. Biol.* **2012**, *29*, 118–143.
[113] W.-C. Lin, C. D. Blanchette, T. V. Ratto, M. L. Longo, *Biophys. J.* **2006**, *90*, 228–237.
[114] H. P. Wacklin, *Langmuir* **2011**, *27*, 7698–7707.
[115] G. M. Cooper, *Structure of the Plasma Membrane. 2nd Edition*, Sunderland (MA): Sinauer Associates, **2000**.
[116] D. E. Discher, A. Eisenberg, *Science* **2002**, *297*, 967–973.
[117] J.-F. L. Meins, O. Sandre, S. Lecommandoux, *Eur. Phys. J. E* **2011**, *34*, 1–17.
[118] Y. Zhang, F. Wu, W. Yuan, T. Jin, *J. Control. Release Off. J. Control. Release Soc.* **2010**, *147*, 413–419.
[119] A. Blanazs, M. Massignani, G. Battaglia, S. P. Armes, A. J. Ryan, *Adv. Funct. Mater.* **2009**, *19*, 2906–2914.
[120] G. Liu, S. Ma, S. Li, R. Cheng, F. Meng, H. Liu, Z. Zhong, *Biomaterials* **2010**, *31*, 7575–7585.
[121] L. Luo, A. Eisenberg, *J. Am. Chem. Soc.* **2001**, *123*, 1012–1013.
[122] J. Li, S. Xiao, Y. Xu, S. Zuo, Z. Zha, W. Ke, C. He, Z. Ge, *ACS Appl. Mater. Interfaces* **2017**, *9*, 17727–17735.
[123] Z. Yu, F. Tantakitti, L. C. Palmer, S. I. Stupp, *Nano Lett.* **2016**, *16*, 6967–6974.
[124] P. Tanner, P. Baumann, R. Enea, O. Onaca, C. Palivan, W. Meier, *Acc. Chem. Res.* **2011**, *44*, 1039–1049.
[125] C. G. Palivan, O. Fischer-Onaca, M. Delcea, F. Itel, W. Meier, *Chem. Soc. Rev.* **2012**, *41*, 2800–2823.
[126] J. Gaitzsch, X. Huang, B. Voit, *Chem. Rev.* **2016**, *116*, 1053–1093.
[127] *The Minimal Cell - The Biophysics of Cell Compartment and | Pier Luigi Luisi | Springer*, **n.d.**
[128] G. Murtas, Y. Kuruma, P. Bianchini, A. Diaspro, P. L. Luisi, *Biochem. Biophys. Res. Commun.* **2007**, *363*, 12–17.
[129] C. Martino, S.-H. Kim, L. Horsfall, A. Abbaspourrad, S. J. Rosser, J. Cooper, D. A. Weitz, *Angew. Chem. Int. Ed.* **2012**, *51*, 6416–6420.
[130] K. Kurihara, M. Tamura, K. Shohda, T. Toyota, K. Suzuki, T. Sugawara, *Nat. Chem.* **2011**, *3*, 775–781.
[131] J. Chalmeau, N. Monina, J. Shin, C. Vieu, V. Noireaux, *Biochim. Biophys. Acta* **2011**, *1808*, 271–278.
[132] S. F. M. van Dongen, M. Nallani, J. J. L. M. Cornelissen, R. J. M. Nolte, J. C. M. van Hest, *Chem. – Eur. J.* **2009**, *15*, 1107–1114.
[133] D. M. Vriezema, P. M. L. Garcia, N. Sancho Oltra, N. S. Hatzakis, S. M. Kuiper, R. J. M. Nolte, A. E. Rowan, J. C. M. van Hest, *Angew. Chem. Int. Ed.* **2007**, *46*, 7378–7382.
[134] D. M. Vriezema, A. Kros, R. de Gelder, J. J. L. M. Cornelissen, A. E. Rowan, R. J. M. Nolte, *Macromolecules* **2004**, *37*, 4736–4739.
[135] M. Nallani, H.-P. M. de Hoog, J. J. L. M. Cornelissen, A. R. A. Palmans, J. C. M. van Hest, R. J. M. Nolte, *Biomacromolecules* **2007**, *8*, 3723–3728.
[136] C. Nardin, S. Thoeni, J. Widmer, M. Winterhalter, W. Meier, *Chem. Commun.* **2000**, 1433–1434.
[137] C. Nardin, T. Hirt, J. Leukel, W. Meier, *Langmuir* **2000**, *16*, 1035–1041.
[138] H. Nikaido, *Mol. Microbiol.* **1992**, *6*, 435–442.

[139] M. Dezi, A. Di Cicco, P. Bassereau, D. Lévy, *Proc. Natl. Acad. Sci. U. S. A.* **2013**, *110*, 7276–7281.
[140] C. Nardin, J. Widmer, M. Winterhalter, W. Meier, *Eur. Phys. J. E* **2001**, *4*, 403–410.
[141] P. Tanner, O. Onaca, V. Balasubramanian, W. Meier, C. G. Palivan, *Chem. – Eur. J.* **2011**, *17*, 4552–4560.
[142] M. Lomora, F. Itel, I. A. Dinu, C. G. Palivan, *Phys. Chem. Chem. Phys.* **2015**, *17*, 15538–15546.
[143] J. Du, Y. Tang, A. L. Lewis, S. P. Armes, *J. Am. Chem. Soc.* **2005**, *127*, 17982–17983.
[144] H. Lomas, J. Du, I. Canton, J. Madsen, N. Warren, S. P. Armes, A. L. Lewis, G. Battaglia, *Macromol. Biosci.* **2010**, *10*, 513–530.
[145] X. Chen, X. Ding, Z. Zheng, Y. Peng, *New J. Chem.* **2006**, *30*, 577–582.
[146] A. Napoli, M. Valentini, N. Tirelli, M. Müller, J. A. Hubbell, *Nat. Mater.* **2004**, *3*, 183–189.
[147] D. Gräfe, J. Gaitzsch, D. Appelhans, B. Voit, *Nanoscale* **2014**, *6*, 10752–10761.
[148] K. T. Kim, J. J. L. M. Cornelissen, R. J. M. Nolte, J. C. M. van Hest, *Adv. Mater.* **2009**, *21*, 2787–2791.
[149] T. D. James, K. R. A. S. Sandanayake, S. Shinkai, *Angew. Chem. Int. Ed. Engl.* **1996**, *35*, 1910–1922.
[150] Z. Cao, P. Nandhikonda, M. D. Heagy, *J. Org. Chem.* **2009**, *74*, 3544–3546.
[151] O. Kreft, M. Prevot, H. Möhwald, G. B. Sukhorukov, *Angew. Chem. Int. Ed.* **2007**, *46*, 5605–5608.
[152] R. J. R. W. Peters, M. Marguet, S. Marais, M. W. Fraaije, J. C. M. van Hest, S. Lecommandoux, *Angew. Chem. Int. Ed.* **2014**, *53*, 146–150.
[153] Y. Elani, R. V. Law, O. Ces, *Nat. Commun.* **2014**, *5*, DOI 10.1038/ncomms6305.
[154] L. Song, M. R. Hobaugh, C. Shustak, S. Cheley, H. Bayley, J. E. Gouaux, *Science* **1996**, *274*, 1859–1865.
[155] B. Städler, R. Chandrawati, A. D. Price, S.-F. Chong, K. Breheney, A. Postma, L. A. Connal, A. N. Zelikin, F. Caruso, *Angew. Chem. Int. Ed.* **2009**, *48*, 4359–4362.
[156] Z. Wang, M. C. M. van Oers, F. P. J. T. Rutjes, J. C. M. van Hest, *Angew. Chem. Int. Ed.* **2012**, *51*, 10746–10750.
[157] R. Chandrawati, M. P. van Koeverden, H. Lomas, F. Caruso, *J. Phys. Chem. Lett.* **2011**, *2*, 2639–2649.
[158] P.-Y. Bolinger, D. Stamou, H. Vogel, *Angew. Chem. Int. Ed.* **2008**, *47*, 5544–5549.
[159] R. Chandrawati, P. D. Odermatt, S.-F. Chong, A. D. Price, B. Städler, F. Caruso, *Nano Lett.* **2011**, *11*, 4958–4963.
[160] S.-F. Chong, A. Sexton, R. De Rose, S. J. Kent, A. N. Zelikin, F. Caruso, *Biomaterials* **2009**, *30*, 5178–5186.

CHAPTER 2: ***Asymmetric hybrid polymer-lipid giant vesicles as biological membrane mimics***

Adapted from:

Asymmetric hybrid polymer-lipid giant vesicles as biological membrane mimics.

Ariane Peyret, Emmanuel Ibarboure, Jean-François Le Meins, Sébastien Lecommandoux, *Submited*.

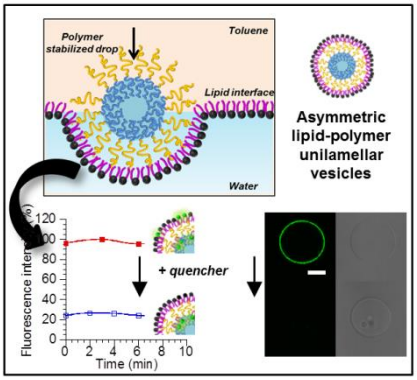

Abstract: Lipid membrane asymmetry plays an important role in cell function and activity, being for instance an indicator of its integrity. The development of artificial asymmetric membranes that can be used to mimic and understand fundamental biophysics aspects of membranes is still challenging. In this context, an emulsion-centrifugation method was developed to prepare giant biomimetic vesicles with an asymmetric membrane composed of an inner monolayer of poly(butadiene)-*b*-poly(ethylene oxide) (PBut-*b*-PEO) and outer monolayer of 1-palmitoyl-2-oleoyl-sn-glycero-3-phosphocholine (POPC). The formation of a complete membrane asymmetry with a fluorescence quenching assay was demonstrated and its stability with time was followed by measuring lipid transverse diffusion from the outer to the inner monolayer. From the fluorescence spectroscopy measurements, the lipid half-life was estimated to be 7.5 hours. Using the fluorescence recovery after photobleaching (FRAP) technique, the diffusion coefficient of 1,2-dioleoyl-sn-glycero-3-phosphoethanolamine-N-(lissamine rhodamine B sulfonyl) (DOPE-rhod, inserted into the POPC leaflet) was determined to be about D=1.8±0.50 μm^2/s at 25 °C and D =2.3±0.7 μm^2/s at 37 °C, between the characteristic values of pure POPC and pure polymer giant vesicles and close to the diffusion of lipids in a variety of biological membranes. Taken together, these results demonstrated our ability to prepare a relevant cell-like model system that displays an asymmetric membrane with transverse and translational diffusion properties similar to that of real biological cells. This system constitutes a step forward in the field of cell biomimicry and a significant advance in the design of model membrane platforms.

1. Introduction

The mimicking and reproduction of natural components or systems is a fantastic source of inspiration and innovation in materials science from many decades.[1–3] Among these biomimetic systems, cells are certainly the most fascinating, but also the most difficult to reproduce both from structural and functional view points. Some key properties have been reproduced, such as compartmentalization,[3–14] cytoskeleton mimics,[15–19] or simple (bio)chemical reactions.[20–29] The cell membrane structure is often simplified using lipids, or lipid mix with addition of cholesterol, which is really far from reality, not only considering the chemical structure, but also the biophysical properties of the membrane.[30] Another important feature that is often neglected concerns the asymmetric composition of the membrane.

As such, the concept of lipid bilayer asymmetry was introduced shortly after the idea of the fluid mosaic model to describe biological cell membranes.[30–33] The two leaflets of the membrane are structurally and functionally different in many aspects, this heterogeneity being crucial in maintaining cell activity and cellular events. The main source of asymmetry in cell membranes resides in the lateral and transversal heterogenous distribution of lipids between both sides. For instance, choline derivatives such as phosphatidylcholine or sphingomyelin are exposed in higher proportions on the external monolayer. On the other hand, negatively charged lipids like phosphatidylserine (PS) are located mainly on the cytoplasmic side.[31,32] This uneven distribution of lipids affects membrane physical properties such as curvature, stability or permeability and warrants efficient signal transduction.[33] In addition, asymmetry is a consequence of differing enzymatic activities between both sides of the membrane and also results from the positioning and orientation of membrane proteins, such as glycoproteins that are located on the outer leaflet and are involved in cell recognition.[34,35] The proper functioning of membrane-regulated cellular phenomena is highly influenced by the asymmetric positioning of membrane constituents and therefore, a lot of energy is invested to maintain it. Perturbation or breakdown of asymmetry often has significant physiological consequences.[36] For example, PS exposure on the outer leaflet is a sign for cell death and recognition by macrophages.[37–39] While many aspects of cellular membrane asymmetry have been unveiled, how asymmetry is assembled and maintained as well as its full implication in membrane-regulated cellular events is still not entirely understood. Hence, it is of major interest to better understand the importance of membrane heterogeneity and one way to do that is by developing asymmetric cell-like biomimetic systems with well-defined membrane properties.

In order to study and better understand the structure and function of biological membranes, model artificial bilayer asymmetric membranes have been prepared, in the context of cell biomimicry.[40,41] There are only a handful of reports on the preparation of such systems, mainly because of the difficulties to control and characterize the asymmetry. Different approaches have been considered, mainly through the fabrication of supported bilayers (i.e. bilayer on a solid surface) or the preparation of vesicles. A number of techniques have been developed to afford asymmetric lipid vesicles (so-called liposomes) such as microfluidic devices[42–44] or droplet-transfer over an interface[45,46] while supported asymmetric lipid bilayers have been prepared mainly through vesicle fusion[47,48] or lipid exchange techniques[49]. However, other types of

amphiphiles namely peptides, polymers or lipid/polymer hybrids were also used to afford various structures, respectively nanoribbons[50], polymer vesicles[51,52] or tubular vesicles[53] with an asymmetric membrane. While all these systems allow new insight into bilayer asymmetry and how it impacts membrane physical properties, there still is a need to further push the frontiers of cell biomimicry by developing stable systems with higher control of membrane properties, many challenges still need to be addressed. For instance, supported bilayers are limited as models of cell membranes as compared with vesicular structures.

Combining the advantages of polymer chemical versatility and robustness with lipid biocompatibility is a powerful way to better modulate and mimic cell membrane properties. The association of block copolymers and phospholipids is a relatively recent approach that have been developed to design bioinspired vesicular structures whose membrane properties could be modulated by composition and membrane structuration.[54–56] These systems, so called Giant Hybrid polymer-lipid Unilamellar vesicles (GHUV) or Large Hybrid polymer lipid Vesicles (LHUV) are especially investigated to generate lateral heterogenous distribution of the components (formation of "raft-like" nanodomains of lipids),[57] but to our knowledge the association of lipids and polymers has never been investigated so far to develop entirely asymmetric membranes.

We herein introduce a versatile protocol to produce asymmetric Giant Hybrid polymer-lipid Unilamellar Vesicles (aGHUV) that closely mimic the properties of biological cell membrane. In the present work, the vesicles are constituted of an inner leaflet of poly(butadiene)-*block*-poly(ethylene oxide) copolymer and outer leaflet of tunable lipid type *via* an emulsion-centrifugation method. We also show how we can prepare the reverse structures with the lipid leaflet facing the interior of the vesicle. We demonstrate the complete asymmetry of the membrane and follow its stability by fluorescence quenching measurements. In addition, we further investigate lipid dynamic responses such as lateral and transverse diffusion (flip-flop). We thus provide an efficient method to afford aGHUV that exhibit close resemblance to the architecture and membrane diffusion dynamics of biological cells. This system could serve as a tool and scaffold to better understand the importance of asymmetry and how it is maintained in biological systems. It is to our knowledge the first report on the preparation of totally asymmetric giant polymer-lipid vesicles and the study of their membrane diffusion properties with the aim to more accurately mimic biological cell membranes.

2. Experimental Section

2.1. Materials

The phospholipids used for the liposomal systems were 1-palmitoyl-2-oleoyl-sn-glycero-3-phosphocholine (POPC) and 1,2-dimyristoyl-sn-glycero-3-phosphocholine (DMPC). The dyes used were 1,2-diphytanoyl-sn-glycero-3-phosphoethanolamine-N-(7-nitro-2-1,3-benzoxadiazol-4-yl) (PE-NBD) (ammonium salt) and 1,2-dioleoyl-sn-glycero-3-phosphoethanolamine-N-(lissamine rhodamine B sulfonyl) (DOPE-rhod, ammonium salt). These materials were purchased from Avanti Polar Lipids Inc., (Albaster, AL, USA) and used without further purification. Poly(butadiene)-*b*-poly(ethylene oxide) ($PBut_{2.5}$-*b*-$PEO_{1.3}$) was ordered from Polymer Source (P18422-BdEO, Mw/Mn 1.04, 89% 1,2-addition of butadiene). All other solvents and reagents used were of analytical grade and purchased from Sigma–Aldrich Chemical Co.

2.2. Methods

UV-Visible experiments were carried out on a Spectra Max M2 microplate spectrophotometer (Molecular Devices). Laser scanning confocal microscopy images were acquired on an inverted Leica TCS SP5 microscope equipped with an HCX PL APO 63×, NA 1.4 oil immersion objective in fluorescence mode. Samples (≈20 μL) were injected in a homemade chamber that was sealed to prevent evaporation. The laser outputs were controlled via the Acousto-Optical Tunable filter and the two collection windows using the Acousto-Optical Beam Splitter and photomultipliers as follows: NBD was excited with an argon laser at 488 nm and DOPE-rhod was excited at 561 nm. The Helium-Neon laser at 633 nm (10 %) was used in transmission mode.

2.3. Fluorescence recovery after photobleaching

Fluorescence recovery after photobleaching (FRAP) was performed using the FRAP-Wizard of the LAS-AF microscope software which allowed to control and tune the scanning conditions: pre-bleach, photo-bleach and post-bleach phases. DOPE-rhod was excited and bleached with the 561 nm laser line and the emission was collected in the 600-700 nm range. Regions of interest (ROIs) were defined over the vesicles with a diameter of 3 μm. FRAP acquisition was started with 10 images scan at low (3-5 %) laser power. Then the dye was bleached locally inside the ROIs at 100

% laser power using a scan of 3 frames. Finally, fluorescence recovery was monitored by the acquisition of a series of 150-200 images at the same low laser power as the pre-bleach phase. The images were acquired with a 6x zoom, using a 256 x 256 pixel frame and bidirectional scan at a 1400 Hz line frequency speed. The pinhole was set to 222.92 µm (2 Airy). To control the temperature, the microscope was equipped with a heating and cooling stage (PE120XY stage size 160*116mm) from Linkam Scientific Instruments,UK, with temperature range: -25°C to 120°C, heating/cooling rate: 0.1 to 20°C/min, and control and stability: +/-0.1°C. FRAP experiments were performed at 25 or 37 °C. The FRAP Analyzer software was used for quantitative analysis of the FRAP data. After normalization (double normalization), the data were fitted with the circular spot model in 2D diffusion. It is important to note that the preparation method used to generate AGHUV, described below, allows the sedimentation of the vesicles in the bottom of the cover slip and perfect immobilization, obviously necessary for FRAP experiments.

2.4.Preparation of asymmetric giant hybrid unilamellar vesicles

Asymmetric giant hybrid unilamellar poly(butadiene)-*b*-poly(ethylene oxide) ($PBut_{2.5}$-*b*-$PEO_{1.3}$) - lipid vesicles (aGHUV) were prepared by a previously reported emulsion-centrifugation method.[58] Briefly, 5 µL of a sucrose solution (0.3 M sucrose, 0.01 M HEPES, 0.15 M NaCl, pH 7.4) was poured into 3 mg/mL $PBut_{2.5}$-*b*-$PEO_{1.3}$ in 500 µL toluene. The solution was vigorously hand-shaken for 30 seconds to create a water-in-oil emulsion. An interface was prepared by pouring 30 µL of the desired lipid (1.5 mg/mL) in toluene over 30 µL glucose solution (0.3 M glucose, 0.01 M HEPES, 0.15 M NaCl, pH 7.4) and allowed to stabilize for 2 hours. 75 µL of the above emulsion was slowly poured over the interface and the sample was immediately centrifuged (3 min, 500 g) at the same temperature the interface was formed. The resulting aGHUV were recovered in the lower phase. For fluorescence quenching experiments, 0.15 mol% PE-NBD (or DOPE-rhod) was added to the lipid solution. The fluorescence intensity was monitored over time on a spectrophotometer (λ_{exc}=488 nm) and data were normalized with the average fluorescence obtained for unquenched vesicles. For the preparation of reverse asymmetric vesicles, an interface was formed and left to rest for 30 mins with 3 mg/mL PBut-*b*-PEO. The emulsion was prepared with different concentrations of lipid and sonicated 10-15 seconds in a bath sonicator.

3. Results and discussion

A previously reported emulsion-centrifugation protocol[58] was adapted to afford asymmetric giant hybrid unilamellar vesicles with an asymmetric polymer-lipid membrane (aGHUV) consisting of an inner leaflet of poly(butadiene)-*b*-poly(ethylene oxide) ($PBut_{2.5}$-*b*-$PEO_{1.3}$) and an outer leaflet of 1-palmitoyl-2-oleoyl-sn-glycero-3-phosphocholine (POPC) lipid. Briefly, an emulsion of sucrose droplets in toluene stabilized by $PBut_{2.5}$-*b*-$PEO_{1.3}$ was poured over a POPC-stabilized glucose/toluene interface. With help of centrifugation and the difference of density between sucrose and glucose, the polymer-stabilized sucrose droplets cross the interface while getting coated with an outer monolayer of lipid, and the resulting POPC/ $PBut_{2.5}$-*b*-$PEO_{1.3}$ aGHUV can be recovered in the lower glucose phase (Figure 1. a)). Additionally, as shown in Figure 1. b), the reverse aGHUV with an outer leaflet of polymer can be obtained.

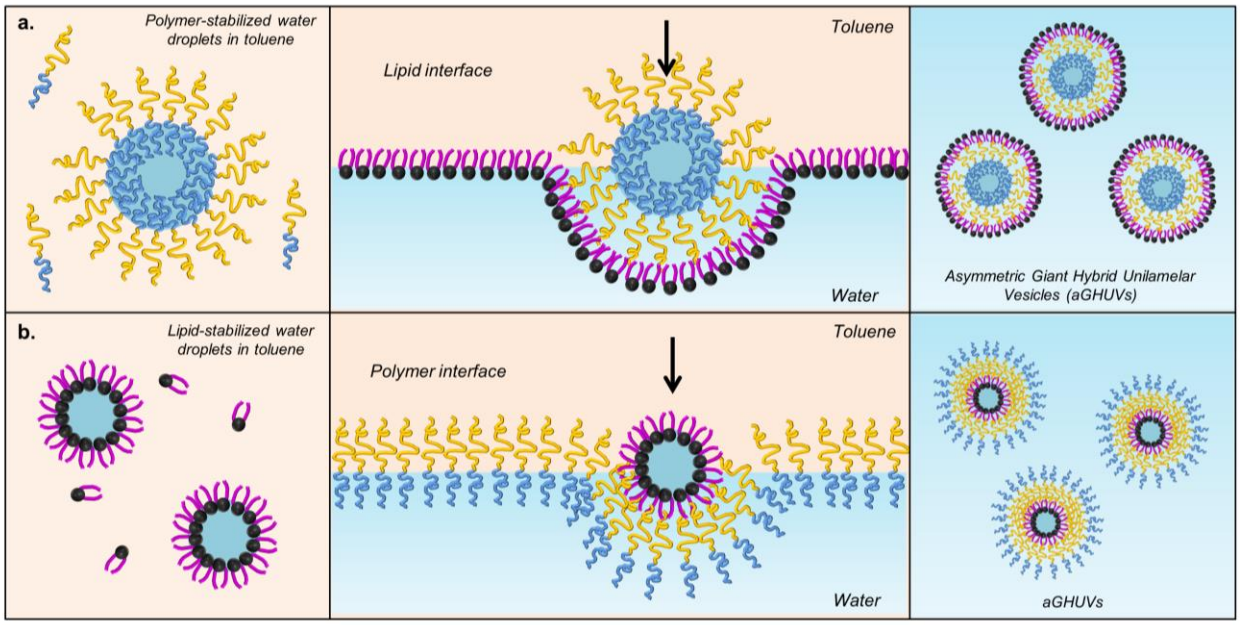

Figure 1. Schematic representation describing the preparation of asymmetric giant hybrid unilamellar vesicles (aGHUV). a) Preparation of aGHUV with an outer monolayer of lipid and inner monolayer of polymer and b) reverse aGHUV with an outer monolayer of polymer and inner monolayer of lipid.

Examples of asymmetric vesicles are scarce and most reported systems consist of a bilayer formed from two different lipid types[42–45] or two different polymers[51,52]. We believe that combining the properties of a lipid and a polymer to afford a hybrid asymmetric synthetic membrane would

improve functional and structural resemblance to a biological cell's membrane. To our knowledge there is only one reported example of such a system, but no clear evidence was provided to fully support the membrane asymmetry because of the impossibility to perform a fluorescence quenching assay.[45] The lipid-stabilized interface induced exposition of the lipid monolayer on the external side while the polymer monolayer is on the internal side of the vesicle. POPC was first chosen as a model lipid because it is one of the most represented lipids on the exoplasmic side of human red blood cells membrane and we hypothesized that it would add more flexibility and permeability as compared to a pure polymer membrane.[59] Similarly, keeping a polymer leaflet should provide increased stability and influence membrane diffusion properties in contrast with a purely lipidic bilayer. For confocal observation, the vesicles were loaded with fluorescein and the membrane was tagged with 0.1 wt% DOPE-rhod (λ_{exc}=561 nm), which has a preferential positioning in the lipid phase (Figure 2. a) and b)). The images show a homogeneous red membrane and a vesicle population with sizes ranging from 10 to 30 µm. This homogeneous distribution of the lipid can be qualitatively interpreted as a first sign of membrane asymmetry.

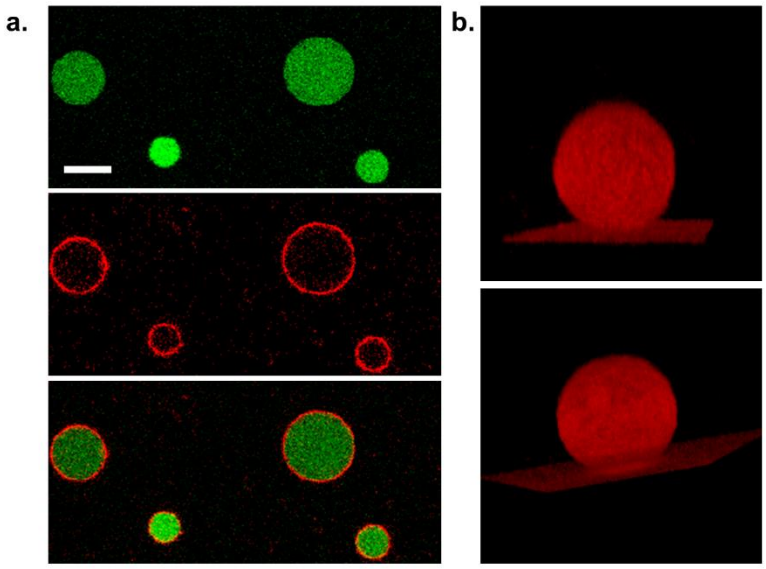

Figure 2. Confocal observations of POPC/PBut2.5-b-PEO1.3 asymmetric vesicles. a) The membrane is tagged with DOPE-rhodamine (red) and the vesicles are loaded with fluorescein (green). Top: emission of fluorescein; middle: emission of rhodamine; bottom: overlay. Scale bar: 10 µm. b) 3D reconstruction of an asymmetric vesicle (≈ 20 µm diameter). Two different views of the same vesicle (red channel).

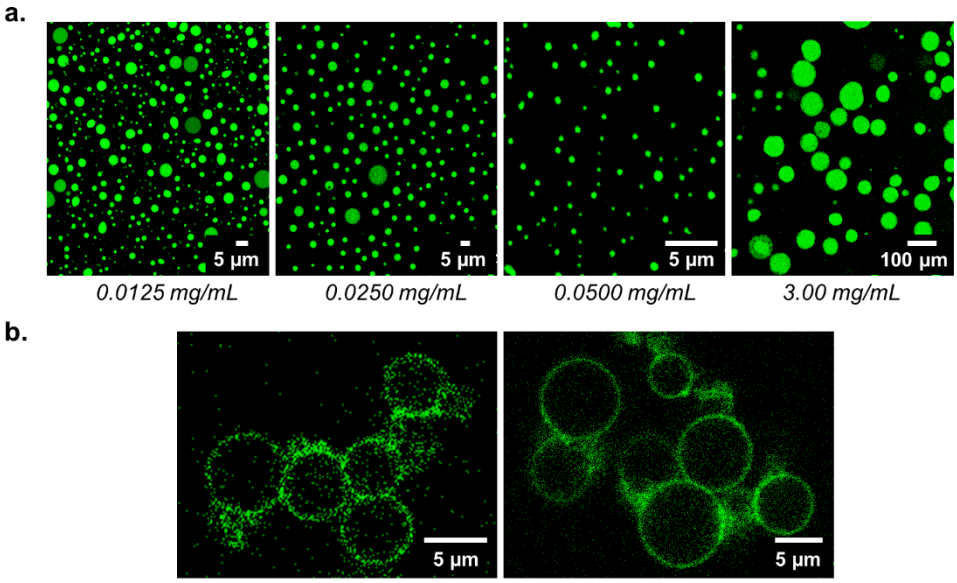

Figure 3. Asymmetric PBut2.5-b-PEO1.3 (outer leaflet) / POPC (inner leaflet) vesicles. Confocal images of a) POPC stabilized emulsions of sucrose droplets (0.1 mg/mL fluorescein) in toluene for different POPC concentrations and b) asymmetric PBut-b-PEO / POPC vesicles.

The reverse asymmetric vesicles (Scheme 1, route b), lipid facing the inside) could also be obtained using the same process. The emulsion conditions had to be optimized since obtaining a stable homogeneous emulsion with a lipid turned out to be more complex than with PBut-*b*-PEO. Different concentrations of POPC were tested and fluorescein was added to the sucrose solution to visualize the droplets under confocal microscopy, as shown in Figure 3. a). Using 0.025 mg/mL POPC gave the most stable emulsion with droplet sizes ranging from 4 to 6 µm approximately after sonication. Other concentrations either gave inhomogeneous droplets (0.0125 mg/mL) or too small or too large sizes (respectively 0.050 mg/mL and 3.0 mg/mL). Figure 3. b) shows the resulting reverse asymmetric polymer / lipid vesicles. The sizes (about 5 µm) are consistent with the sizes measured for the emulsion droplets which led to assume that the reverse asymmetric vesicles were effectively formed. However, owing to their limited yield and stability, these vesicles were not subjected to further experiments.

In order to demonstrate and quantify the asymmetric repartition of lipids in the membrane, a small fraction of 1,2-diphytanoyl-sn-glycero-3-phosphoethanolamine-N-(7-nitro-2-1,3-benzoxadiazol-

4-yl) (PE-NBD, λ_{exc}=488 nm) was added to the lipid interface in order to recover it in the external lipid monolayer after vesicle formation. NBD is a green fluorescent dye that can be reduced upon reaction with sodium dithionite leading to a complete loss of fluorescence.[60] A total loss of fluorescence from the vesicles after addition of dithionite to the solution would indicate 100 % asymmetry assuming that the quencher does not cross the membrane. To verify this assumption, we added a small fraction of PE-NBD in the $PBut_{2.5}$-*b*-$PEO_{1.3}$ solution in toluene used to form the emulsion as well as in the POPC solution for the interface. After vesicle formation, the green-tagged lipid was consequently present in both leaflets and the aGHUV could be visualized under confocal microscopy (Figure 4. a).

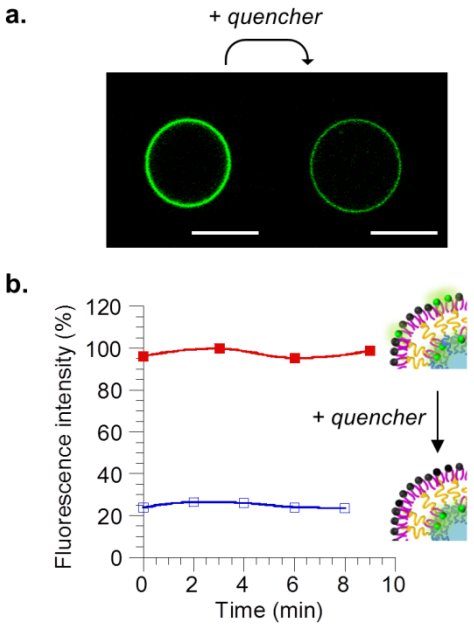

Figure 4. Spectral and microscopy analysis of POPC/ PBut2.5-b-PEO1.3 asymmetric vesicle solution incorporating PE-NBD on both sides of the membrane, before and after addition of dithionite as fluorescence quencher. a) Confocal microscopy observations before (left column) and after (right column) addition of dithionite. Scale bar = 10 µm. b) Fluorescence intensity of vesicle solution before (■) and after (□) addition of quencher.

Immediately after addition of the quencher (final concentration: 60 mM), a decrease of fluorescence intensity was observed on all of the vesicles. This decrease came from the reduction of NBD on the lipid outer leaflet of the membrane, which resulted in an extinction of the

fluorescence. The remaining fluorescence observed could be attributed to the PE-NBD inserted in the inner polymer monolayer. We further quantified the fraction of tagged lipid in each leaflet by means of fluorescence spectroscopy (Figure 4. b). Fluorescence of the tagged-vesicle solution was monitored over time before and after addition of dithionite. The results confirmed the confocal observations and showed that the major fraction of PE-NBD was inserted into the lipid monolayer during vesicle formation while the rest remained in the polymer inner layer. The fact that we did not observe a complete loss of fluorescence confirmed that dithionite does not cross the membrane most likely because of its negatively charged character that is known to prevent membrane penetration.

To further demonstrate the bilayer asymmetry, aGHUV vesicles were prepared with addition of a fraction of PE-NBD only in the lipid solution. One can hypothesize that if the vesicles are completely asymmetric, with an inner monolayer of polymer and outer monolayer of lipid, the fluorescence signal should completely disappear upon addition of the dithionite quencher to the vesicle solution. On the contrary, if lipids distribute symmetrically, or if a portion goes into the polymer phase, the fluorescence intensity should only decrease but not completely disappear upon reduction of the NBD dye. Figure 5. a) shows confocal images taken 6 hours after vesicle formation. Before addition of the quencher, the vesicles presented a homogeneous green membrane upon excitation at 488 nm. The addition of sodium dithionite to the vesicle solution (final concentration: 60 mM) resulted in a complete disappearance of the fluorescence signal, suggesting a total asymmetry of the vesicle membrane. In order to get more quantitative measurements on an ensemble of vesicles, the same experiments were performed by fluorescence spectroscopy: no residual fluorescence after addition of the quencher could be detected, confirming the complete asymmetric character of the membrane, with the lipid constituting the external leaflet of the membrane (Figure 5. b)). To demonstrate the versatility of our protocol, the same experiment was conducted with 1,2-dimyristoyl-sn-glycero-3-phosphocholine (DMPC) instead of POPC, (see supporting information Figure S1). Again, a complete loss of fluorescence upon addition of sodium dithionite was observed, confirming the membrane asymmetry of the formed vesicles.

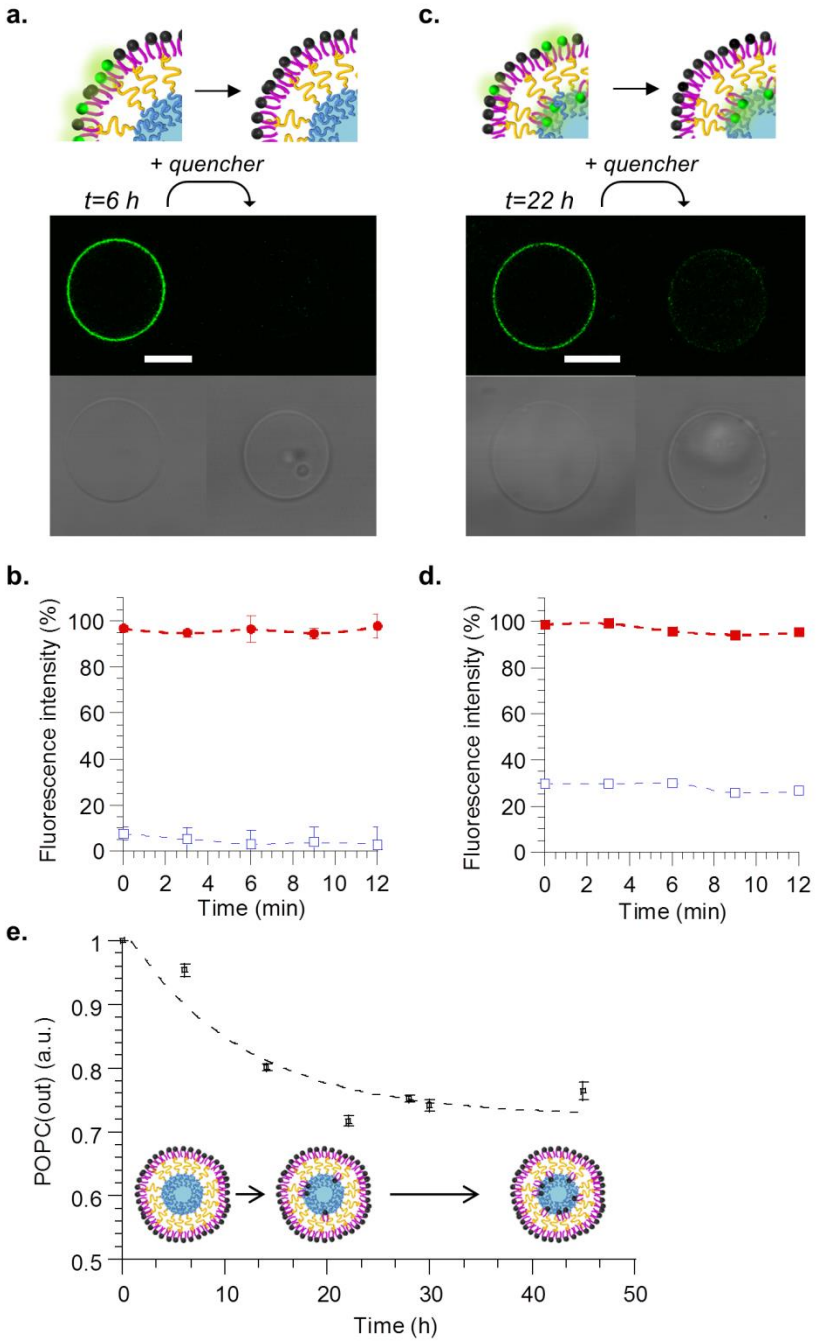

Figure 5. Spectral analyses and microscopy observation of asymmetric vesicles as function of time. Confocal microscopy observations a) after 6 hours and c) after 22 hours before (left column) and after (right column) addition of dithionite quencher. Top images: NBD emission, bottom images: white light. Scale bar = 10 μm. Fluorescence intensity of vesicle suspension b) after 6 hours and d) after 22 hours, before (■) and after (□) addition of quencher. e) Kinetics of POPC transverse diffusion from the outer to the inner leaflet of the membrane. Measurements were performed in triplicate at 25 °C. For every time point, data were normalized with the total fluorescence intensity of the vesicle suspension before addition of the quencher.

An important characteristic of biological membranes resides in the ability of lipids to move from the exoplasmic side to the cytoplasmic side and *vice versa*.[61] This transverse diffusion, also called flip-flop, is energetically unfavorable and happens at rather slow rates and with the help of enzymes. Flip-flop rates have been evaluated for different types of lipids and lipid bilayers in several synthetic systems such as supported bilayers or large unilamellar vesicles.[47,62–64] However, owing to the much larger sizes of biological cells, membrane properties such as curvature (and thus lipid diffusion rates) would be more accurately represented by giant vesicle systems.[65] We thus investigated POPC trans-bilayer diffusion on the aGHUV by following the stability of the asymmetry over time with fluorescence spectroscopy measurements. Figure 5. c) shows confocal images taken 22 hours after vesicle formation, before and after addition of sodium dithionite quencher. In contrast with vesicles visualized after 6 hours, some residual fluorescence on the membrane could be observed, suggesting lipid flip-flop to the polymer leaflet. One should note that the diffusion rates are attributed to the PE-NBD lipid across the polymer-lipid bilayer. We could estimate by fluorescence spectroscopy that 75% of the initial fluorescence signal on the outer monolayer was lost following the addition of quencher after 22 hours (Figure 5. d). We then followed the kinetics of lipid flip-flop to estimate the half-life for POPC to move from the outer to the inner side of the membrane, assuming that the dye exhibits the same fluorescence on both sides of the membrane. Therefore the loss of fluorescence was assumed to be directly related to the amount of POPC diffusing in the inner leaflet. Figure 5. e) shows the evolution of remaining POPC on the outside of the membrane (POPC(out)) after several hours and allowed us to determine a half-life around 7.5 hours, a value that is consistent with previously reported values of 5-6 hours for giant asymmetric lipid vesicles.[44]

In addition, it is well established that lipid transverse diffusion across the cell's bilayer membrane occurs at much slower rates than translational diffusion, *i.e.* the motion of lipids in one monolayer, which was first evidenced in 1970.[66] Translational or lateral diffusion has been quantified in synthetic membrane systems using the standard fluorescence recovery after photobleaching (FRAP) technique which consists in measuring the recovery of fluorescence in a determined region of interest of a membrane (ROI) that was exposed to photo-bleaching.[67] The motion of unbleached lipids in the membrane allows a recovery of fluorescence in the bleached ROI with kinetics that can be monitored and fitted with appropriate models. Lateral diffusion coefficients in the literature for pure POPC or pure PBut-*b*-PEO giant vesicles, were reported to be respectively D=0.22 and

9.8 μm^2/s.[68] Using giant hybrid unilamellar vesicles presenting homogenous distribution of the lipid and polymer content at the micron-scale, it was shown that lipid lateral diffusion coefficient could be modulated by the lipid/polymer composition. We thus hypothesized that an asymmetric POPC/PBut-*b*-PEO membrane would give intermediate diffusion values closer to those observed in biological membranes which are around 1 μm^2/s.[69] We used confocal microscopy imaging (Figure 6. a)) and the FRAP analyzer software to measure the diffusion coefficients of a DOPE-rhodamine (DOPE-rhod) probe inserted into the POPC outer monolayer of the aGHUV for different temperatures and different membrane types. Rhodamine was chosen as a fluorescent probe because of its photo-stability as compared with other dyes. After collecting the intensity profiles from the confocal images, we analyzed the results with the FRAP software. The data were first double-normalized to remove the fluorescence variations between samples, by taking into account the background fluorescence and the slow bleaching of the dye during fluorescence recovery at low laser intensity. We used the circular spot diffusion model described by the following equation to fit the data:

$$FRAP(t) = a_0 + a_1 . e^{-\frac{\tau}{2(t-t_{bleach})}} . \left(I_0\left(\frac{\tau}{2(t-t_{bleach})}\right) + I_1\left(\frac{\tau}{2(t-t_{bleach})}\right)\right)$$

with $\tau = \frac{\omega^2}{D}$, where ω is the radius of the bleach spot, D the diffusion coefficient, a_0 and a_1 normalizing coefficients and t_{bleach} the bleach time.

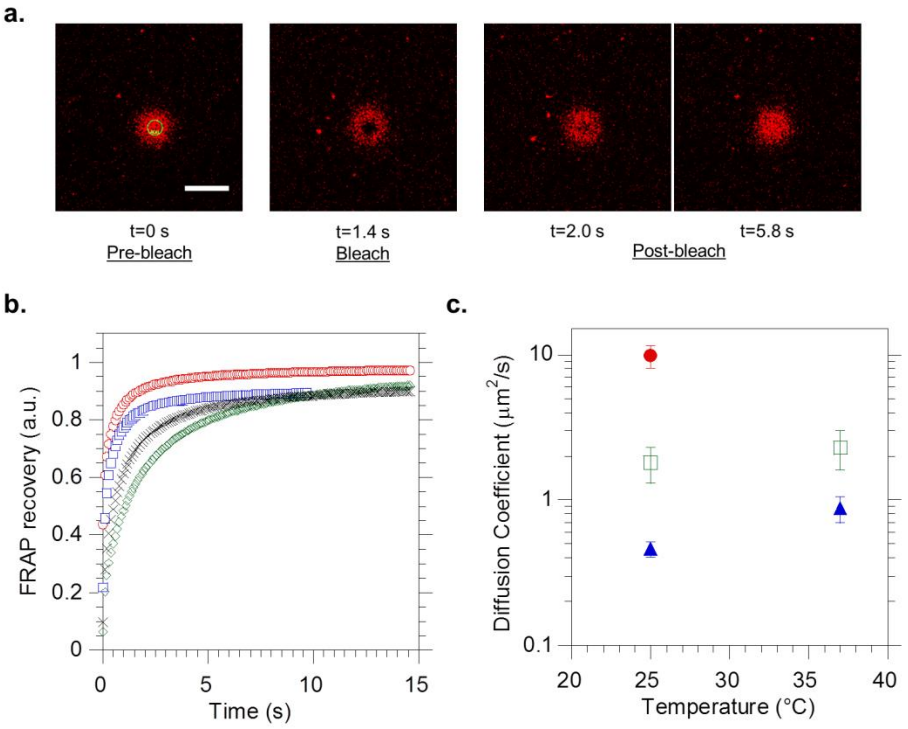

*Figure 6. FRAP measurements on DOPE-rhodamine inserted into the membrane of PBut$_{2.5}$-b-PEO$_{1.3}$ and asymmetric POPC/ PBut$_{2.5}$-b-PEO$_{1.3}$ (aGHUV) giant vesicles. a) Confocal images of a vesicle during the three phases of FRAP experiment, namely pre-beach, bleach and post-bleach. We observe the recovery of fluorescence inside the ROI with time. Scale bar: 10 µm. b) Normalized fluorescence intensity profiles during recovery. Pure PBut$_{2.5}$-b-PEO$_{1.3}$ giant vesicles (25 °C green, 37 °C black), POPC/PBut$_{2.5}$-b-PEO$_{1.3}$ AGHUV (25 °C red, 37 °C blue). c) Measured lipid lateral diffusion coefficients (**D** (µm^2/s)) for different membranes and temperatures: pure POPC giant vesicles (●) (ref [39]), POPC/PBut$_{2.5}$-b-PEO$_{1.3}$ aGHUV (□), pure PBut$_{2.5}$-b-PEO$_{1.3}$ giant vesicles (▲). Measurements were performed and averaged on 5-10 vesicles for each system.*

As can be seen in Figure 6. a), FRAP measurements were performed at the top of the giant vesicles that consequently appear as fluorescent disks under confocal observation. The experiment can be decomposed into three different phases: the pre-bleach phase where the ROI chosen on the top of the vesicles is irradiated at low laser power, followed by a defined bleaching phase at high laser power and a longer post-bleach phase to monitor the recovery of fluorescence inside the ROI induced by the diffusion of lipids in the POPC outer leaflet. Figure 6. b) shows the obtained intensity profiles during the post-bleach phase after normalization. These data were fitted with the model described previously to obtain the lateral diffusion coefficients (D, (µm^2/s)) of the probe in

the lipid monolayer (Figure 6. c)). For POPC/$PBut_{2.5}$-*b*-$PEO_{1.3}$ aGHUV we found D=1.8±0.50 $\mu m^2/s$ for DOPE-rhod at 25 °C. Under the same experimental conditions, the diffusion coefficient for DOPE-rhod in pure $PBut_{2.5}$-*b*-$PEO_{1.3}$ giant vesicles was found to be D=0.46±0.055 $\mu m^2/s$ and it has been shown that for pure POPC giant vesicles D=9.8±1.7 $\mu m^2/s$.[68] Therefore, as for GHUV, an intermediate diffusion coefficient value is found, and shows that despite the asymmetric character of the membrane, the lipid lateral diffusion coefficient is lowered by the copolymer chains, suggesting some interdigitation between lipids and copolymer chains in the membrane. The lipid lateral diffusion has been also evaluated in aGHUV at 37°C and is found to be 2.3±0.7 $\mu m^2/s$ confirming the impact of temperature on membrane's fluidity,[30,70,71] and the relevance of our systems, with a lateral diffusion coefficient close to those reported in cells' membrane.

Overall, our technique provides a method for controlled assembly of giant vesicles exhibiting an asymmetric lipid-polymer membrane that can easily be tuned. The qualitative confocal observations and the quantitative diffusion coefficient and flip-flop values that were measured are intermediate between those of pure lipid or pure polymer membranes and support the presence of an asymmetric membrane. Because of their biological relevance, we believe that synthetic vesicles possessing an asymmetric bilayer constitute appropriate models to get more insight into the cell membrane diffusion dynamics.

4. Conclusion

We have demonstrated for the first time the preparation of giant hybrid polymer-lipid vesicles exhibiting total asymmetry with an outer leaflet of tunable lipid type and inner leaflet of copolymer. We also showed that the reverse asymmetric structures with the lipid leaflet facing the inside of the vesicle could be obtained. The total asymmetry was proven using a fluorescence quenching assay. Interestingly the lateral lipid diffusion coefficient is perturbed by the presence of the copolymer chains, probably because of slight interdigitation between the two leaflets, leading to a lateral diffusion coefficient comparable to the ones known for lipids in biological cells. The originality of our approach was to prepare a mix-system combining lipid and polymer advantages to afford a cell-sized giant vesicle with an asymmetric membrane. As compared with previously reported lipid/lipid or polymer/polymer asymmetric membranes, this approach represents a step forward towards preparing model systems for cell biomimicry.

5. References

[1] J. M. Benyus, *Biomimicry: Innovation Inspired by Nature*, Harper Collins, **2009**.

[2] R. Chandrawati, F. Caruso, *Langmuir* **2012**, *28*, 13798–13807.

[3] M. Marguet, C. Bonduelle, S. Lecommandoux, *Chem. Soc. Rev.* **2012**, *42*, 512–529.

[4] A. Perro, C. Nicolet, J. Angly, S. Lecommandoux, J.-F. Le Meins, A. Colin, *Langmuir* **2011**, *27*, 9034–9042.

[5] H. C. Shum, Y. Zhao, S.-H. Kim, D. A. Weitz, *Angew. Chem. Int. Ed.* **2011**, *50*, 1648–1651.

[6] H.-C. Chiu, Y.-W. Lin, Y.-F. Huang, C.-K. Chuang, C.-S. Chern, *Angew. Chem. Int. Ed.* **2008**, *47*, 1875–1878.

[7] M. Marguet, L. Edembe, S. Lecommandoux, *Angew. Chem. Int. Ed.* **2012**, *51*, 1173–1176.

[8] A. Peyret, E. Ibarboure, A. Tron, L. Beauté, R. Rust, O. Sandre, N. D. McClenaghan, S. Lecommandoux, *Angew. Chem.* **2017**, *129*, 1588–1592.

[9] Y. Elani, A. Gee, R. V. Law, O. Ces, *Chem. Sci.* **2013**, *4*, 3332.

[10] L. Hosta-Rigau, S. F. Chung, A. Postma, R. Chandrawati, B. Städler, F. Caruso, *Adv. Mater.* **2011**, *23*, 4082–4087.

[11] S.-H. Kim, H. C. Shum, J. W. Kim, J.-C. Cho, D. A. Weitz, *J. Am. Chem. Soc.* **2011**, *133*, 15165–15171.

[12] C. Schmitt, A. H. Lippert, N. Bonakdar, V. Sandoghdar, L. M. Voll, *Front. Bioeng. Biotechnol.* **2016**, *4*, 19.

[13] A. H. Chen, P. A. Silver, *Trends Cell Biol.* **2012**, *22*, 662–670.

[14] L. Schoonen, J. C. M. van Hest, *Adv. Mater.* **2016**, *28*, 1109–1128.

[15] M. Marguet, O. Sandre, S. Lecommandoux, *Langmuir* **2012**, *28*, 2035–2043.

[16] J. S. Lee, W. Zhou, F. Meng, D. Zhang, C. Otto, J. Feijen, *J. Control. Release Off. J. Control. Release Soc.* **2010**, *146*, 400–408.

[17] H.-K. Lee, S. Soukasene, H. Jiang, S. Zhang, W. Feng, S. I. Stupp, *Soft Matter* **2008**, *4*, 962–964.

[18] C. C. Campillo, A. P. Schroder, C. M. Marques, B. Pépin-Donat, *Mater. Sci. Eng. C* **2009**, *29*, 393–397.

[19] L. Limozin, E. Sackmann, *Phys. Rev. Lett.* **2002**, *89*, 168103.

[20] R. J. R. W. Peters, M. Marguet, S. Marais, M. W. Fraaije, J. C. M. van Hest, S. Lecommandoux, *Angew. Chem. Int. Ed.* **2014**, *53*, 146–150.

[21] N. P. Kamat, J. S. Katz, D. A. Hammer, *J. Phys. Chem. Lett.* **2011**, *2*, 1612–1623.

[22] Y. Elani, R. V. Law, O. Ces, *Phys. Chem. Chem. Phys.* **2015**, *17*, 15534–15537.

[23] G. Murtas, Y. Kuruma, P. Bianchini, A. Diaspro, P. L. Luisi, *Biochem. Biophys. Res. Commun.* **2007**, *363*, 12–17.

[24] V. Noireaux, A. Libchaber, *Proc. Natl. Acad. Sci. U. S. A.* **2004**, *101*, 17669–17674.

[25] K. Kurihara, M. Tamura, K. Shohda, T. Toyota, K. Suzuki, T. Sugawara, *Nat. Chem.* **2011**, *3*, 775–781.

[26] O. Kreft, M. Prevot, H. Möhwald, G. B. Sukhorukov, *Angew. Chem. Int. Ed.* **2007**, *46*, 5605–5608.

[27] B. Städler, R. Chandrawati, A. D. Price, S.-F. Chong, K. Breheney, A. Postma, L. A. Connal, A. N. Zelikin, F. Caruso, *Angew. Chem. Int. Ed.* **2009**, *48*, 4359–4362.

[28] R. Chandrawati, P. D. Odermatt, S.-F. Chong, A. D. Price, B. Städler, F. Caruso, *Nano Lett.* **2011**, *11*, 4958–4963.

[29] P.-Y. Bolinger, D. Stamou, H. Vogel, *Angew. Chem. Int. Ed.* **2008**, *47*, 5544–5549.

[30] S. J. Singer, G. L. Nicolson, *Science* **1972**, *175*, 720–731.
[31] M. S. Bretscher, *Nature* **1972**, *236*, 11–12.
[32] P. F. Devaux, *Biochemistry (Mosc.)* **1991**, *30*, 1163–1173.
[33] J. E. Rothman, J. Lenard, *Science* **1977**, *195*, 743–753.
[34] R. B. Gennis, in *Biomembranes*, Springer New York, **1989**, pp. 138–165.
[35] H. Herrmann, *Comput. Math. Appl.* **1986**, *12*, 155–167.
[36] B. Fadeel, D. Xue, *Crit. Rev. Biochem. Mol. Biol.* **2009**, *44*, 264–277.
[37] V. A. Fadok, P. M. Henson, *Curr. Biol.* **1998**, *8*, R693–R695.
[38] V. A. Fadok, D. R. Voelker, P. A. Campbell, J. J. Cohen, D. L. Bratton, P. M. Henson, *J. Immunol. Baltim. Md 1950* **1992**, *148*, 2207–2216.
[39] B. Verhoven, R. A. Schlegel, P. Williamson, *J. Exp. Med.* **1995**, *182*, 1597–1601.
[40] D. Marquardt, B. Geier, G. Pabst, *Membranes* **2015**, *5*, 180–196.
[41] F. Fernandez-Trillo, L. M. Grover, A. Stephenson-Brown, P. Harrison, P. M. Mendes, *Angew. Chem. Int. Ed.* **2017**, *56*, 3142–3160.
[42] D. L. Richmond, E. M. Schmid, S. Martens, J. C. Stachowiak, N. Liska, D. A. Fletcher, *Proc. Natl. Acad. Sci. U. S. A.* **2011**, *108*, 9431–9436.
[43] P. C. Hu, S. Li, N. Malmstadt, *ACS Appl. Mater. Interfaces* **2011**, *3*, 1434–1440.
[44] K. Kamiya, R. Kawano, T. Osaki, K. Akiyoshi, S. Takeuchi, *Nat. Chem.* **2016**, *8*, 881–889.
[45] S. Pautot, B. J. Frisken, D. A. Weitz, *Proc. Natl. Acad. Sci.* **2003**, *100*, 10718–10721.
[46] T. Hamada, Y. Miura, Y. Komatsu, Y. Kishimoto, M. Vestergaard, M. Takagi, *J. Phys. Chem. B* **2008**, *112*, 14678–14681.
[47] W.-C. Lin, C. D. Blanchette, T. V. Ratto, M. L. Longo, *Biophys. J.* **2006**, *90*, 228–237.
[48] G. J. Hardy, R. Nayak, S. Zauscher, *Curr. Opin. Colloid Interface Sci.* **2013**, *18*, 448–458.
[49] I. Visco, S. Chiantia, P. Schwille, *Langmuir ACS J. Surf. Colloids* **2014**, *30*, 7475–7484.
[50] Z. Yu, F. Tantakitti, L. C. Palmer, S. I. Stupp, *Nano Lett.* **2016**, *16*, 6967–6974.
[51] Y. Zhang, F. Wu, W. Yuan, T. Jin, *J. Control. Release Off. J. Control. Release Soc.* **2010**, *147*, 413–419.
[52] A. F. Mason, P. Thordarson, *ACS Macro Lett.* **2016**, 1172–1175.
[53] S. K. Lim, A. S. W. Wong, H.-P. M. de Hoog, P. Rangamani, A. N. Parikh, M. Nallani, S. Sandin, B. Liedberg, *Soft Matter* **2017**, *13*, 1107–1115.
[54] J.-F. Le Meins, C. Schatz, S. Lecommandoux, O. Sandre, *Mater. Today* **2013**, *16*, 397–402.
[55] M. Schulz, W. H. Binder, *Macromol. Rapid Commun.* **2015**, *36*, 2031–2041.
[56] T. P. T. Dao, A. Brûlet, F. Fernandes, M. Er-Rafik, K. Ferji, R. Schweins, J.-P. Chapel, A. Fedorov, M. Schmutz, M. Prieto, et al., *Langmuir* **2017**, *33*, 1705–1715.
[57] T. P. T. Dao, F. Fernandes, E. Ibarboure, K. Ferji, M. Prieto, O. Sandre, J.-F. L. Meins, *Soft Matter* **2017**, *13*, 627–637.
[58] S. Pautot, B. J. Frisken, D. A. Weitz, *Langmuir* **2003**, *19*, 2870–2879.
[59] G. van Meer, D. R. Voelker, G. W. Feigenson, *Nat. Rev. Mol. Cell Biol.* **2008**, *9*, 112–124.
[60] J. C. McIntyre, R. G. Sleight, *Biochemistry (Mosc.)* **1991**, *30*, 11819–11827.
[61] F.-X. Contreras, L. Sánchez-Magraner, A. Alonso, F. M. Goñi, *FEBS Lett.* **2010**, *584*, 1779–1786.
[62] K. Matsuzaki, O. Murase, N. Fujii, K. Miyajima, *Biochemistry (Mosc.)* **1996**, *35*, 11361–11368.
[63] H. M. McConnell, R. D. Kornberg, *Biochemistry (Mosc.)* **1971**, *10*, 1111–1120.
[64] J. Bai, R. E. Pagano, *Biochemistry (Mosc.)* **1997**, *36*, 8840–8848.
[65] T. Zhu, Z. Jiang, Y. Ma, *Colloids Surf. B Biointerfaces* **2012**, *97*, 155–161.
[66] L. D. Frye, M. Edidin, *J. Cell Sci.* **1970**, *7*, 319–335.

[67] D. Axelrod, D. E. Koppel, J. Schlessinger, E. Elson, W. W. Webb, *Biophys. J.* **1976**, *16*, 1055–1069.
[68] J. Nam, P. A. Beales, T. K. Vanderlick, *Langmuir* **2011**, *27*, 1–6.
[69] J. M. Berg, J. L. Tymoczko, L. Stryer, in *Biochem. 5th Ed.*, W. H. Freeman, New York, **2002**.
[70] A. J. Jin, M. Edidin, R. Nossal, N. L. Gershfeld, *Biochemistry (Mosc.)* **1999**, *38*, 13275–13278.
[71] A. Nenninger, G. Mastroianni, A. Robson, T. Lenn, Q. Xue, M. C. Leake, C. W. Mullineaux, *Mol. Microbiol.* **2014**, *92*, 1142–1153.

6. Supporting information

DMPC (outer layer) / PBut$_{2.5}$-b-PEO$_{1.3}$ (inner layer) asymmetric vesicles

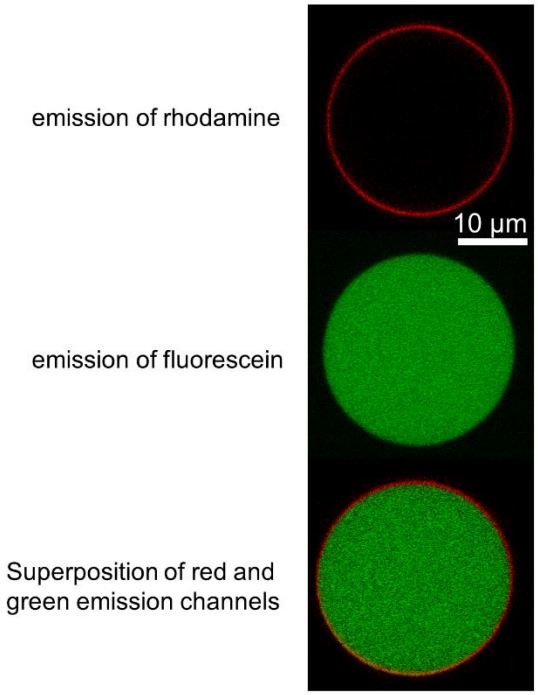

Figure S 1. Confocal observation of DMPC/PBut$_{2.5}$-b-PEO$_{1.3}$ asymmetric vesicles. The membrane is tagged with DOPE-rhodamine (red) and the vesicles are loaded with fluorescein (green). Top: emission of rhodamine; middle: emission of fluorescein; bottom: overlay.

CHAPTER 3: ***Liposomes in Polymersomes (LiPs), multi-compartment system with temperature-triggered release***

Adapted from:

Liposomes in Polymersomes (LiPs), multi-compartment system with temperature-triggered release.

Ariane Peyret, Emmanuel Ibarboure, Natassa Pippa, Sebastien Lecommandoux*, *Langmuir,* **2017**, *33*, 7079-7085.

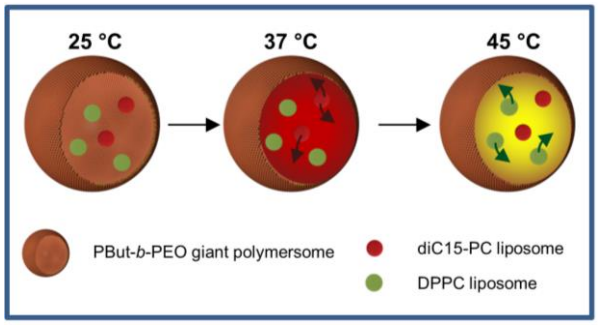

Abstract: Multi-compartmentalization is a key feature of eukaryotic cells, allowing separation and protection of species within the membrane walls. During the last years, several methods have been reported to afford synthetic multi-compartment lipidic or polymeric vesicles that mimic biological cells and that allow cascade chemical or enzymatic reactions within their lumen. We hereby report on the preparation and study of liposomes in polymersomes (LiPs) systems. We discuss on the loading and co-loading of lipidic nano-vesicles made of 1-palmitoyl-2-oleoyl-sn-glycero-3-phosphocholine (POPC), 1,2-dimyristoyl-sn-glycero-3-phosphocholine (DMPC), 1,2-dipentadecanoyl-*sn*-glycero-3-phosphocholine (diC15-PC), or 1,2-dipalmitoyl-*sn*-glycero-3-phosphocholine (DPPC) inside the lumen of giant poly(butadiene)-*b*-poly(ethylene oxide) (PBut-*b*-PEO) polymersomes. These LiPs systems were characterized by confocal microscopy and UV-visible spectroscopy. We further demonstrate that we can achieve controlled sequential release of dyes from diC15-PC and DPPC liposomes at defined temperatures inside the giant PBut-*b*-PEO polymersomes. This controlled release could be used as a means to initiate cascade reactions on demand in confined micro-reactors.

1. Introduction

Lipidic vesicles, currently named liposomes, are self-assembled colloidal systems that consist of one or more phospholipid bilayers. They can be prepared through a number of methods such as thin film hydration, sonication or extrusion to afford small to large unilamellar or multilamellar spherical vesicles.[1] Due to their tunable size, as well as their hydrophobic (bilayer membrane) or hydrophilic (aqueous core) character, they can load a variety of species. Liposomes were especially developed of the last 30 years in the areas ranging from personal to health care, and especially in pharmaceutical nanotechnology.[1–3] In addition, their biocompatibility and their structure make them suitable candidates as models of biological membranes, that are composed by about 60% of phospholipids.[4]

Over the last decade, polymersomes have been developed and used as structural analogues of liposomes in order to overcome the stability issues and the chemical versatility limitations of such lipidic vesicles.[5] Polymer-based vesicle are obtained from the controlled self-assembly of amphiphilic block copolymers through a number of ways.[6,7] As for liposomes, they can

enclose hydrophilic compounds, but also hydrophobic ones in large quantities, and both, and are nowadays presented as promising systems to be used as nanocarriers and artificial cells or organelles.[8–11] The synthetic nature of block copolymers makes them highly versatile materials with tunable structural and mechanical properties. By varying the copolymer molecular weight, it is possible to tune the membrane thickness of the polymersomes, and thus, to control membrane properties such as permeability, elasticity and mechanical stability.[7,12,13] The higher molecular weight of polymers as compared with lipids make polymersomes more stable and robust than liposomes.[5] In addition, the chemical versatility conferred by polymers allow the design of complex stimuli-responsive vesicles for triggered cargo-release.[14–16]

The mixing of different biomaterials (i.e. lipids and polymers) is a new attractive orientation that widens the use of vesicular carrier platforms for cell mimicry and/or targeting and controlled release.[13,17–21] Recently, multi-compartmentalized systems have been developed both for controlled delivery purpose and as models for cell biomimicry.[22,23] Compartmentalization in eukaryotic cells is a crucial feature that allows separation and protection of species as well as simultaneous different enzymatic reaction to take place independently in a confined space with high spatio-temporal control.[9,11,24–31] A number of techniques have been developed to afford such multi-compartment systems, such as double-emulsion, film rehydration, layer-by-layer assembly, micro-fluidics or phase transfer of emulsion droplets over an interface, also referred as emulsion-centrifugation.[32–40] Liposomes in liposomes, also named vesosomes, are the first compartmentalized systems that appeared in the literature from Zasadzinski.[41–43] More recently, polymeric vesosomes (polymersomes in polymersomes, PiPs) were developed by emulsion-centrifugation and used as scaffolds for cascade enzymatic reactions.[44,45] These complex systems both mimic the structural and functional characteristics of the eukaryotic cell and thus provide a simplified biomimetic model that can serve as a tool for the understanding and the study of complex cellular mechanism.

In this context, the aim of this contribution is to design and develop multi-compartmentalized systems composed of nano-sized liposomes encapsulated into micron-sized polymersomes. Our main purpose is to combine different vehicles in order to produce mixed multi-compartmentalized systems based on biologically inspired technology. As compared with purely lipidic or purely polymeric vesosomes, these systems benefit both from the softness and thermosensitivity conferred by lipids and the robustness and chemical versatility of polymers.

The main feature of LiPs is the ability to trigger the *in vitro* release of species from the inner liposomes inside a robust polymeric vesicle through temperature-controlled permeability. In addition, the temperature-controlled permeability of liposomes can allow triggered release of species in the lumen of the giant polymersomes. This could give access to controlled cascade chemical or enzymatic reactions confined in micro-compartments. Confocal microscopy and specific labeling using dyes was used to access the multi-compartmentalized structure and morphology. As a proof of concept, we show an *in vitro* double-triggered release of dyes from the encapsulated liposomes using temperature variations as well as a thermally-initiated enzymatic reaction.

2. Experimental section

2.1. Materials

The phospholipids used for the liposomal systems were 1-palmitoyl-2-oleoyl-sn-glycero-3-phosphocholine (POPC), 1,2-dimyristoyl-sn-glycero-3-phosphocholine (DMPC), 1,2-dipentadecanoyl-*sn*-glycero-3-phosphocholine (diC15-PC), and 1,2-dipalmitoyl-s*n*-glycero-3-phosphocholine (DPPC). The dyes used were 1,2-diphytanoyl-s*n*-glycero-3-phosphoethanolamine-N-(7-nitro-2-1,3-benzoxadiazol-4-yl) (NBD) (ammonium salt) and 1,2-dioleoyl-s*n*-glycero-3-phosphoethanolamine-N-(lissamine rhodamine B sulfonyl) (LRB, ammonium salt). These materials were purchased from Avanti Polar Lipids Inc., (Albaster, AL, USA) and used without further purification. Poly(butadiene)-*b*-poly(ethylene oxide) $PBut_{46}$-*b*-PEO_{30} (Mn x 10^3 PBut-*b*-PEO: 2.5-*b*-1.3; Mw/Mn 1.04) was ordered from Polymer Source (P18422-BdEO, 89% 1,2-addition of butadiene). Chloroform and all other solvents and reagents used were of analytical grade and purchased from Sigma–Aldrich Chemical Co.

2.2. Methods

UV-Visible experiments were carried out on a Spectra Max M2 microplate spectrophotometer (Molecular Devices). Dynamic Light Scattering (DLS) was used to determine the average size of extruded liposomes in solution. The measurements were performed on a Malvern ZetaSizer Nano ZS instrument with detection at 90°. Samples were analyzed at room temperature. Laser scanning confocal microscopy images were acquired on an inverted Leica TCS SP5 microscope

equipped with an HCX PL APO 63×, NA 1.4 oil immersion objective in fluorescence mode. Samples (≈20 µL) were injected in a homemade chamber that was sealed to prevent evaporation. The laser outputs were controlled via the Acousto-Optical Tunable filter and the two collection windows using the Acousto-Optical Beam Splitter and photomultipliers as follows: NBD and fluorescein were excited with an argon laser at 488 nm, rhodamine was excited at 561 nm and methylene blue at 633 nm. The Helium-Neon laser at 633 nm (10 %) was also used in transmission mode. For the dye-release studies, the microscope was equipped with a heating and cooling stage (PE120XY stage size 160*116mm) from Linkam Scientific Instruments,UK, with temperature range: -25°C to 120°C, heating/cooling rate: 0.1 to 20°C/min, and control and stability: +/-0.1°C.

2.3.Preparation of giant unilamellar polymersomes

Poly(butadiene)-*b*-poly(ethylene oxide) ($PBut_{2.5}$-*b*-$PEO_{1.3}$) giant unilamellar vesicles (GUVs) were prepared by a previously reported emulsion-centrifugation method.[46] Briefly, 5 µL of sucrose 0.38 M was poured into 3 mg/mL $PBut_{2.5}$-*b*-$PEO_{1.3}$ in 500 µL toluene. The solution was vigorously hand-shaken for 30 seconds to create a water-in-oil emulsion. An interface was prepared by pouring 30 µL of $PBut_{2.5}$-*b*-$PEO_{1.3}$ (3 mg/mL) in toluene over 30 µL glucose 0.38 M and allowed to stabilize for 30 minutes. 60 µL of the above emulsion was slowly poured over the interface and the sample was immediately centrifuged (3 min, 500 g, ambient temperature). The resulting polymersomes were recovered in the lower phase.

2.4.Preparation of liposomes and incorporation into giant polymersomes

Different types of liposomes were prepared using the thin-film hydration method followed by extrusion. POPC, DMPC, diC15-PC or DPPC lipids were dissolved in chloroform/methanol (9:1 v/v; 10 mg/mL). The dyes 1,2-dioleoyl-*sn*-glycero-3-phosphoethanolamine-N-(lissamine rhodamine B sulfonyl) (ammonium salt) or 1,2-diphytanoyl-*sn*-glycero-3-phosphoethanolamine-N-(7-nitro-2-1,3-benzoxadiazol-4-yl) (ammonium salt) were added to the lipid solutions (0.1 mg/mL). The resulting solution was evaporated using a rotary evaporator and a thin film was formed by slow removal of the solvent. The films were maintained under vacuum for at least 24h in a desiccator to remove traces of solvent and then rehydrated in sucrose 0.38 M, by slowly stirring for 1h in a water bath above the phase transition temperature

of lipids (-2 °C for POPC, 23 °C for DMPC, 35 °C for diC15-PC and 41 °C for DPPC). In the case of fluorescein or methylene blue encapsulation, the films (DPPC and diC15-PC) were hydrated respectively with 80 mM fluorescein in sucrose 0.30 M and 10 mM methylene blue in sucrose 0.37 M. The resultant multilamellar vesicles were subjected to extrusion (Avanti Mini-Extruder, Avanti Polar Lipids, 11 times/cycles of extrusion) in order to produce large unilamellar vesicles. Removal of free dye was achieved by performing a size exclusion chromatography column packed with a Sephadex G-100 gel (15 cm). For the encapsulation into the giant polymersomes, the emulsion centrifugation protocol described above was followed. The liposomes suspension was used to form the emulsion. The concentration of the glucose solution for the interface was adjusted to the same osmotic pressure as the liposomes in sucrose solution to avoid any destabilization.

2.5.Estimation of dilution factor after dye release in the GUVs

We estimated the value of the dilution factor if the total internal volume of the liposomes encapsulated in 1 GUV is emptied inside the lumen of the vesicle. The details of the calculation are given as an example for 100 nm liposomes composed of DPPC lipid (9.1 mM) encapsulated into a 20 μm polymersome. The total number of DPPC lipid molecules per liposomes (N_{Tot}) can be calculated with equation (1):

$$N_{Tot} = \frac{[4\pi\left(\frac{d}{2}\right)^2 + 4\pi\left[\left(\frac{d}{2}\right) - h\right]^2]}{a} \approx 88000 \qquad (1)$$

where d is the diameter of the liposome, h is the thickness of the bilayer (approx. 5nm), and a the lipid head group area (estimated at 0.65 nm^2 for DPPC)[47]. The number of liposomes per GUV (N_{Lipo}) can be calculated according to equation (2):

$$N_{Lipo} = \frac{M_{Lipid} \times Na}{N_{Tot} \times 1000} \times V_{Int\ GUV} \approx 260000 \qquad (2)$$

where M_{Lipid} is the molar concentration of lipid, Na the Avogadro number, and $V_{Int\ GUV}$ the internal volume of a 20 μm polymersome ($V_{Int\ GUV} = \frac{4}{3}\pi {R_{GUV}}^3$). Finally, the dilution factor n is given from equation (3):

$$n = \frac{V_{Int\ GUV}}{N_{Lipo} \times V_{Int\ Lipo}} \approx 40 \qquad (3)$$

where $V_{Int\ Lipo}$ is the internal volume of a 100 nm liposome ($V_{Int\ Lipo} = \frac{4}{3}\pi {R_{Lipo}}^3$). As a result, for an initial fluorescein concentration of 80 mM, the final concentration will be $\frac{[fluorescein]}{n} \approx 2$ mM.

3. Results and discussion

3.1. Encapsulation of liposomes in giant unilamellar vesicles (GUVs)

The preparation of liposomes in polymersomes (LiPs) compartmentalized systems was performed using an emulsion-centrifugation process, for which pre-formed liposomes were encapsulated into giant unilamellar PBut-*b*-PEO vesicles (GUVs).[46] Four different types of lipid were selectively chosen: 1-palmitoyl-2-oleoyl-sn-glycero-3-phosphocholine (POPC), 1,2-dimyristoyl-sn-glycero-3-phosphocholine (DMPC), 1,2-dipentadecanoyl-sn-glycero-3-phosphocholine (diC15-PC), and 1,2-dipalmitoyl-sn-glycero-3-phosphocholine (DPPC) with melting temperatures (Tm) respectively equal to -2 °C, 23 °C, 35 °C and 41 °C. A thin film hydration protocol followed by extrusion was used to afford large unilamellar liposomes tagged with either 1,2-diphytanoyl-sn-glycero-3-phosphoethanolamine-N-(7-nitro-2-1,3-benzoxadiazol-4-yl) (NBD) or 1,2-dioleoyl-sn-glycero-3-phosphoethanolamine-N-(lissamine rhodamine B sulfonyl) (LRB). A size of 400 nm was chosen for extrusion of the giant vesicles obtained after rehydration to allow better observation under confocal microscopy. Figure 1 shows images in white light (left), fluorescence emission (center) and overlays (right) of the four encapsulated liposome types. Liposomes were either prepared with 0.1 % of NBD (diC15-PC, green) or LRB (POPC, DMPC and DPPC, red). The images show a successful encapsulation of the liposomes into the PBut-*b*-PEO GUVs regardless of the transition temperature of the lipids. Indeed, the experiments were performed at 24 °C (room temperature), above the Tm of POPC and DMPC but below the Tm of diC15-PC and DPPC. In addition, the confinement of the liposomes at rather high concentration did not induce any destabilization, as they can still be observed individually dispersed and freely moving into the lumen of the polymersomes (SI, video S1).[48] Finally, no interaction between the liposomes and the PBut-*b*-PEO membrane was observed (as would have been indicated by a subsequent appearance of fluorescence on the membrane), even after a few hours of observation, proving that any kind of liposomes can successfully be encapsulated into giant polymersomes using such a process.

Indeed, four examples are provided in the context of this work, but we are confident that a wide variety of lipids and mixed-lipid systems of comparable sizes could be used.

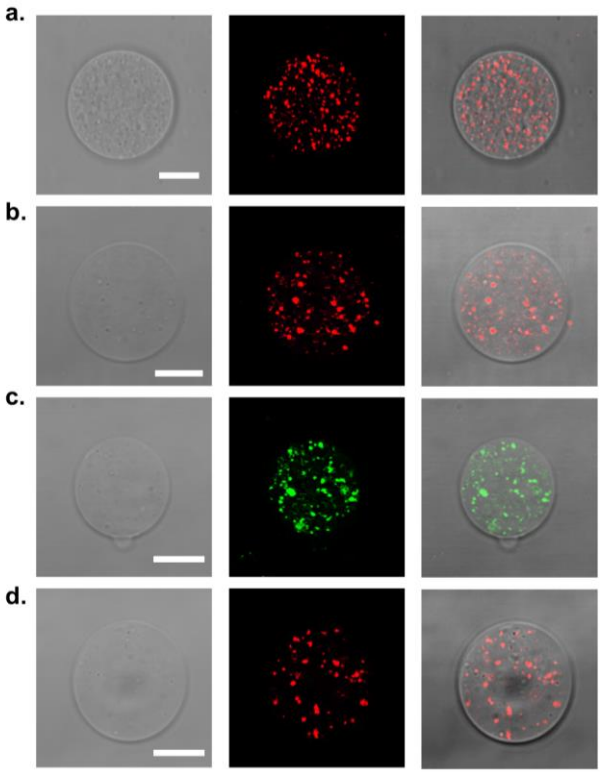

Figure 1. Loading of 400 nm liposomes into giant polymersomes. a) POPC labelled with rhodamine, b) DMPC labelled with rhodamine, c) diC15-PC labelled with NBD, d) DPPC labelled with rhodamine. Left images: view in transmission, center: emission of liposomes, right: overlay. Scale bar = 10 µm.

The same process was then used to load different kind of liposomes together in a single polymersome: 400 nm POPC with DPPC liposomes and diC15-PC with DPPC liposomes were then loaded in PBut-*b*-PEO polymersomes (Figure 2). POPC and diC15-PC liposomes were tagged with 0.1 wt % NBD (green) and DPPC liposomes were tagged with 0.1 wt % LRB (red). Similarly to the previous experiments, the different liposomes did not noticeably interact together or with the polymersome's membrane as observed by confocal observations. In addition, these systems were stable over time, as no aggregation or sedimentation was observed for at least 72 hours.

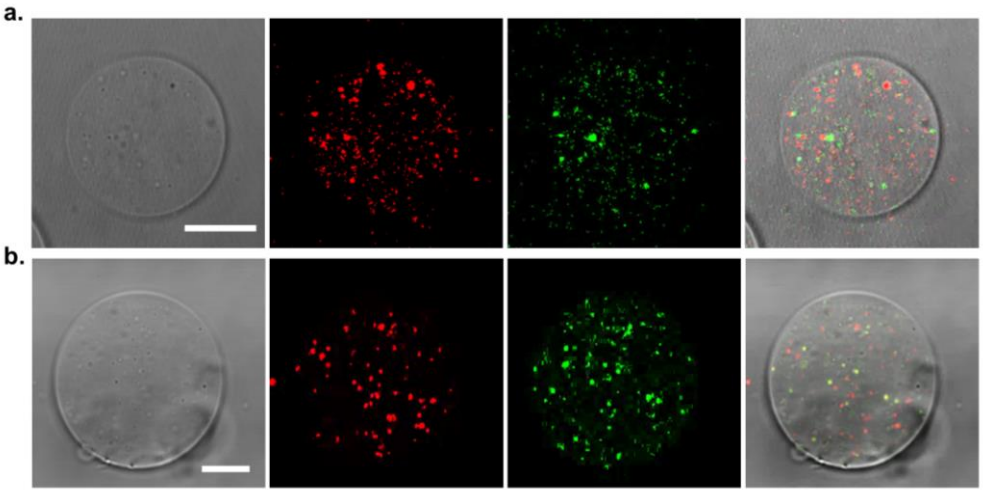

Figure 2. Co-loading of two 400 nm liposome types in giant polymersomes. a) POPC tagged with NBD and DPPC tagged with rhodamine, b) diC15-PC tagged with NBD and DPPC tagged with rhodamine. Left column: view in transmission, center: emission of liposomes, right: overlay. Scale bar = 10 μm.

3.2. Triggered release of encapsulated dyes inside GUVs

The major goal of this contribution is to demonstrate the potential use of this LiPs system as a model for triggered release of species from compartmentalized systems in a confine environment. For this purpose, we loaded fluorescein, a green hydrophilic fluorescent dye with λ_{exc}=488 nm inside the 100 nm DPPC liposomes. By increasing the temperature above the melting transition of the lipid (DPPC, Tm=41 °C), one can anticipate that the liposome membrane transitions from a gel phase into a fluid phase will allow the release of the dye due to the permeabilization of the membrane.[49] In order to accurately follow this process, an appropriate concentration of fluorescein has to be used in order to observe an increase of fluorescence with time. The dependence of the fluorescence intensity of fluorescein with concentration is shown in Figure 3. a). At high concentration (i.e. above 10 mM) the intensity decreases, due to the self-quenching of fluorescence. We then decided to load 80 mM fluorescein (Figure 3. a), red arrow) inside the DPPC liposomes. The liposomes were then purified with a size exclusion gel chromatography column to eliminate the free dye. By increasing the temperature above the Tm of the lipids, the dye can be released from the lumen of the liposomes and is slowly diluted in the external solution, meaning the lumen of the large polymersomes. This was confirmed by a strong recovery of the fluorescence intensity after

heating (Figure 3. a), green arrow). The emission of fluorescein was monitored over time at different temperatures for the liposome suspension (Figure 3. b)). The percentage of dye released was calculated according to equation (4):

$$Released\ dye\ (\%) = \frac{I_t - I_0}{I_T - I_0} \times 100 \qquad (4)$$

where I_0 is the initial fluorescence intensity, I_t is the fluorescence intensity at a given time and I_T is the fluorescence intensity after disruption of the liposomes with Triton X-100 (10%). No dye release was observed at 25 and 30 °C. The liposomes started to leak at 37 °C, close to the transition temperature of DPPC and a complete and fast release was observed at 45 °C, in less than 10 minutes. These experiments clearly demonstrated the ability to accurately control the release of fluorescein from the DPPC liposomes with temperature.

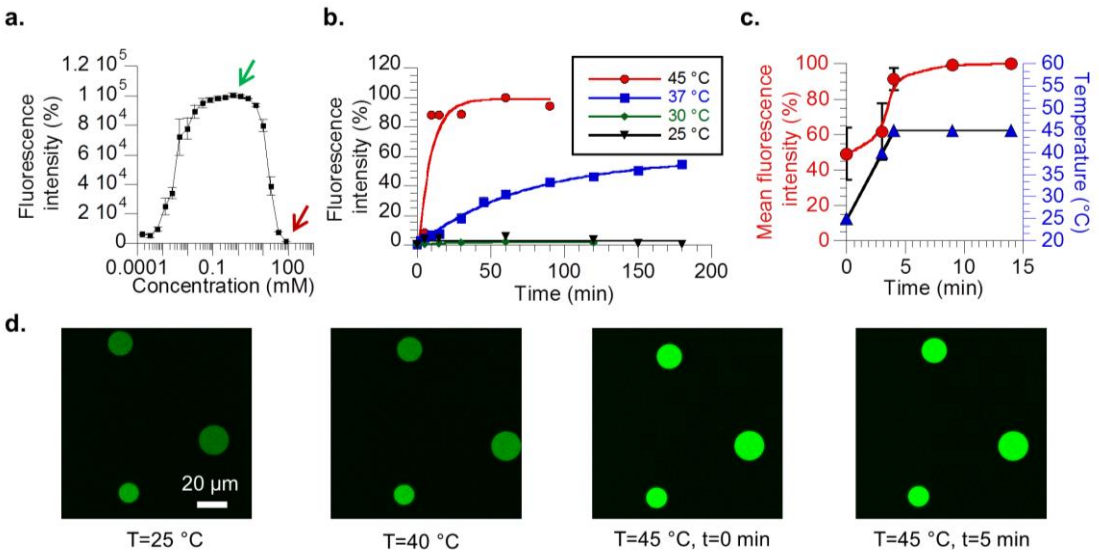

Figure 3. Fluorescein release studies from 100 nm DPPC liposomes. a) Dependence of the fluorescence intensity of fluorescein with concentration. Red arrow: 80 mM, green arrow: 1 mM, b) Release from 80 mM fluorescein-loaded 100 nm DPPC liposomes at T= 25, 30, 37 and 45 °C, c) Temperature dependence of fluorescence intensity of 80 mM fluorescein-loaded 100 nm DPPC liposomes encapsulated inside giant PBut-b-PEO polymersomes, and d) Confocal microscopy observation of fluorescein emission of liposomes inside giant PBut-b-PEO polymersomes at different times and temperatures. Plain lines are used only as a visual guide.

The next challenge consisted in the quantification of the '*in vitro*' release of fluorescein with temperature from liposomes into the confined environment created by PBut-*b*-PEO GUVs. Indeed, in such a compartmentalized system, the release medium for liposomes will be limited to the lumen of the giant polymersomes, allowing a control of the final concentration that can be programmed to reach the maximum fluorescence intensity. Theoretical calculations were thus performed in order to determine the appropriate fluorescein concentration to be loaded inside the liposomes. Indeed, once the dye gets released and diluted into the lumen of polymersomes, its concentration should be high enough (i.e. highest fluorescence intensity, Figure 3. a)) to be detectable by fluorescence emission under confocal observation. From the estimated number of liposomes loaded in 1 GUV (about 260000, see materials and methods), the theoretical internal volumes of a 100 nm liposome and a 20 µm GUV, the theoretical dilution factor after release of the dye inside the lumen of the polymersomes could be calculated as: $n = \frac{V_{Int\ GUV}}{V_{T\ liposomes}} \approx 40$. As a consequence, one can estimate that for an initial fluorescein concentration of 80 mM, the final concentration after release of the dye with temperature inside the polymersomes would be about 2 mM (red to green arrow in Figure 3. a)). For the experiment, the confocal microscope was equipped with a heating and cooling stage that allowed heating and cooling of the visualized samples at controlled rates. The mean fluorescence intensity was collected on a defined area at the center of the vesicles by image analysis on 10 to 15 vesicles over time and for different temperatures (Figure 3. c)). First, the GUVs loaded with the fluorescein-DPPC liposomes were visualized at 25 °C in the green channel (emission of fluorescein). The sample was then heated to 45 °C (5 °C/min) and images were taken with time to monitor the increase of fluorescence inside the vesicles (dye release from the loaded liposomes). A clear increase in fluorescence intensity was noticeable already after 5 mins heating at 45 °C (Figure 3. d)) and mean average intensity measurements over time confirmed the effective *in vitro* dye release (Figure 3. c)).

In order to generalize the phenomenon, similar experiments were conducted with methylene blue (MB)-loaded 200 nm diC15-PC liposomes (Figure 4). Interestingly, MB is a red hydrophilic fluorescent dye often used in photodynamic therapy.[50] As shown in Figure 4. a), the MB fluorescence self-quenches for concentrations above 1 mM. We thus used 10 mM loaded MB-liposomes to perform dye release tests at different temperatures from the diC15-PC liposomes (Tm=35 °C) (Figure 4. b)). As for DPPC liposomes, the dye rapidly released when

the temperature exceeded the transition temperature of the diC15-PC lipids (i.e. MB is fully released at 37 °C). The *in vitro* triggered release inside the PBut-*b*-PEO GUVs led to a visible increase of fluorescence intensity in the emission range of MB after several minutes at 37 °C while no change in intensity was observed for samples kept at room temperature (Figure 4. c)).

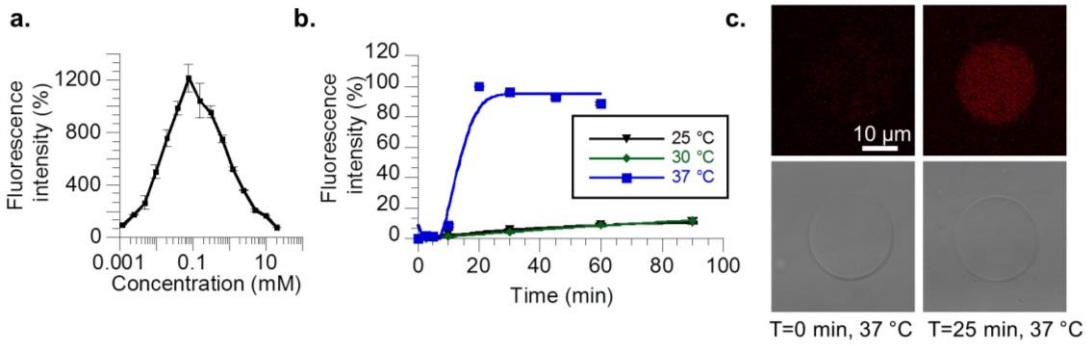

Figure 4. Methylene blue (MB) release studies from 200 nm diC15-PC liposomes. a) Dependence of the fluorescence intensity of MB with concentration, b) Release from 10 mM MB-loaded 200 nm diC15-PC liposomes at T= 25, 30, and 37 °C, and c) Confocal microscopy observation of MB emission of liposomes inside giant PBut-b-PEO polymersomes at different times and temperatures. Plain lines are used only as a visual guide.

In a final experiment, both dye-loaded liposome types (DPPC and diC15-PC loaded with 80 mM fluorescein and 10 mM MB respectively) were encapsulated into PBut-*b*-PEO polymersomes. A successive triggered dye-release from the LiPs was achieved and characterized by placing the sample on the heating and cooling stage over the objective of the microscope, to allow direct visualization of dye release during the controlled heating process. As observed in Figure 5. a), the presence of both DPPC and diC15-PC liposomes, respectively loaded with quenched fluorescein and MB, is confirmed by the low fluorescence intensity signal in the emission channels of both dyes (green and red, 520 and 660 nm respectively) at 25 °C. The sample was then heated at 37 degrees (heating rate: 8 °C/min). We observed a release of methylene blue from diC15-PC liposomes after 10 min, as confirmed by the increase of fluorescence intensity (Figure 5. d)). The fact that fluorescein also gets slowly released from the DPPC liposomes is consistent with the dye-release studies in solution at 37 °C (Figure 3. b)). To allow complete release of fluorescein, the sample was then heated to 45 °C (8 °C/min)

(Figure 5. c). Once both dyes are released, the overlay of images taken from the green and red channels (emission of fluorescein and emission of MB respectively) give a yellow color characteristic of the mixing of the two fluorophores inside the lumen of the giant polymersomes.

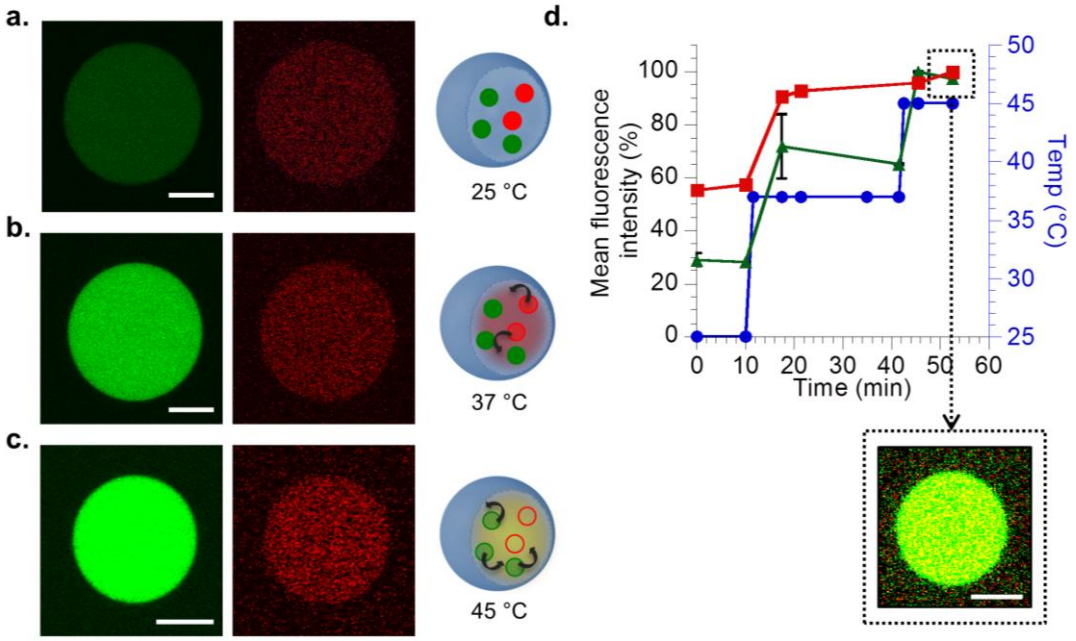

Figure 5. Co-loading of MB-loaded diC15-PC liposomes and fluorescein-loaded DPPC liposomes into giant PBut-b-PEO polymersomes and successive temperature-triggered dye release. a) 25 °C, T=0 min, b) 37 °C, T=25 min, and c) 45 °C, T=10 min. Left column: emission of fluorescein, right: emission of MB. Scale bar = 10 µm.

3.3.Proof of concept: temperature-triggered enzymatic reaction

In a last experiment, we aimed at demonstrating the potential use of this compartmentalized system as a bioreactor for temperature-triggered confined reactions. Laccase was chosen as a catalytic enzyme for the oxidation of the substrate 2,2'-azino-bis(3-ethylbenzothiazoline-6-sulphonic acid) (ABTS) into its radical cationic blue-colored product. $ABTS^{\bullet+}$ is generated by reaction of ABTS with oxidizing species and is thus often used to evaluate the anti-oxidant activity of compounds or the reaction rate of various enzymes.[51,52] Laccase is part of a group of enzymes termed the multicopper oxidases found in many organisms including bacteria and humans.[53] Laccases exhibit low stability and catalytic activity in a variety of environmental conditions and thus immobilization methods have been developed to improve their stability and

reactivity.[54,55] Especially, laccases immobilized in polystyrene sulphonate and polyallylamine microcapsules have been prepared based on a layer-by-layer (lbl) technique.[56]

As schematically represented in Figure 6, the concept developed here was to encapsulate laccase-loaded lbl capsules together with ABTS-loaded liposomes inside GUVs and trigger the *in situ* oxidation of ABTS by temperature-release of ABTS from the liposomes. ABTS subsequently enters the capsules and is oxidized into blue-colored $ABTS^{\bullet+}$.

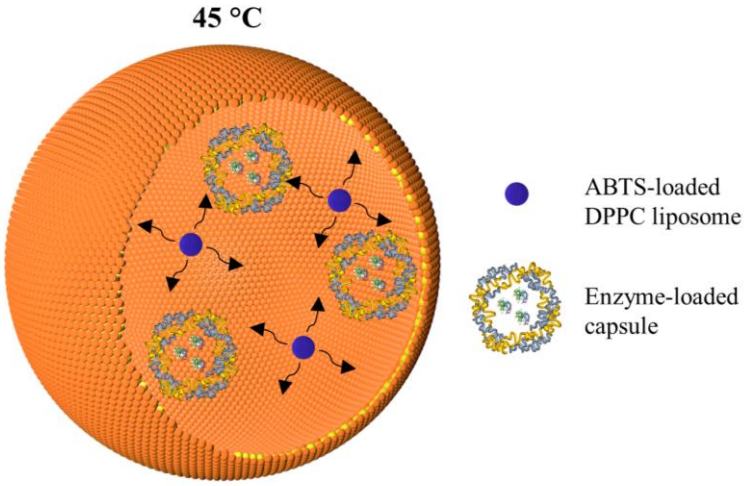

Figure 6. Schematic representation of the laccase-loaded lbl capsules and ABTS-loaded DPPC liposomes inside a PBut-b-PEO GUV. Upon temperature increase to 45 °C, ABTS is released from the liposomes and diffuses into the capsules to react with the laccase. The subsequent blue radical $ABTS^{\bullet+}$ cation is produced inside the GUV.

To verify the operating conditions, the oxidation reaction was initially performed in bulk and followed by absorbance measurements at 414 nm, the maximal absorption of $ABTS^{\bullet+}$. The laccase-loaded lbl capsules were prepared according to a previously established protocol.[56] Briefly, sequential layers of polyelectrolytes are deposited onto a sacrificial polycarbonate template and the enzyme is subsequently loaded by varying the pH into the open or closed form of the capsule.[56] ABTS (20 mM) was loaded into DPPC liposomes following the film rehydration method. The liposomes were extruded at 100 nm and their size was confirmed by DLS measurements.

An initial experiment was performed with free enzymes. Laccase was added to a solution of ABTS-loaded DPPC liposomes and the absorbance (414 nm) was monitored at ambient temperature. As can be seen in Figure 7. a), upon addition of free enzyme, the absorbance of the solution increases with time indicating the formation of the colored oxidized product of ABTS. This result was not expected since the DPPC liposomes should remain impermeable below the lipid transition temperature (41 °C). It was hypothesized that the free enzyme destabilizes the liposomes and provokes a diffusion of ABTS in the outer medium. Thus, loading the enzymes in capsules should prevent their destabilizing action towards the liposomes.

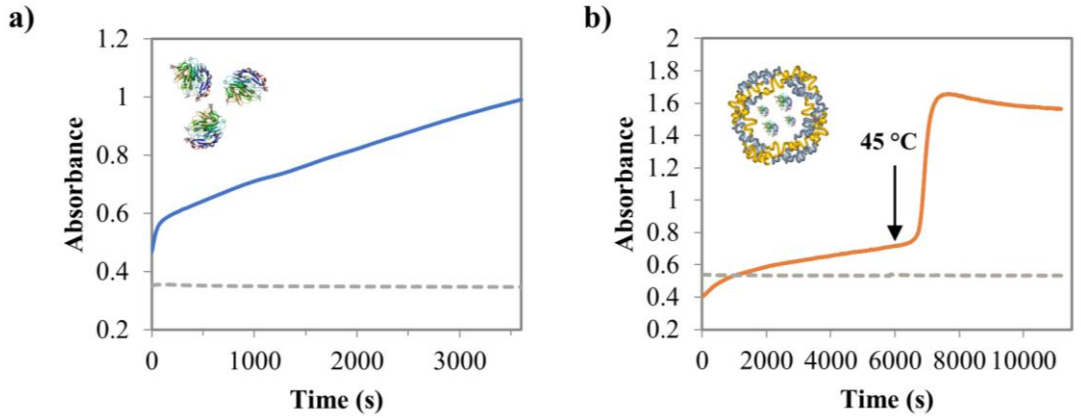

Figure 7. Oxidation of ABTS from DPPC 100 nm liposomes following the addition of laccase. a) Free laccase (15 mg/mL), ambient temperature. b) Laccase (15 mg/mL)-loaded lbl capsules added at ambient temperature. The increase to 45 °C is noted by the arrow. In a) and b), the dotted line represents the absorbance of the ABTS-loaded DPPC liposomes without addition of the enzyme.

The same experiment was then repeated with the laccase enzymes loaded and protected inside the lbl capsules (Figure 7. b)). The absorbance slowly increases upon addition of the capsules at 25 °C indicating that the liposomes might still be a little destabilized. However, a burst of absorbance is observed few minutes after temperature increase to 45 °C. This increase of absorbance is due to the release of ABTS from the permeabilized DPPC liposomes and its subsequent oxidation into blue $ABTS^{\bullet+}$ by the enzymes. These results further confirm the

efficient release of the substrate upon temperature permeabilization of the DPPC liposomal membrane and the possibility to perform a triggered compartmentalized reaction.

In a last step, the same reaction was performed inside the PBut-*b*-PEO GUVs under confocal observation. While the oxidized ABTS is not fluorescent, its blue coloring should be clearly visible under white light observation. The emulsion-centrifugation protocol was followed for the encapsulation of the capsules and the ABTS-loaded DPPC liposomes inside the giant polymersomes. Figure 8 a) shows the enzyme-loaded lbl capsules observed in transmission well dispersed, free in solution, with a size of about 2 µm. These capsules were then successfully loaded inside the sucrose polymer-stabilized emulsion droplets (Figure 8. b)). Unfortunately, the loaded-emulsion droplets could not cross the polymer-stabilized oil-water interface and thus the GUVs could not be formed. We believe that owing to the relatively large size of the capsules, the emulsion droplets ruptured during centrifugation. Thus, in order to perform the *in situ* reaction, the encapsulation process should be optimized and the emulsion-centrifugation process needs optimization.

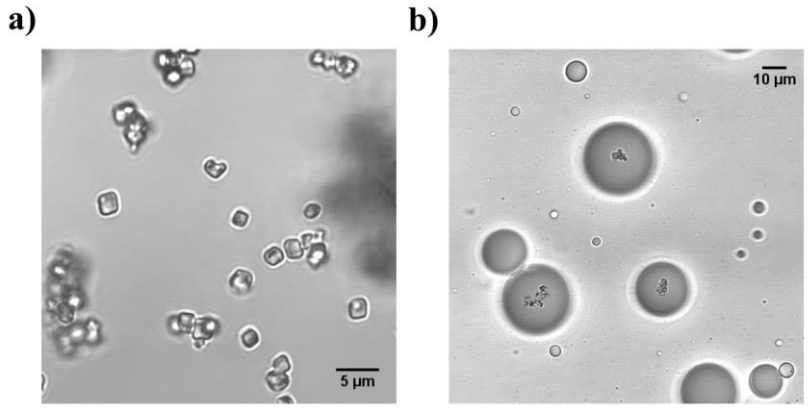

Figure 8. Confocal observations of enzyme-loaded lbl-capsules a) free in solution and b) loaded in PBut-b-PEO emulsion droplets (water in oil).

4. Conclusion

We have demonstrated that different kinds of liposomes can be effectively loaded into giant polymersomes using an emulsion-centrifugation approach, thus affording original compartmentalized liposomes in polymersomes (LiPs). The thermo-sensitivity of liposomes

has been used as reservoirs that can be thermally activated on demand to release their cargo at a specific temperature. A sequence-controlled release of molecules has also been demonstrated with two different kinds of vesicles (and dyes). In addition, an attempt was made to use these LiPs as a scaffold to perform a thermally activated cascade enzymatic reaction in a confined system. To the best of our knowledge, this contribution represents the first report on a co-loading of different liposomes into a same polymersome (LiPs). We herein provide a novel multicompartment system with a versatile and tunable structure that could have potential interest for compartmentalized micro-reactors or sensors and delivery systems.

5. References

[1] A. Akbarzadeh, R. Rezaei-Sadabady, S. Davaran, S. W. Joo, N. Zarghami, Y. Hanifehpour, M. Samiei, M. Kouhi, K. Nejati-Koshki, *Nanoscale Res. Lett.* **2013**, *8*, 102.
[2] R. A. Schwendener, *Ther. Adv. Vaccines* **2014**, *2*, 159–182.
[3] T. M. Allen, P. R. Cullis, *Adv. Drug Deliv. Rev.* **2013**, *65*, 36–48.
[4] C. Peetla, A. Stine, V. Labhasetwar, *Mol. Pharm.* **2009**, *6*, 1264–1276.
[5] L. Messager, J. Gaitzsch, L. Chierico, G. Battaglia, *Curr. Opin. Pharmacol.* **2014**, *18*, 104–111.
[6] D. E. Discher, *Science* **2002**, *297*, 967–973.
[7] B. M. Discher, Y.-Y. Won, D. S. Ege, J. C.-M. Lee, F. S. Bates, D. E. Discher, D. A. Hammer, *Science* **1999**, *284*, 1143–1146.
[8] B. Städler, A. D. Price, A. N. Zelikin, *Adv. Funct. Mater.* **2011**, *21*, 14–28.
[9] P. Tanner, S. Egli, V. Balasubramanian, O. Onaca, C. G. Palivan, W. Meier, *FEBS Lett.* **2011**, *585*, 1699–1706.
[10] G. Pasparakis, N. Krasnogor, L. Cronin, B. G. Davis, C. Alexander, *Chem. Soc. Rev.* **2009**, *39*, 286–300.
[11] N. P. Kamat, J. S. Katz, D. A. Hammer, *J. Phys. Chem. Lett.* **2011**, *2*, 1612–1623.
[12] R. Rodríguez-García, M. Mell, I. López-Montero, J. Netzel, T. Hellweg, F. Monroy, *Soft Matter* **2011**, *7*, 1532–1542.
[13] J.-F. L. Meins, O. Sandre, S. Lecommandoux, *Eur. Phys. J. E* **2011**, *34*, 1–17.
[14] F. Meng, Z. Zhong, *J. Phys. Chem. Lett.* **2011**, *2*, 1533–1539.
[15] F. Meng, Z. Zhong, J. Feijen, *Biomacromolecules* **2009**, *10*, 197–209.
[16] J. S. Lee, J. Feijen, *J. Controlled Release* **2012**, *161*, 473–483.
[17] S. Pispas, *Soft Matter* **2011**, *7*, 8697–8701.
[18] S. K. Lim, H.-P. de Hoog, A. N. Parikh, M. Nallani, B. Liedberg, *Polymers* **2013**, *5*, 1102–1114.
[19] K. Hadinoto, A. Sundaresan, W. S. Cheow, *Eur. J. Pharm. Biopharm.* **2013**, *85*, 427–443.
[20] J.-F. Le Meins, C. Schatz, S. Lecommandoux, O. Sandre, *Mater. Today* **2013**, *16*, 397–402.
[21] B. Städler, R. Chandrawati, A. D. Price, S.-F. Chong, K. Breheney, A. Postma, L. A. Connal, A. N. Zelikin, F. Caruso, *Angew. Chem. Int. Ed.* **2009**, *48*, 4359–4362.
[22] C. Schmitt, A. H. Lippert, N. Bonakdar, V. Sandoghdar, L. M. Voll, *Front. Bioeng. Biotechnol.* **2016**, *4*, 19.
[23] M. Marguet, C. Bonduelle, S. Lecommandoux, *Chem. Soc. Rev.* **2012**, *42*, 512–529.
[24] A. H. Chen, P. A. Silver, *Trends Cell Biol.* **2012**, *22*, 662–670.
[25] Y. Zhang, W. C. Ruder, P. R. LeDuc, *Trends Biotechnol.* **2008**, *26*, 14–20.
[26] A. Pohorille, D. Deamer, *Trends Biotechnol.* **2002**, *20*, 123–128.
[27] S. Mann, *Acc. Chem. Res.* **2012**, *45*, 2131–2141.
[28] J. W. Szostak, D. P. Bartel, P. L. Luisi, *Nature* **2001**, *409*, 387–390.
[29] J. Gaitzsch, X. Huang, B. Voit, *Chem. Rev.* **2016**, *116*, 1053–1093.
[30] L. Schoonen, J. C. M. van Hest, *Adv. Mater.* **2016**, *28*, 1109–1128.
[31] A. Peyret, E. Ibarboure, A. Tron, L. Beauté, R. Rust, O. Sandre, N. D. McClenaghan, S. Lecommandoux, *Angew. Chem.* **2017**, *129*, 1588–1592.
[32] A. Perro, C. Nicolet, J. Angly, S. Lecommandoux, J.-F. Le Meins, A. Colin, *Langmuir* **2011**, *27*, 9034–9042.
[33] H. C. Shum, Y. Zhao, S.-H. Kim, D. A. Weitz, *Angew. Chem.* **2011**, *123*, 1686–1689.
[34] E. Mabrouk, D. Cuvelier, F. Brochard-Wyart, P. Nassoy, M.-H. Li, *Proc. Natl. Acad. Sci.* **2009**, *106*, 7294–7298.
[35] M. Marguet, L. Edembe, S. Lecommandoux, *Angew. Chem. Int. Ed.* **2012**, *51*, 1173–1176.
[36] Y. Elani, A. Gee, R. V. Law, O. Ces, *Chem. Sci.* **2013**, *4*, 3332.
[37] L. Hosta-Rigau, S. F. Chung, A. Postma, R. Chandrawati, B. Städler, F. Caruso, *Adv. Mater.* **2011**, *23*, 4082–4087.

[38] S.-H. Kim, H. C. Shum, J. W. Kim, J.-C. Cho, D. A. Weitz, *J. Am. Chem. Soc.* **2011**, *133*, 15165–15171.
[39] O. Kreft, M. Prevot, H. Möhwald, G. B. Sukhorukov, *Angew. Chem. Int. Ed.* **2007**, *46*, 5605–5608.
[40] P.-Y. Bolinger, D. Stamou, H. Vogel, *Angew. Chem. Int. Ed.* **2008**, *47*, 5544–5549.
[41] S. A. Walker, M. T. Kennedy, J. A. Zasadzinski, *Nature* **1997**, *387*, 61–64.
[42] C. Boyer, J. A. Zasadzinski, *ACS Nano* **2007**, *1*, 176–182.
[43] J. A. Zasadzinski, B. Wong, N. Forbes, G. Braun, G. Wu, *Curr. Opin. Colloid Interface Sci.* **2011**, *16*, 203–214.
[44] R. J. R. W. Peters, M. Marguet, S. Marais, M. W. Fraaije, J. C. M. van Hest, S. Lecommandoux, *Angew. Chem. Int. Ed.* **2014**, *53*, 146–150.
[45] Y. Elani, R. V. Law, O. Ces, *Nat. Commun.* **2014**, *5*, DOI 10.1038/ncomms6305.
[46] S. Pautot, B. J. Frisken, D. A. Weitz, *Langmuir* **2003**, *19*, 2870–2879.
[47] S. Leekumjorn, A. K. Sum, *Biophys. J.* **2006**, *90*, 3951–3965.
[48] M. Marguet, O. Sandre, S. Lecommandoux, *Langmuir* **2012**, *28*, 2035–2043.
[49] S. Nagarajan, E. E. Schuler, K. Ma, J. T. Kindt, R. B. Dyer, *J. Phys. Chem. B* **2012**, *116*, 13749–13756.
[50] J. P. Tardivo, A. Del Giglio, C. S. de Oliveira, D. S. Gabrielli, H. C. Junqueira, D. B. Tada, D. Severino, R. de Fátima Turchiello, M. S. Baptista, *Photodiagnosis Photodyn. Ther.* **2005**, *2*, 175–191.
[51] R. B. Walker, J. D. Everette, *J. Agric. Food Chem.* **2009**, *57*, 1156–1161.
[52] R. Bourbonnais, D. Leech, M. G. Paice, *Biochim. Biophys. Acta BBA - Gen. Subj.* **1998**, *1379*, 381–390.
[53] A. M. Mayer, R. C. Staples, *Phytochemistry* **2002**, *60*, 551–565.
[54] S. Rodríguez Couto, J. F. Osma, V. Saravia, G. M. Gübitz, J. L. Toca Herrera, *Appl. Catal. Gen.* **2007**, *329*, 156–160.
[55] S. Rodríguez Couto, J. L. Toca Herrera, *Biotechnol. Adv.* **2006**, *24*, 500–513.
[56] C. Crestini, R. Perazzini, R. Saladino, *Appl. Catal. Gen.* **2010**, *372*, 115–123.

6. Supporting Information

The following file is visible online at:

http://pubs.acs.org/doi/suppl/10.1021/acs.langmuir.7b00655

Video S1: 400 nm POPC and DPPC liposomes encapsulated in giant polymersome (avi).

CHAPTER 4: *Effect of osmotic pressure imbalance on giant polymer vesicles*

One of the main objectives of this PhD research project was to find triggers to control the independent release of multiple species from separated compartments. In the previous chapter, we detailed our findings on temperature-triggered release of encapsulated dyes from nano-liposomes inside giant polymersomes. We showed that upon temperature increase, permeabilization of the lipid membrane led dyes to diffuse from the nano-liposomes into the lumen of giant polymersomes. This technique is tunable and could be used to trigger the release of various molecules and especially to initiate a confined cascade reaction. However, temperature-induced membrane permeabilization of liposomes does not allow a real control over the diffusion rate of the loaded species that can be rather slow and thus not desired for applications that need a fast burst release. In addition, the technique only applies to small molecules able to permeate through the membrane.

Osmotic pressure variations are known to have an effect on cell morphology and, as will be further discussed, they can be responsible for the rupture of a lipid or polymer membrane. Hence, in this chapter, we present our findings on the effects of hypo- or hypertonic shocks (respectively linked to an increase or a decrease of the concentration of species) on giant polymer vesicles. A critical point concerned the design of a system allowing a rapid change of osmotic pressure, fast enough to induce an osmotic imbalance that can cause the vesicle rupture. We showed that these osmotic shocks can be used to trigger the release of encapsulated species from polymersomes.

In the first part of this chapter, we present our findings on hypotonic shocks induced on polymersomes by photo-cleavage of encapsulated fluorescent dyes upon light irradiation at different wavelengths. In a second part, hypertonic UV-induced shocks were provoked by photo-polymerization of an acrylamide monomer inside polymer vesicles.

PART 1: ***Polymersome popping by light-induced osmotic shock under temporal, spatial and spectral control***

Adapted from:

Polymersome popping by light-induced osmotic shock under temporal, spatial and spectral control

Ariane Peyret, Emmanuel Ibarboure, Arnaud Tron, Louis Beauté, Ruben Rust, Olivier Sandre, Nathan D. McClenaghan*, Sebastien Lecommandoux*

COMMUNICATION

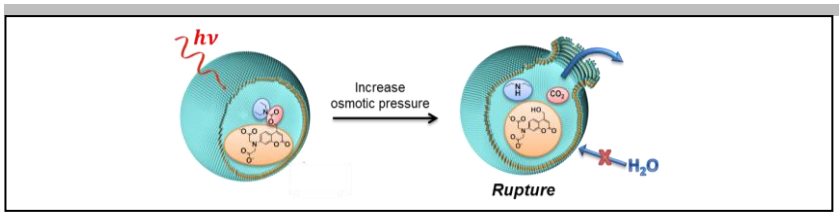

A simple and versatile protocol is described for the controlled light-triggered rupture of giant polymersomes. This method allows precise and selective liberation of a range of encapsulated species with full control in time, space and excitation wavelength.

A. Peyret, E. Ibarboure, A. Tron, L. Beauté, R. Rust, O. Sandre, N. D. McClenaghan, S. Lecommandoux**

Angew. Chem. Int. Ed., **2017**, *129*, 1688-1592.

Polymersome popping by light-induced osmotic shock under temporal, spatial and spectral control.

Abstract: A high precision approach allowing light-triggered, programmed cell-sized vesicle rupture is described, with particular emphasis on self-assembled polymersome capsules. The mechanism involves a hypotonic osmotic imbalance created by accumulation of new photogenerated species inside the lumen, which cannot be compensated due to the low water permeability of the membrane. This simple and versatile mechanism can be adapted to a wealth of hydrosoluble molecules, which are either able to generate reactive oxygen species or undergo photocleavage. Ultimately, in a multi-compartmentalized and cell-like system, the possibility to selectively burst polymersomes with high specificity and temporal precision, and consequently deliver small encapsulated vesicles (both polymersomes and liposomes) is demonstrated.

1. Introduction

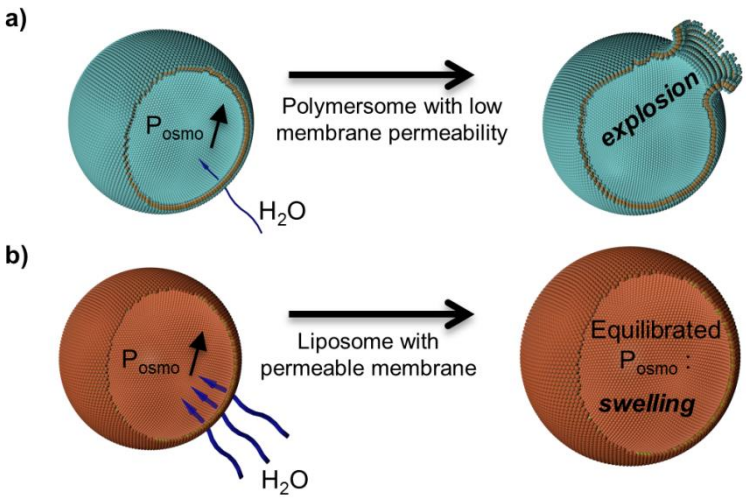

Scheme 1. a) Schematic representation of osmotic pressure increase in polymersomes. The impermeable membrane prevents water from entering the vesicle or the internal solution to leak out and the osmotic pressure remains imbalanced until the vesicle ruptures. b) Schematic representation of osmotic pressure increase in liposomes. The internal osmotic pressure increases transiently but it is rapidly compensated by water diffusion through the tenfold more permeable membrane of the liposome or through sub-critical viz. resealing pores, resulting in vesicle swelling without irreversible rupture.

Polymersomes are mechanically robust self-assembled vesicular structures that are widely studied and are proving central in increasing research and application areas ranging from

nanomedicine to artificial cell design.[1] Control over their membrane diffusion properties and structural integrity is crucial for the development of new complex systems, such as artificial cells. Compartmentalization is central in biological cells. Indeed, physical separation of biochemical species allows metabolic reactions to take place independently and simultaneously in a confined and crowded space.[2–10] For decades, different methods have been proposed to construct elaborate structures that have been developed in the field of lipid and polymer chemistry.[11–14] Amongst others, double emulsion techniques[15–17], phase transfer of emulsion droplets over an interface[18–20], layer-by-layer assembly[21] or microfluidics[22] have proved efficient in affording micron-sized vesicles, allowing the encapsulation of distinct biochemical species in different compartments and the ability to control simple biomimetic enzymatic reactions in a confined space.[13,23–25]

One additional major characteristic of natural cells is their ability to initiate metabolic reactions at a specific time and at a desired location, independently and repeatedly. In this regard, temporal control is crucial in artificial cell systems. However, most of the designed synthetic systems to date lack some control over the initiation of the reactions, which are generally induced by passive diffusion of species across semi-permeable membranes, either as a result of intrinsic membrane permeability[23] or by the incorporation of channels or pores into the membrane, resulting in a slow release of reactants.[26–28] As a result, a remaining major challenge concerns the ability to trigger specific reactions by selectively and rapidly inducing the release of species from independent compartments, while controlling their concentration.[29,30]

Herein, we introduce a tunable protocol for light-driven specific polymersome rupture in time and space, which combines the advantages of utilizing light as a trigger and the fast release of components from bursting vesicles. Our system is based on laser excitation of hydrophilic dyes encapsulated in the lumen of distinct giant poly(butadiene)-*b*-poly(ethylene oxide) (PBut-*b*-PEO) polymersomes, across the whole visible spectrum gamut. Upon excitation the dye is degraded, either through photofragmentation or reactive oxygen species (ROS)-mediated degradation, leading to an increase of the internal osmotic pressure until subsequent polymersome rupture. This process allows for a precise and fast release of entrapped species from different compartments. Additionally, such a selective mechanism allows discrimination

between two types of polymersomes within a group of many and to successively trigger the release of their content without altering the remaining vesicles. This system offers great potential for the development of cell mimics where different species encapsulated in distinct organelle-like compartments have to be released independently, in a controlled manner, but also for the release of other (bio)active compounds.

2. Experimental Section

2.1. Materials

Poly(butadiene)-*b*-poly(ethylene oxide) $PBut_{46}$-*b*-PEO_{30} and $PBut_{23}$-*b*-PEO_{14} (Mn x 10^3 PBut-*b*-PEO: 2.5-*b*-1.3 and 1.2-*b*-0.6; Mw/Mn 1.04 and 1.09) were ordered from Polymer Source (P18422-BdEO and 10191-BdEO batches respectively, both comprising 89% 1,2-addition of butadiene). 1-Palmitoyl-2-oleoyl-*sn*-glycero-3-phosphocholine (POPC), 1,2-dipalmitoyl-*sn*-glycero-3-phosphocholine (DPPC) and L-α-phosphatidylethanolamine-N-(lissamine rhodamine B sulfonyl) (rhod-PE) were purchased from Avanti Polar Lipids (reference numbers: 850457, 850355 and 810146 respectively). Sodium azide (NaN_3), sucrose, glucose, calcein, methylene blue and rhodamine were purchased from Sigma Aldrich and used as received. Hydrosoluble caged coumarin and a dibenzofuran-based singlet oxygen trap were synthesized using standard protocols.

2.2. Methods

NMR experiments were performed at 25 °C on a Bruker Advance 400 spectrometer operating at 400 MHz calibrated to the solvent peak in reference to the tetramethylsilane standard. Electronic absorption experiments were carried out on a Varian Cary 5000 UV-vis-NIR spectrophotometer. Mass spectrometry was performed by the CESAMO analytical centre (University of Bordeaux, France) on a QStar Elite mass spectrometer (Applied Biosystems). The instrument is equipped with an ESI source and spectra were recorded in the positive mode. The electrospray needle was maintained at 5000 V and operated at room temperature. Samples were introduced by injection through a 10 μL sample loop into a 200 μL/min flow of methanol from the LC pump. Dynamic Light Scattering (DLS) was used to determine the average size of

extruded liposomes and polymersomes in solution. The measurements were performed on a Malvern ZetaSizer Nano ZS instrument with detection at 90°. Samples were analyzed at room temperature. Osmolarity measurements were performed with a freezing point Type-15M automatic osmometer (Löser, Berlin, Germany). Irradiation experiments were carried with a Mercury-Xenon 200 W lamp. A filter was used to cut UV light below 400 nm. The wavelength range was 400-550 nm. Samples (≈1-2 mL) were placed 1 cm from the light guide output end and irradiated in the dark under magnetic stirring for a defined time. Osmolarities were measured before and after irradiation. Viscosities were determined with a DMA generation M density meter equipped with a Lovis 2000 M/ME rolling ball micro-viscometer from Anton Paar at 20°C.

2.3. Vesicle preparation

Poly(butadiene)-*b*-poly(ethylene oxide) ($PBut_{2.5}$-*b*-$PEO_{1.3}$) giant polymersomes were prepared by a previously reported emulsion-centrifugation method. Briefly, 5 µL of sucrose 0.38 M was poured into 3 mg/mL $PBut_{2.5}$-*b*-$PEO_{1.3}$ in 500 µL toluene. The solution was vigorously hand-shaken for 30 seconds to create a water-in-oil emulsion. An interface was prepared by pouring 30 µL of $PBut_{2.5}$-*b*-$PEO_{1.3}$ (3 mg/mL) in toluene over 30 µL glucose 0.38 M and allowed to stabilize for 30 minutes. 60 µL of the above emulsion was slowly poured over the interface and the sample was immediately centrifuged (3 min, 500 g, ambient temperature). The resulting polymersomes were recovered in the lower phase. In the case of calcein or methylene blue (MB)-loaded polymersomes, the dye was dissolved in a sucrose solution to reach the desired concentration and 5 µL of this solution was used to form the emulsion. The concentration of glucose was adjusted to the same osmotic pressure as the dye in sucrose solution. For the ROS quenching experiment with sodium azide (NaN_3), the desired concentration of NaN_3 was added to the calcein in sucrose solution and 5 µL of this solution was used to form the emulsion. The concentration of glucose was adjusted to the same osmotic pressure (sucrose and dye-containing solution).

2.4. Confocal microcopy observations

Laser scanning confocal microscopy images were acquired on an inverted Leica TCS SP5 microscope equipped with an HCX PL APO 63×, NA 1.4 oil immersion objective in fluorescence mode. Samples (≈20 µL) were injected in a homemade chamber that was sealed to prevent evaporation. The laser outputs were controlled *via* the Acousto-Optical Tunable filter (AOTF) and the two collection windows using the Acousto-Optical Beam Splitter (AOBS) and photomultipliers (PMT) as follows: Alexa Fluor 405 was excited with a diode laser at 405 nm and measured with emission settings at 415-455 nm, calcein was excited with an argon laser at 488 nm (3-20 %) using a 418-423 nm window, rhodamine was excited at 561 nm using a 575-600 nm window and MB was excited at 633 nm with emission settings at 650–700 nm (90%). The Helium-Neon laser at 633 nm (10 %) was also used in transmission mode. Images were collected in simultaneous mode using a resonant scanner at 8000 Hz in bidirectional mode at a resolution of either 512×512, 1024×1024 or 1024×256 pixels. For the pore opening measurements, a lower resolution was used (128×128) to acquire 1frame/10ms. The FRAP wizard using the fly mode for faster time resolution was used to define regions of interest (ROIs) around chosen vesicles. Processing of fluorescence confocal acquisitions was performed with the ImageJ freeware.

2.5. Gel assisted giant unilamellar vesicle (GUV) formation

Giant liposomes were prepared by spin-coating and film rehydration on polyvinyl alcohol (PVA, Mw=143 000 g·mol^{-1}, 100 % hydrolyzed, Merck S6585 194 247) gel.[31] A few drops of 30 mM calcein in 5 % PVA solution in water (pH adjusted to 7.4) were spin coated on a microscope coverslip (2500 rpm, 3 minutes). 1-Palmitoyl-2-oleoyl-*sn*-glycero-3-phosphocholine (POPC) lipids (1 mg/mL) tagged with rhod PE and dissolved in chloroform were spread out on the dried calcein-PVA film. After solvent evaporation, small chambers were formed and filled with 1 mL sucrose solution (0.35 M). GUV formation was followed under the confocal microscope (bright field). Glass micropipettes used to aspire the GUVs were prepared using a pipette puller (from Sutter Instrument: Model P97) followed by micro-forge treatment of the tip to adjust the inner diameter of the capillary around 5-10 µm. A micromanipulator (Eppendorf PatchMan NP2) connected to a water reservoir was used to move the micropipette. A micrometer allowed both to move the water reservoir with precision and to measure the low pressures applied to the aspired GUVs.

2.6. Photocapture of singlet oxygen

Photocapture of singlet oxygen was determined upon excitation at 488 nm (calcein) or 633 nm (methylene blue) on an optical bench equipped with a 150 W Hg-Xe lamp and a monochromator. Samples (ratio fluorescent dye/oxygen trap : 10 µM / 40 µM in sucrose 0.35 M) were stirred during the irradiation and the amount of converted material was determined by UV-visible spectroscopy following the disappearance of the absorption band of the oxygen trap at 425 nm.

2.7. Small unilamellar liposome/polymersome preparation and incorporation in giant polymersomes

Liposomes were prepared by the thin film rehydration method, followed by extrusion. 1,2-Dipalmitoyl-*sn*-glycero-3-phosphocholine (DPPC) lipids (6 mg/mL) and L-α-phosphatidylethanolamine-N-(lissamine rhodamine B sulfonyl) (rhod PE) (0.1 mg/mL) were solubilized in chloroform. 1 mL of the above solution was evaporated on a rotary evaporator and rehydrated under magnetic stirring with 1.5 mL milliQ water (50 °C, overnight). The resulting suspension was extruded (Avanti Mini-Extruder, Avanti Polar Lipids) through a 400 nm poly-carbonate filter. For the encapsulation in the giant polymersomes, the vesicle preparation protocol was followed. 15 µL of the liposomes suspension was added to 15 µL of 30 mM calcein in sucrose 0.35 M and 5 µL of this solution was used to form the emulsion. The concentration of the glucose solution for the interface was adjusted to the same osmotic pressure as the liposomes in calcein-sucrose solution. The same procedure was applied to form PBut-*b*-PEO (Mn x 10^3: 1.2-*b*-0.6) polymersomes with ≈ 3 wt. % PBut (Mn=1700 g·mol^{-1}) tagged with Alexa Fluor 405.[19]

2.8. Synthesis of N-diethyl, O-({7-[bis(carboxymethyl)-amino]coumarin-4-yl}methyl carbamate (11)

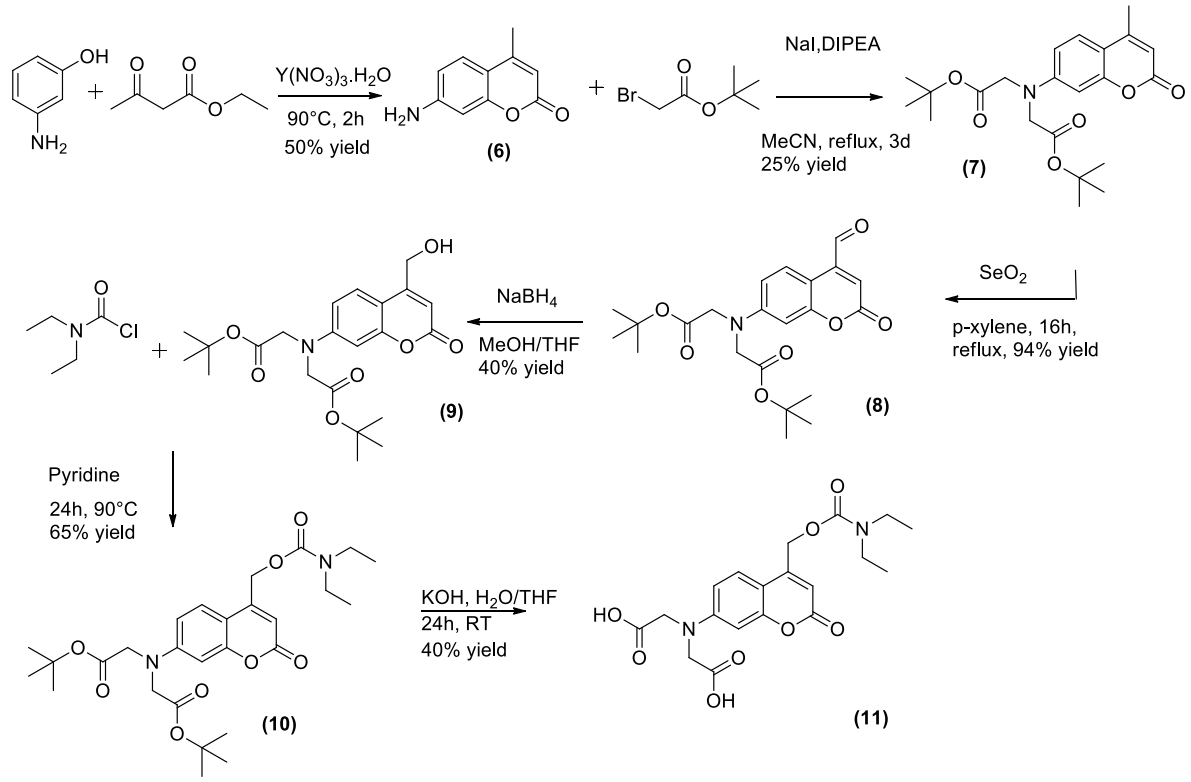

Scheme 2. Synthesis reaction scheme of N-diethyl, O-({7-[bis(carboxymethyl)-amino]coumarin-4-yl}methyl carbamate

The synthesis protocol was adapted from literature procedures for a structurally-related photoactive conjugate.[32,33]

7-amino-4-methylcoumarin (6): Ethyl acetoacetate (45.8 mmol, 1eq) was added to a mixture of 3-aminophenol (45.8 mmol, 1eq) and $Y(NO3)_3.6H_2O$ (4.58 mmol, 0.1 eq) in a 100 mL round bottom flask. The reaction mixture was stirred at 90°C for 2 hours. The mixture was dispersed in water and the solid was filtered. The resulting crude product was then recrystallized from EtOH to give a yellow/green crystalline powder (50% yield).

^{1}H NMR (DMSO, 300 MHz) δ (ppm): 7.41 (d, 1H), 6.57 (dd, 1H), 6.41 (d, 1H), 6.12 (s, 2H), 5.91 (s, 1H), 3.35 (s, 1H), 2.31 (s, 3H).

Di-tert-butyl 2,2'-((4-methyl-2-oxo-2H-chromen-7-yl)azanediyl)diacetate (7): Compound **6** (22.8 mmol, 1eq) was dissolved in MeCN (120 mL) in a round-bottom flask of 250 mL and then *t*-butylbromoacetate (114 mmol, 5 eq) , NaI (45.4 mmol, 2eq) and DIPEA (91 mmol, 4eq) were added. The mixture was heated at reflux for 3 days. Then the mixture was concentrated in vacuo and the residue was dissolved in EtOAc (100 mL) and washed with water (100 mL) and brine (100 mL) and dried over $MgSO_4$. Following purification by column chromatography on silica gel (cyclohexane/EtOAc, 5:1) and solvent removal, an orange solid was obtained (25% yield).

^{1}H NMR (DMSO, 300 MHz) δ (ppm): 7.57 (d, 1H), 6.58 (dd, 1H), 6.43 (d, 1H), 6.05 (d, 1H), 4.19 (s, 4H), 2.36 (d, 3H), 1.43 (s, 18H).

Di-tert-butyl 2,2'-((4-formyl-2-oxo-2H-chromen-7-yl)azanediyl)diacetate (8): Selenium dioxide (10.9 mmol, 2eq) was added to a solution of compound **7** (5.45 mmol, 1eq) in *p*-xylene (55 mL). The resulting mixture was heated at reflux for 16 h and filtered while hot. The filtrate was concentrated in vacuo yielding a dark orange solid (94%).

^{1}H NMR (DMSO, 300 MHz) δ (ppm): 10.10 (s, 1H), 8.25 (d, 1H), 6.78 (s, 1H), 6.66 (dd, 1H), 6.53 (d, 1H), 4.22 (s, 4H), 1.44 (s, 18H).

Di-tert-butyl 2,2'-((4-(hydroxymethyl)-2-oxo-2H-chromen-7-yl)azanediyl)diacetate (9): Compound **8** (4.8 mmol, 1 eq) was dissolved in a mixture of methanol (50 mL) and THF (50 mL) and the solution was cooled on ice. $NaBH_4$ (7.2 mmol, 1.5 eq) was added in small portions and the reaction mixture was stirred for 3 h. After this time, the reaction was quenched by addition of 1 N aqueous HCl (20 mL) and the mixture was extracted twice with EtOAc. The combined organic layers were washed with brine and dried ($MgSO_4$). The product was purified by column chromatography over silica gel (cyclohexane:AcOEt; 1:1 *v*/*v*) and resulted in a green solid (40% yield).

^{1}H NMR (DMSO, 300 MHz) δ (ppm): 7.50 (d, 1H), 6.55 (dd, 1H), 6.45 (d, 1H), 6.16 (s, 1H), 5.56 (t, 1H), 4.70 (d, 2H), 4.19 (s, 4H), 1.43 (s, 18H).

Di-tert-butyl-2,2'-((4-(((diethylcarbamoyl)oxy)methyl)-2-oxo-2H-chromen-7-yl)azanediyl)diacetate (10): Diethylcarbamoyl chloride (0.5 mL, excess) was added to a solution of compound **9** (0.24 mmol, 1 eq) in pyridine (3 mL) at ambient temperature. Then the mixture was heated to 90°C for 48 hours under a nitrogen atmosphere. After the reaction mixture was cooled to ambient temperature, 1N HCl was added and the mixture was extracted with EtOAc. The combined organic layers were washed with saturated $NaHCO_3$ solution and concentrated. Then the crude product was purified by silica column chromatography, eluting with cyclohexane:EtOAc (5:1, *v*/*v*) yielding the product (40% yield) upon solvent removal.

^{1}H NMR ($CDCl_3$, 300 MHz) δ (ppm): 7.40 (d, 1H), 6.54 (m, 2H), 6.24 (s, 1H), 5.29 (d, 2H), 4.09 (s, 4H), 3.38 (q, 4H), 1.52 (s, 18H), 1.2 (t, 6H).

^{13}C NMR ($CDCl_3$, 400 MHz) δ (ppm): 167.9, 160.7, 154.6, 153.8, 150.2, 149.5, 123.5, 108.1, 107.3, 106.8, 98.2, 81.5, 61.1, 53.3, 41.2, 40.4, 28.7, 27.1, 13.1, 13.4.

MS-TOF: m/z = 541.2520 calculated for $C_{27}H_{38}N_2O_8Na$; m/z = 541.2504 $[M+Na]^+$

2,2'-((4-(((diethylcarbamoyl)oxy)methyl)-2-oxo-2H-chromen-7-yl)azanediyl)diacetic acid (11) : Compound **10** (0.058 mmol, 1eq) was dissolved in THF (0.5 mL). Then 0.13 mL of a water solution containing 100 mg of KOH in 1 mL of water was added (KOH = 4eq). The mixture was stirred at room temperature overnight. Water and THF were removed and the product was dissolved in water and precipitated on adding a small amount of HCl until precipitate formation was complete. The product, which was a red powder, was filtered off and dried in vacuo (50% yield).

^{1}H NMR (DMSO, 600 MHz, 60°C) δ (ppm): 7.53 (d, 1H), 6.64 (dd, 1H), 6.5 (d, 1H), 6.01 (s, 1H), 5.28 (s, 2H), 4.22 (s, 4H), 3.31 (q, 4H), 1.12 (t, 6H).

^{13}C NMR (MeOD, 400 MHz) δ (ppm): 175.8, 162.3, 155.6, 155.2, 152.0, 150.7, 125.0, 109.0, 107.7, 106.4, 98.0, 62.1, 56.3, 41.9, 41.3, 13.0, 12.2.

TOF-MS $[M-H]^+$: m/z=405.1303 calculated for $C_{19}H_{21}N_2O_8$; Found: m/z=405.1301

3. Results and discussion

3.1. Photo-cleavable dyes

3.1.1. Coumarin

Poly(butadiene)-*b*-poly(ethylene oxide) ($PBut_{2.5}$-*b*-$PEO_{1.3}$) giant unilamellar vesicles (GUVs) were prepared by a previously reported emulsion-centrifugation method.[34] As suggested in Scheme 1. a), due to the limited water permeability of the polymersome membrane, compared to liposomes, we initially hypothesized that a sudden increase in the internal osmotic pressure of the vesicles would lead to efficient rupture of the membrane. Indeed, water would be unable to diffuse into the cavity fast enough to compensate for the pressure difference between the lumen and the external medium. The outcome is that the membrane is exposed to a large lateral tension and ruptures irreversibly to release pressure. On the other hand, liposomes exhibit a tenfold larger permeability towards water compared to polymersomes, and whenever a pore opens up, the lateral stress on the membrane can be relaxed by hydrodynamic flow from inner to outer solutions through transient pores reported by many groups on large or giant liposomes irrespective of the means used to stress their bilayer: osmotic pressure[35], applied electric field[36], lipid photo-oxidation[37] or membrane dye illumination[38] (Scheme 1. b). Osmotic pressure was also shown to induce shell rupture of layer-by-layer coated gel beads releasing micro-capsules.[39]

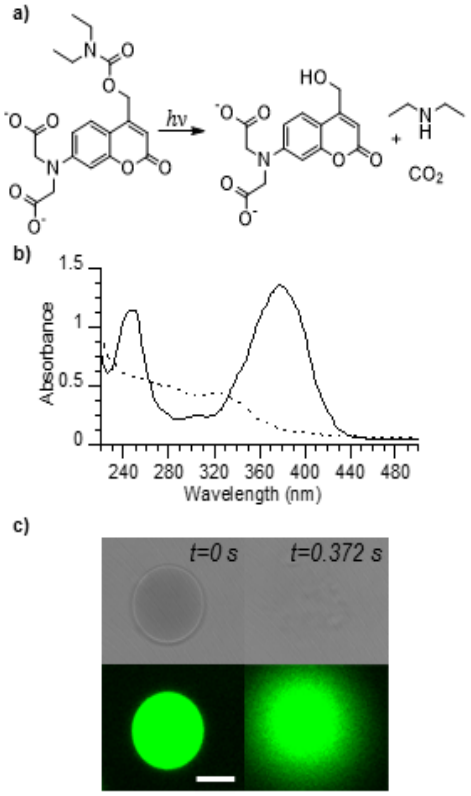

Figure 1. a) Photocleavage of N-diethyl, O-({7-[bis(carboxymethyl)-amino]coumarin-4-yl}methyl carbamate (coumarin derivative) under irradiation. b) Electronic absorption spectrum of a 80 μM coumarin derivative in aqueous solution before and after (dashed line) 30 min irradiation at 365 nm with a 200 W Hg-Xe lamp. c) Confocal observation of a 10 mM coumarin-loaded GUV (green channel, emission range of coumarin, 485 nm). The vesicle undergo fast (few milliseconds) rupture upon irradiation at 405 nm (50 mW, 25%). Scale bar = 10 μm.

To test our hypothesis, a photodegradation experiment was performed to confirm that fast *in situ* molecule fragmentation and subsequent osmotic pressure increase in the lumen of giant polymersomes could indeed cause vesicle rupture. In this context, N-diethyl, O-({7-[bis(carboxymethyl)-amino]coumarin-4-yl}methyl carbamate (coumarin derivative (**11**)) was synthesized, inspired by a previously described procedure.[32] It has been established that coumarin derivatives undergo heterolytic C-O bond cleavage under UV irradiation. This cleavage results in the formation of a carbamate ion. After decarboxylation of the carbamate, carbon dioxide and diethylamine are released ($\Phi_{reaction}$ = 0.003 on irradiating at 405 nm) (Figure 1. a).[40] Cleavage of the molecule was confirmed by a decrease and a shift of the absorption band after 30 min UV irradiation (365 nm, 200 W Hg-Xe lamp) (Figure 1. b). This photoinduced coumarin cleavage feature was used as a way to increase the osmotic pressure

inside the polymersomes. The molecule was encapsulated inside the $PBut_{2.5}$-*b*-$PEO_{1.3}$ GUVs. The vesicles were then irradiated under confocal observation (405 nm, 50 mW, 25%) resulting in a fast (few milliseconds) explosion (Figure 1. c). As a control, dye-free (sucrose-loaded) polymersomes were irradiated at 405 nm and coumarin-loaded polymersomes were irradiated at 488 nm and 561 nm. In all cases, no rupture was observed, confirming that the explosion results from coumarin selective irradiation.

3.1.2. Calcein and methylene blue

In order to broaden the scope and versatility of the release process, we reasoned that as increased osmolarity is a colligative process, any molecule able to degrade/cleave following illumination would potentially provide a complementary alternative release pathway. In this context, we chose two hydrophilic fluorescent dyes, calcein and methylene blue (MB), that are known to be effective photosensitizers.[41,42] Upon irradiation in the visible region, they generate reactive oxygen species (ROS) including singlet oxygen ($^1O_2$) *via* energy transfer from the excited triplet state of the dye to the triplet ground state of molecular oxygen ($^3O_2$).[43]

We hypothesized that the fast generation of reactive species upon irradiation would result in increasing the osmotic pressure inside the lumen of the polymersomes and would lead to vesicle bursting. As shown in the confocal images of Figure 2. a), and b), irradiation of GUVs loaded with either 15 mM calcein (λ_{exc}=488 nm,) or 10 mM MB (λ_{exc}=633 nm,) led to a rapid (t <10 s) rupture of the membrane and content release (SI, videos S1, S2). For both dye-loaded vesicles, no bursting occurred on illuminating at wavelengths outside the dye absorption bands, nor for dye-free vesicles (sucrose-loaded only) at any available wavelength (SI, video S3), confirming that the mechanism is not related to direct local heating or any other disturbance of the membrane due to the laser excitation.

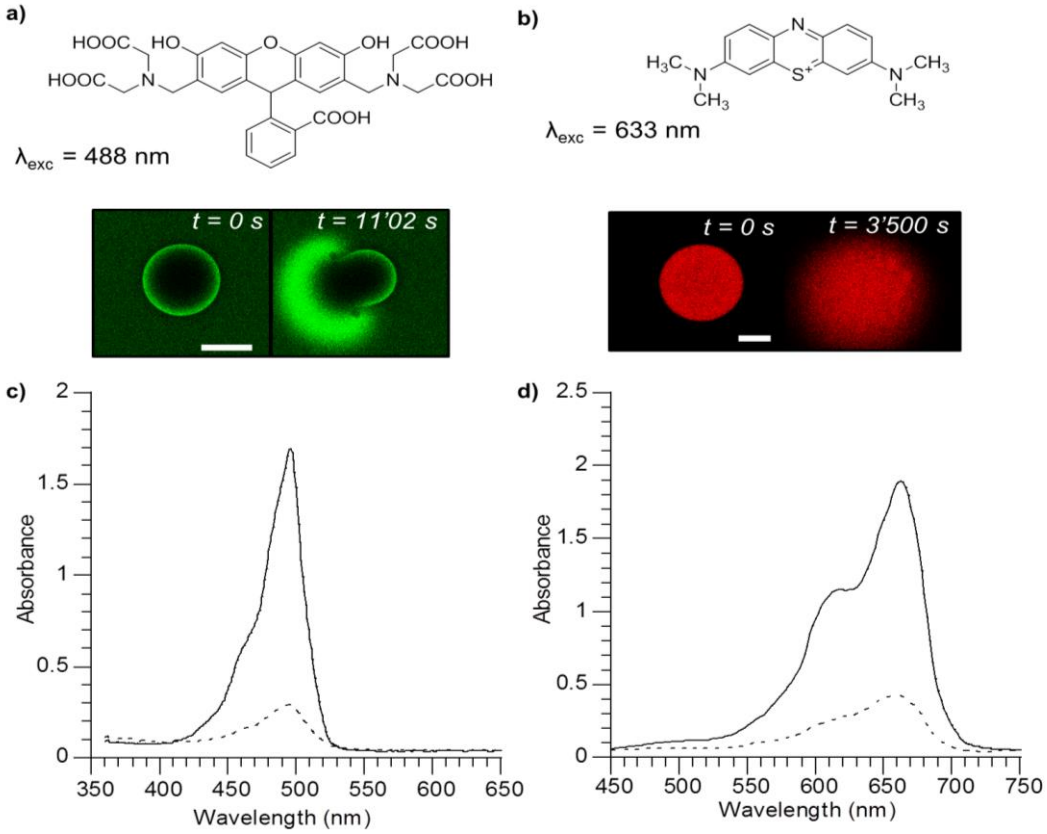

Figure 2. a) Chemical structure of calcein and confocal images of a 15 mM calcein-loaded polymersome irradiated at 488 nm, with laser intensity 40 mW, 5% (green channel, emission range of calcein, 520 nm). b) Chemical structure of methylene blue (MB) and confocal images of a 10 mM MB-loaded polymersome irradiated at 633 nm with laser intensity 10 mW, 90% (red channel, emission range of MB, 660 nm). c) Electronic absorption spectrum of a 30 μM calcein photosensitizer in aqueous solution before and after (dashed line) 30 min irradiation in the 400 – 550 nm range with a 200 W Hg-Xe lamp equipped with a bypass filter, showing photoinduced degradation. d) Electronic absorption spectrum of a 30 μM methylene blue in water solution before and after

3.2.ROS-mediated vesicle rupture

3.2.1. ROS generation

To further understand the mechanism of vesicle bursting at the molecular level, we investigated the role of ROS production in the overall phenomenon.

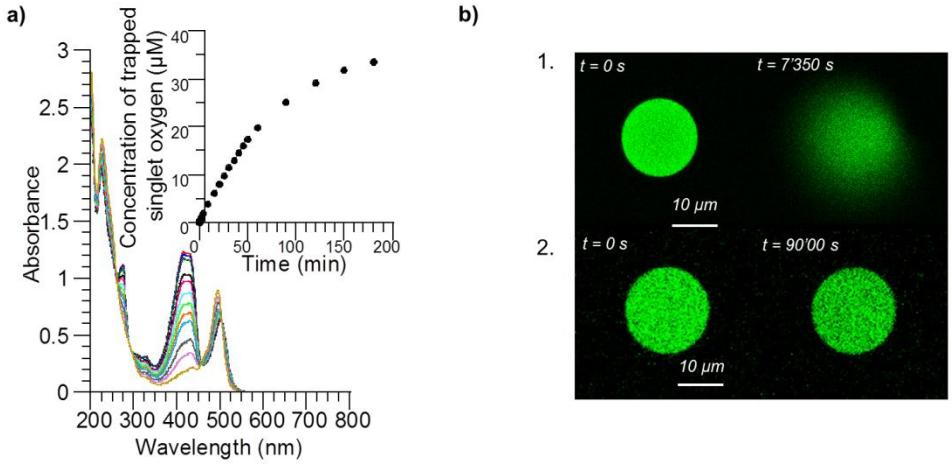

Figure 3. a) UV-visible absorption spectra of a solution of calcein (λ_{max} = 488 nm) and singlet oxygen scavenger (λ_{max} = 425 nm) (ratio 1:4) during irradiation at 488 nm and singlet oxygen consumption over time. The decrease of the absorption of the scavenger indicates the consumption of singlet oxygen during irradiation. b) Confocal images of 5 mM calcein-loaded $PBut_{2.5}$-b-$PEO_{1.3}$ polymersomes during irradiation (488 nm) 1. without and 2. with 3 eq. sodium azide (NaN_3). NaN_3 efficiently prevents vesicle rupture (verified on ~15 vesicles).

We first evaluated the generation of ROS using a scavenger for singlet oxygen ($^1O_2$), known to be predominantly generated by excited calcein in the presence of oxygen.[43] The scavenger is a hydrophilic derivative of 1,3-diphenylisobenzofuran (DPBF), used for the detection of $^1O_2$ in vitro.[44] A mixture of calcein in sucrose was prepared with a four-fold excess of the scavenger. The evolution of the absorption band of the scavenger was followed spectrophotometrically during excitation of the solution at 488 nm on an optical bench (Figure 3. a). The disappearance of the main emission band at 425 nm (arrow) as a function of illumination time, which is directly correlated with the consumption of $^1O_2$, confirmed that ROS were effectively generated by calcein upon irradiation. If ROS generation is part of the process leading to membrane rupture, then the use of a scavenger should prevent vesicles from bursting, as confirmed in Figure 3. b using sodium azide (NaN_3) as a $^1O_2$ quencher.[45] Under the same irradiation conditions, explosion was inhibited by the presence of the oxygen scavenger, meaning that the scavenger efficiently trapped the generated singlet oxygen. In order to evaluate the consequence of singlet oxygen generation on the osmotic pressure change, a solution of calcein in sucrose (at varying concentration) was prepared at the same concentration as that used in polymersome formation (15 mM). The solution was irradiated at wavelengths ranging between 400 nm and 550 nm for 30 min using a mercury-xenon (Hg-Xe) lamp equipped with a broadband filter, and the

osmolarity of the solutions was measured before and after the irradiation by the freezing point determination method.

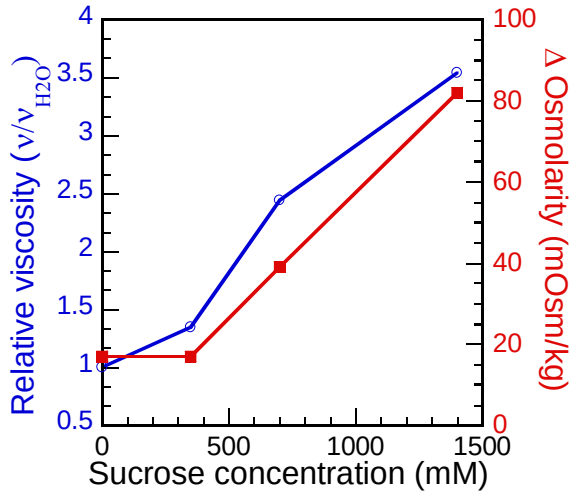

Figure 4. Evolution of osmolarity increase upon irradiation correlated with the relative viscosity of 15 mM calcein in increasing sucrose concentrations. Calcein solutions (15 mM) with different sucrose concentrations were irradiated for 30 min in the 400 - 550 nm range with a 200 W Hg-Xe lamp equipped with a filter. Osmolarites were measured before and after irradiation. The difference in osmolarity after irradiation increases with the sucrose concentration, which determines the relative viscosity of the solution (ratio compared to pure water).

Solution osmolarity was found to significantly increase (up to 80 mOsm/kg) with increasing sucrose concentration (Figure 4**)**. For a solution of 0.35 M sucrose and 15 mM calcein, there was an increase of 18 mOsm/kg after irradiation, whereas no increase was observed when irradiating pure sucrose solutions. Irradiation of calcein in the absence of sucrose led to the same increase of osmotic pressure, thus proving the non-interference of sucrose in the process. Then, we observed that increasing viscosity was correlated with a higher osmolarity difference after irradiation. Indeed, for 0.7 M sucrose, the osmolarity increase was about 40 mOsm/kg and it doubled for 1.4 M sucrose. We propose the interpretation that the viscosity of the solution has an impact on the diffusion of ROS and promotes degradation of the dye by lowering their diffusion away from the dye molecule.

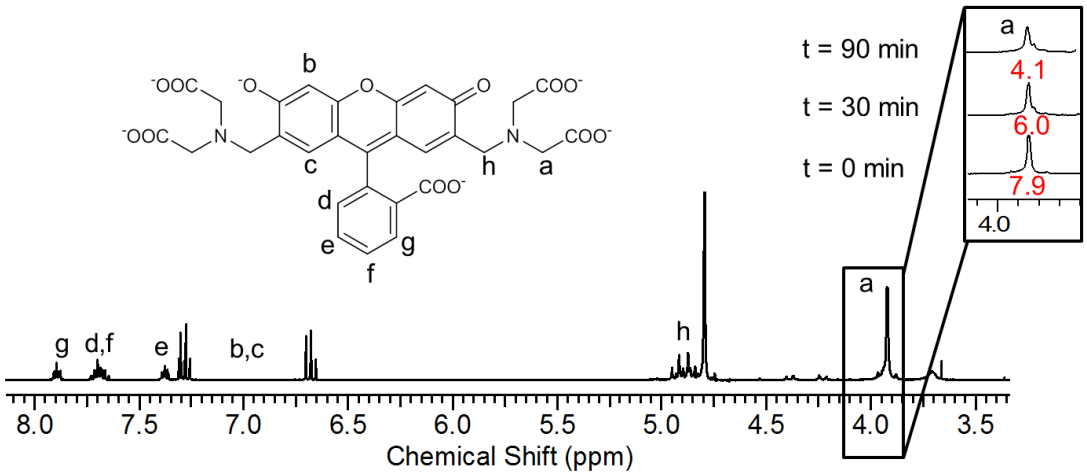

Figure 5. ^{1}H NMR in D_2O of calcein before and during irradiation (t=30 and 90 min). Integration of proton a resonance (-CH2-COOH, δ=3.9 ppm) decreases with irradiation time indicating a probable cleavage of the –CH_2-COOH arm mediated by ROS. Reference resonance for integration: aromatic proton e (H, δ=7.9 ppm).

^{1}H NMR analysis of calcein in D_2O during irradiation (Figure 5) proved that the changes in osmolarity were most certainly due to its degradation. Indeed, a decrease of the intensity of the resonance of the CH_2 proton adjacent to the carboxylic moiety (**a**, δ=3.93 ppm, -CH_2-COOH) was observed as a function of irradiation time. Moreover, the apparition of a peak at 8.46 ppm after irradiation was consistent with the presence of formic acid, one of the probable degradation products.[46] The control experiment, which consisted of irradiating solutions without calcein, did not show any change (Figure S 1and Figure S 2). Additional control ^{1}H NMR experiments were performed in order to verify the non-interference of ROS with the membrane of the polymersomes (Figure S 3 and Figure S 4). Based on these results, as well as previous studies of ROS-mediated oxidation[46], the suggested mechanism is based on a radical-mediated oxidation of calcein, leading to an increase of the internal osmotic pressure of the vesicle caused by the degradation products, arising through bond cleavage at the position labeled **a** on Figure 5 (and also most likely at the two quasi-equivalent methylene groups adjacent to the carboxylate moiety). The same experiments were performed with MB and showed that the dye underwent auto-degradation through the same process (Figure S 5 and Figure S 6).

3.2.2. Vesicle permeability and water diffusion

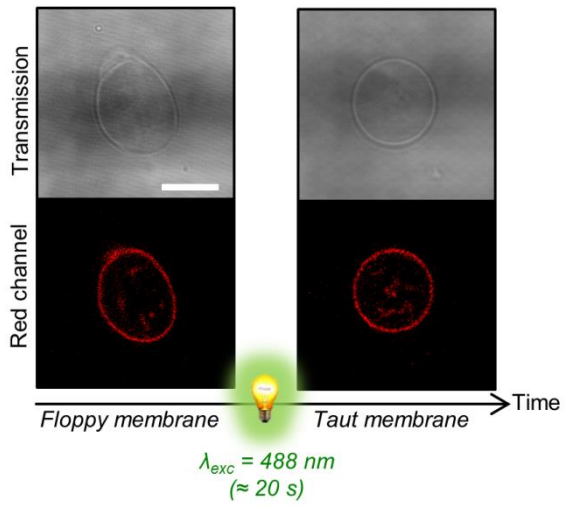

Figure 6. Confocal observations of POPC GUVs loaded with 30 mM calcein before and after irradiation at 488 nm. The membrane is doped with L-α-Phosphatidylethanolamine-N-(lissamine rhodamine B sulfonyl) to allow observation in the red channel. Upon irradiation, the vesicle membrane tightens without rupturing.

If the limited diffusion of water across the membrane is responsible for the explosion, using a much more permeable membrane should prevent it. In order to test this hypothesis, we formed 1-palmitoyl-2-oleoyl-sn-glycero-3-phosphocholine (POPC) GUVs[31], as lipidic membranes are known to exhibit tenfold higher permeability towards water than polymersomes.[47] Figure 6 represents confocal images of a POPC GUV loaded with 30 mM calcein before and after irradiation. For visualization in the red channel, the membrane was tagged with rhodamine. The images clearly show a floppy membrane before irradiation. After being excited (λ_{exc}= 488 nm; 5 % laser intensity; 20 s), the vesicle swelled without rupturing, even if higher laser intensity and/or illumination times were applied. These observations confirmed that water indeed diffused into the interior of such permeable lipidic vesicles to compensate for the osmotic imbalance, inducing its swelling, but without a rupture of the membrane. This scenario was confirmed by an additional experiment where a POPC GUV was partially aspired through a micropipette to evaluate its internal volume increase and hence the initial osmotic pressure increase upon calcein irradiation (Figure 7).

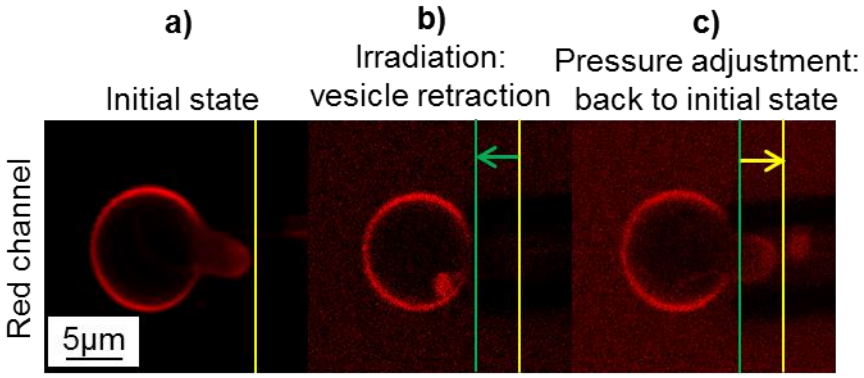

Figure 7. Controlled membrane deformation of a phospholipid GUV by pressure adjustments through aspiration in a capillary. Confocal images of a 30 mM calcein-loaded POPC GUV aspired inside a micropipette. The membrane is tagged with rhodamine for visualization in the red channel. Image a) shows the vesicle before irradiation. In image b), the vesicle is irradiated at 488 nm (calcein) and then (image c)) the pressure is adjusted (i.e. the level of the tank is decreased by a 55 mm height, corresponding to a negative pressure of 540 Pa) to aspire the vesicle portion within the capillary back to its initial position $\boldsymbol{L_P = 5}$ *µm.*

In the initial state (**a**), the vesicle has not been irradiated at 488 nm and the floppy membrane is rendered tauter by aspiration inside the capillary. When the vesicle is irradiated at 488 nm (**b**), calcein generates ROS that degrade the dye and induce an increase of the osmotic pressure. As the lipid membrane is permeable, water is able to enter the GUV to compensate for the osmotic imbalance. This results in a swelling of the vesicle and a retraction of the membrane tongue from the capillary by a length $\Delta L_\mathrm{P} \approx -4$ µm. Using an equation introduced by Olbrich *et al.* for osmotically-swollen giant liposomes under micropipette aspiration,[48] we can estimate the volume increase of liposomes caused by irradiation and ROS production: $\Delta V = -\pi D_\mathrm{P}(D_\mathrm{V} - D_\mathrm{P})\Delta L_\mathrm{P}/4 = 91$ µm^3 for a vesicle of diameter $D_\mathrm{V} = 10.8$ µm (initial volume $V_\mathrm{i} = 660$ µm^3) aspired in a pipette of diameter $D_\mathrm{P} = 5$ µm. The ratio $\Delta V/V_\mathrm{i} \approx 0.14$ can give an estimate of the osmotic pressure variation under illumination $\Delta C/C_\mathrm{i} \approx 0.14$ where the initial osmolarity is $C_\mathrm{i} = 380$ mOsm $\cdot$ kg^{-1}. Therefore we can estimate the osmolarity increase build up by light-induced ROS production and dye degradation at $\Delta C \approx 52$ mOsm $\cdot$ kg^{-1} . When the pressure inside the capillary (**c**) was adjusted to pull the vesicle tether end back to its initial position, the lateral tension was raised up to $\sigma = 1.3$ mN.m^{-1}, a value still below the maximum lateral tension that a phospholipic GUV can withstand σ_lys~10 mN·m^{-1}.[48]

3.3.Membrane pore opening dynamics

The dynamics of pore opening were experimentally monitored and fitted with a theoretical model proposed by Mabrouk *et al.* in which they describe the curling of polymersome membranes induced by nucleation of a pore as a result of creation of an excess area on one of the two leaflets of the membrane through photo-isomerization of azobenzene moieties.[49] We show that our system exhibits the same trends in pore opening dynamics although the initial constraint needed to induce membrane rupture is different in the two cases.

According to their model, the opening of a pore in the membrane can be compared with the curling rim instability of a bimetallic spring or an asymmetric elastic sheet. The dynamics of pore growth is governed by a transfer of the membrane surface elastic energy S into viscous dissipation of the curling rim within the solution (either the inside solution of the polymersome if the rim curls inward, or the outside solution if the rim curls outwards, depending on whether the photoisomerizable groups are located on the outer or inner leaflet of the asymmetric block copolymer bilayer, respectively). In our case, Figure 2**.** a) clearly shows the calcein outward flow through the pore (the fluorescence bursts arising from a suddenly unquenched signal by dye dilution), whereas the still quenched solution pocket trapped inside the rim is moving into the external medium. Our experiments are thus consistent with their model: the vesicles might also experience a change of spontaneous curvature due to the photo-osmotic phenomenon described to occur in the inner compartment. The pore opening dynamics has two regimes:[49] constant velocity at the early stages, followed by a quasi-diffusive regime at longer times. More precisely, the effective diffusion constant of the rim (governing the rate of pore opening at long times) is expected to have a bulk (external) solution viscosity dependence when the rim is directed outwards (provoked by azobenzene groups in the inner leaflet in the previous case or internal osmotic pressure in the current case). In their initial publication,[49] Mabrouk *et al.* gave an oversimplified form $r^2 + 2\,r\,r_c = D_{\text{eff}}t$ that simply reduces to linear regime $r \sim (D_{\text{eff}}/2r_c)\,t$ at early stages and to pure diffusive regime $r \sim \sqrt{D_{\text{eff}}t}$ at long stages. Subsequently, they considered a slightly modified form of the growth dynamics of a pore of radius r at time t as given by Equation (1) [50]:

$$2r_c\,\dot{r}/D_{\text{eff}} = 2/(1+\frac{r}{r_c})^{\frac{1}{2}} - 1/(1+\frac{r}{r_c}) \qquad \text{Eq. (1)}$$

where D_{eff} is the effective diffusion coefficient and r_c is defined as the critical pore radius, $r_c = \pi\kappa/(eS_0)$, κ being the bending modulus of the membrane, e the membrane thickness and S_0 the stored elastic energy per unit area at initial time t=0). As the line tension (or line energy) of a pore in the membrane is usually expressed as $\tau = \kappa/2e$, we can also write $r_c = 2\pi\,\tau/S_0$ which represents well the balance between the 2 driving forces that determine the nucleation pore radius: on one side the elastic energy that tends to open up the pore ($\pi {r_c}^2 S_0$) and on the opposite the line energy that closes it ($2\pi r_c\,\tau$).

The effective diffusion coefficient D_{eff} is given by:

$$D_{\text{eff}} = 2r_c S_0/(\eta\, ln) = 2\pi\kappa/(e\eta ln) = 4\pi\tau/(\eta ln) \approx 5\tau/2\eta \quad \text{Eq. (2)}$$

where η represents the viscosity of the solution in which the membrane curls (the outside glucose solution in our case) and *ln* is a logarithmic term arising from the drag coefficient of a cylinder that is considered as constant:[49] $ln = \ln(2\pi\, r/L) + 1/2 \approx 5$, and $4\pi/ln \approx 5/2$ (hence the simplified right term on Eq. (2).)

To compare our system with the aforementioned one, we prepared three different batches of giant vesicles with the emulsion-centrifugation technique (see experimental methods) with varying glucose concentrations. In each experiment, the concentration of the inner sucrose solution was adjusted to reach an osmotic equilibrium with the outer glucose solution. Calcein (15 mM) was encapsulated within the vesicles to enable bursting under laser irradiation (488 nm, 5-10 % laser intensity). Movies of pore bursting were obtained at the highest achievable speed of the Leica SP5 resonant scanner (100 frames/s). The extracted frames of the explosions were processed with ImageJ freeware to track and measure membrane pore growth. For each glucose concentration, the experiment was repeated on an average of ten vesicles of equivalent sizes, and the results were plotted on a master curve (horizontal error bars represent standard deviations from different vesicles and horizontal error bars correspond to ± 5 ms, i.e. half of the interval between successive frames) (Figure 8).

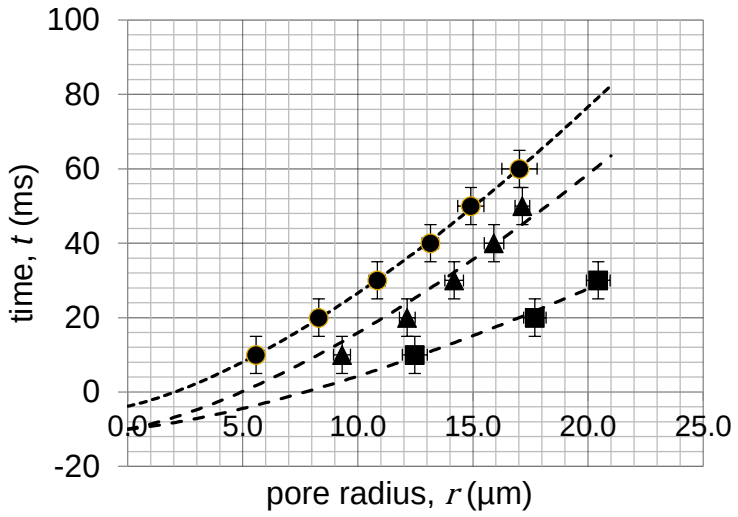

Figure 8. Variations of pore opening dynamics in $PBut_{2.5}$-b-$PEO_{1.3}$ vesicles containing sucrose and calcein 15 mM depending on viscosity of the external glucose solution. Pore radius as a function of time for three different glucose viscosities as averaged on several pore dynamics: (●) η=1.33 mPa·s, (▲) η=2.46 mPa·s, (■) η=4.19 mPa·s. Equation (1) was used to fit the experimental data with two parameters: the critical pore radius (r_c) and the effective diffusion constant (D_{eff}). The external glucose concentrations were chosen to balance osmolarity of the internal sucrose/calcein mixtures: (●) sucrose 20% in glucose 10% (0.6 M), (▲) sucrose 50% in glucose 26% (1.475M), (■) sucrose 70% in glucose 36% (2.06 M). Negative points on the time scale arise from the uncertainty about the initial time of pore nucleation (on the order of 10 ms, i.e. the interval between successive frames).

Glucose concentration (M)	**Glucose viscosity η (mPa·s)**	**Apparent diffusion coefficient D_{eff}, (µm²·s⁻¹)**
0.6	1.33	1111
1.475	2.46	612
2.060	4.19	522

Table 1. Variation of the apparent diffusion coefficient with external glucose solution viscosity (measured independently by rolling ball viscosimetry) as obtained by fitting the pore dynamics (Figure 8) with Eq. (1) with a constant critical radius $\boldsymbol{r_c = 0.38}$ µ$\boldsymbol{m}$. The calcein concentration is maintained at 15 mM.

From the fits derived from the experimental data (Eq. (1)), the effective diffusion coefficients D_{eff} could be calculated by fixing the value of the critical radius r_c to 0.38 µm for each viscosity. In agreement with the model proposed by Mabrouk *et al.*, the diffusion coefficient is roughly

inversely proportional to the viscosity of the solution into which the membrane curling rim advances (which determines the viscous losses) as in Eq. (2). The slight deviation from the perfect $\sim 1/\eta$ dependency might be ascribed to a weak variation also of the line tension of the PBut$_{2.5}$-*b*-PEO$_{1.3}$ membrane with the sucrose and glucose concentrations, as with the reported modification of the mechanical properties (κ and thus τ) for phospholipid bilayers exposed to high sugar concentrations.[51] Regarding quantification, we can estimate the structural (hydrophobic thickness *e*) and mechanical (bending modulus κ) properties of the PBut$_{2.5}$-*b*-PEO$_{1.3}$ membrane from their reported experimental values: $e = 9.6$ nm and $\kappa = 24.7 \pm 11.1 k_B T$, according respectively to cryo-TEM image analysis and micropipette measurements.[52] Scaling laws versus the molar mass M_h of the hydrophobic block were proposed by Bermudez *et al.*:[53] $e \sim {M_h}^{1/2}$ and $\kappa \sim K_a e^2 \sim M_h$ since the area expansion elastic modulus was shown to be constant material property $K_a = 102 \pm 11$ mN/m for all the PBut-*b*-PEO copolymer series. Therefore we deduce $e = 6.7$ nm and $\kappa = 11.9 \pm 5.3 k_B T$ for the less commonly used PBut$_{1.2}$-*b*-PEO$_{0.6}$ copolymer. From these values, we can obtain an estimate of the pore line tension: $\tau = \kappa/2e = 3.7 \pm 1.7$ pN and 5.3 ± 2.4 pN for PBut$_{1.2}$-*b*-PEO$_{0.6}$ and PBut$_{2.5}$-*b*-PEO$_{1.3}$, respectively. Such line energies compare well to the value $\tau =$ 4 pN estimated by Mabrouk *et al.* for PBut-*b*-PEO copolymers,[49] and are significantly lower than those measured on DPPC large liposomes at 46°C by Taupin *et al.* through the leakage of parametric probes under various hypotonic shocks (from $\tau = 6.5$ pN for irreversible pores to $\tau = 5.5 - 8$ pN on sub-critical resealing pores)[35], on DOPC giant liposomes by Karatekin *et al.*[54] through the closure dynamics of transient pores (from $\tau = 6.9 \pm 0.4$ pN to $\tau = 20.7 \pm$ 3.5 pN depending on the supplier, and thus of purity, of DOPC), or by Levadny *et al.*[55] by statistical analysis of the pore induction rate under micropipette pulling ($\tau = 10.5 \pm 0.5$ pN). Although the pore dynamics here are qualitatively equivalent to the experiment of Mabrouk *et al.* with photo-isomerizable liquid crystalline copolymers, in our case with PBut$_{2.5}$-*b*-PEO$_{1.3}$ the critical radius $r_c = 0.38\ \mu m$ is much lower, which implies that the initial elastic tension is higher: $S_0 = 8.8 \cdot 10^{-2}\ \mathrm{mN.m^{-1}}$. From the expression of the initial elastic tension $S_0 = \frac{1}{2}\kappa(c_0)^2$, we get an estimate of the spontaneous curvature c_0 of the membrane, from which we deduce the spontaneous radius of curvature $(c_0)^{-1} \approx 24$ nm. Interestingly, this value is typically comparable to the smallest radius that large unilamellar vesicles (LUV) of a given copolymer can withstand from the rule-of-thumb $e/R_{min} \approx 0.25$ as shown by Salva *et al.* after

LUV rupture by hypertonic shocks,[56] thus here $R_{\min} \approx 38\,\mathrm{nm}$ for $PBut_{2.5}$-*b*-$PEO_{1.3}$ polymersomes.

To interpret the different fates between liposomes and polymersomes exposed to increased internal osmotic pressure through dye irradiation at its maximum absorption wavelength, we propose a kinetic control of the membrane pore induction in these two different types of vesicles as opposed to a mere thermodynamic control sometimes put forward by several authors.[57,58] To give quantitative values, the water permeability of monounsaturated phospholipids like POPC measured by the Evans micropipette aspiration method is P~30 µm·s^{-1} and their lysis tension is σ_{lys}~10 mN·m^{-1},[48] whereas values for $PBut_{2.5}$-*b*-$PEO_{1.3}$ polymersomes are respectively P~3.1±1.6 µm·s^{-1} from osmotic inflation experiments[59] and σ_{lys}~16 mN·m^{-1} from micropipette aspiration measurements[60]. In brief, polymersomes resist larger applied lateral stresses than fluid-phase liposomes and exhibit a higher toughness (*i.e.* a larger surface area below the curve of lateral tension *versus* membrane expansion coefficient), but they are 10 times less permeable to water, which is mainly ascribed to their thicker hydrophobic membrane (~6–10 nm as compared to ~3–5 nm). The lateral tension arising from the increased osmotic pressure relative to the external solution after dye photo-degradation can be estimated by the Laplace law of fluid interfaces $\Delta\pi = 2\sigma_0/R_0$ where R_0 is the initial vesicle radius and σ_0 is the lateral tension just before pore aperture. Converting the estimated osmolarity difference $\Delta\pi \approx 18\,\mathrm{mOsm \cdot kg^{-1}}$ into an osmotic pressure through the perfect gas law $\Delta\pi = \Delta cRT = 4.5 \cdot 10^4\mathrm{Pa}$ and using the Laplace law, we obtain a lateral tension σ_0~225 mN·m^{-1} with R_0=10 µm, well above the rupture tension σ_{lys}.

In the case of liposomes, the lateral tension on the membrane built up by the increase of solute concentration inside the vesicles can relax by internal volume reduction through outwards flow across "sub-critical" pores, *i.e.* holes in the bilayer that have a size insufficient to expand (below the critical radius r_c) but nevertheless contribute to increase permeability. Their existence has been evidenced more than four decades ago by the pioneering work of Taupin *et al.*[35] using electron paramagnetic resonance (EPR) probes. These authors also demonstrated that the frequency of vesicle leakage (*i.e.* inverse of mean leakage time) through transient pores for a given solute over-concentration inside the vesicles is inversely proportional to τ^2, the square of line tension. This mechanism of transient or "pulsatile" pore formation relaxing the pressure in

response to an osmotic shock, classical for liposomes,[61] can certainly not work in the case of polymersomes due to their too low line energy τ compared to liposomes, not sufficient to reseal the membrane once a pore is nucleated. This is why for the same osmotic pressure imposed (same solutes encapsulated and same conditions of illumination), polymersomes leak much more slowly than liposomes, and thus they stay longer in a taut state without relaxing their lateral tension, until they eventually burst irreversibly. The osmotically driven vesicle rupture triggered by illumination described in this article corresponds to a kinetic control of rupture, the lower permeability of polymersomes letting them for longer in a tense state and maximizing their probability to undergo rupture with less possibility of resealing (since the driving force for pore closure is τ).

3.4. Selective vesicle rupture and controlled release of internalized cargo

In order to demonstrate the role and versatility of compartmentalization and polymersome explosion in vesicle-based chemical factories or proto-cell design, further series of experiments were conducted. In a first series (Figure 9. a), calcein-loaded $PBut_{2.5}$-*b*-$PEO_{1.3}$ polymersomes were observed with a confocal microscope in bright field (transmission) and in the green channel (emission range of calcein). Regions of interest (ROIs) in the form of circles were defined over several distinct polymersomes. At a defined time, these ROIs and consequently the chosen vesicles were subjected to intense irradiation (488 nm, 40 mW, 30%) corresponding to calcein absorption. The fluorescence intensity inside the ROIs could be followed during excitation. As shown in a series of snapshot images taken from the videos of the confocal observations, the chosen polymersomes rupture shortly (≈3 s) after being excited. The rupture is associated with the appearance of a peak (arrows) during the fluorescence intensity decay inside the ROIs. This decay corresponds to the bleaching of the dye. Because of its high concentration, calcein fluorescence that was initially quenched inside the polymersomes is rapidly recovered when diluted in the external medium due to vesicle rupture (see arrows on Figure 9. a). This method allows fast release of loaded species with high precision in space and time. In another series of experiments, calcein-, methylene blue -loaded and dye-free (sucrose-loaded) giant polymersomes were prepared, mixed together and visualized using confocal microscopy (Figure 9. b). MB-loaded vesicles were visualized in the red channel, calcein-loaded vesicles in the green channel and the native vesicles were only visible in bright field.

First, the whole solution was illuminated in the absorption range of MB. As expected, only the red polymersome ruptured while the green and empty ones remained stable. Then, we excited calcein (λ_{ex}=488 nm) and selectively-induced rupture of the green polymersome. The sucrose-loaded vesicles remained stable through the whole process. This method of wavelength selectivity for explosion allows targeting of one or more types of vesicles within a group of many, and to specifically address them.

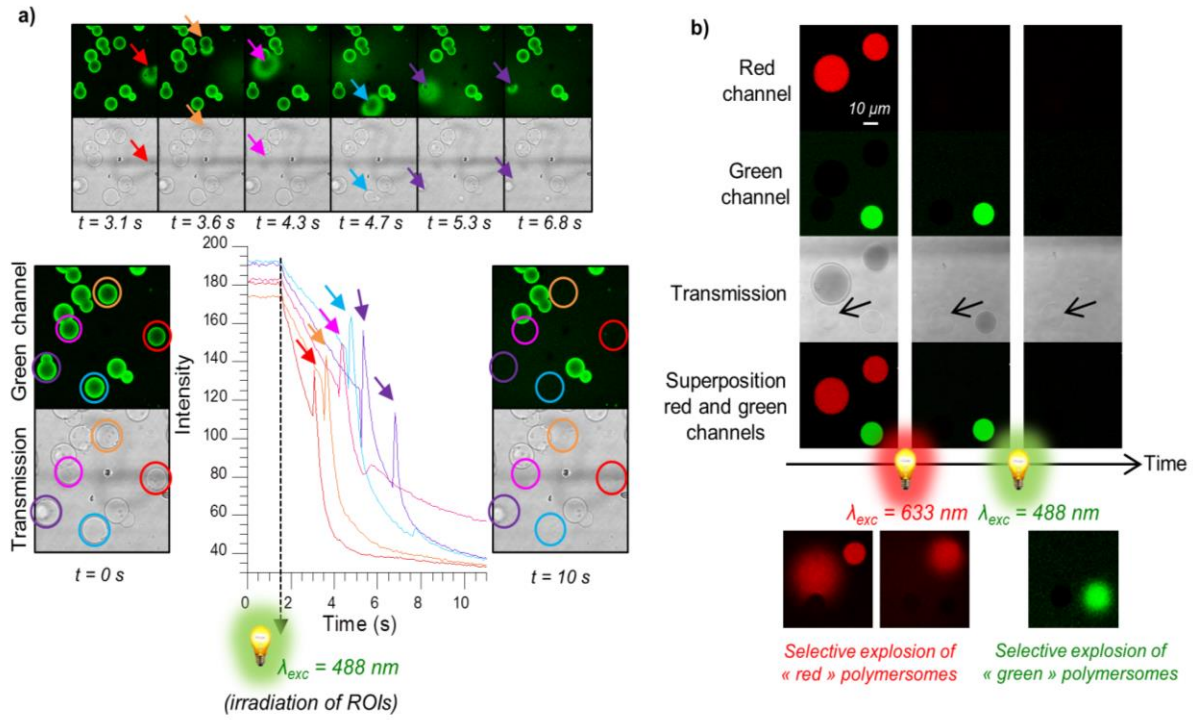

Figure 9. Selective rupture of vesicles. a) Time and space. *Confocal microscopy observation of 15 mM calcein-loaded $PBut_{2.5}$-b-$PEO_{1.3}$ vesicles. Regions of interest (ROIs) are defined around chosen vesicles (circles) and allow specific irradiation of those vesicles. The fluorescence intensity inside the ROIs is monitored over time. At t=0 s, 5 vesicles (circled) are subjected to high irradiation intensity at 488 nm. Rapid vesicle rupture (t=3.1, 3.6, 4.3, 4.7 and 5.3 s) is indicated by a sudden burst in fluorescence intensity (arrows) in the 5 defined ROIs. The global decay of fluorescence intensity corresponds to the bleaching of the dye upon irradiation.* ***b) Time and wavelength.*** *Confocal observation of $PBut_{2.5}$-b-$PEO_{1.3}$ vesicles loaded with methylene blue (10 mM; red), calcein (15 mM; green) or sucrose (0.35 M; arrow). The first column of pictures shows vesicles subjected to low laser intensity irradiation at 488 nm (40 mW, 2%, green channel) and 633 nm (10 mW, 10%, red channel). Then, vesicles are irradiated at 633 nm (high laser intensity), resulting in a rupture of red vesicles followed by an irradiation at 488 nm (high laser intensity), provoking rupture of green vesicles. Empty vesicles remain intact as can be seen in the transmission channel. (The movies corresponding to these two series of experiments are presented in SI, video S4 and video S5).*

To illustrate and generalize this last example of controlled species release, an experiment was designed where nano-polymersomes and nano-liposomes (100 nm diameter) were encapsulated separately in $PBut_{2.5}$-*b*-$PEO_{1.3}$ GUVs (Figure S 7 and Figure S 8). The $PBut_{1.2}$-*b*-$PEO_{0.6}$ nano-polymersomes tagged with Alexa fluor 405 were encapsulated with calcein in $PBut_{2.5}$-*b*-$PEO_{1.3}$ GUVs and the rhodamine tagged 1,2-dipalmitoyl-*sn*-glycero-3-phosphocholine (DPPC) nano-liposomes were loaded with MB in another batch of $PBut_{2.5}$-*b*-$PEO_{1.3}$ GUVs. Figure 10 shows confocal images of two neighboring GUVs. Visualization in the emission range of Alexa fluor and L-α-Phosphatidylethanolamine-N-(lissamine rhodamine B sulfonyl) (blue and red channel respectively) confirmed the effective encapsulation of the nano-vesicles (polymersomes and liposomes) in the cavity of the GUVs. A first irradiation (λ_{ex}=488 nm) triggered selective rupture of calcein-loaded GUVs and a consequent release of $PBut_{1.2}$-*b*-$PEO_{0.6}$ "blue" nano-polymersomes, as schematically represented in Figure 10. Then, the sample was irradiated (λ_{ex}=633 nm) to induce the DPPC "red" liposomes release after MB-loaded GUV explosion. This is, to the best of our knowledge, the first reported example of selective triggered release of nano-vesicles (liposomes or polymersomes) loaded in giant polymersomes.

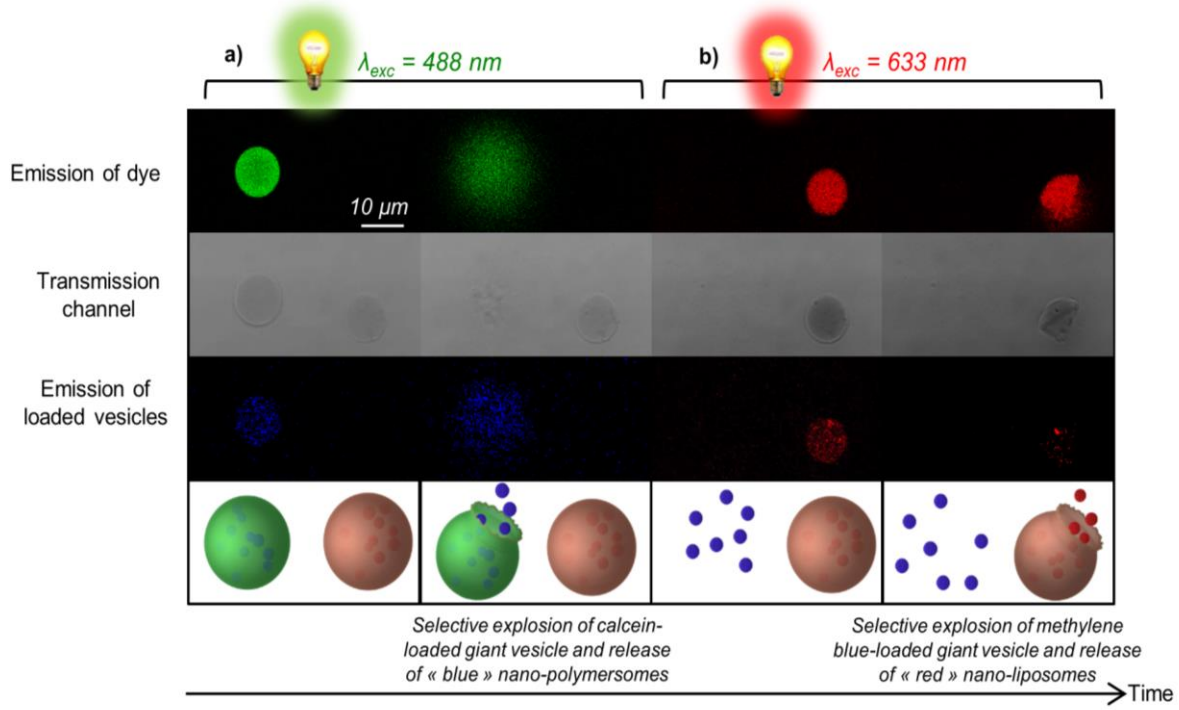

Figure 10. Controlled release of internalized cargo by selective vesicle rupture. *Confocal observation of two neighbouring $PBut_{2.5}$-b-$PEO_{1.3}$ GUVs loaded with 15 mM calcein (green) or 10 mM methylene blue (red). Nano-$PBut_{1.2}$-b-$PEO_{0.6}$ polymersomes tagged with Alexa Fluor 405 (blue) dye are loaded in the green GUV and nano-DPPC liposomes doped with fluorescent L-α-Phosphatidylethanolamine-N-(lissamine rhodamine B sulfonyl) dye (red) are loaded in the red GUV. After a) irradiation at 488 nm (high laser intensity) the green vesicle ruptures and releases the nano-polymersomes. Then, b) irradiation at 633 nm (high laser intensity) caused rupture of the red vesicle and subsequent release of the nano-DPPC liposomes. (Movies corresponding to these two series of experiments are presented in SI, video S6).*

4. Conclusion

To summarize, photoirradation of vesicles (both polymersomes and liposomes) loaded with photofragmenting dyes (either via the intermediacy of ROS activity or direct photodecaging) is proposed as an efficient external trigger to modulate their membrane properties and structural integrity. Considering much more permeable phospholipid vesicles, the direct consequence of this dye photo-degradation process is vesicle swelling, which renders their membrane more taut. The ability to tune membrane surface tension of these micron-sized capsules can offer scope in studies of surface tension effect on motility in aqueous solution. Concerning polymersomes, which are much less capable of exchanging water with external bulk solution

through passive permeability and cannot open up transiently (due to lower line energy), an increase in osmolarity accompanying photo-irradiation provokes bursting of their membrane, which is shown to release any cargo initially sequestered within the lumen (such as internalized molecules or nano-polymersomes and liposomes). We anticipate that such behavior can be generalized to any other kind polymersomes or membranes with low water permeability. Additionally, this process is subject to spatial and temporal control based on the appropriate choice of the illumination source and of the irradiation wavelength, depending on the selected photosensitizer, making this phenomenon a universal and versatile approach. Envisioned applications range from directed delivery in nanomedicine, as well as controlled dosing of nutrients and cofactors locally, which may prove decisive in decrypting biochemical interplays in cascade reactions and enzyme function.

5. References

[1] D. E. Discher, *Science* **2002**, *297*, 967–973.
[2] A. H. Chen, P. A. Silver, *Trends Cell Biol.* **2012**, *22*, 662–670.
[3] Y. Zhang, W. C. Ruder, P. R. LeDuc, *Trends Biotechnol.* **2008**, *26*, 14–20.
[4] N. P. Kamat, J. S. Katz, D. A. Hammer, *J. Phys. Chem. Lett.* **2011**, *2*, 1612–1623.
[5] A. Pohorille, D. Deamer, *Trends Biotechnol.* **2002**, *20*, 123–128.
[6] P. Tanner, S. Egli, V. Balasubramanian, O. Onaca, C. G. Palivan, W. Meier, *FEBS Lett.* **2011**, *585*, 1699–1706.
[7] S. Mann, *Acc. Chem. Res.* **2012**, *45*, 2131–2141.
[8] J. W. Szostak, D. P. Bartel, P. L. Luisi, *Nature* **2001**, *409*, 387–390.
[9] J. Gaitzsch, X. Huang, B. Voit, *Chem. Rev.* **2016**, *116*, 1053–1093.
[10] L. Schoonen, J. C. M. van Hest, *Adv. Mater.* **2016**, *28*, 1109–1128.
[11] R. Chandrawati, F. Caruso, *Langmuir* **2012**, *28*, 13798–13807.
[12] R. Chandrawati, M. P. van Koeverden, H. Lomas, F. Caruso, *J. Phys. Chem. Lett.* **2011**, *2*, 2639–2649.
[13] M. Marguet, C. Bonduelle, S. Lecommandoux, *Chem. Soc. Rev.* **2012**, *42*, 512–529.
[14] W. M. Aumiller Jr, C. D. Keating, *Nat. Chem.* **2016**, *8*, 129–137.
[15] A. Perro, C. Nicolet, J. Angly, S. Lecommandoux, J.-F. Le Meins, A. Colin, *Langmuir* **2011**, *27*, 9034–9042.
[16] H. C. Shum, Y. Zhao, S.-H. Kim, D. A. Weitz, *Angew. Chem. Int. Ed.* **2011**, *50*, 1648–1651.
[17] H.-C. Chiu, Y.-W. Lin, Y.-F. Huang, C.-K. Chuang, C.-S. Chern, *Angew. Chem. Int. Ed.* **2008**, *47*, 1875–1878.
[18] E. Mabrouk, D. Cuvelier, F. Brochard-Wyart, P. Nassoy, M.-H. Li, *Proc. Natl. Acad. Sci.* **2009**, *106*, 7294–7298.
[19] M. Marguet, L. Edembe, S. Lecommandoux, *Angew. Chem. Int. Ed.* **2012**, *51*, 1173–1176.
[20] Y. Elani, A. Gee, R. V. Law, O. Ces, *Chem. Sci.* **2013**, *4*, 3332.
[21] L. Hosta-Rigau, S. F. Chung, A. Postma, R. Chandrawati, B. Städler, F. Caruso, *Adv. Mater.* **2011**, *23*, 4082–4087.
[22] S.-H. Kim, H. C. Shum, J. W. Kim, J.-C. Cho, D. A. Weitz, *J. Am. Chem. Soc.* **2011**, *133*, 15165–15171.
[23] R. J. R. W. Peters, M. Marguet, S. Marais, M. W. Fraaije, J. C. M. van Hest, S. Lecommandoux, *Angew. Chem. Int. Ed.* **2014**, *53*, 146–150.
[24] R. J. R. W. Peters, I. Louzao, J. C. M. van Hest, *Chem. Sci.* **2012**, *3*, 335–342.
[25] B. Städler, A. D. Price, R. Chandrawati, L. Hosta-Rigau, A. N. Zelikin, F. Caruso, *Nanoscale* **2009**, *1*, 68–73.
[26] B. Kim, T. Y. Lee, A. Abbaspourrad, S.-H. Kim, *Chem. Mater.* **2014**, DOI 10.1021/cm503831t.
[27] M. Lomora, F. Itel, I. A. Dinu, C. G. Palivan, *Phys. Chem. Chem. Phys.* **2015**, *17*, 15538–15546.
[28] Y. Elani, R. V. Law, O. Ces, *Nat. Commun.* **2014**, *5*, DOI 10.1038/ncomms6305.
[29] J. Du, R. K. O'Reilly, *Soft Matter* **2009**, *5*, 3544–3561.
[30] F. Meng, Z. Zhong, J. Feijen, *Biomacromolecules* **2009**, *10*, 197–209.
[31] A. Weinberger, F.-C. Tsai, G. H. Koenderink, T. F. Schmidt, R. Itri, W. Meier, T. Schmatko, A. Schröder, C. Marques, *Biophys. J.* **2013**, *105*, 154–164.

[32] W. A. Velema, J. P. van der Berg, W. Szymanski, A. J. M. Driessen, B. L. Feringa, *ACS Chem. Biol.* **2014**, *9*, 1969–1974.
[33] B. Karami, M. Kiani, *J. Chin. Chem. Soc.* **2014**, *61*, 213–216.
[34] S. Pautot, B. J. Frisken, D. A. Weitz, *Langmuir* **2003**, *19*, 2870–2879.
[35] C. Taupin, M. Dvolaitzky, C. Sauterey, *Biochemistry (Mosc.)* **1975**, *14*, 4771–4775.
[36] K. A. Riske, R. Dimova, *Biophys. J.* **2005**, *88*, 1143–1155.
[37] W. Caetano, P. S. Haddad, R. Itri, D. Severino, V. C. Vieira, M. S. Baptista, A. P. Schröder, C. M. Marques, *Langmuir* **2007**, *23*, 1307–1314.
[38] O. Sandre, L. Moreaux, F. Brochard-Wyart, *Proc. Natl. Acad. Sci.* **1999**, *96*, 10591–10596.
[39] B. G. De Geest, S. De Koker, K. Immesoete, J. Demeester, S. C. De Smedt, W. E. Hennink, *Adv. Mater.* **2008**, *20*, 3687–3691.
[40] P. Klán, T. Šolomek, C. G. Bochet, A. Blanc, R. Givens, M. Rubina, V. Popik, A. Kostikov, J. Wirz, *Chem. Rev.* **2013**, *113*, 119–191.
[41] H. Diehl, J. L. Ellingboe, *Anal. Chem.* **1956**, *28*, 882–884.
[42] J. P. Tardivo, A. Del Giglio, C. S. de Oliveira, D. S. Gabrielli, H. C. Junqueira, D. B. Tada, D. Severino, R. de Fátima Turchiello, M. S. Baptista, *Photodiagnosis Photodyn. Ther.* **2005**, *2*, 175–191.
[43] C. Beghetto, C. Renken, O. Eriksson, G. Jori, P. Bernardi, F. Ricchelli, *Eur. J. Biochem.* **2000**, *267*, 5585–5592.
[44] D. Arian, E. Cló, K. V. Gothelf, A. Mokhir, *Chem. Weinh. Bergstr. Ger.* **2010**, *16*, 288–295.
[45] M. Bancirova, *Luminescence* **2011**, *26*, 685–688.
[46] T. F. Zhu, J. W. Szostak, *J. Syst. Chem.* **2011**, *2*, 4.
[47] J.-F. L. Meins, O. Sandre, S. Lecommandoux, *Eur. Phys. J. E* **2011**, *34*, 1–17.
[48] K. Olbrich, W. Rawicz, D. Needham, E. Evans, *Biophys. J.* **2000**, *79*, 321–327.
[49] E. Mabrouk, D. Cuvelier, F. Brochard-Wyart, P. Nassoy, M.-H. Li, *Proc. Natl. Acad. Sci.* **2009**, *106*, 7294–7298.
[50] E. Mabrouk, *Vésicules Polymères (Polymersomes) Stimulables*, Paris 6, **2010**.
[51] R. Dimova, *Adv. Colloid Interface Sci.* **2014**, *208*, 225–234.
[52] H. Bermúdez, D. A. Hammer, D. E. Discher, *Langmuir* **2004**, *20*, 540–543.
[53] H. Bermudez, A. K. Brannan, D. A. Hammer, F. S. Bates, D. E. Discher, *Macromolecules* **2002**, *35*, 8203–8208.
[54] R. Salva, J.-F. Le Meins, O. Sandre, A. Brûlet, M. Schmutz, P. Guenoun, S. Lecommandoux, *ACS Nano* **2013**, *7*, 9298–9311.
[55] E. Karatekin, O. Sandre, H. Guitouni, N. Borghi, P.-H. Puech, F. Brochard-Wyart, *Biophys. J.* **2003**, *84*, 1734–1749.
[56] V. Levadny, T. Tsuboi, M. Belaya, M. Yamazaki, *Langmuir* **2013**, *29*, 3848–3852.
[57] M. A. S. Karal, M. Yamazaki, *J. Chem. Phys.* **2015**, *143*, 81103.
[58] J. C. Shillcock, U. Seifert, *Biophys. J.* **1998**, *74*, 1754–1766.
[59] A. Carlsen, N. Glaser, J.-F. Le Meins, S. Lecommandoux, *Langmuir* **2011**, *27*, 4884–4890.
[60] P. P. Ghoroghchian, J. J. Lin, A. K. Brannan, P. R. Frail, F. S. Bates, M. J. Therien, D. A. Hammer, *Soft Matter* **2006**, *2*, 973–980.
[61] D. Popescu, *Proc. Romanian Acad.* **2010**, *11*, 108–115.

6. Supporting Information

Supplementary Movies can be seen online at

http://onlinelibrary.wiley.com/doi/10.1002/anie.201609231/abstract

Video S1: bursting of calcein-loaded $PBut_{2.5}$-*b*-$PEO_{1.3}$ polymersome (0.35 M sucrose, 30 mM calcein, λ_{ex} = 488 nm, 3% laser intensity).

Video S2: bursting of methylene blue-loaded $PBut_{2.5}$-*b*-$PEO_{1.3}$ polymersomes (0.37 M sucrose, 10 mM methylene blue, λ_{ex} = 633 nm, 90% laser intensity).

Video S3: selective explosion of 30 mM calcein-loaded PBut-*b*-PEO polymersomes in the presence of empty ones (λ_{ex} = 488 nm, 3% laser intensity).

Video S4: spatio-temporal selective rupture of calcein loaded-vesicles.

Video S5: temporal and spectral selective rupture of calcein and methylene blue-loaded vesicles.

Video S6: controlled release of internalized cargo by selective vesicle rupture in time and wavelength.

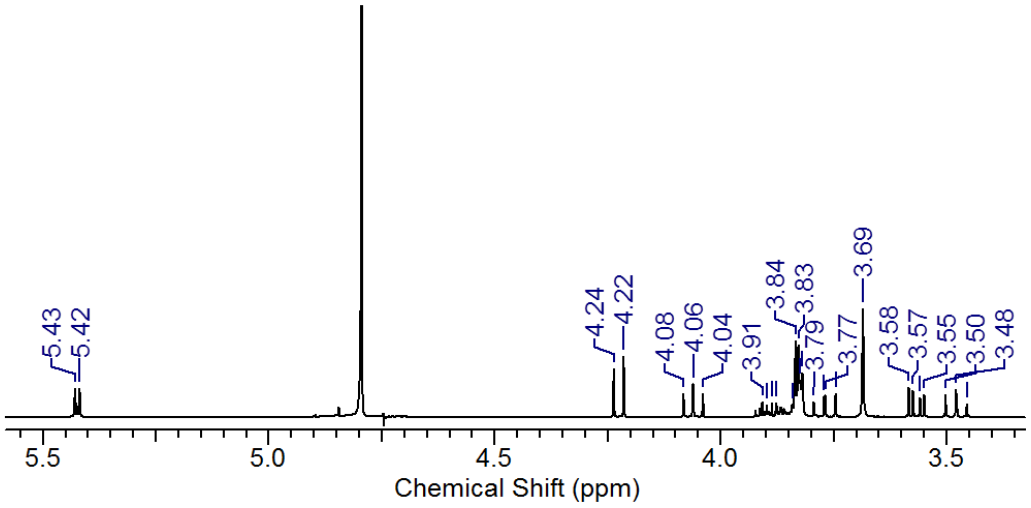

Figure S 1. ^{1}H NMR of sucrose. (400 MHz, D_2O), δ (ppm): 5.42 (d, J=3.8 Hz, 1H), 4.22 (d, J=8.6 Hz, 1H), 4.06 (t, J=8.6 Hz, 1H), 3.91 – 3.86 (m, 1H), 3.84 (m, 1H), 3.81 – 3.78 (m, 4H), 3.77 (t, J=10.1 Hz, 1H,), 3.69 (s, 2H), 3.57 (dd, J=13.1 Hz, J=3.8 Hz, 1H), 3.48 (t, J=9.1 Hz, 1H).

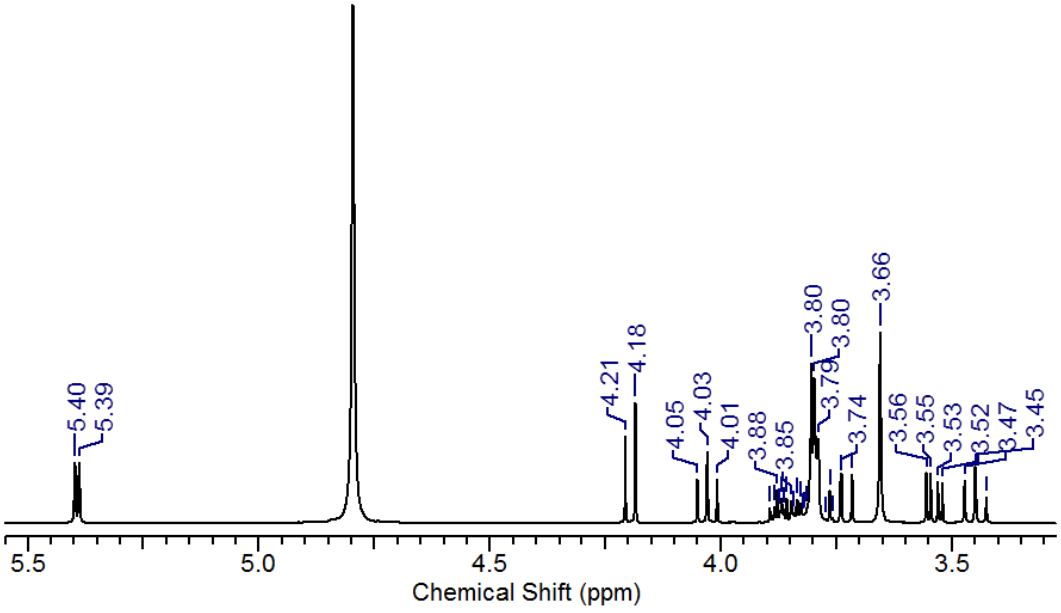

Figure S 2. ^{1}H NMR of sucrose after 30 min irradiation between 400 and 550 nm. (400 MHz, D_2O), δ(ppm): 5.40 (d, J=4 Hz, 1H), 4.21 (d, J= 8.6 Hz, 1H), 4.03 (t, J=8.5 Hz, 1H), 3.89 – 3.86 (m, 1H), 3.84 (m, 1H), 3.81 – 3.78 (m, 4H), 3.74 (t, J=9.9 Hz, 1H), 3.66 (s, 2H), 3.55 (dd, J=9.9 Hz, J=3.8 Hz, 1H), 3.45 (t, J=9.3 Hz, 1H).

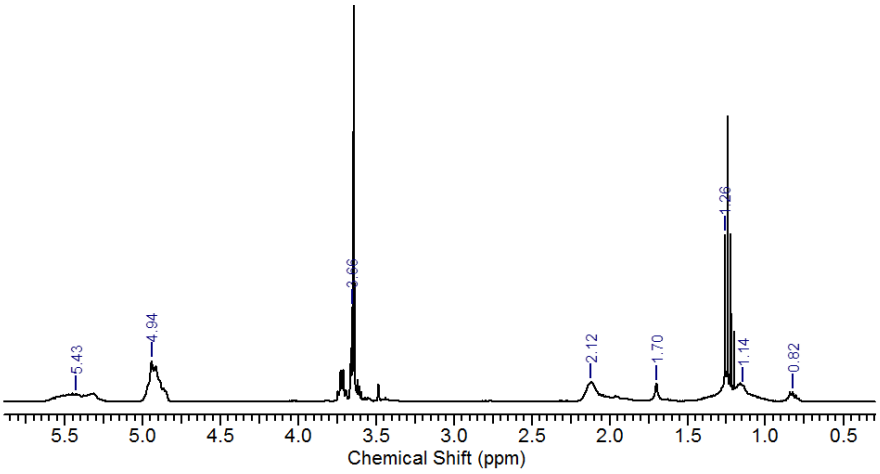

Figure S 3. ^{1}H NMR spectrum of $PBut_{1.2}$-b-$PEO_{0.6}$. (400 MHz, $CDCl_3$), δ (ppm): 5.65 – 5.30 (m, 1H), 5.0 – 4.75 (m, 2H), 3.64 (s, 4H), 1.25 (s, 2H).

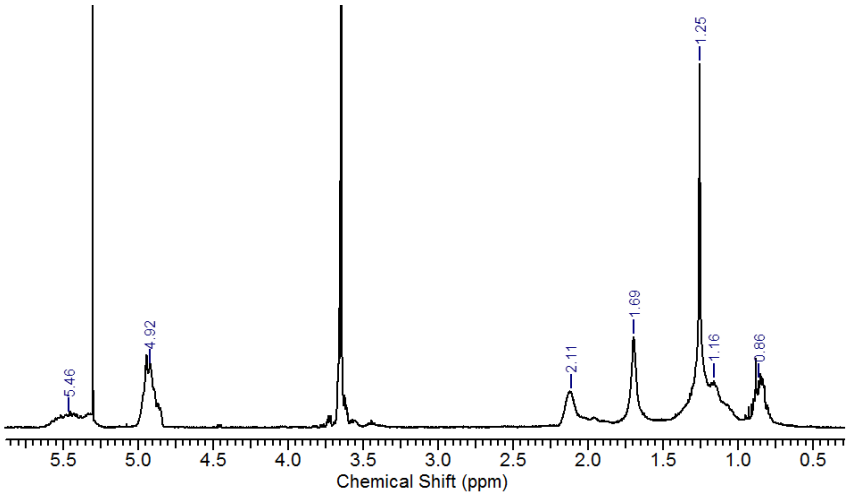

Figure S 4. ^{1}H NMR spectrum of $PBut_{1.2}$-b-$PEO_{0.6}$ after irradiation at 488nm in presence of calcein. (400 MHz, $CDCl_3$), δ (ppm): 5.65 – 5.30 (m, 1H), 5.0 – 4.75 (m, 2H), 3.64 (s, 4H), 1.25 (s, 2H).

$PBut_{1.2}$-*b*-$PEO_{0.6}$ polymer LUVs of 100 nm diameter were formed by the thin film rehydration method. Briefly, a polymer film was dried in a round bottom flask and rehydrated overnight with 3 mL of a solution of 30 mM calcein in 0.35 M sucrose. The resulting suspension was extruded through a 100 nm polycarbonate filter (Avanti Polar Lipids). The calcein-loaded polymersomes were then irradiated at 488 nm overnight on an optical bench equipped with a 150 W Hg-Xe lamp and a monochromator. The polymer was recovered for NMR analyses by extraction with dichloromethane.

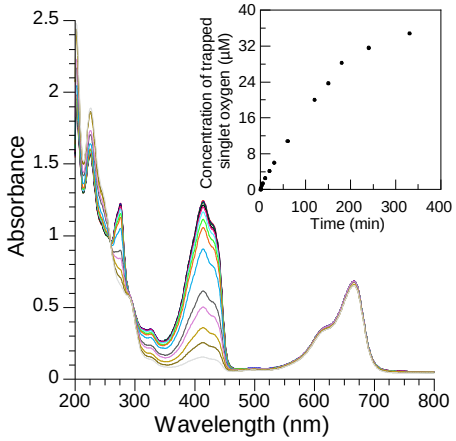

Figure S 5. Electronic absorption spectrum showing ROS photogeneration by methylene blue. UV-visible absorption spectrum of a solution of methylene blue (λ_{abs} = 500 -700 nm) and singlet oxygen scavenger (λ_{abs} = 360-460 nm) (ratio 1:4) during irradiation at 633 nm and singlet oxygen consumption over time (inset). The decrease of the absorption band of the scavenger indicates the consumption of singlet oxygen generated during irradiation.

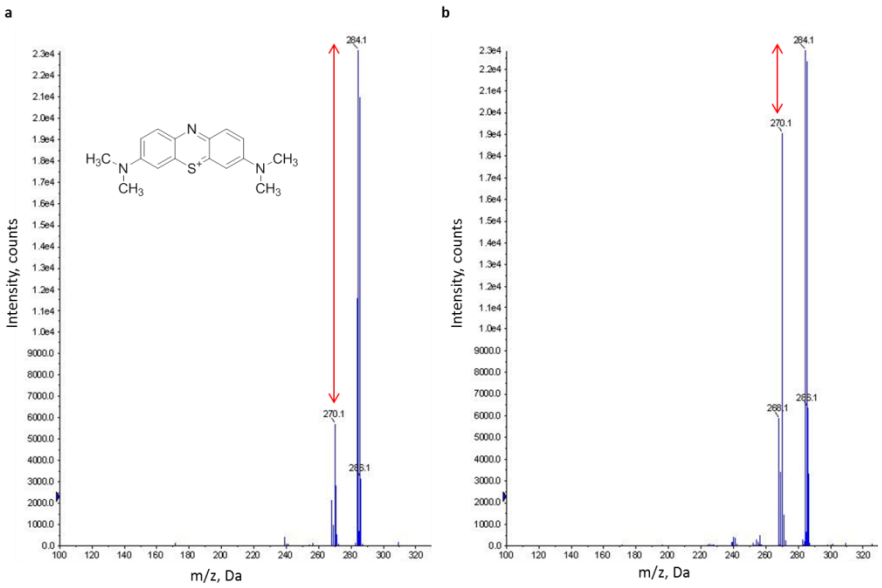

Figure S 6. ESI mass spectrum of methylene blue before and after overnight irradiation. A solution of 5 mM methylene blue in D_2O was irradiated overnight at 633 nm and ESI analyses were performed a) before and b) after irradiation.

After irradiation of methylene blue the ESI spectrum shows an increase of the peak at 270.1 m/z that corresponds to dye degradation. The same peak is present in a smaller proportion in the spectrum before irradiation because the sample was left unprotected from light a few hours before the analysis.

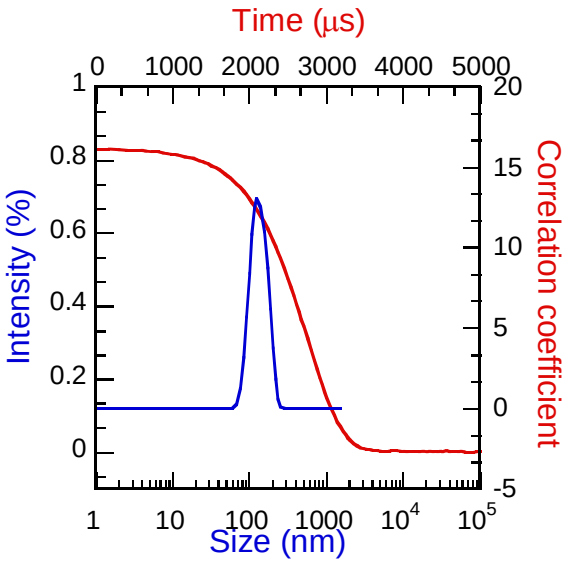

Figure S 7. DLS measurement of a solution of extruded 100 nm DPPC liposomes.

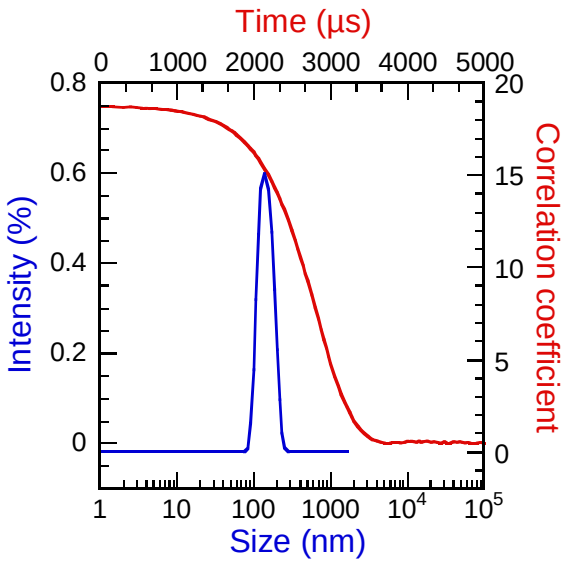

Figure S 8. DLS measurement of a solution of extruded 100 nm $PBut_{1.2}$-b-$PEO_{0.6}$ polymersomes.

PART 2: ***Hypertonic shock in giant vesicles induced by in situ UV photo-polymerization of acrylamide***

1. Introduction

The osmotic pressure gradient between the two sides of a cell (or any synthetic) membrane is related to the osmolarity difference between the inside and outside medium. Biological cells compensate for osmotic imbalances by swelling or deswelling as a response to influxes of water. For example, a hypotonic shock (increase of the osmolarity inside the cell) will generate a swelling of the cell as a consequence to water entry.[1–3] However, contrary to biological cells which exhibit rather permeable membranes, polymersomes show low and selective permeability. A difference in the permeation rate of species can thus easily induce an osmotic disequilibrium between the lumen of the vesicle and the outer medium and could lead to a shape modification or rupture. Vesicle swelling, shrinkage, collapse or bursting has been demonstrated as a response to hypo- or hypertonic shocks on lipid or polymer vesicles.[1,2,4–9] Taken together, these studies show the impact of membrane permeability on morphological changes triggered by osmotic variations.

The first part of this chapter was focused on studying the behavior of giant poly(butadiene)-*b*-poly(ethylene oxide) (PBut-*b*-PEO) vesicles loaded with photo-cleavable dyes. It was showed that polymersome popping could be triggered under irradiation of photo-cleavable fluorescent dyes at specific wavelengths.[5] Photo-cleavage led to an increase of the internal osmotic pressure which is equivalent to a hypotonic shock. The low permeability of the polymer membrane prevented an influx of water from the outer medium to compensate for the osmotic imbalance which led to opening of a pore and subsequent rupture of the vesicle.

This second part aims at presenting the consequences of an induced hypertonic shock in the lumen of PBut-*b*-PEO giant polymersomes. As previously discussed, the hypotonic shock provoked an influx of water from the outer medium, which exerted pressure on the vesicle membrane and led to pore opening and vesicle rupture. We here wonder how would the same vesicles react as a consequence of an induced decrease of the internal osmotic pressure (hypertonic shock).

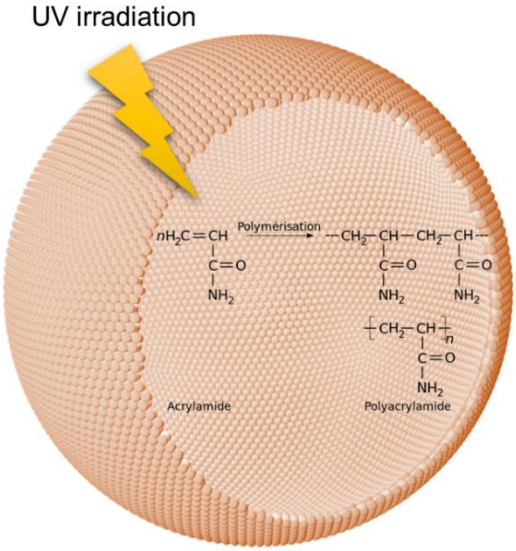

Figure 1. Schematical representation of UV photo-induced polymerization of acylamide inside the lumen of a giant polymersome.

As depicted in Figure 1, an experiment was designed where acrylamide and a hydrophilic radical photo-initiator are encapsulated together inside the lumen of giant PBut-*b*-PEO vesicles. Upon UV irradiation, poly(acrylamide) is generated inside the vesicles from the acrylamide monomer leading to a decrease of the internal osmotic pressure and increase of viscosity.[10–12] We hypothesized that if the osmotic imbalance from the photo-polymerization reaction was sufficient and generated fast enough, the vesicles could rupture similarly to the previous hypotonic experiments discussed in the first part of this chapter, or some vesicle deformation would occur. Herein are thus presented the results obtained on the study of the behavior of PBut-*b*-PEO giant polymersomes submitted to a hypertonic shock induced by *in situ* photo-polymerization of acrylamide.

2. Experimental section

2.1. Materials

Poly(butadiene)-*b*-poly(ethylene oxide) $PBut_{46}$-*b*-PEO_{30} (Mn x 10^3 PBut-*b*-PEO: 2.5-*b*-1.3; Mw/Mn 1.04) was ordered from Polymer Source (P18422-BdEO, 89% 1,2-addition of butadiene).

2-Hydroxy-4′-(2-hydroxyethoxy)-2-methylpropiophenone (Irgacure 2959), acrylamide monomer, sucrose and glucose were purchased from Sigma Aldrich and used as received.

2.2. Methods

Electronic absorption experiments were carried out on a Varian Cary 5000 UV-vis-NIR spectrophotometer. Osmolarity measurements were performed with a freezing point Type-15M automatic osmometer (Löser, Berlin, Germany). Irradiation experiments were carried with a Mercury-Xenon 200 W lamp. A filter was used to cut UV light below 300 nm and over 480 nm. Samples (≈1-2 mL) were placed 1 cm from the light guide output end and irradiated in the dark for a defined time. Osmolarities and viscosities were measured before and after irradiation. Viscosities were determined with a DMA generation M density meter equipped with a Lovis 2000 M/ME rolling ball micro-viscometer from Anton Paar at 20°C. Laser scanning confocal microscopy images were acquired on an inverted Leica TCS SP5 microscope equipped with an HCX PL APO 63×, NA 1.4 oil immersion objective in transmission mode. Samples (≈20 µL) were injected in a homemade chamber that was sealed to prevent evaporation. The light guide output end of the UV lamp was placed 1 cm away from the chamber for optimized irradiation. Images were collected in simultaneous mode using a resonant scanner at 8000 Hz in bidirectional mode and processed with the ImageJ freeware. Size exclusion chromatography in water was performed on a Wyatt apparatus. Samples (≈1 mL) were prepared from the dissolution of 5 mg lyophilised polymer in a 0.1 M $NaNO_3$ + 0.1 M H_2O_4P buffer and were filtered (0.45 µm) before injection.

2.3. Vesicle preparation

Poly(butadiene)-*b*-poly(ethylene oxide) ($PBut_{2.5}$-*b*-$PEO_{1.3}$) giant polymersomes were prepared from the previously discussed emulsion-centrifugation method. Briefly, 5 µL of sucrose 0.38 M was poured into 3 mg/mL $PBut_{2.5}$-*b*-$PEO_{1.3}$ in 500 µL toluene. The solution was vigorously hand-shaken for 30 seconds to create a water-in-oil emulsion. An interface was prepared by pouring 30 µL of $PBut_{2.5}$-*b*-$PEO_{1.3}$ (3 mg/mL) in toluene over 30 µL glucose 0.38 M and allowed to stabilize for 30 minutes. 60 µL of the above emulsion was slowly poured over the interface and the sample was immediately centrifuged (3 min, 500 g, ambient temperature). The resulting polymersomes were recovered in the lower phase. In the case of acrylamide and irgacure-loaded polymersomes,

the monomer and initiator were dissolved in a sucrose solution to reach the desired concentration and 5 µL of this solution was used to form the emulsion. The concentration of glucose was adjusted to the same osmotic pressure as the sucrose solution. Samples were kept in the dark prior to irradiation.

3. Results and discussion

The idea of this research was to induce a fast decrease of the overall osmotic pressure inside the lumen of giant PBut-*b*-PEO vesicles to study their behavior under such hypertonic shock as compared with the hypotonic shock generated from the cleavage of fluorescent dyes under irradiation and leading to vesicle rupture. We thus looked for a way to induce a fast decrease of the osmotic pressure inside the lumen of the polymersomes, or in other words, a way to rapidly reduce the number of species at a defined time. In such a way, polymerization reactions involve monomers building up to single polymer chains and thus can lead to a decrease of the osmotic pressure by a decrease of the total number of species. The polymerization of acrylamide was chosen as a model reaction to be confined inside the lumen of the polymersomes (Figure 1). Poly(acrylamide) is obtained from the polymerization of an acrylamide monomer, both being well soluble in water at room temperature.[11] It has been well studied for many years and is known to be a fast reaction with a high yield.[10] Very often, a cross-linking agent is added to form a gel used for electrophoresis applications.[13] It was hypothesized that, if fast enough, the polymerization of acrylamide into poly(acrylamide) would generate a sufficient osmotic imbalance to trigger a rupture or deformation of the PBut-*b*-PEO giant polymersomes as a response to the hypertonic shock.

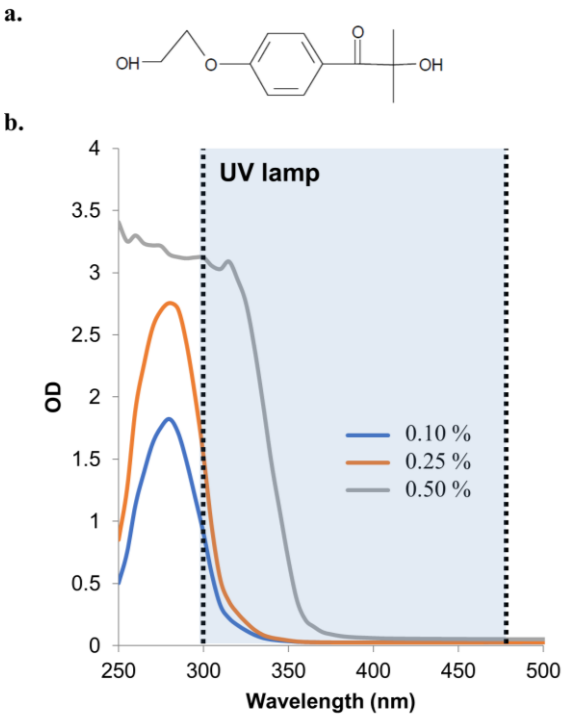

Figure 2. a) Chemical structure of Irgacure photo-initiator; b) absorbance spectra of Irgacure with varying wt/v %.

2-Hydroxy-4′-(2-hydroxyethoxy)-2-methylpropiophenone (Irgacure, Figure 2. a)) was chosen as a photo-initiator because it is rather water soluble and has proven effective in photo-initiated polymerization reactions.[14–16] The absorbance spectra for different Irgacure concentrations were monitored with a spectrophotometer to verify that they could be activated in the wavelength range of a mercury-xenon 200 W UV lamp (300-480 nm) (Figure 2. b)). While 0.10 and 0.25 wt/v % Irgacure only show low signal in that area, a great increase in absorbance is noticeable for 0.5 wt/v % Irgacure.

In photo-polymerization processes, both the monomer and the initiator should have an impact on the rate of the reaction.[17] Therefore, the photo-polymerization was first performed in bulk using different monomer-to-initiator ratio to verify the effective polymerization of acrylamide under these conditions and, on the other hand, to monitor the changes in viscosity and osmolarity required to observe a change in the behavior of the vesicles.

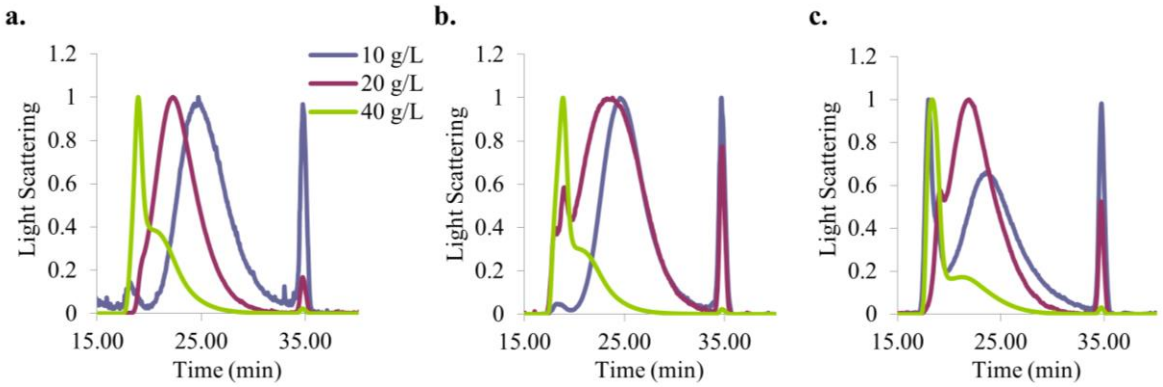

Figure 3. Size exclusion chromatography (water) traces of generated poly(acrylamide) for different monomer (10, 20 and 40 g/L) and Irgacure concentrations: a) 0.50 wt/v %; b) 0.25 wt/v % and c) 0.10 wt/v % under 5 min UV irradiation (300 – 480 nm) with a mercury-xenon 200 W lamp in 0.3 M sucrose.

In each experiment, the monomer and initiator were mixed in a 0.3 M sucrose solution and irradiated 5 minutes with a mercury-xenon 200 W lamp between 300 and 480 nm. Figure 3. a), b) and c) show the chromatograms obtained for the size exclusion chromatography in water of the poly(acrylamides) generated after photo-polymerization with different concentrations of monomer and initiator. The large peaks indicate the high polydispersity of the samples. However, a net shift between the peaks confirm the influence of the concentration of the monomer on the final molar masses of the polymers. Indeed, the highest concentrations of monomer induce higher molar masses and thus probably higher changes in osmolarity and viscosity.

To confirm this hypothesis, osmolarity and viscosity measurements were performed on the samples before and after irradiation (Figure 4. a) and b) respectively). As expected, a decrease in osmolarity and increase in viscosity was observed for every monomer-to-initiator ratio with the highest differences most often attributed to the 0.5 wt/v % Irgacure concentration. In the absence of initiator, no changes in either osmolarity or viscosity were observed proving that polymerization cannot occur without the presence of Irgacure as a source of radicals.

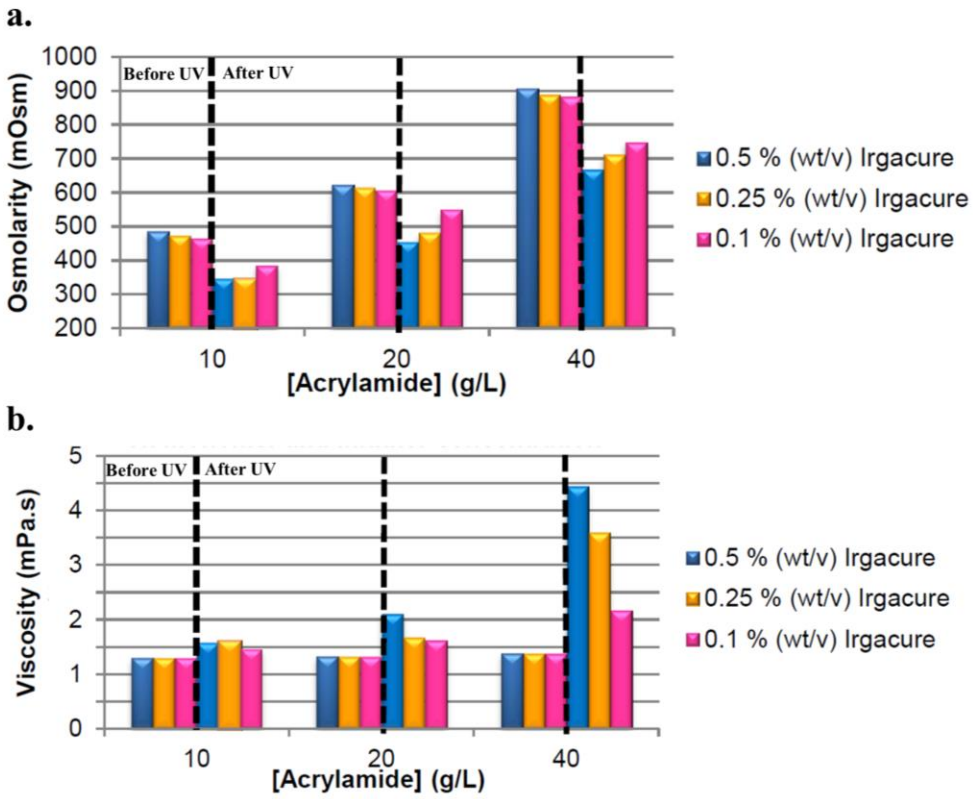

Figure 4. a) Osmolarity and b) viscosity measurements on obtained poly(acrylamides) for different monomer and initiator concentrations before (left of dotted line) and after (right of dotted line) 5 min UV irradiation (300 – 480 nm) with a mercury-xenon 200 W lamp in 0.3 M sucrose.

Having determined the optimal concentration conditions to induce the highest osmotic shock, the photo-initiated reaction was then triggered inside the lumen of the giant PBut-*b*-PEO polymersomes as schematically represented in Figure 1. According to the previous results, different ratios of monomer and initiator solubilized in sucrose were loaded in the giant vesicles following the emulsion-centrifugation protocol. The light guide output end of the mercury-xenon 200 W UV lamp was placed over the hermetic chamber containing the sample under the confocal lens as shown in Figure 5. The irradiation of the vesicles could thus be followed by confocal microscopy under white light observation.

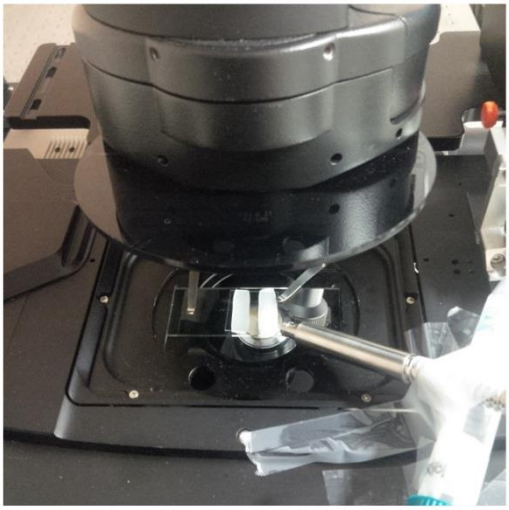

Figure 5. Confocal setup. The light guide output end of a mercury-xenon UV 200 W lamp is placed over the hermetic chamber containing the sample.

Vesicles containing 0.1 wt/v % Irgacure did not show any change, even after 10 min irradiation at maximum lamp intensity, most probably because this percentage of initiator gave the smallest osmotic pressure and viscosity differences (Figure 6. a)). However, fast vesicle rupture (less than 1 minute UV irradiation between 300 and 480 nm) was observed for a majority of vesicles loaded with either 0.25 or 0.50 wt/v % initiator with respectively 40 and 20 g/L monomer (Figure 6). Controls were made (data not shown) to verify that no explosions occurred in empty (sucrose-loaded) vesicles under the same conditions, confirming that there is no heating effect due to the UV radiation. Figure 6. a) and b) show vesicles during rupture (images acquired from a video). Interestingly, the membrane rim seems to curl in the inner medium, where the viscosity is supposedly higher, as discussed in previous studies.[5,18] These results confirm our hypothesis that the low membrane permeability of polymer vesicles prevents effective water diffusion and thus prevents a re-equilibration of concentrations of species between both sides, as would have been the case with more permeable lipidic vesicles.

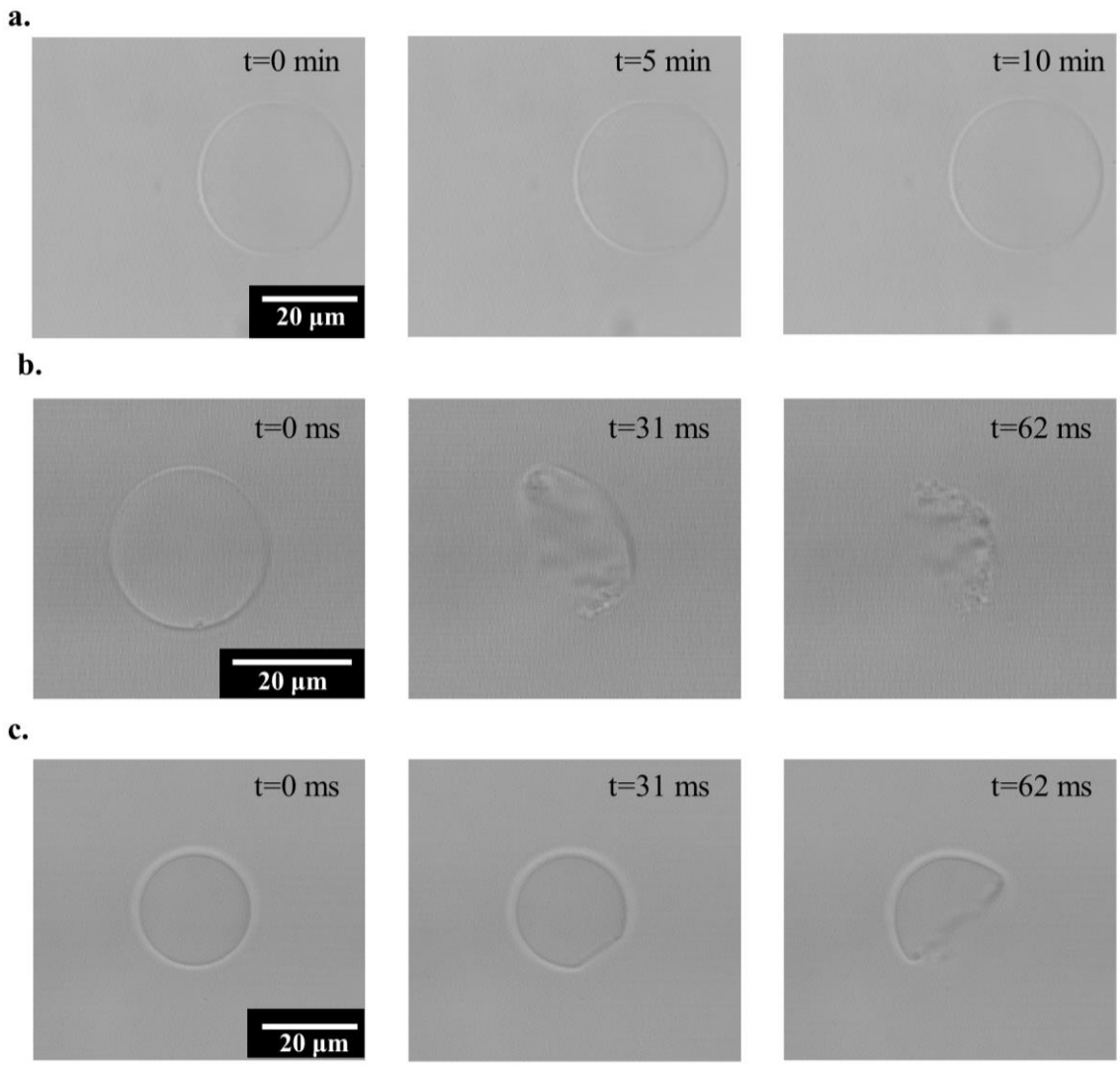

Figure 6. Confocal images of vesicle following in situ polymerization of acrylamide in the presence of an Irgacure initiator under UV irradiation (300 – 480 nm). The images are acquired from a video. a) 0.1 wt/v% Irgacure, 40g/L monomer, b) 0.50 wt/v % Irgacure, 20 g/L monomer and b) 0.25 wt/v % Irgacure and 40 g/L monomer.

4. Conclusion

This study demonstrates the impact of light-induced hypertonic shocks on giant polymer vesicles. An external trigger was used to induce a fast polymerization reaction inside the lumen of the vesicles. This reaction generates a decrease of the internal osmotic pressure, linked to an increase

in viscosity which, in turns, leads to vesicle rupture due to the low water diffusion conferred by the impermeable membrane.

This research aimed at confirming the results discussed in the first part of this chapter on light-induced dye photo-degradation inside giant polymersomes. Whether the shock is hypo- or hypertonic (respectively increase or decrease of the total internal osmotic pressure), we have shown that vesicle rupture could be effectively and precisely externally triggered. This phenomenon could possibly have applications in drug release studies or cascade reactions where a control on the initiation of the reaction is needed.

5. References

[1] R. Salva, J.-F. Le Meins, O. Sandre, A. Brûlet, M. Schmutz, P. Guenoun, S. Lecommandoux, *ACS Nano* **2013**, *7*, 9298–9311.

[2] W. Li, T. S. Aurora, T. H. Haines, H. Z. Cummins, *Biochemistry (Mosc.)* **1986**, *25*, 8220–8229.

[3] V. W. Sidel, A. K. Solomon, *J. Gen. Physiol.* **1957**, *41*, 243–257.

[4] A. Carlsen, N. Glaser, J.-F. Le Meins, S. Lecommandoux, *Langmuir* **2011**, *27*, 4884–4890.

[5] A. Peyret, E. Ibarboure, A. Tron, L. Beauté, R. Rust, O. Sandre, N. D. McClenaghan, S. Lecommandoux, *Angew. Chem.* **2017**, *129*, 1588–1592.

[6] C. Ménager, V. Cabuil, *J. Phys. Chem. B* **2002**, *106*, 7913–7918.

[7] C. Mm, L. Fa, H. Fa, S. Ma, *Biochim. Biophys. Acta* **2008**, *1778*, 890–895.

[8] A.-L. Bernard, M.-A. Guedeau-Boudeville, L. Jullien, J.-M. di Meglio, *Biochim. Biophys. Acta* **2002**, *1567*, 1–5.

[9] J. Pencer, G. F. White, F. R. Hallett, *Biophys. J.* **2001**, *81*, 2716–2728.

[10] G. Delzenne, S. Toppet, G. Smets, *J. Polym. Sci.* **1960**, *48*, 347–355.

[11] S. A. Seabrook, R. G. Gilbert, *Polymer* **2007**, *48*, 4733–4741.

[12] L. Villegas, M. V. Encinas, A. M. Rufs, C. Bueno, S. Bertolotti, C. M. Previtali, *J. Polym. Sci. Part Polym. Chem.* **2001**, *39*, 4074–4082.

[13] A. Chrambach, D. Rodbard, *Science* **1971**, *172*, 440–451.

[14] B. D. Fairbanks, M. P. Schwartz, C. N. Bowman, K. S. Anseth, *Biomaterials* **2009**, *30*, 6702–6707.

[15] A. Sabnis, M. Rahimi, C. Chapman, K. T. Nguyen, *J. Biomed. Mater. Res. A* **2009**, *91*, 52–59.

[16] C. G. Williams, A. N. Malik, T. K. Kim, P. N. Manson, J. H. Elisseeff, *Biomaterials* **2005**, *26*, 1211–1218.

[17] E. Andrzejewska, *Prog. Polym. Sci.* **2001**, *26*, 605–665.

[18] E. Mabrouk, D. Cuvelier, F. Brochard-Wyart, P. Nassoy, M.-H. Li, *Proc. Natl. Acad. Sci.* **2009**, *106*, 7294–7298.

CHAPTER 5: *Co-culture between synthetic cells and eukaryotic cells*

1. Introduction

In the previous chapters, was discussed and presented the work carried out during this PhD thesis on the development of innovative structural and functional artificial mimics of biological cells to reach accurate synthetic cell-like systems. Especially, a method was proposed to selectively release encapsulated cargo from light-induced rupture of polymer vesicles with high precision as a way to mimic the controlled release of species from biological cells.[1] In this last on-going work, we questioned how biological cells would co-exist with artificial biomimetic polymer cells and especially how they would physically respond to the nearby delivery of therapeutic or toxic species from polymersomes.

Cell-based assays have proven extremely useful in the design of new therapeutic agents as they provide a simple and cost-effective means to avoid intensive animal testing. The majority of cell biological studies are performed on two-dimensional (2D) monolayer cell culture media (flat substrates) and consist on observing cellular response to external agents. This method, while having proven efficient and useful for many years, still has some limitations.[2] In particular, the 2D environment conferred by cell cultures on flat substrates does not accurately represent the natural biological cell environment. It has been demonstrated that 2D cell cultures can provide misleading data attributed to differing cell behavior as compared to 3D cultures especially because 2D cultures force cells to grow in an unnatural flat monolayer.[3] For example, Bissell's group showed that breast cancer cells exposed to a particular antibody completely changed their behavior when grown in 3D culture.[4] *In vivo,* cells are almost all surrounded by other cells and connect to each other and to a support structure called the extra-cellular matrix (ECM) in a three-dimensional (3D) fashion. The ECM contains proteins that provide tissues their physical properties and that help communication between cells.[5,6] It has been shown to highly influence cell morphological changes and differentiation.[7] Hence, the behavior of 3D-cultured cells would be more reflective of *in vivo* cellular responses.[8]

For a few years now, some groups have focused on engineering 3D cell culture media as they would constitute more appropriate models and would provide more physiologically relevant information to study cell growth as compared with cultures on flat substrates which do not accurately reflect the *in vivo* cell physical constraints.[9–11] Settings that resemble *in vivo* environments have been elaborated and particularly, cellular spheroids as *ex vivo* 3D cultures have been described since the 1980s.[12] Spheroids are self-assembled spherical clusters of cells that adhere together in an ECM. They are either grown on a matrix or in suspension in a liquid

medium and form perfect spheres if the cells are normal or distorted structures if they are malignant.[9,13,14] In addition, because all the cells are not exposed to the same environment, 3D spheroids are composed of cells in various stages. The outer layers are more exposed to the medium and thus contain viable proliferating cells. On the contrary, the core of the spheroid receives less oxygen and nutrients and tend to enter a hypoxic state.[15,16] These conditions are very similar to the ones found in tissues or tumors and thus make 3D cultured spheroids highly relevant to study *in vivo* processes.

In this context, the team of P. Nassoy has developed a simple and reproducible method to prepare size-controlled spheroids using a microfluidic device.[17–19] Cells are encapsulated in permeable hydrogel micro-capsules formed by polymerization of alginate in the presence of calcium.[20] A microfluidic setup comprising a 3D-printed 3-way co-extrusion device was designed and used to form a hydrogel shell comprising a suspension of cells as depicted in Figure 1. The cell suspension, an intermediate solution and an alginate solution (CS, IS and AL in Figure 1. B)) respectively flow from the innermost to the outermost inlets of the co-extrusion device to generate size controlled microdroplets that fall into a calcium bath to allow gelation of the shell by polymerization of alginate. Hollow micro-capsules are subsequently obtained (Figure 1. E)) with a size that can be tuned depending on the flow rate ratio between the CS + IS solutions and the AL solution. Typically, ≈ 150 μm capsules comprising a few tens of cells are produced.

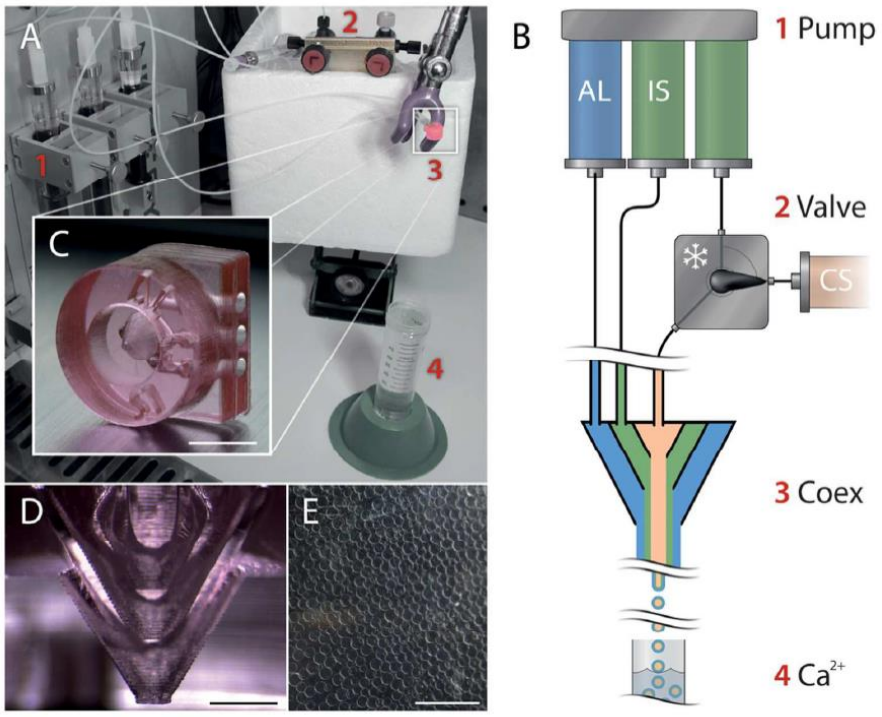

Figure 1. Operating principle of the microfluidic device.[19]

These alginate capsules were shown to be highly efficient as scaffolds to allow long-term culture of spheroids and permit study of their mechanical properties under confinement.[17]

In the context of this PhD work, a research project combining the 3D cell culture technology implemented by Nassoy's group and the controlled delivery of species from laser-induced rupture of polymersomes (CHAPTER 4) was designed. The main goal of this collaboration, schematically presented in Figure 2, is to study the chemical and physical impact of species (toxic or therapeutic) released in close proximity of normal or tumorous cells. Herein are presented the initial results obtained on the optimization of the co-encapsulation (polymersomes and cells) protocol and the cell viability assays in presence of the polymersomes. We aimed at providing solid bases for this study to be implemented as a continuing collaboration between the LP2N and LCPO laboratories in the coming years.

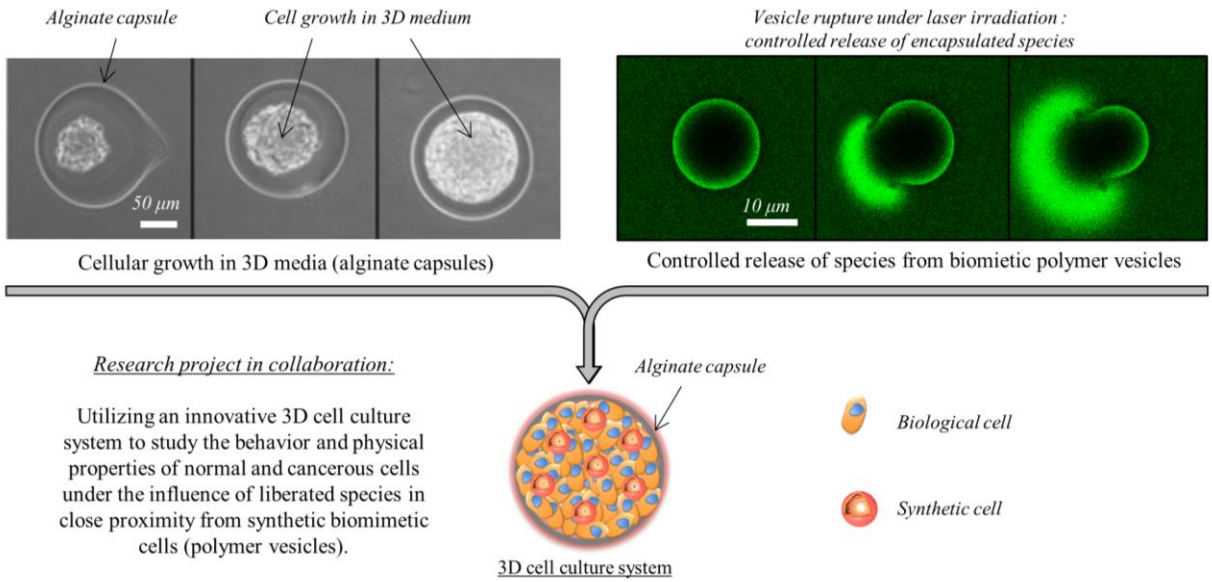

Figure 2. Schematical presentation of the research project in collaboration with Dr. P. Nassoy (LP2N, CNRS 5298) on the encapsulation and study of coexistence of biomimetic synthetic polymersomes and biological cells in 3D alginate capsules.[1,17]

2. Experimental section

2.1. Materials

Poly(butadiene)-*b*-poly(ethylene oxide) $PBut_{46}$-*b*-PEO_{30} (Mn x 10^3 PBut-*b*-PEO: 2.5-*b*-1.3; Mw/Mn 1.04) was ordered from Polymer Source (P18422-BdEO batch, comprising 89% 1,2-addition of butadiene). Calcium chloride was purchased from VWR international. Tween 20 surfactant was purchased from Merck. Fluorescein, glucose, sorbitol and sucrose were purchased from Sigma Aldrich and used as received.

Two cell lines were used for this study: human induced pluripotent stem cells (cell line BC1, MTI-Globalstem) cultivated in Matrigel MT1 medium and adipocytes (mouse pre-adipocytes, cell-line 3T3-F442A, ECACC general collection).

2.2.Methods

2.1.1. Polymersome preparation

Poly(butadiene)-*b*-poly(ethylene oxide) ($PBut_{2.5}$-*b*-$PEO_{1.3}$) giant polymersomes were prepared by an emulsion-centrifugation method. Briefly, 5 µL of sucrose 0.38 M was poured into 3 mg/mL $PBut_{2.5}$-*b*-$PEO_{1.3}$ in 500 µL toluene. The solution was vigorously hand-shaken for 30

seconds to create a water-in-oil emulsion. An interface was prepared by pouring 30 µL of $PBut_{2.5}$-*b*-$PEO_{1.3}$ (3 mg/mL) in toluene over 30 µL glucose or sorbitol at the desired concentration and allowed to stabilize for 30 minutes. 75 µL of the above emulsion was slowly poured over the interface and the sample was immediately centrifuged (3 min, 500 g, ambient temperature). The resulting polymersomes were recovered in the lower phase. In the case of fluorescein-loaded polymersomes, the dye was dissolved at 1 mM in a sucrose solution and 5 µL of this solution was used to form the emulsion.

2.1.2. Loading in alginate capsules and microscope observation

The detailed protocol of alginate capsule formation by the microfluidic setup is described in a recently published article from Roux and co-authors and is schematically represented in Figure 1.[19] Briefly, the intermediate solution (IS, 300 mM sorbitol), the alginate solution (AL, 2 % wt/vol sodium alginate in water with 0.5 mM sodium dodecyl sulfate) and the innermost cell solution phase (CS) were loaded in syringes mounted on pumps used at the same flow rate for all experiments (CS and IS : 20 mL/hr and AL : 30 mL/hr). The microdroplets were recovered in a calcium gelation bath (calcium 100 mM and traces of tween 20 surfactant). It was estimated that about 10^4 capsules could be formed in a few seconds. The capsules were then washed and placed in an appropriate culture medium. For the co-encapsulation, the same procedure was followed with polymersomes initially mixed with cells at the desired ratio.

The obtained loaded capsules were visualized under an optical or confocal microscope (inverted Leica TCS SP5 microscope equipped with an HCX PL APO 63x, NA 1.4 oil immersion objective in fluorescence mode). The fluorescein-loaded polymersomes were excited with an argon laser (λ= 488 nm, 15 % laser intensity). Processing of fluorescence confocal acquisitions was performed with the ImageJ freeware.

3. Results

3.1. Optimization of the co-encapsulation protocol

3.1.1. Encapsulation of polymersomes in alginate capsules

A first prerogative to put in place a series of experiments on synthetic and biological cell co-existence was to determine the critical parameters affecting polymersome encapsulation in alginate capsules. Indeed, the alginate capsule formation method was carefully designed to

allow encapsulation of biological cells in such a way that specific flow rates, tubing sizes, or solutions were chosen to avoid cell death and to optimize the encapsulation yield. Thus the initial objective of this study was to find encapsulating conditions that would both fit biological cells and polymersomes (synthetic cells).

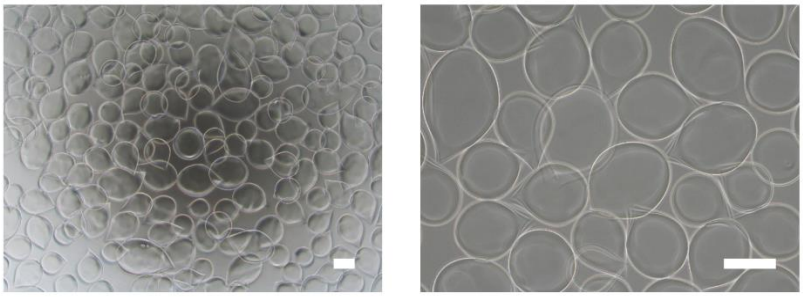

Figure 3. Optical microscope observation of empty alginate capsules. Scale bar = 150 µm.

Figure 3 shows optical microscope images of empty alginate capsules. As clearly noticeable, a monodisperse population of about 150 µm in diameter is obtained with a uniform capsule shape. A first concern was that because of the differences in membrane composition and mechanical stability between cells (lipid, flexible permeable membrane) and poly(ethylene oxide)-*b*-poly(butadiene) (PBut-*b*-PEO) vesicles (polymer, rigid low permeable membrane), the shape and dispersity of the capsules would be altered upon polymersome encapsulation. The second main concern was that polymersomes could suffer from the encapsulation process and osmotic pressure variations and be disrupted. To evaluate these potential limitations, it was first tried to load alginate capsules with polymersomes alone without changing any experimental conditions regarding the microfluidic setup or the vesicle preparation protocol. Hence, the polymer vesicles were prepared as previously described, in 0.38 M glucose and were loaded with 0.38 M sucrose and encapsulated in the capsules 4 hours after preparation.

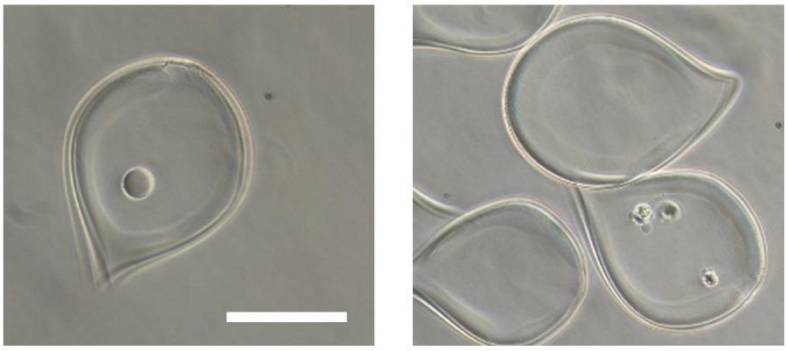

Figure 4. Optical microscope observation of polymersome-loaded alginate capsules. Scale bar = 150 µm.

Figure 4 shows optical microscope images of some of the obtained polymersome-loaded alginate capsules. Overall, only a very low vesicle encapsulation yield was obtained and most of the capsules were empty or contained only few vesicles. However, these initial results gave confirmation that PBut-*b*-PEO vesicles could resist the encapsulation process and especially the high flow rates (up to 30 mL/hr) and shear stress occurring during the capsule assembly. It was thus decided not to change the microfluidic setup operating conditions, as many parameters could be modified from the polymersome preparation alone, to try to increase vesicle encapsulation yield. The tested experimental conditions are summarized in Table 1.

Test N°	Concentration	Number of batches	Ratio polymersomes : cells	Rest time before encapsulation	Outer phase
1	*0.38 M*	*1*	- - -	*4 hours*	*Glucose*
2	*0.38 M*	*3*	- - -	*4 hours*	*Glucose*
3	*0.38 M*	*3*	- - -	*12 hours*	*Glucose*

Table 1. Main tunable parameters for PBut-b-PEO polymersome preparation and encapsulation in alginate capsules. In red: modified parameter.

After all these experiments, it was found that the number of encapsulated polymersomes could considerably be increased by combining several batches of vesicles prior to injection in the microfluidic setup. In addition, the combined batches were left to rest overnight before encapsulation to allow the sediment obtained after the vesicle preparation process to fully re-

disperse and thus avoid injecting any polymersome aggregates that could alter capsule formation. Thus the optimal conditions were to combine 3 polymersome batches and leave them to rest for a minimum of 12 hours before encapsulation.

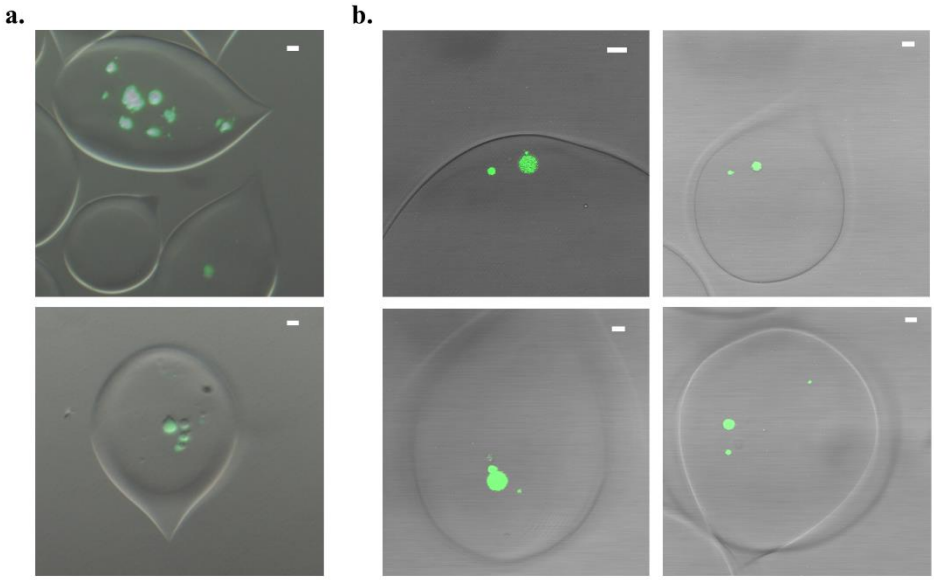

Figure 5. Microscope observations of polymersome-loaded alginate capsules. The polymersomes are loaded with 1 mM fluorescein.a) Optical microscope ; b) confocal microscope. The white light and green fluorescence images were superposed. Scale bar = 20 μm.

These modified parameters allowed to notice a clear increase in the number of polymersomes per capsules. Figure 5. a) and b) respectively show optical and confocal images of the prepared vesicle-loaded capsules. For better visualization, polymersomes were filled with 1 mM fluorescein (λexc=488 nm). One should note that lots of capsules remained empty, even after having optimized the encapsulation parameters. This last statement however can be explained by the fact that during the encapsulation process, capsules were started to be collected before injection of the polymersome sample and after the injection was finished, to make sure that the totality of the batch was encapsulated and avoid any loss.

3.1.2. Co-loading of polymersomes and cells in alginate capsules

The second series of experiments consisted in verifying that the defined parameters for polymersome loading would fit the co-encapsulation process with biological cells. For the experiments, human stem cells were chosen as they would be of great interest for potential

studies with therapeutic applications, and the vesicles were prepared in sterile conditions to avoid cell contamination.

Test N°	Concentration	Number of batches	Ratio polymersomes : cells	Rest time before encapsulation	Outer phase
4	*0.38 M*	*3*	*1:1*	*12 hours*	*Glucose*
5	*0.30 M*	*3*	*1:1*	*12 hours*	*Glucose*
6	*0.30 M*	*3*	*1:1*	*12 hours*	*Sorbitol*
7	*0.30 M*	*3*	*3:1*	*12 hours*	*Sorbitol*
8	*0.30 M*	*3*	*1,5:1*	*12 hours*	*Sorbitol*

Table 2. Main tunable parameters for PBut-b-PEO polymersome preparation and encapsulation with cells in alginate capsules. In red: modified parameter.

As summarized in Table 2 (tests 4-8), key parameters still had to be modified to allow co-encapsulation. Indeed, the stem cells (re-suspended in a Matrigel culture medium) and the polymersomes (glucose, 0.38 M) were injected with sorbitol 0.3 M buffer. Several co-encapsulations were performed in these conditions but no survival of the vesicles was observed which indicated that they probably suffered from the difference in osmotic pressure between both buffers. Consequently, for the next experiments, polymersomes were prepared in sorbitol 0.3 M to avoid any instability issues. Finally, the polymersome-to-cell ratio was optimized in order to increase the probability to find vesicles and cells in a single capsule as the majority of capsules most often comprise cells alone.

3.2. Cell viability assays

After having determined the optimal vesicle preparation and encapsulation conditions, it was necessary to assess cell survival with time. Indeed, stem cells need a few days to grow inside the capsules and the presence of polymersomes could affect their replication.

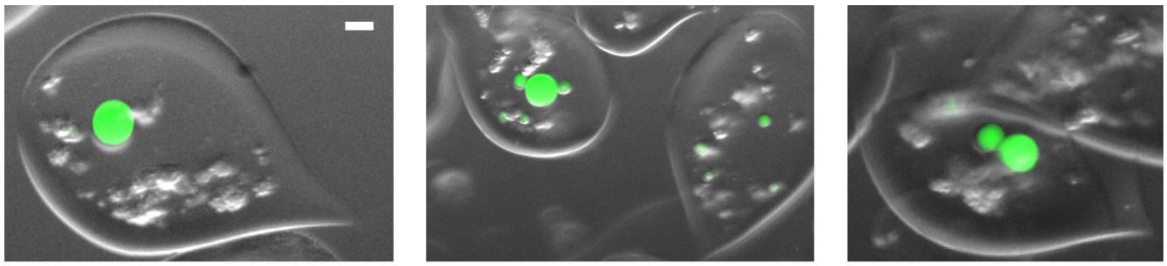

Figure 6. Optical microscope observation of polymersomes (loaded with 1 mM fluorescein) and human stem cells co-encapsulated in alginate capsules. Superposition of green channel and bright field.

Figure 6 shows optical microscope images of co-encapsulated polymersomes and stem cells a few hours after encapsulation. As can be noticed, the vesicles look unaltered and the cells are still alive (cell death would have been noticeable by a change of emitted intensity). However, viable cells were only observed a few hours after the encapsulation thus suggesting a probable contamination of the medium by the polymersomes or an incompatibility between the polymer vesicle membrane and the cells. As several parameters could be the source of cell death, such as the presence of residual solvent (toluene) from the polymersome preparation process, and because stem cells are extremely sensitive to the external environment, it was decided to use alternative cell lines. Mouse adipocytes were chosen because of their robustness, ease of handling and imaging. They are present in adipose tissues and are specialized in storing energy as fat.

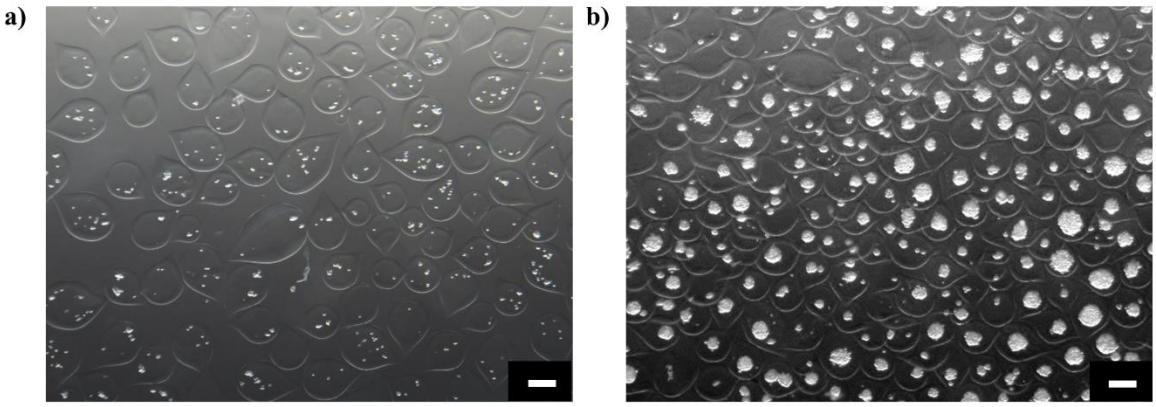

Figure 7. Optical microscope observation of adipocyte growth in alginate capsules. a) one day after encapsulation and b) one week after encapsulation.

As an initial control, adipocytes were encapsulated alone in alginate capsules and their growth was studied over a few days. Figure 7. a) and b) shows optical microscope images of the capsules respectively one and seven days after encapsulation. From the images, it is clearly noticeable that the cells have expanded inside the capsules and that their growth is not affected by the process.

In a second series of experiments, co-encapsulation with polymersomes was performed using the previously determined optimized parameters. As can be seen in microscope images taken four days after encapsulation (Figure 8. a) and b)) cells have grown suggesting that the presence of polymersomes did not affect cell viability. Unfortunately, one can note that very few capsules containing both polymer vesicles and adipocytes were found (Figure 8. c)) and thus the encapsulation conditions defined for co-encapsulation with stem cells have to be optimized for using adipocytes. However, cell viability is a good sign that once fully optimized, this process can be applied for the co-culture of any kind of synthetic and biological cells.

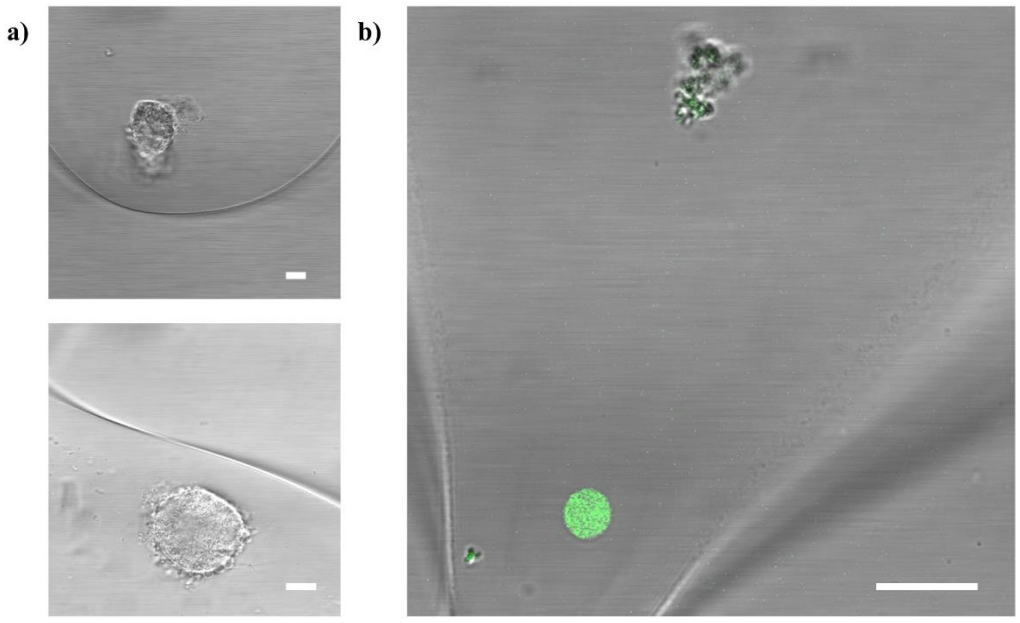

Figure 8. Confocal microscope observation of co-encapsulated pre-adipocytes and polymersomes 4 days after encapsulation. a) adipocytes forming in capsules and b) bright field and green channel overlay of a green fluorescent polymersome and adipocytes during differentiation in an alginate capsule. Scale bar = 10 µm.

4. Conclusion and future perspectives

In this part, we have shown the optimization a microfluidic setup, initially engineered to prepare 3D cell culture alginate capsules, for co-encapsulation of synthetic vesicles (polymersomes) with biological cells (stem cells or adipocytes). We have demonstrated that the polymersome preparation protocol could be optimized to allow an increase of vesicle yield and an efficient encapsulation with cells. Additionally, in a last series of experiments, we established the first evidence that vesicles are not toxic to cells and that they can be co-cultured.

This preliminary contribution was aimed to be a proof of concept for an innovative collaboration project put in place with the team of P. Nassoy (LP2N, UMR 5298). In future work, cell viability has to be validated with different kinds of cell lines, and especially stem cells which are known to be very sensitive to external environment. The polymersome preparation and encapsulation protocols still have to be optimized to increase vesicle yield inside the capsules.

The next steps of this project will be to observe and evaluate the interactions of polymer vesicles with cells inside the alginate capsules and to study the impact of released species in close proximity to biological cells from temperature-induced membrane permeabilization (work presented in Chapter 3) or controlled vesicle rupture (work presented in Chapter 4).

5. References

[1] A. Peyret, E. Ibarboure, A. Tron, L. Beauté, R. Rust, O. Sandre, N. D. McClenaghan, S. Lecommandoux, *Angew. Chem.* **2017**, *129*, 1588–1592.

[2] Z. F. Bielecka, K. Maliszewska-Olejniczak, I. J. Safir, C. Szczylik, A. M. Czarnecka, *Biol. Rev.* **2017**, *92*, 1505–1520.

[3] K. E. Sung, X. Su, E. Berthier, C. Pehlke, A. Friedl, D. J. Beebe, *PLoS ONE* **2013**, *8*, DOI 10.1371/journal.pone.0076373.

[4] V. M. Weaver, O. W. Petersen, F. Wang, C. A. Larabell, P. Briand, C. Damsky, M. J. Bissell, *J. Cell Biol.* **1997**, *137*, 231–245.

[5] C. Frantz, K. M. Stewart, V. M. Weaver, *J Cell Sci* **2010**, *123*, 4195–4200.

[6] E. D. Hay, *Cell Biology of Extracellular Matrix: Second Edition*, Springer Science & Business Media, **2013**.

[7] E. Cukierman, R. Pankov, D. R. Stevens, K. M. Yamada, *Science* **2001**, *294*, 1708–1712.

[8] M. W. Tibbitt, K. S. Anseth, *Biotechnol. Bioeng.* **2009**, *103*, 655–663.

[9] R. Edmondson, J. J. Broglie, A. F. Adcock, L. Yang, *Assay Drug Dev. Technol.* **2014**, *12*, 207–218.

[10] D. Antoni, H. Burckel, E. Josset, G. Noel, *Int. J. Mol. Sci.* **2015**, *16*, 5517–5527.

[11] A. Abbott, *Nature* **2003**, *424*, 870–872.

[12] R. M. Sutherland, *Science* **1988**, *240*, 177–184.

[13] S. Breslin, L. O'Driscoll, *Drug Discov. Today* **2013**, *18*, 240–249.

[14] M. Rimann, U. Graf-Hausner, *Curr. Opin. Biotechnol.* **2012**, *23*, 803–809.

[15] D. Khaitan, S. Chandna, M. Arya, B. Dwarakanath, *J. Transl. Med.* **2006**, *4*, 12.

[16] G. Mehta, A. Y. Hsiao, M. Ingram, G. D. Luker, S. Takayama, *J. Control. Release Off. J. Control. Release Soc.* **2012**, *164*, 192–204.

[17] K. Alessandri, B. R. Sarangi, V. V. Gurchenkov, B. Sinha, T. R. Kießling, L. Fetler, F. Rico, S. Scheuring, C. Lamaze, A. Simon, et al., *Proc. Natl. Acad. Sci. U. S. A.* **2013**, *110*, 14843–14848.

[18] H. Doméjean, M. de la M. S. Pierre, A. Funfak, N. Atrux-Tallau, K. Alessandri, P. Nassoy, J. Bibette, N. Bremond, *Lab. Chip* **2016**, *17*, 110–119.

[19] K. Alessandri, M. Feyeux, B. Gurchenkov, C. Delgado, A. Trushko, K.-H. Krause, D. Vignjević, P. Nassoy, A. Roux, *Lab. Chip* **2016**, *16*, 1593–1604.

[20] A. D. Augst, H. J. Kong, D. J. Mooney, *Macromol. Biosci.* **2006**, *6*, 623–633.

General conclusion

The main motivation of the research project developed during this PhD was to find inspiration from biological cells to expand the already existing toolbox of biomimetic structures. Our main objective was to propose new tools to help researchers develop innovative autonomous "smart" systems for various applications including cell biomimicry and nanomedicine.

During the past years, significant progress was made in the field of cell biomimetics especially with the use of polymers or polymer-based materials to construct artificial cells and organelles. Owing to their chemical tunability and versatility, polymers have helped develop synthetic membranes and compartments with physical properties that more and more resemble the ones of biological cells. In the context of this PhD work, we focused on improving structural and functional characteristics of artificial polymer cells for a better biomimicry.

A first project was dedicated to the development of a biomimetic synthetic membrane (**chapter 2**). Many artificial lipid-based membranes have been proposed in the literature but most of them are lacking an important common feature that biological membranes share, which is their asymmetric structure. Indeed, the outer and inner leaflets of the bilayer membranes are different in terms of lipid composition. This asymmetric lipid distribution is crucial for many membrane-related phenomena and most importantly, it is an indicator of cell integrity. A few asymmetric synthetic membranes have been described, mostly composed of lipids, but for the most, the asymmetry is not totally controlled and the preparation pathway is often tedious. We thus presented the preparation of original giant hybrid vesicles composed of an asymmetric polymer (inner lealet) – lipid (outer leaflet) membrane. We modified the emulsion-centrifugation protocol (also termed droplet over an interface) to prepare the vesicles with poly(butadiene)-*b*-poly(ethylene oxide) (PBut-*b*-PEO) as choice of polymer and 1-palmitoyl-2-oleoyl-sn-glycero-3-phosphocholine (POPC) lipid (Figure 1). This protocol offers a facile and reproducible way to afford giant asymmetric polymer-lipid giant vesicles. We showed that the reverse vesicles could also be obtained (with a lower yield) and that the lipid content could be tuned (an example is shown with 1,2-dimyristoyl-sn-glycero-3-phosphocholine (DMPC)). Additionally, membrane diffusion properties were evaluated by inserting a fluorescently-tagged probe into the outer lipid leaflet. Fluorescence recovery after photobleaching (FRAP) and fluorescence spectroscopy allowed to evaluate respectively lipid lateral diffusion to be D=1.8±0.50 μm^2/s at 25 °C and D =2.3±0.7 μm^2/s at 37 °C (lateral) and a half-life of about 7.5 hours for lipid transverse diffusion. These values were found to be close to the diffusion of lipids in a variety of biological membranes and confirmed the relevance of our cell-like model membrane.

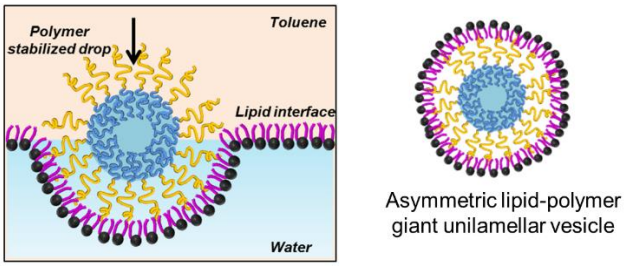

Figure 1. Schematic representation of the formation of hybrid polymer-lipid asymmetric vesicles following the emulsion-centrifugation protocol.

Biological cells are capable of releasing substrates and enzymes from organelles at precise timing to initiate metabolic reactions with high precision. Most presented biomimetic systems exhibit complex compartmentalized structures with the possibility to perform cascade confined chemical or enzymatic reactions. However, for a large majority of these systems, there is no real control over the beginning of the reactions, which are most often initiated by the slow diffusion of species from their respective compartments.

Thus, another major challenge of my PhD research project was to find different triggers to release species independently inside compartmentalized systems to afford a better level of control and precision and further push the boundaries of artificial cell development. We decided to use the emulsion-centrifugation process to encapsulate nano-liposomes inside giant PBut-*b*-PEO vesicles (**chapter 3**). This is to our knowledge one of the first examples of lipid vesicles loaded inside a giant polymersome. We demonstrated that different kinds of liposomes could be encapsulated simultaneously following this approach. One of the main reasons of utilizing liposomes is to take advantage of their phase transition from a gel phase to a fluid phase when modifying the temperature. Membrane permeability can thus be tuned by increasing or decreasing the temperature above or below the lipid melting temperature (Tm). Hence, to go a bit further, we decided to use temperature to trigger the release of species from the nano-liposomes into the lumen of the outer polymer giant vesicle. Two different lipids were chosen for this study, 1,2-dipentadecanoyl-*sn*-glycero-3-phosphocholine (diC15-PC, Tm=35°C) and 1,2-dipalmitoyl-sn-glycero-3-phosphocholine (DPPC, Tm=41 °C). As an example, methylene blue and fluorescein were respectively loaded inside the diC15-PC and DPPC liposomes which were encapsulated together in the giant PBut-*b*-PEO polymersomes. Two different temperature steps (respectively 37 and 45 °C) were then applied to successively release methylene blue from the diC15-PC liposomes, and then fluorescein from the DPPC liposomes (Figure 2).

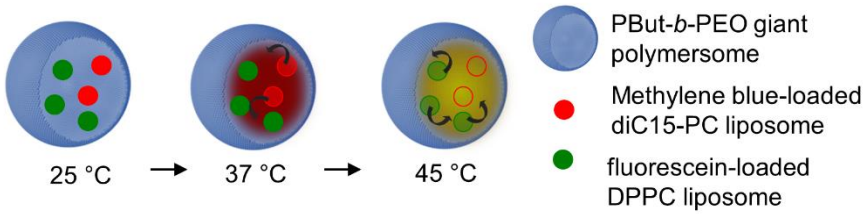

Figure 2. Schematic representation of temperature triggered release of methylene blue and fluorescein from diC15-PC and DPPC liposomes (chapter 3).

We propose this system as a scaffold to perform compartmentalized triggered cascade reactions and provide a first attempt with the enzymatic oxidation of an encapsulated substrate by laccase.

We next explored for a faster and more precise way to have an "on-demand" release of species from compartments, since diffusion through a lipidic membrane is not kinetically well controlled and constitutes a rather slow process. Hence, we focused on osmotic pressure variations which have been shown to have an impact on cell morphological changes (**chapter 4**). We studied the effects of osmotic hypotonic or hypertonic shocks on PBut-*b*-PEO polymersomes and optimized them to trigger vesicle rupture.

First, photo-cleavable dyes (a coumarin derivative (λexc=405 nm), calcein (λexc=488 nm) and methylene blue (λexc=633 nm)) were loaded inside the polymer vesicles. We demonstrated that irradiation under confocal observation at high laser intensity and subsequent photo-cleavage of the dyes inside the vesicles, are responsible for the opening of a pore on the membrane (Figure 3). We further proved that this pore opening is a consequence of the generated increase in osmotic pressure (hypotonic shock) inside the lumen of the vesicles which causes external water to exert pressure on the membrane. We then demonstrated the high precision and control conferred by this method by successively and independently triggering the release of nano-liposomes and nano-polymersomes loaded inside the PBut-*b*-PEO giant vesicles. Overall, we provided a method that allows achieving spatial and temporal control on the release of species, which is another major step forward to artificial cell design.

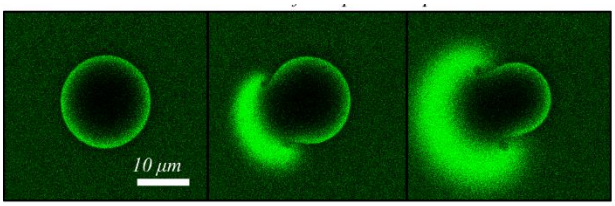

Figure 3. Confocal observation of a PBut-b-PEO vesicle rupturing under light irradiation.

In a second part, we demonstrated how vesicle rupture could be triggered with a hypertonic shock. We hypothesized that the same rupture phenomenon that we observed on giant polymersomes with an osmotic pressure increase could also be induced as a consequence of a fast osmotic pressure decrease. We thus studied the effects of osmolarity and viscosity changes on the UV-polymerization of acrylamide monomers and optimized the reaction conditions to have both a decrease of osmotic pressure and increase of viscosity after short irradiation time. Acrylamide and the irgacure 2959 UV photo-initiator were then loaded inside the PBut-*b*-PEO vesicles and the UV photo-induced polymerization was performed under confocal observation (Figure 4). As expected, a fast rupture was observed for a majority of the vesicles under irradiation, a result that further confirms the impact of osmotic variations on vesicles with a rather impermeable polymer membrane.

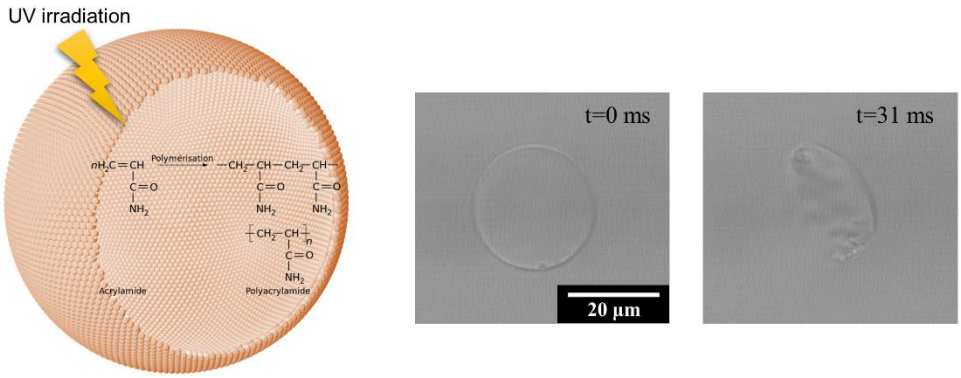

Figure 4. Schematic representation of the UV photopolymerization of acrylamide inside a giant PBut-b-PEO vesicle (left) and the resulting polymersome rupture observed under confocal microscopy (right).

Finally, a new research project in collaboration with the team of Dr. P. Nassoy (LP2N, UMR 5298) was initiated in the context of this PhD thesis. After having proposed tools to help the development of structural and functional mimics of cells, we wondered how would artificial polymer cells interact with biological cells. The team of Dr. P. Nassoy has engineered a method based on microfluidics to prepare alginate capsules as three-dimensional (3D) culture media for biological cells. In **chapter 5**, we described how the process was optimized to allow a co-encapsulation of PBut-*b*-PEO giant polymersomes with human stem cells inside the alginate capsules. The emulsion-centrifugation operating conditions were adapted to the process in order to enhance vesicle yield and increase the probability of co-location of polymersomes and cells in the capsules. Optical and confocal microscopy allowed evidencing that co-encapsulation was

feasible with stem cells. However the survival rate was very poor especially because these cells are very fragile. Hence, the process was successfully repeated with adipocytes (which are much more robust). These preliminary results on this innovative project confirm that artificial and biological cells can be grown together in 3D media and that they are not toxic to each other, even if some optimization is still necessary if working with sensitive cells such as stem cells. The next steps would be to study the impact of released species in close vicinity to biological cells from temperature-induced membrane permeabilization (chapter 3) or light-induced vesicle rupture (chapter 4). This on-going research offers many possible developments, especially in the field of cell therapy.

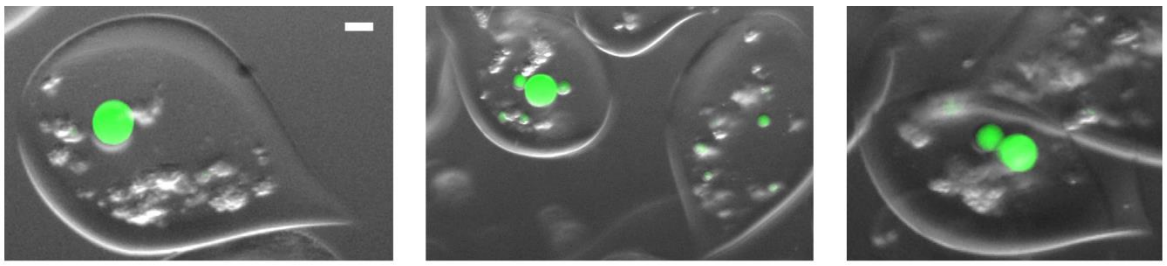

Figure 5. Optical microscope observation of polymersomes (green) and human stem cells co-encapsulated in alginate capsules. Superposition of green channel and bright field.

What comes next ?

The work carried out during this PhD project could have impact in several domains, the first being **1) the building of a complete artificial cell**. Combining all the different parts of biological cells that have been synthetically mimicked by us and others and especially the membrane, organelles, cytoplasm and metabolic confined reactions would help reach a robust simplified cell-model. This model could be of great interest for chemists, physico-chemists, and biologists for studying cellular-related phenomena and to better understand the cell complex machinery. In addition, as already previously mentioned, a compartmentalized structure with triggers the release encapsulated species could be used by chemists or biochemists as **2) a (bio)reactor** with the possibility to perform a temperature- or osmotic pressure-induced cascade confined reaction. A first example was given in chapter 3 with the enzymatic oxidation of an encapsulated substrate. More generally, these systems could be of major interest in the field of therapeutics. One could imagine using compartmentalized systems as **3) multiple-drug reservoirs** released autonomously, independently, and separately as a response to

environmental triggers. Each internal compartment could encapsulate a different active or pro-drug that would be released at appropriate timing. These “smart” systems could be of great interest in diseases that involve combination therapies (such as cancer or HIV) and would avoid having to take multiple drugs every day. Such a system would most surely facilitate patient’s everyday life.

We believe that the fields of synthetic biology and cell mimicry are on the verge of major breakthroughs and that research in these domains has a lot more to offer and is only limited by one’s imagination.

Résumé

Les copolymères à blocs amphiphiles peuvent s'auto-assembler sous forme de vésicules, appelées polymersomes. Ces vésicules ont été développées et étudiées depuis de nombreuses années notamment pour l'encapsulation et la délivrance contrôlée de médicaments. Depuis quelques temps, elles connaissent des applications dans le domaine du biomimétisme cellulaire. Plus robustes que leurs analogues lipidiques (liposomes), les avantages à utiliser les polymersomes comme mimes synthétiques de cellules biologiques ne sont plus à démontrer. Ainsi, des structures compartimentées à base de polymères ont été développés comme mimes structurels de cellules. Ces systèmes ont été utilisés comme bioréacteurs, avec la réalisation de réactions chimiques ou enzymatiques en cascade en milieu confiné. Toutefois, l'un des obstacles qu'il reste à franchir est de trouver des moyens simples et efficaces pour déclencher la réaction au sein de ces systèmes. C'est dans ce contexte que s'inscrivent les travaux de cette thèse. Une membrane synthétique asymétrique à base de lipide et polymère a été développée et la méthode d'émulsion-centrifugation a été utilisée pour produire des systèmes compartimentés biomimétiques. De plus, deux approches différentes ont été suivies pour provoquer la libération contrôlée d'espèces encapsulées, l'une utilisant la température et l'autre la lumière. Enfin, des études de co-encapsulation de cellules synthétiques (polymersomes) et biologiques au sein de milieux 3D ont été réalisées dans le but d'évaluer leur compatibilité et la possibilité de les co-cultiver.

Mots-clés : vésicules, polymères, polymersomes, lipides, biomimétisme cellulaire, multicompartimentation, auto-assemblage, membrane asymétrique, libération contrôlée

Summary

Amphiphilic block copolymers can self-assemble into vesicles, also called polymersomes. These vesicles have been developed and studied for many years especially in the field of drug loading and controlled release. More recently, their use as cell mimics have attracted a lot of attention, mainly because polymersomes exhibit many advantages in contrast to their lipidic analogues (liposomes). In such, compartmentalized polymer systems have especially been developed as structural mimics of cells. These systems have found applications as bioreactors that can confine cascade chemical or enzymatic reactions. However, a major goal that still remains to achieve is to find ways to trigger the beginning of these chemical reactions inside the compartmentalized structures. The work carried out during this PhD thesis was actually to tackle this challenge. A synthetic asymmetric lipid – polymer membrane, that mimics the membrane of biological cells was developed and the emulsion-centrifugation protocol was followed to prepare biomimetic compartmentalized structures. In addition, two different ways to control the independent release of multiple species from individual compartments were developed, based on temperature or light activation. Lastly, co-encapsulation of synthetic cells (polymersomes) and biological cells were performed in 3D media with the aim to study their compatibility for co-culture experiments.

Key words : vesicles, polymers, polymersomes, lipids, cell biomimicry, multicompartment, self-assembly, asymmetric membrane, controlled release